THE ROLE OF MAGMATIC PROCESSES IN THE DEVELOPMENT OF HYPOGENE MINERALISATION AT QUEBRADA BLANCA, NORTHERN CHILE.

Matthew Gareth Rowland

A thesis submitted for the degree of
Doctor of Philosophy
of the University of London,
October 1998.

Department of Geology,
Royal School of Mines,
Imperial College,
Prince Consort Road,
London, SW7 2BP

BRITISH LIBRARY HSIIB

IMAGING SERVICES NORTH

Boston Spa, Wetherby
West Yorkshire, LS23 7BQ
www.bl.uk

PAGINATED BLANK PAGES ARE SCANNED AS FOUND IN ORIGINAL THESIS

NO INFORMATION IS MISSING

PAGE NUMBERING AS ORIGINAL

ABSTRACT

This thesis presents data relating to the intrusive lithologies, hydrothermal veins, and styles of alteration which record the evolution of the magmatic-hydrothermal system associated with the porphyry copper deposit of Quebrada Blanca, the most northern of such deposits of Late Eocene-Early Oligocene age in Chile. Data presented include field and petrographic observations, elemental and isotopic geochemistry of whole rocks and mineral separates, and microthermometric analyses of fluid inclusions. A comparison of these data with those reported for other porphyry copper deposits indicates that the components of the magmatic-hydrothermal system at Quebrada Blanca and their temporal relationships are typical of porphyry copper deposits in general.

Analysis of data from Quebrada Blanca suggests that the evolution of the magmatic-hydrothermal system was driven by a series of processes in a sub-volcanic environment. There are two fundamental processes in this series: (1) Equilibration between a layer of magma at the base of a physically stratified felsic chamber and a melt volatile phase derived from a mafic magma; (2) Dyking of this layer of felsic magma upwards through the dominantly crystalline regions of the chamber. Hypogene mineralisation is bracketed by these two processes and is thought to be a product of equilibration between dominantly crystalline magma in the upper parts of the felsic chamber and volatiles sourced from the layer of felsic magma at the base of the chamber.

Combined, the proposed processes form a genetic model for magmatic-hydrothermal systems associated with porphyry copper deposits and for the development of hypogene mineralisation. This model accounts more completely for the nature and interrelationships of the characteristic components of such magmatic-hydrothermal systems than previous genetic models. The model can be used to explain some of the variations displayed by magmatic-hydrothermal systems and so is of value both for the better understanding of existing deposits and in the exploration for new prospects.

ACKNOWLEDGEMENTS

It goes without saying that a great many people have contributed towards this project, both in Chile and in the UK. Special mention must be made of Adrian King and the staff at Minera Cominco Chile Ltda. who made me so welcome during my visits to Chile. Thanks must also be extended to the geological staff at Quebrada Blanca for, above all, their patience.

Back in the UK, the high level of technical support provided by Liz Morris & Mark Thompson (thin sectioning), Dick Giddens (EPMA) and Peter Watkins & Gillian Wragg (whole-rock geochem.) at Imperial College, and by Adrian Boyce and his team at SURRC (isotopes) is gratefully acknowledged.

Closer to home still, I'd like to thank my parents for all the support they have provided over the years and for putting-up with all the comings and goings – I may think about getting a "proper" job now... maybe. And also Nic, Sal, and Karen – for the beginning, the middle and the end ☺.

Lastly, I'd like to acknowledge Jamie Wilkinson. In truth, he deserves far more than an acknowledgement; without his support, encouragement and enthusiasm, I would not have gained nearly as much from this piece of research as I feel I have done.

TABLE OF CONTENTS

List of tables 10

List of figures 12

Chapter 1 Introduction

1.1 Project rationale 17

1.1.1 Burnham and the orthomagmatic model 17

1.1.2 Limitations of the Burnham model and its derivatives 20

1.2 The study area 21

1.2.1 Why Quebrada Blanca? 21

1.2.2 Exploration and discovery 22

1.2.3 Stratigraphic and structural setting 22

1.3 Modus Operandi 23

1.4 About the layout of this thesis 24

Chapter 2 Data relating to the magmatic system at Quebrada Blanca

2.1 Lithologies in the field area 25

2.1.1 Monzogranite-granodiorite 25

2.1.2 Andesite 25

2.1.3 Feldspar porphyry 27

2.1.4 Aplite 28

2.2 Petrography 29

2.2.1 Technique 29

2.2.2 Fresh samples 29

2.2.3 Samples exhibiting evidence of hypogene alteration 33

2.3 Whole-rock geochemistry 34

2.3.1 Technique 34

2.3.2 Data 36

2.4 Biotite geochemistry 39

2.4.1 Technique 39

2.4.2 Data 40

2.5 Plagioclase zonation 44

2.5.1 Technique 44

2.5.2 Zonation of plagioclase in the feldspar porphyry 44

2.6 Hydrogen and oxygen isotope geochemistry 46
2.6.1 Technique 46
2.6.2 Data 47
2.7 Fluid inclusions 47
2.7.1 Technique 47
2.7.2 Fluid inclusions within quartz phenocrysts in the feldspar porphyry 47

Chapter 3 Data relating to the hydrothermal system at Quebrada Blanca

3.1 Vein classification 49
3.2 Vein paragenesis and spatial distribution 52
3.3 Petrography 53
3.3.1 Techniques 53
3.3.2 Data 54
3.4 Fluid inclusion microthermometry 58
3.4.1 Technique 58
3.4.2 Data 62
3.5 Light stable isotope geochemistry 69
3.5.1 Techniques 69
3.5.2 Data 69
3.6 Data relating to breccias 70

Chapter 4 A comparison of Quebrada Blanca with other porphyry copper deposits

4.1 Magmatic components associated with porphyry copper deposits 72
4.1.1 The mineralised stock 72
4.1.2 The mineralising porphyry 73
4.1.3 Other intrusives 74
4.2 Hydrothermal components associated with porphyry copper deposits 75
4.2.1 Vein paragenesis 75
4.2.2 Morphology, internal structure and spatial distribution of veins 76
4.2.3 Fluid inclusions 78
4.2.4 Isotopes 80
4.2.5 Hydrothermal breccias 81
4.3 Timing of mineralisation and magmatism 82
4.4 Summary 83

Chapter 5 Evolution of the magmatic system at Quebrada Blanca

5.1 Monzogranite 84
5.1.1 Petrography 84
5.1.2 Whole-rock geochemistry 86
5.1.3 Biotite geochemistry 86
5.1.4 Summary 87
5.2 Andesite 88
5.2.1 Petrography 88
5.2.2 Whole-rock geochemistry 88
5.2.3 Biotite geochemistry 90
5.2.4 Isotope geochemistry 91
5.2.5 Summary 91
5.3 Feldspar porphyry 92
5.3.1 Petrography 92
5.3.2 Whole-rock geochemistry 93
5.3.3 Biotite geochemistry 94
5.3.4 Plagioclase zonation 95
5.3.5 Isotope geochemistry 99
5.3.6 Fluid inclusions within the quartz phenocrysts 99
5.3.7 Summary 100
5.4 Aplite and igneous breccia 101
5.4.1 Petrography 101
5.4.2 Biotite geochemistry 101
5.4.3 Summary 102
5.5 Relationships between lithologies 102
5.6 Summary 104

Chapter 6: Evolution of the hydrothermal system at Quebrada Blanca

6.1 Processes influencing the evolution of the MVP 105
6.1.1 Regimes of fluid flow associated with porphyry copper deposits 105
6.1.2 Phase relations in evolving magmatic fluids 106
6.2 Early stage veins 106
6.2.1 Petrography 106
6.2.2 Fluid inclusions 107
6.2.3 Oxygen isotopes 108

6.2.4 Sulphur isotopes 109

6.2.5 Evolution of early stage hydrothermal assemblages 110

6.3 Late stage hydrothermal assemblages 111

6.3.1 Petrography 111

6.3.2 Reliability of fluid inclusion data 114

6.3.3 Fluid inclusions 116

6.3.4 Oxygen isotopes 119

6.3.5 Sulphur isotopes 120

6.3.6 Evolution of late stage hydrothermal assemblages 120

6.3.7 Summary 123

6.4 Summary 123

Chapter 7: A model for the development of hypogene mineralisation in porphyry copper deposits

7.1 Introduction 124

7.1.1 Previous models 124

7.1.2 Relationships between magmatic and hydrothermal events at Quebrada Blanca 125

7.1.3 This model 126

7.2 Stage 1: Establishment of a stratified felsic magma chamber 127

7.2.1 Physical stratification 127

7.2.2 Rheological variations in the magma chamber 128

7.2.3 Variation in melt composition within the magma chamber 128

7.2.4 Magma chamber processes 130

7.3. Stage 2: Introduction of mafic magma into the felsic chamber and exchange of components 131

7.3.1 Effects of magma juxtaposition 131

7.3.2 Nature of material exchange 131

7.3.3 Limits on the volume of volatiles introduced 132

7.3.4 Composition of the mafic MVP 133

7.3.5 Effects of MVP transfer 133

7.4 Stage 3: Generation of a MVP in equilibrium with the suspension layer 135

7.4.1 Composition of the melt in the suspension layer 135

7.4.2 The MVP in equilibrium with the suspension layer 136

7.5 Stage 4: Fluid flow 138

7.5.1 Disseminated mineralisation and alteration 138
7.5.2 Fracture-related mineralisation 139
7.6 Stage 5: Chamber evacuation 140
7.7 Stage 6: Dyke degassing 142
7.7.1 Behaviour of volatiles during dyke ascent 142
7.7.2 Loss of the volatile phase from the magma 142
7.6.3 Decompression of the system 142
7.8 Summary 143

Chapter 8 Applications and implications of the model

8.1 Variations on a theme 144
8.1.1 Barren systems with evidence of mafic-felsic magma interaction 144
8.1.2 Contrasting styles of hypogene alteration 146
8.2 Implications for mineral exploration 147
8.3 Areas for further research 147
8.3.1 Validation of the model 147
8.3.2 The model as a framework 150

Chapter 9 Conclusions

Conclusions 151

Reference list

Reference list 154

Appendices

A.1 Method of preparation for whole-rock compositional analysis 174

A.2 Results of whole-rock compositional analysis 175

A.3 Compositions of biotite determined by EPMA 180

A.4 EPMA transects across plagioclase from the feldspar porphyry 185

A.5 Oxygen and hydrogen isotopic compositions of biotite phenocryst from the feldspar porphyry and of the andesite dykes and their selvedges. 197

B.1 Data for EPMA transects across veins 198

B.2 Microthermometric data from fluid inclusions by vein type 201

B.3 Oxygen isotopic results for vein quartz and magnetite 226

B.4 Sulphur isotopic results for vein sulphides 227

C.1 Calculation of water solubility in the melt of the suspension layer at Quebrada Blanca 228

C.2 Calculation of the melt composition of the suspension layer at Quebrada Blanca 229

C.3 Calculation of the melt composition of the suspension layer at Yerington 230

D Sample list 231

LIST OF TABLES

TABLE 2.1 Averaged compositions of the sulphides-only and magnetite-bearing groups of the monzogranite. 36

TABLE 2.2 Compositional variation in the samples of andesite 37

TABLE 2.3 Averaged compositions of the three groups of samples of the feldspar porphyry. 38

TABLE 2.4 Averaged compositions of the aplite and magnetite-bearing samples of the monzogranite 39

TABLE 2.5 $\delta^{18}O$ and δD values of biotite separates from samples of the feldspar porphyry 47

TABLE 3.1 The vein paragenesis at Quebrada Blanca. 49

TABLE 3.2 Summary of fluid inclusion properties for type 1 veins. 62

TABLE 3.3 Summary of fluid inclusion properties for type 2 veins. 63

TABLE 3.4 Summary of fluid inclusion properties for type 3 veins. 64

TABLE 3.5 Summary of fluid inclusion properties for type 4 veins. 65

TABLE 3.6 Summary of fluid inclusion properties for veins of type 5(a and b). 68

TABLE 3.7 Summary of fluid inclusion properties for type 6 veins. 68

TABLE 4.1 A comparison of the vein parageneses at various porphyry copper deposits. 75

TABLE 4.2 Summary of salinity and homogenisation temperature data for fluid inclusions in veins at Quebrada Blanca. 78

TABLE 5.1 Metal contents of volcanic exhalations. 89

TABLE 6.1 Critical temperatures of fluids trapped in type V inclusions within intermediate stage veins. 115

TABLE 6.2 Minimum formation pressures of late stage veins. 118

TABLE 6.3 Calculated $\delta^{18}O$ of fluids in equilibrium with vein quartz. 119

TABLE 7.1 Normalised composition and modal mineralogy of samples 164 and R5. 129

TABLE 7.2 Normalised composition of the residual melt and modal mineralogy of the solid assemblage at the boundaries between layers in the felsic magma chamber. 130

TABLE 7.3 Composition of melt and relative composition of fluid within the suspension layer. 135

TABLE 8.1 Composition of melt and equilibrium MVP of the porphyritic intrusives at Yerington, Nevada. 146

LIST OF FIGURES

FIG. 1.1	Types of hydrothermal mineral deposit spatially associated with granitoid intrusives	17
FIG. 1.2	Comparison of the empirical model for porphyry copper deposits of Lowell & Guilbert (1970) with the Burnham (1979) model for the genesis of porphyry copper mineralisation	19
FIG. 1.3	Map showing the location of Quebrada Blanca and selected porphyry copper deposits in Chile	21
FIG. 2.1	Simplified map of the geology of Quebrada Blanca	26
FIG. 2.2	Schematic section through and below the deposit of Quebrada Blanca	27
FIG. 2.3	Andesite enclave	30
FIG. 2.4	Backveining of an andesite dyke by the monzogranite	30
FIG. 2.5	Entrainment of plagioclase phenocrysts from the monzogranite in the selvedge of an andesite dyke	30
FIG. 2.6	Contact relationships of the aplite with the monzogranite	30
FIG. 2.7	Photomicrograph of intergrown plagioclase and quartz in the andesite	32
FIG. 2.8	Photomicrograph of acicular apatite in the andesite	32
FIG. 2.9	Photomicrograph of oxyhornblende in the feldspar porphyry	32
FIG. 2.10	Photomicrographs of quartz phenocrysts in the feldspar porphyry	32
FIG. 2.11	Photomicrograph of biotite pseudomorphing hornblende in the feldspar porphyry	35
FIG. 2.12	Photomicrograph of sphene replaced by magnetite/ilmenite in the feldspar porphyry	35
FIG. 2.13	Styles of potassic alteration within the monzogranite	35
FIG. 2.14	Coarse graphic texture developed in the monzogranite	35
FIG. 2.15	Scatter plot showing the variation of K_2O with Na_2O in whole-rock samples of the monzogranite	36
FIG. 2.16	Scatter plot showing the variation of Sr with CaO in whole-rock samples of the feldspar porphyry	38
FIG. 2.17	Scatter plot showing the variation of Ba with K_2O in whole-rock samples of the feldspar porphyry	38
FIG. 2.18	Scatter plot showing the variation of MgO with $FeO_{(total)}$ in biotite from samples of the monzogranite	41

FIG. 2.19 Scatter plot showing the variation of K_2O with $MgO/(MgO+FeO_{(total)})$ in biotite from samples of the monzogranite 41

FIG. 2.20 Scatter plot showing the variation of SiO_2 with $MgO/(MgO+FeO_{(total)})$ in biotite from samples of the monzogranite 41

FIG. 2.21 Scatter plot showing the variation of Cl with $MgO/(MgO+FeO_{(total)})$ in biotite from samples of the monzogranite 41

FIG. 2.22 Scatter plot showing the variation of TiO_2 with $MgO/(MgO+FeO_{(total)})$ in biotite from samples of the monzogranite 41

FIG. 2.23 Scatter plot showing the variation of $FeO_{(total)}$ with TiO_2 in biotite from samples of the monzogranite 41

FIG. 2.24 Scatter plot showing the variation of TiO_2 with $MgO/(MgO+FeO_{(total)})$ in biotite from a sample of the andesite and samples of selvedges on andesite dykes 42

FIG. 2.25 Scatter plot showing the variation of SiO_2 with $MgO/(MgO+FeO_{(total)})$ in biotite from a sample of the andesite and samples of selvedges on andesite dykes 42

FIG. 2.26 Histogram of $MgO/(MgO+FeO_{(total)})$ in biotite from samples of the feldspar porphyry 43

FIG. 2.27 Scatter plot showing the variation of SiO_2 with $MgO/(MgO+FeO_{(total)})$ in biotite from samples of the feldspar porphyry 43

FIG. 2.29 Variation in mol. % anorthite and wt. % K_2O along traverses across large feldspar phenocrysts from the feldspar porphyry 45

FIG. 2.30 Variation in mol. % anorthite and wt. % K_2O along traverses across small feldspar phenocrysts from the feldspar porphyry (a) Plateau subtype (b) Atoll subtype (c) Hiatal subtype 45

FIG. 2.31 Photomicrgraph of small plagioclase phenocryst from the feldspar porphyry 45

FIG. 2.32 Histogram of fluid inclusion salinities in quartz phenocrysts from the feldspar porphyry 48

FIG. 2.33 Scatter plot of homogenisation temperature vs. salinity for fluid inclusions in quartz phenocrysts from the feldspar porphyry 48

FIG. 3.1 Petrographic characteristics of type 1 veins 50

FIG. 3.2 Petrographic characteristics of type 3 veins 50

FIG. 3.3 Spatial distribution of vein types at Quebrada Blanca 52

FIG. 3.5 Petrographic characteristics of type 5a veins 57

FIG. 3.6	Petrographic characteristics of type 5b veins	57
FIG. 3.8	EPMA traverses across type 5a veins showing variation in concentration of selected trace elements in quartz	58
FIG. 3.9	Histogram of fluid inclusion salinities in type 1 veins	62
FIG. 3.10	Scatter plot of homogenisation temperature vs. salinity for fluid inclusions in type 1 veins	62
FIG. 3.11	Histogram of homogenisation temperatures for fluid inclusions in type 1 veins	62
FIG. 3.12	Histogram of homogenisation temperatures for fluid inclusions in type 2 veins	63
FIG. 3.13	Scatter plot of homogenisation temperature vs. salinity for fluid inclusions in type 2 veins	63
FIG. 3.14	Histogram of fluid inclusion salinities in type 3 veins	64
FIG. 3.15	Scatter plot of homogenisation temperature vs. salinity for fluid inclusions in type 3 veins	64
FIG. 3.16	Scatter plot showing temperature of halite dissolution vs. liquid-vapour homogenisation for saturated inclusions in type 3 veins	65
FIG. 3.17	Histogram of fluid inclusion salinities in type 4 veins	66
FIG. 3.18	Histogram of homogenisation temperatures for fluid inclusions in type 4 veins	66
FIG. 3.19	Scatter plot of homogenisation temperature vs. salinity for fluid inclusions in type 4 veins	66
FIG. 3.20	Scatter plot of homogenisation temperature vs. salinity for fluid inclusions in type 5 veins	67
FIG. 3.21	Histogram of homogenisation temperatures for fluid inclusions in type 5 veins	67
FIG. 3.22	Scatter plot of homogenisation temperature vs. salinity for fluid inclusions in type 6 veins	68
FIG. 3.23	Histogram of measured $\delta^{18}O$ values for vein quartz for all vein types	69
FIG. 3.24	Petrographic characteristics of the hydrothermal breccias	71
FIG. 4.1	Schematic diagram showing the two stages of development characteristic of porphyry copper deposits. (a) Development of disseminated protore (b) Overprinting by fracture hosted assemblages associated with sericitic alteration	83
FIG. 5.1	Variation of copper and molybdenum contents of arc lavas with SiO_2 content	89

FIG. 5.2	Transect across one of the large plagioclase phenocrysts from the feldspar porphyry showing the variation in anorthite and potassium, and the calculated potassium content of the melt	97
FIG. 6.1	Schematic pressure-temperature diagram showing phase relations in an evolving magmatic fluid	106
FIG. 6.2	Schematic diagram showing the environment in which type 2 veins are postulated to have formed	108
FIG. 6.3	Diagram summarising the effects of annealing	113
FIG. 6.4	Scatter plot of homogenisation temperature vs. salinity for fluid inclusions in vein types 3, 4, and 5a	117
FIG. 6.5	Schematic graph of measured $d^{18}O$ value of quartz vs. temperature showing the position of quartz from vein types 3, 4 and 5	119
FIG. 6.6	Schematic diagram summarising the evolution of late stage veins	122
FIG. 7.1	Stratification of the modelled felsic magma chamber	127
FIG. 7.2	Enlargement of the area of interest on the phase diagram contoured for melt fraction and showing the proposed cooling trajectory of the modelled magma	129
FIG. 7.3	Schematic view of the modelled mgma chamber following introduction of the mafic magma	131
FIG. 7.4	Phase diagram for the modelled magma modified for the addition of the components of biotite.	134
FIG. 7.5	Flows within the modelled magma chamber during the development of protore.	138
FIG. 7.6	Evacuation of the chamber and ascent of magmas as dykes.	141
FIG. 8.1	Mineralisation as an intermediate condition between magma mixing and bimodal volcanism	145

INTRODUCTION 1

This thesis concerns the magmatic-hydrothermal evolution of the porphyry copper deposit of Quebrada Blanca, and the implications of this study for the evolution of porphyry copper systems in general. This chapter summarises the rationale for the research project and its main objectives, and briefly presents the *modus operandi*.

1.1 Project rationale

1.1.1 Burnham and the orthomagmatic model

A variety of hydrothermal mineral deposit types are spatially associated with granitoid intrusives (Fig. 1.1). In some of these deposits, most notably the high sulphidation epithermal and porphyry-associated types, the metals within the ore bodies and the fluids that transported them are both thought to have been supplied by the associated intrusive while it was still at least partially molten, i.e. in the magmatic state. Models developed on the basis of this concept have been termed orthomagmatic, and contrast with models in which

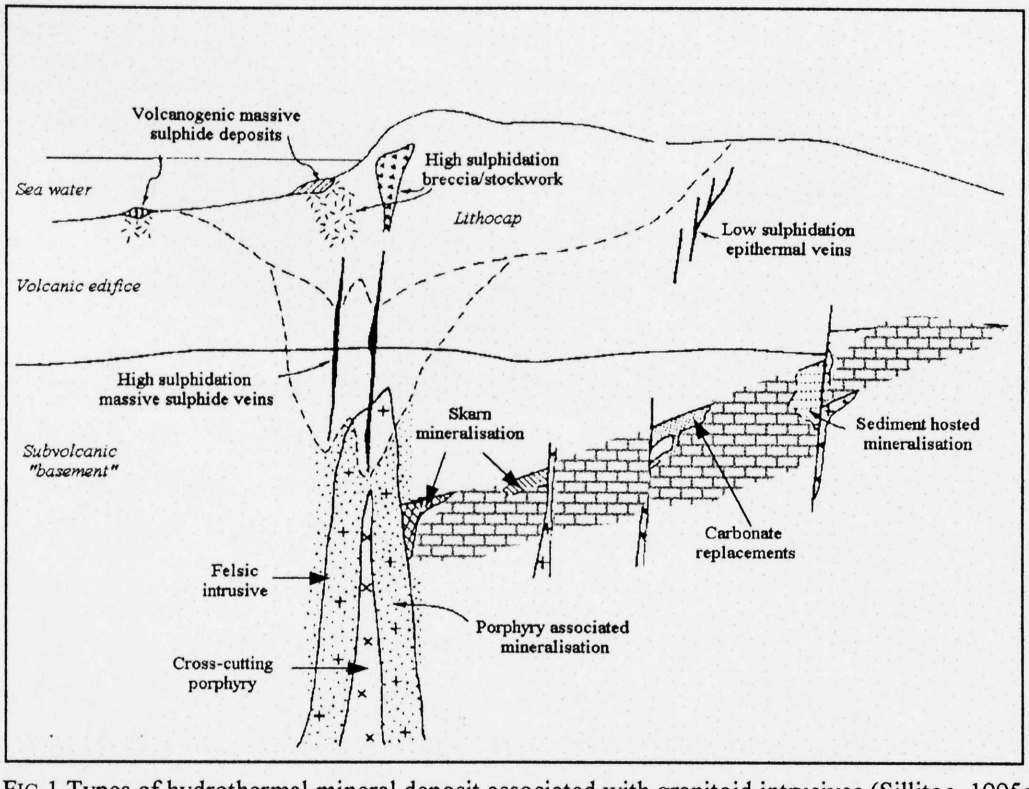


FIG.1 Types of hydrothermal mineral deposit associated with granitoid intrusives (Sillitoe, 1995a)

the associated intrusive only provides the heat required to drive hydrothermal circulation (Norton, 1978). Distinction between the two types of model has been hindered by the modification of deep hypogene assemblages by later supergene processes following uplift and erosion.

Of the ore deposit types shown in Figure 1.1, the porphyry-associated type is the most closely related to the intrusives thought to source the ore fluid(s) and our understanding of the role magmatic processes play in the development of hypogene mineralisation is largely based on theoretical, experimental and field-based studies of the porphyry environment. Assuming an orthomagmatic origin for fluids and ore elements, the development of hypogene mineralisation in porphyry-associated systems can be split into two stages: (1) A magmatic stage, in which a fluid phase enriched in metals is produced from, and is initially in equilibrium with, a magma; (2) A hydrothermal stage, in which this fluid phase migrates such that the fluid and magma cease to be in physical contact and the fluid phase precipitates ore phases in response to re-equilibration with its new environment.

Our understanding of the magmatic stage of hypogene mineralisation was pioneered by Burnham (1979). He recognised that although water, the main component of hydrothermal fluids, was dispersed in large quantities (2-6 wt. %) in many granitic magmas, the diffusivity of water in felsic magmas was too small to account for its redistribution from this disperse state to form significant accumulations within a geologically reasonable length of time. Consequently, saturation of the melt with respect to water was required so that the two could exist as independent phases. In this respect water, and the less abundant volatile species, CO_2, H_2S and SO_2, could be regarded as being similar to the components of a crystallising solid phase: they were always present within the melt but only when their concentration reached saturation did they exsolve as a separate, immiscible, phase. This phase will hereafter be referred to as a melt volatile phase (MVP).

Burnham proposed two mechanisms of MVP saturation in granitic magmas. Since the solubility of water in silicate melts is highly pressure dependent, magmas could become saturated with a MVP as they were emplaced and underwent decompression. This he termed first boiling. Alternatively, having established a closed system magma chamber, volatile saturation of the melt could result from the crystallisation of anhydrous phases (those which do not incorporate volatile components) increasing the concentration of volatile components within the residual melt until the saturation level for the appropriate conditions of temperature, pressure and melt composition was exceeded. Once the magma has become saturated with a volatile phase, the enrichment in ore elements of the MVP relative to the

magma is a natural consequence of the partitioning behaviour of the ore elements between fluid and magma, assuming no solid phase, such as a sulphide, has sequestered the ore elements prior to volatile saturation (Kilinc, 1969; Candela & Holland, 1986).

In a series of papers, Burnham and his co-authors (Burnham, 1979, 1981; Burnham & Ohmoto, 1980) used the premise outlined above to explain the production of ore-bearing fluids in porphyry-copper deposits. A zoned intrusive was envisaged, consisting of a solidified outer casing, a marginal "carapace" of H_2O-saturated melt, thick close to the chamber's apex but thinning rapidly with depth, and an inner zone filled with crystallising magma that was undersaturated with respect to H_2O. Fluid exsolution within the carapace led to an increase in pressure within the system as the two phases (magma plus volatile) occupied a greater volume than the melt with dissolved volatiles. This build-up of pressure eventually exceeded the strength of the solidified casing, producing fractures through which the MVP escaped, marking the onset of the hydrothermal stage. Fluid escape resulted in decompression of the system and pressure-induced fluid exsolution, termed second boiling.

The model proposed by Burnham has been widely embraced by geologists: the build-up of fluid pressures leading to fracturing of the overlying casing ties in well with the empirical models of mineralised stockworks developed in the apical regions of small intrusive stocks (Lowell & Guilbert, 1970). The two are compared in Figure 1.2. As noted by Gustafson (1978) the empirical model presented by Lowell & Guilbert (1970) is a static model, as is the model presented by Burnham and his co-workers. Hypogene mineralisation in porphyry-associated deposits, however, clearly occurs as a series of distinct events.

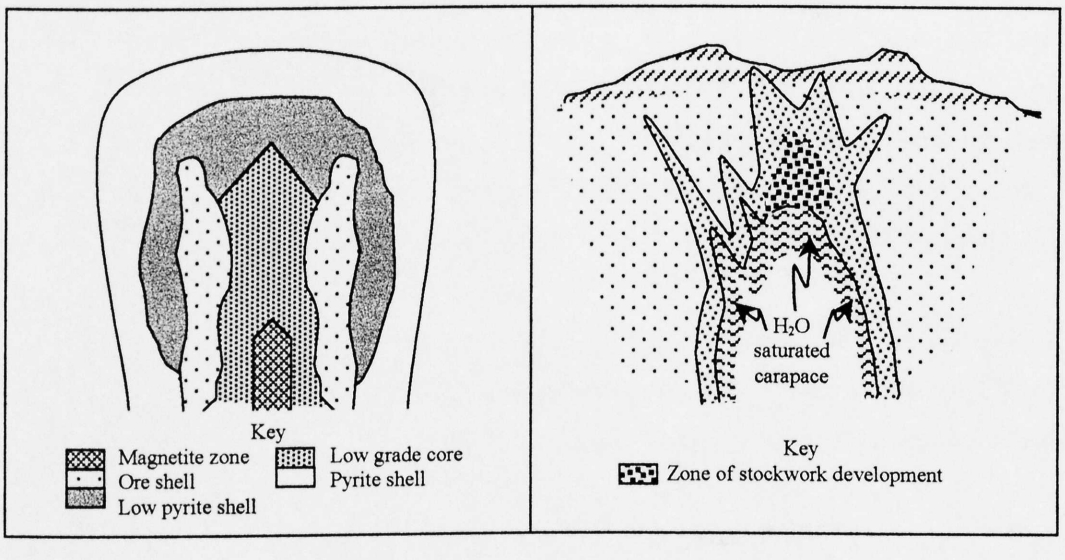


FIG. 1.2 Comparison of the empirical model for porphyry copper deposits (left; Lowell & Guilbert, 1970) with the Burnham (1979) model for the genesis of porphyry copper mineralisation (right)

As an explanation for these events, Whitney (1975a, 1989) suggested the occurrence of resurgent boiling. At constant conditions of pressure, temperature and composition, the carapace, or crystallisation interval, as it will be referred to hereafter, would become smaller and eventually be eliminated. Changes in these conditions, such as attendant on a further influx of melt, could lead to renewed or resurgent boiling. With each successive boiling event the crystallisation interval would retreat to a greater depth within the stock and the pressures required to initiate fracturing would be higher. Subsequent boilings could result in the relative enrichment or depletion of a given volatile depending upon the pressure, the partitioning coefficient and whether the system was open or closed. Consequently, the composition of the aqueous phase could vary spatially and temporally.

Recent models of hypogene mineralisation in porphyry-associated deposits have attempted to reconcile chemical models for MVP exsolution with physical models of the crystallisation of hydrous, felsic magmas. These models are discussed in more detail in Chapter 6. Fundamentally, however, all have been based on the idea of vapour saturation of a magma occurring in a closed chamber as a result of second boiling, as proposed by Burnham in 1979.

1.1.2 Limitations of the Burnham model and its derivatives

The model presented by Burnham in 1979 was based on the assumption that the volatile content of the magma involved originated from the initial fluid-absent partial melting of the source rocks. Burnham himself admitted (Burnham, 1997) that many of the model's predictions were "critically dependent on the specific mode of origin of the magma", and that his view of magma generation in subduction zones was "at odds" with that of more recent workers in the field. Although many of the later theoretical models have not made inferences about the origins of the magma involved, most have assigned it a composition which constrains the modelled results (Candela & Holland, 1986; Candela, 1989, 1994).

Despite the ultimate dependence of models concerned with hypogene mineralisation on the composition of the magma from which the volatiles were sourced, there has only been a single study of the magmatic system beneath a porphyry copper deposit: that which underlies the deposits of Yerington, Nevada (Dilles, 1987). This study has been used as a test-case for some theoretical models published in the last ten years (Cline & Bodnar, 1991; Cline, 1995), and as an analogue for magmatic systems that are concealed at depth beneath other deposits

(Shinohara & Hedenquist, 1997). Clearly there is a need for more studies of the magmatic systems underlying porphyry-associated deposits.

The principal objective of this piece of research is to detail both the development of the magmatic system underlying a porphyry-associated deposit and the hydrothermal evolution of that deposit in order to provide an integrated model for hypogene mineralisation.

1.2 The study area

1.2.1 Why Quebrada Blanca?

The deposit selected for study is the porphyry-copper deposit of Quebrada Blanca, located in northern Chile (Fig. 1.3; Hunt *et al.*, 1983). Dating using the K-Ar method suggests that the intrusives hosting mineralisation and the potassic alteration assemblage at Quebrada Blanca both have an age of approximately 35 Ma (Maksaev & Zentilli, 1988). Consequently, Quebrada Blanca represents the northern-most of the economic deposits of the Late Eocene-Early Oligocene porphyry belt of Chile (Sillitoe, 1988). A deposit from the central Andean orogen, and more particularly from the Eocene-Oligocene belt, makes a good choice for study as the deposits within the orogen are well documented and display similar characteristics (see Chapter 4 for a detailed review) as typified by the deposit of El Salvador (Gustafson & Hunt, 1975). A model accounting for the characteristics of one of these deposits may therefore be of general application.



FIG. 1.3 Map showing the location of Quebrada Blanca and selected porphyry copper deposits in Chile.

An additional reason for the choice of Quebrada Blanca as the study site was the amount of exploration core available for examination. Working with core is a necessity when studying porphyry copper mineralisation in general and for this project in particular, concerned as it is with the evolution of the system below the level of currently economic mineralisation. Such levels are poorly documented, partly reflecting the fact that they are rarely exposed during mineral

extraction. The system described at Yerington, Nevada (Dilles, 1987) was exposed by fortuitous tilting during Basin and Range faulting.

1.2.2 Exploration and discovery

The porphyry copper deposit of Quebrada Blanca is located in the Chilean altiplano at 21°00S, 68°48W. The deposit has a long exploration history that is discussed in more detail by Hunt *et al.* (1983) and Sillitoe (1995b) from which the following is summarised. The location was noted for its potential in 1957 by the Chile Exploration Company, Anaconda's subsidiary in Chile. Drilling was first carried out by CODELCO-Chile in 1975 following expropriation of all Anaconda's assets by the state in 1971. Enriched copper mineralisation was intersected in the only hole. In 1977, Superior Oil-Falconbridge obtained a 51% share of the project (the remainder still being owned by the state) and its Chilean subsidiary, Compañia Minera Exploradora Dona Ines, commenced exploration on the site. Between 1977 and 1982, nearly 44,000 metres of drilling was carried out, and an exploration tunnel constructed. In 1983, the resource was put on care and maintenance due to the low price of copper, and in 1984, Mobil Oil, who by that time had acquired Superior Oil, abandoned the project. In 1988 the state agency ENAMI tendered the resource and it was won by Cominco. Following a feasibility study using heap-leach technology, the deposit entered production as an open-pit SX-EW operation in 1994. This research is the first to address the genesis of the deposit.

1.2.3 Stratigraphic and structural setting

During this study, little emphasis has been placed on the structural evolution of the deposit, or on the country rock hosting the intrusive sequence. A comparison with other deposits (see chapter 4) suggests that while structures may act as foci for magmas at a regional scale or for mineralising fluids at a deposit scale, they do not appear to influence the nature of the elements comprising the magmatic-hydrothermal systems at the various deposits, nor the evolutionary processes which link them. This is also true of the lithologies hosting the magmatic-hydrothermal systems; although reactive lithologies such as mafic volcanics and carbonate-rich sediments may alter the character of some deposits by acting as sinks for mineralising fluids, there is no evidence to suggest that in doing so they influence the processes responsible for fluid production. A brief summary of the structural/stratigraphic evolution of northern Chile is given below to help place Quebrada Blanca in its regional context.

Since the Jurassic, the magmatic arc of Northern Chile has evolved in four separate stages, each characterised by the formation of a spatially distinct arc (Reutter *et al*, 1996). The late Eocene-early Oligocene porphyry belt (Sillitoe, 1988), in which Quebrada Blanca is located, formed at the end of the third (late Cretaceous-Palaeogene) stage. Mesozoic-Cenozoic plutonic rocks are characterised by a predominance of mafic rocks such as tonalite, quartz diorite and diorite, and also of slightly alkaline rocks such as quartzmonzodiorite and quartz monzonite. The granitoids are typically magnetite series and are usually hornblende bearing (Ishihara *et al.*, 1984).

In addition to the intrusion of stocks, there was major volcanic activity in the middle and upper Eocene. This activity was of contrasting composition, andesitic lavas being accompanied by intermediate to acid pyroclastics (Hammerschmidt *et al.*, 1992). Rhyolitic ignimbrites did not occur, contrasting strongly with the present day situation. Volcanic activity had ceased by the onset of the Incaic phase (Hammerschmidt *et al.*, 1992) and it has been suggested that the small volumes of dacitic magma which generated the deposits consituted the terminal phase in this episode of magmatism (Clark, 1993).

The Incaic phase (39-38 Ma; Reutter *et al.*, 1996) was a period of deformation coinciding with an increase in convergence rates and markedly oblique subduction under northern Chile (Clark, 1993). Much of the deformation in the Incaic phase was translated into dextral movements on the large scale, vertical, strike-slip fault systems which parallel the orogen (Reutter *et al*, 1991). Although most of the deposits are located close to one of these systems (Quebrada Blanca is located a few hundred metres to the east of the West Fissure system), the precise role that these faults play in the location of the porphyry copper deposits is not clear (Clark, 1993).

1.3 *Modus operandi*

In order to integrate the evolution of the magmatic and hydrothermal systems it is necessary to first understand how the elements within each system are related to each other; some of the variation observed within each system may reflect the operation of processes internal to that system.

For example, a single batch of MVP, released from a magma and migrating through the overlying material, will evolve in response to changing conditions of pressure and temperature and through reaction and exchange of components with the wall rocks and/or

other fluids. Vein assemblages record the passage of the MVP and reflect its composition. As a result, variation in vein assemblages may be produced by compositional evolution of a single batch of fluid as well as by distinct batches of fluid with differing initial compositions.

Consequently it has been necessary to catalogue all of the types of vein, breccia and intrusive lithology present, and then to determine to which intrusive phase, and, if need be, to which episode of exsolution/fracturing each type of vein relates. Although observations of the spatial and temporal relationships between veins, breccias and intrusive lithologies made in the field provided much of the requisite information, a number of analytical techniques have been used to further refine the interpretation, particularly of processes acting within one of the systems. These have included fluid inclusion microthermometry, geochemistry of the stable isotopes of sulphur, hydrogen and oxygen, and the chemical analysis of whole–rock and mineral separates.

1.4 About the layout of this thesis

Chapters 2 and 3 present data that have been collected as part of this research, with Chapter 2 containing data pertaining to the lithologies that comprise the magmatic system and Chapter 3 detailing data relating to the hydrothermal system. Chapter 4 compares these data with those documented for other deposits in order to assess how representative of porphyry copper deposits Quebrada Blanca is considered to be, and concludes with a summary of the characteristics common to this type of deposit. In Chapters 5 and 6, an interpretation of the data given in Chapters 2 and 3 is presented.

Chapter 7 combines the interpretation given in Chapters 5 and 6 with previously published experimental and theoretical treatments and presents a model for the development of hypogene mineralisation which accounts for the observations of the magmatic-hydrothermal system at Quebrada Blanca and, by reference to the summary concluding Chapter 4, the characteristics of this type of deposit in general. Some applications and implications of this model are then addressed in Chapter 8. Chapter 9 summarises the conclusions of this research.

THE MAGMATIC SYSTEM AT QUEBRADA BLANCA

2

This chapter presents data which relate to the magmatic system associated with the porphyry-copper deposit of Quebrada Blanca. These data include descriptions of the petrography, spatial distribution and cross-cutting relationships of the intrusive lithologies comprising the system, their whole-rock geochemistry and, for certain lithologies, the geochemistry and isotopic characteristics of some of the minerals they contain. Samples exhibiting evidence of supergene alteration were excluded from this study.

2.1 Lithologies in the field area

2.1.1 Monzogranite

The deposit of Quebrada Blanca is located entirely within a stock of monzogranite-granodiorite with a surficial exposure of approximately 2 by 6 km (Fig. 2.1). Alteration has affected all of the stock. Samples on the margin of the deposit are propylitically altered. They are medium-coarse grained and have an equigranular texture. Subhedral to euhedral plagioclase and K-feldspar make up 70-80% of the rock, usually in a ratio of ~3:2. Subhedral quartz is a late crystallising phase. Ferromagnesian minerals represent less than 5% of the rock and have been altered to chlorite. Below the enrichment blanket (Fig. 2.2), the monzogranite is medium grained with a seriate to porphyritic texture. Plagioclase appears to have been the main phenocrystic phase prior to alteration.

2.1.2 Andesite

Distribution and appearance

This lithology only rarely outcrops at surface within the mine area (Fig. 2.1), and was only present at the level of the exploration tunnel in a few exposures. Small dykes of andesite, typically 0.5-2m wide are, however, commonly seen in the deeper drill holes centred in the southwestern area of the monzogranite (Fig. 2.2). In hand specimen the rock is charcoal grey and forms dykes with black margins (Fig. 2.3). These selvedges sometimes form dykelets branching from the larger dykes. Plagioclase is the only phenocryst phase and the groundmass appears aphanitic.

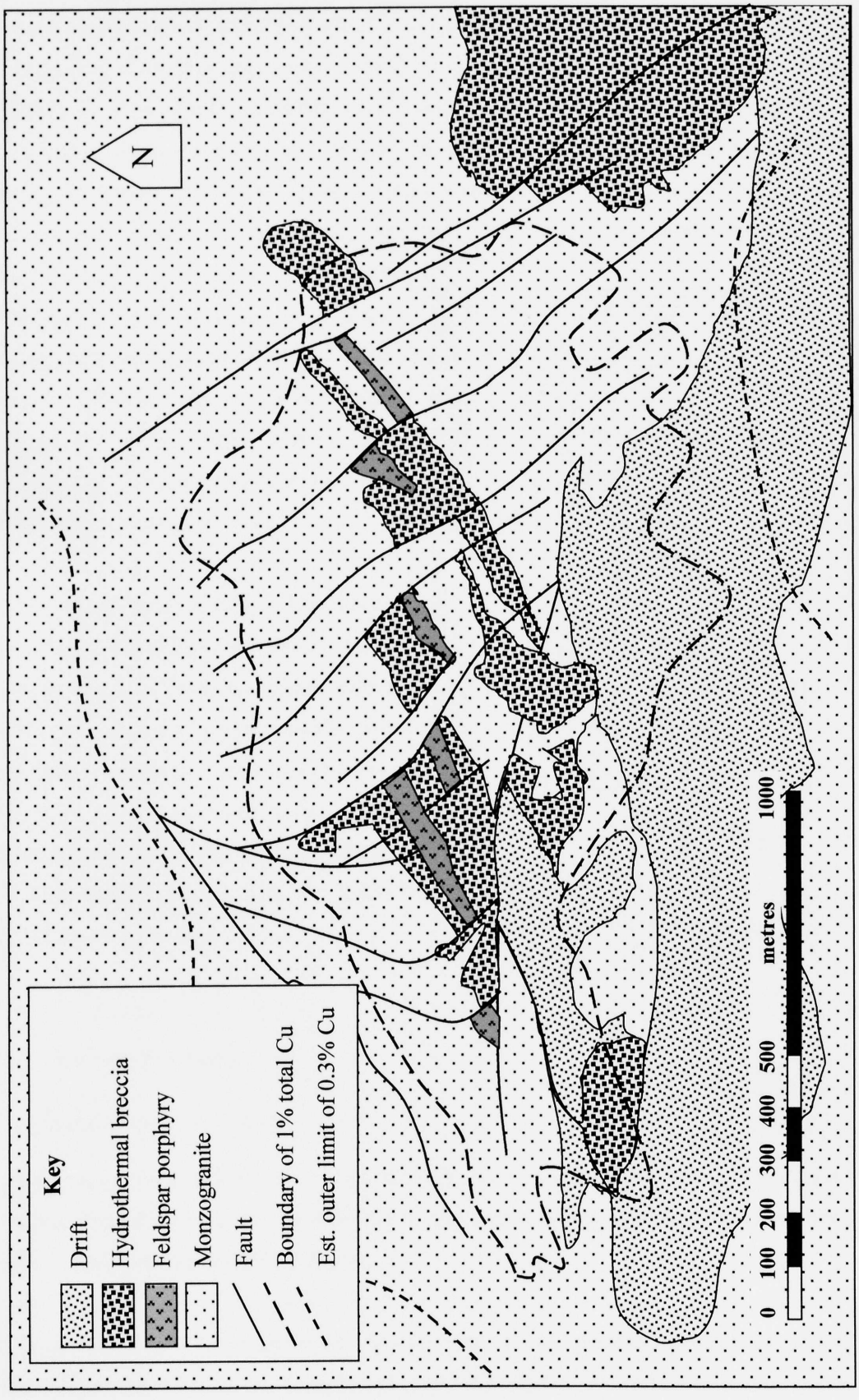


FIG. 2.1. Simplified map of the geology of Quebrada Blanca.

Contacts and cross-cutting relationships

In the monzogranite, clasts of andesite may be seen at the edges of dykes, cemented by felsic material (Fig. 2.4). This felsic material is enriched in feldspar and quartz and also, but more variably, in chalcopyrite, magnetite and copper oxides. It is similar to the reaction rims surrounding some enclaves, and grades into granodiorite with a slightly accentuated porphyritic texture before the texture becomes more typical. Backveining of andesite dykes by the monzogranite is commonly observed (Fig. 2.5), and phenocrysts from the monzogranite may indent or become entrained in the selvedges (Fig. 2.3). Baking of the monzogranite, in which the texture becomes finer and more equigranular and mafic phases are depleted, is occasionally observed in association with andesite dykes.

Well defined cross-cutting relationships with other lithologies are rarely seen. Kinking of the dykes around clasts within the breccia bodies suggests that the two may be broadly contemporaneous, supported by the observation that some dykes clearly cut the bodies while others are brecciated. Contacts with the aplite are diffuse to flame-like.

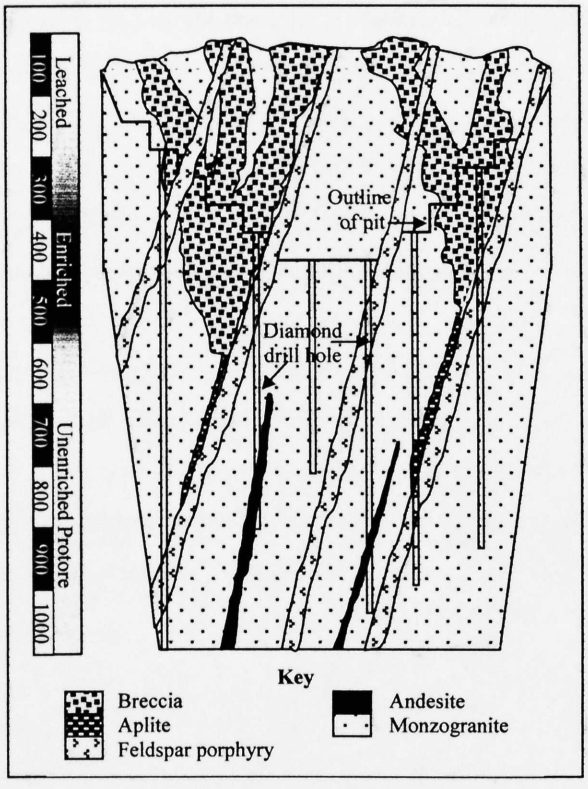


FIG. 2.2 Schematic section through and below the deposit of Quebrada Blanca.

2.1.3 Feldspar Porphyry

Distribution and appearance

This lithology forms dykes with widths of 1-10m with a northeasterly strike. They appear to be concentrated in the south-western end of the monzogranite stock and coincide with the highest grades of mineralisation (Fig. 2.1).

In hand specimen the majority of samples are rich in phenocrysts and have a grey, microcrystalline groundmass. Some samples are so crystal-rich that the porphyritic texture is lost, while others have a low phenocryst to groundmass ratio. Variations in phyricity are

sometimes seen across dykes; on the margins, fine-to-medium grained, matrix-rich zones with few mafic phenocrysts contain drifts of phenocrysts, while in the centre, fine-grained, acicular biotite is present. In the less phyric portions, quartz phenocrysts are all but absent and disseminated pyrite is much more abundant than chalcopyrite.

Contacts and cross-cutting relationships

The nature of the contacts between the monzogranite and the feldspar porphyry varies; some are masked by short zones of brecciation while others are diffuse. In a number of samples, the monzogranite appears to be finely brecciated into the feldspar porphyry. Contact zones with this character grade into homogeneous feldspar porphyry over a few centimetres, though the porphyry in these zones commonly lacks quartz phenocrysts and magnetite is partially replaced by hematite.

Contacts with the aplite tend to be gradational, though the porphyry is sometimes seen as clasts (small and rounded) in the latter lithology and vice-versa. There appears to be a strong spatial relationship between the feldspar porphyry and the andesite and they commonly occur as adjacent clasts or enclaves within the monzogranite. A conclusive cross-cutting relationship between the andesite and the feldspar porphyry has not been observed.

2.1.4 Aplite

Distribution and appearance

This lithology forms dykes and acts as the matrix to the igneous breccia. Where seen as dykes, it is spatially associated with dykes of andesite or feldspar porphyry, and probably has a similar areal extent to these two lithologies, i.e. focused in the southwestern end of the monzogranite (Fig. 2.1). Dykes do not occur at the surface. In hand specimen, they are a dark charcoal grey. Clots of mafic phases are abundant. Laths of plagioclase feldspar, sometimes exhibiting a weak foliation, are locally present and may be xenocrystic. The selvedges seen on the andesite dykes are not present and there may be some coarsening at the contacts.

In the igneous breccia, the aplitic material encloses equant, subangular clasts of monzogranite typically >10cm in diameter displaying either sericitic alteration or moderate K-feldspar enrichment. Quartz-rich veins within these clasts are commonly plastically deformed and many clasts bear vein fragments. The igneous breccia is generally clast

supported. Short (<10cm vertical extent) zones of breccia with a matrix consisting of quartz + magnetite + coarse biotite ± pyrite/chalcopyrite interfinger with the igneous breccia. They are not seen independently of the igneous breccia and appear to be only locally developed.

Contacts and cross-cutting relationships

Contacts with the monzogranite are often convolute and the aplite may form tongues lacking a well-defined orientation. It is also seen spalling into the monzogranite, producing rounded enclaves with intricate margins (Fig. 2.6). This style of interaction is consistent within specific intervals of the monzogranite (perhaps 30-40m sections). Contacts with the feldspar porphyry may be gradational and/or diffuse, though clasts of feldspar porphyry have been observed within the aplite. Both the monzogranite and the feldspar porphyry are seen enriched in potassium-bearing phases where they are in contact with the aplite. In the monzogranite this takes the form of an increase in modal K-feldspar (sometimes to the extent of K-feldspar flooding) and an increase in biotite as stringers.

2.2 Petrography

2.2.1 Technique

Samples were subjected to a microscopic examination using transmitted and reflected light.

2.2.2 Fresh samples

Andesite

Some variation in phyricity is apparent in the andesite when viewed in thin section. In the less phyric samples, small plagioclase laths are found in a groundmass rich in biotite and feldspar. Small clasts of the selvedge material, composed of biotite with accessory opaque phases, may be enclosed in this groundmass. In the more phyric samples, fine-grained, euhedral laths of oligoclase are seen to form an almost interlocking network enclosing interstitial quartz (Fig. 2.7). A few show signs of growth zoning, and typically have altered cores and fresh rims. Primary mafic phases have been pseudomorphed by secondary biotite, which is abundant throughout the groundmass, though some corroded laths of primary biotite remain. Quartz constitutes about 5% of the rock volumetrically. Acicular apatite, showing extreme elongation, is a ubiquitous accessory (Fig. 2.8).

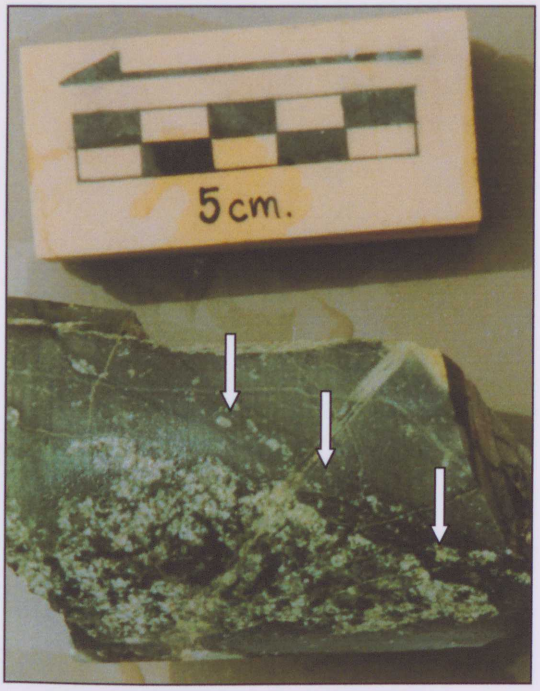


FIG. 2.3 Entrainment of plagioclase crystals (arrowed) from the monzogranite in the selvedge of an andesite dyke. Note the darker colour of the selvedge compared with that of the dyke.

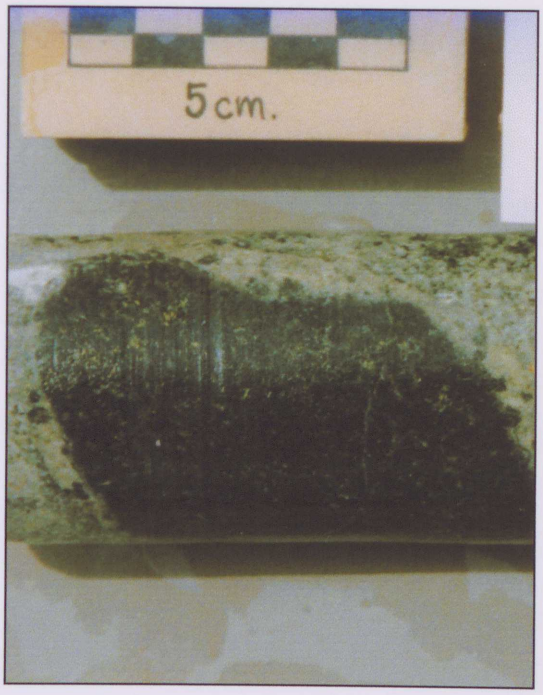


FIG. 2.4 Andesitic enclave in the monzogranite. Note the small rounded enclaves at the contact between the two lithologies.



FIG. 2.5 Backveining of an andesite dyke by the monzogranite. The sinuous contacts of the "vein" suggest that both lithologies were partially molten at the time of interaction.



FIG. 2.6 Contact between monzogranite and a tongue of aplite. The aplite is seen to spall into the monzogranite, forming small enclaves similar to those seen surrounding enclaves of the andesite.

Regardless of the phyricity, samples of this lithology do exhibit some common characteristics. Magnetite is a significant constituent and is variably altered to hematite. Chalcopyrite is also common, and is often intergrown with either magnetite or pyrite. Bornite may be associated with chalcopyrite, but rarely.

Feldspar Porphyry

The majority of the samples of the feldspar porphyry are strongly porphyritic with phenocryst to groundmass ratios of ~1:1. Plagioclase feldspar constitutes 85% of the phenocryst assemblage and is described in more detail below (section 2.5.2). Other phenocrystic phases include biotite, oxyhornblende and quartz, but their occurrence is irregular at thin section scale. Biotite phenocrysts are present as euhedral to subhedral laths of varying size but rarely constitute more than 4% of the phenocrystic phases present. Oxyhornblende is present in similar amounts. Crystals of this phase have a hexagonal section and a strong orange-brown colouration which masks the birefringence. They commonly bear exsolution seams of pyrite and ilmenite, both parallel to and cross-cutting the cleavage (Fig. 2.9). Quartz occurs as hexagonal bipyramidal phenocrysts which in most specimens exhibit some degree of resorption and embayment (Fig. 2.10). The phenocrysts vary in diameter from 2-10mm and may account for as much as 8% of the phenocryst volume in some samples while being all but absent in others. They may contain inclusions of plagioclase, groundmass and magnetite in addition to fluid inclusions, and often have halos of finer grained groundmass enriched in quartz (Fig. 2.10).

Aggregates of secondary biotite completely replace a phenocrystic phase which, judging from the shape of the pseudomorphs (euhedral laths and rhombs) was probably an amphibole (Fig. 2.11). This phase may originally have represented as much as 5% of the phenocryst assemblage. Magnetite phenocrysts are subhedral to euhedral and broadly isodiammetric. They are commonly replaced by hematite and some may contain blebs of chalcopyrite. Magnetite was probably the only opaque phase present as phenocrysts and is sometimes enclosed in plagioclase. Coarse, euhedral sphene exhibiting the characteristic arrowhead habit is present as an accessory phase, though is always replaced by a mixture of magnetite and ilmenite (Fig. 2.12). The groundmass is typically microcrystalline and is composed of plagioclase laths showing a single growth zone mixed with intergrown quartz, biotite and K-feldspar. On average, quartz and feldspar are present in equal amounts within the groundmass, but the proportions do vary between 2:1 and 1:2. Oxyhornblende is not present.

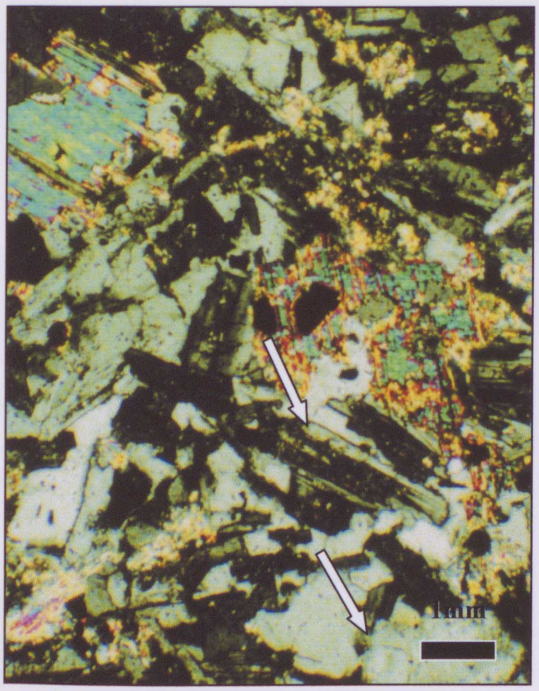


FIG. 2.7 Photomicrograph (XPL) of intergrown plagioclase and quartz in the andesite. Note also the flaky biotite phenocrysts (top left).

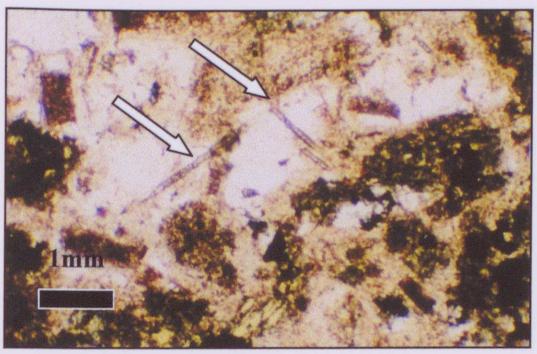


FIG. 2.8 Photomicrograph (PPL) of acicular apatite (arrowed) in the andesite.

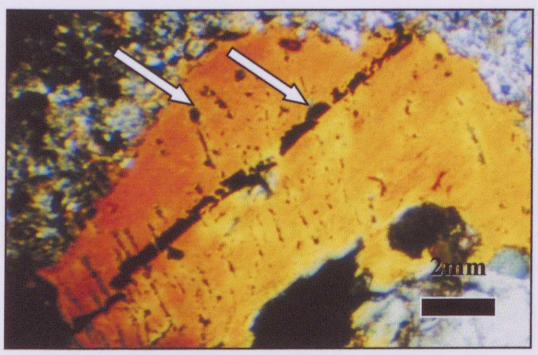


FIG. 2.9 Photomicrograph (XPL) of part of a large crystal of oxyhornblende in the feldspar porphyry. Exsolved opaques (arrowed) are ilmenite and magnetite.

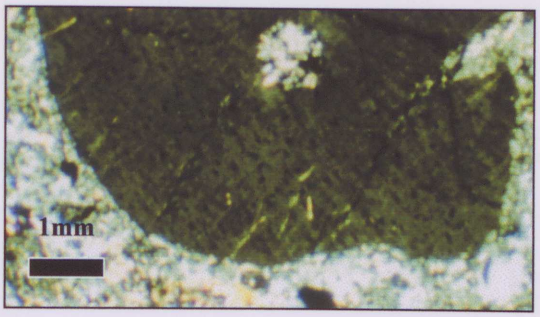


FIG. 2.10A Photomicrograph (XPL) of resorbed quartz phenocryst with a large inclusion of groundmass (centre, top) in the feldspar porphyry.

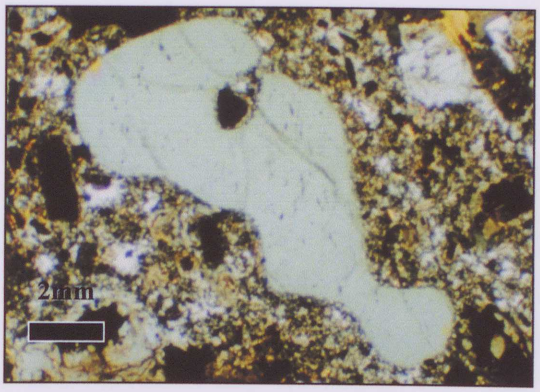


FIG. 2.10B Photomicrograph (XPL) of resorbed quartz phenocryst in the feldspar porphyry. Note remnant hexagonal morphology and liquid-like form.

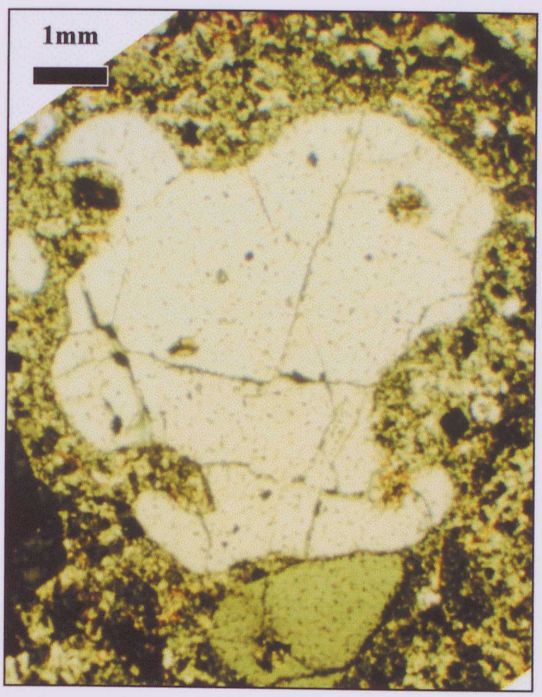


FIG. 2.10C Photomicrograph (XPL) of resorbed quartz phenocryst in the feldspar porphyry. Note the silica-rich halo (particularly evident in the embayments).

Aplite

In the aplite dykes, quartz and plagioclase form an aplitic matrix enclosing plagioclase phenocrysts. These are commonly observed to be glomerophyric and, where fresh, show multiple twinning. Biotite is often acicular and tends to aggregate in clots within the matrix. It rarely constitutes more than 10% of the rock. Hematite is commonly seen to replace magnetite, euhedral cubes of which are abundant in the groundmass. Apatite and zircon are common accessory phases.

2.2.3 Samples exhibiting evidence of hypogene alteration

Monzogranite

All samples of the monzogranite from below the enrichment blanket are potassically altered and display enrichment in perthitic K-feldspar and fine-grained secondary biotite, either as replacements of plagioclase and mafic phases, respectively, or as seams of interstitial material (Fig. 2.13). Plagioclase exhibits varying degrees of alteration. In some samples, alteration is restricted to crystal margins while in others the crystals are completely replaced and the original crystal outlines lost. Enrichment in biotite also shows varying degrees of intensity. Replacement of primary mafic phases represents the minimum degree of enrichment. More enriched samples have interstitial clots or seams of secondary biotite, which may enclose grains of zircon. Biotite enrichment is noticeably more pronounced in the intervals within which clasts of aplite are present. In some samples quartz forms medium grained, subhedral phenocrysts or is interstitial, but more typically it forms clusters of fine, rounded grains showing unit extinction separated by septa of perthite (Fig. 2.14).

Ilmenite is accompanied either by magnetite with minor chalcopyrite or by chalcopyrite and pyrite. Both assemblages are seen associated with secondary biotite as well as interstitially with quartz. The magnetite-chalcopyrite assemblage occurs at greater depths than the chalcopyrite-pyrite assemblage.

In the most porphyritic samples, mafic phases pseudomorphed by secondary biotite and laths of plagioclase are held in a groundmass composed of quartz and K-feldspar. Small enclaves of monzogranite in which plagioclase exhibits more intense potassic alteration than the phenocrysts in the groundmass may be present. The quartz in these enclaves is unusually euhedral, displaying a hexagonal section.

Andesite

It is rare to find fresh samples of this lithology. Most exhibit quite intense potassic alteration in which the plagioclase is replaced by perthitic K-feldspar and the lithology is enriched in biotite.

Feldspar Porphyry

In the feldspar porphyry, two styles of alteration are observed. In some samples, plagioclase is replaced by sericite and magnetite is partially replaced by pyrite. In thicker dykes and in those which outcrop at higher levels within the deposit sericitisation may be so intense that the competence of the rock is destroyed and the lithology becomes friable.

In other samples, plagioclase is replaced by pink K-feldspar. This style of alteration is rare and may be restricted to groundmass-rich samples of the feldspar porphyry (phenocryst:groundmass ~1:2), though sinuous veins and stringers of K-feldspar are commonly seen cutting samples of the feldspar porphyry which are otherwise fresh. The groundmass of the groundmass-rich samples is fine grained and does not have the quenched appearance of the samples in which phenocrysts and groundmass are present in approximately equal proportions. Groundmass-rich samples are unusually rich in magnetite and chalcopyrite, and quartz and oxyhornblende phenocrysts are absent. In one such sample, igneous biotite was observed to be replaced by secondary biotite.

Aplite

This lithology often exhibits extreme potassic alteration. Plagioclase is completely replaced by perthitic K-feldspar and the texture is lost as the feldspar phenocrysts lose their subhedral outlines.

2.3 Whole-rock geochemistry

2.3.1 Technique

Whole-rock geochemistry was determined for the purpose of petrogenetic modelling. Some of the whole-rock geochemical analyses were performed at Imperial College; some were carried out commercially by COMINCO. For those samples analysed at Imperial College,

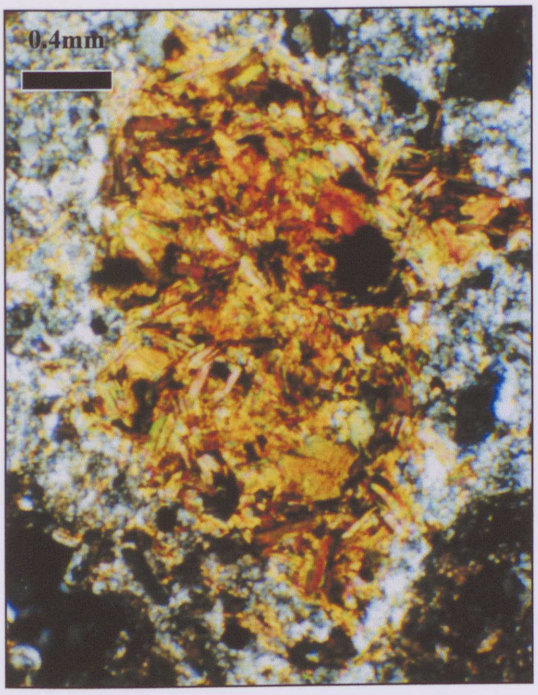


FIG. 2.11 Photomicrograph (XPL) of biotite pseudomorphing a mafic phenocryst in the feldspar porphyry.

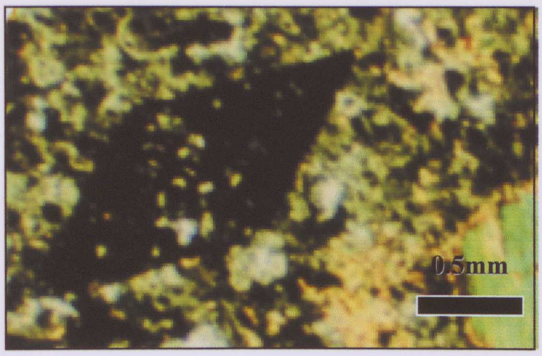


FIG. 2.12 Photomicrograph (XPL) of sphene showing it characteristic arrow-head habit pseudomorphed by magnetite/ilmenite.

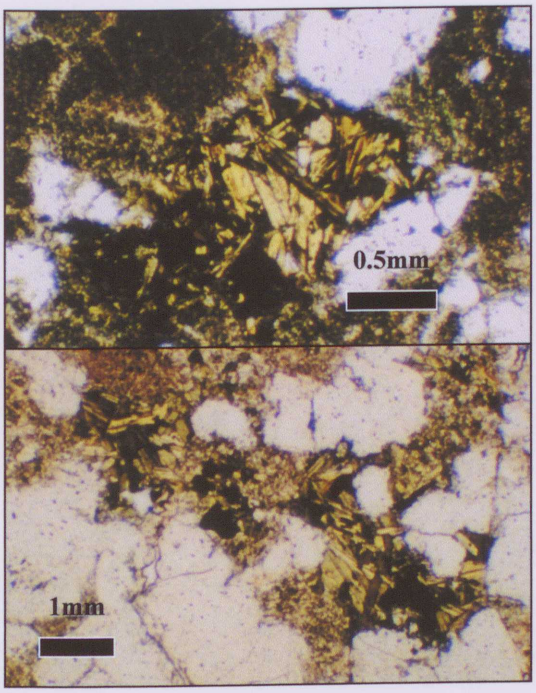


FIG. 2.13 Photomicrograph (PPL) of biotite (A, above) pseudomorphing a mafic phenocryst in the monzogranite. (B, below) Ocurring interstitially with opaques in the monzogranite.

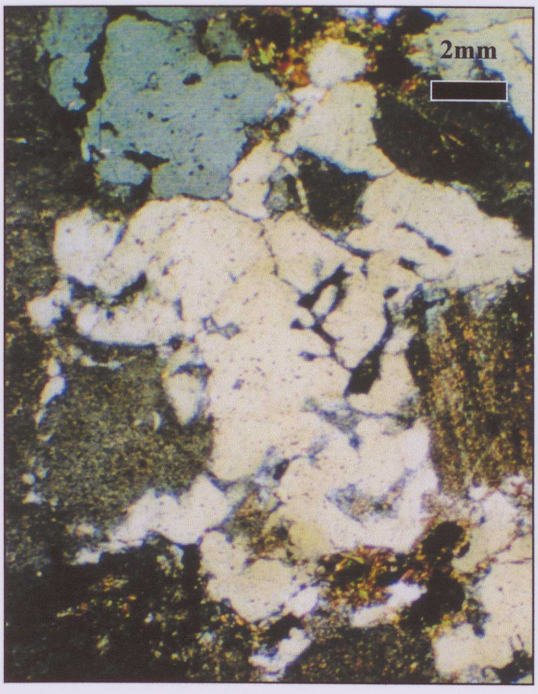


FIG. 2.14 Photomicrograph (XPL) of quartz in the monzogranite. Patches of quartz exhibit unit extinction but are separated by septa of perthitic K-feldspar, forming a crude graphic texture.

ten major and fourteen trace elements were determined by inductively-coupled plasma-atomic emission spectrometry (ICP-AES) of solutions created by the acid dissolution of powdered material that had been fused with a lithium borate flux. A detailed method is given in Appendix A.1. All results, whether collected at Imperial College or determined commercially, are to be found in Appendix A.2. Analytical precision for each element for both laboratories is calculated in Appendix A.1., using data obtained from repeat analyses carried out at those laboratories. Detection limits are calculated for elements determined at Imperial College using data from the analysis of blank samples.

2.3.2 Data

Monzogranite

Samples of monzogranite either contain magnetite and sulphides or only sulphides; neither are considered to be fresh. Average compositions for the two groups are given in Table 2.1. Although the absolute amounts of the elements vary slightly between the groups, the majority of the elemental ratios remain the same. Important exceptions are the ratios of calcium to sodium and calcium to potassium, which are both substantially lower in the samples containing only sulphides. A plot of K_2O vs. Na_2O suggests there may be two trends; one in which sodium varies at constant potassium content and one in which the two are inversely related (Fig. 2.15).

TABLE 2.1 Averaged compositions of the sulphides-only and magnetite-bearing groups of the monzogranite.

	Sulphides only	Magnetite bearing
SiO_2	69.84	68.08
Al_2O_3	14.38	15.24
FeO	2.96	4.34
MgO	1.12	1.60
CaO	0.40	0.68
Na_2O	4.11	4.02
K_2O	4.19	3.60
P_2O_5	0.10	0.13
TiO_2	0.46	0.59
MnO	0.02	0.03
LOI	1.32	1.53
Total	98.90	99.84
Ba	693	598
Sr	129	139
Cr	122	102
Cu	2195	1635
Ni	24	22
Zn	91	209
Zr	226	227
Mo	36	39
Mg/Mg+Fe	28	27
Na/Na+K	50	53
Ca/Ca+K	9	16
Ca/Ca+Na	9	14

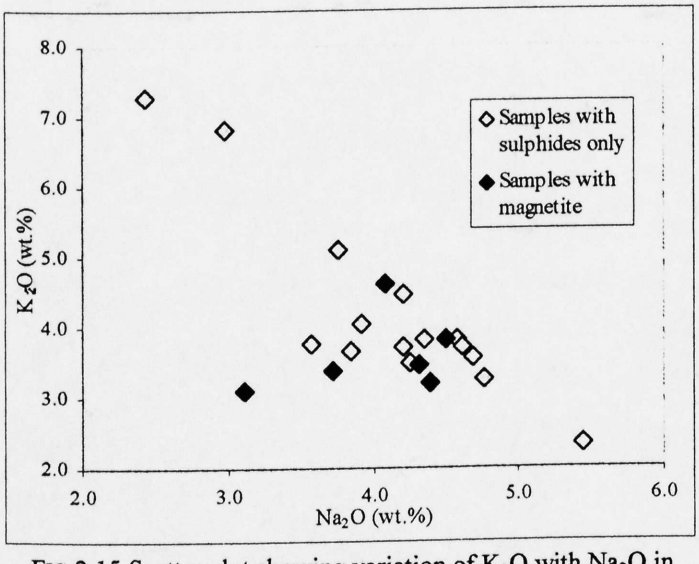


FIG.2.15 Scatter plot showing variation of K_2O with Na_2O in samples of the monzogranite.

Andesite

Of the samples of andesite sectioned, only five were considered fresh enough for their whole-rock compositions to be determined. Of these, two are distinct due to their high ratios of calcium to potassium, and their higher silica contents. Two samples of dyke selvedge were also analysed. One sample has notably higher contents of the transition metals and a higher ratio of magnesium to iron than the other, but otherwise the compositions of the two are comparable. Relative to the end-member composition of the andesite, the selvedge material is very strongly enriched in iron, magnesium and potassium, and very strongly depleted in quartz, calcium, sodium and strontium. The averaged compositions of the two samples of andesite with high ratios of calcium to potassium and the composition of the selvedge material richer in transition metals appear to be end-members to a sequence in which the compositions of the remaining fresh samples are intermediates (Table 2.2).

TABLE 2.2 Compositional variation in the samples of andesite.

	A	Intermediates			B
SiO_2	57.13	54.81	48.34	47.48	42.22
Al_2O_3	17.04	18.3	17.94	18.86	17.33
FeO	8.04	7.73	11.64	10.37	14.43
MgO	3.35	5.66	8.12	7.88	12.12
CaO	3.24	0.79	0.70	0.68	0.07
Na_2O	2.97	3.44	2.66	3.06	0.30
K_2O	2.11	4.59	6.27	7.09	8.58
P_2O_5	0.24	0.14	0.17	0.15	0.04
TiO_2	0.66	0.97	1.16	1.33	1.02
MnO	0.07	0.05	0.1	0.09	0.12
LOI	4.46	2.89	2.5	1.98	2.38
Total	99.31	99.37	99.6	98.97	98.61
Ba	273	548	364	375	237
Sr	237	204	102	92	13
Cr	71	167	99	372	709
Cu	364	1117	1651	2973	2484
Ni	26	79	46	68	204
Zn	112	183	237	96	152
Zr	142	145	99	105	61

A=Andesite, B=Selvedge

Feldspar Porphyry

The composition of six fresh samples, two groundmass-rich samples and six samples exhibiting sericitic alteration was determined. Fresh samples of the feldspar porphyry have a very uniform composition. Iron shows the most variation but shows no consistent correlation with the other elements. Strontium shows a weak correlation with calcium (Fig. 2.16), while barium shows a weak correlation with potassium (Fig. 2.17). Sericitised samples can be distinguished from the fresh samples by their lower contents of calcium and strontium, and their strong enrichment in copper (Table 2.3). Groundmass-rich samples are enriched in magnesium, iron and copper, relative to the fresh samples, and depleted in calcium and strontium (Table 2.3).

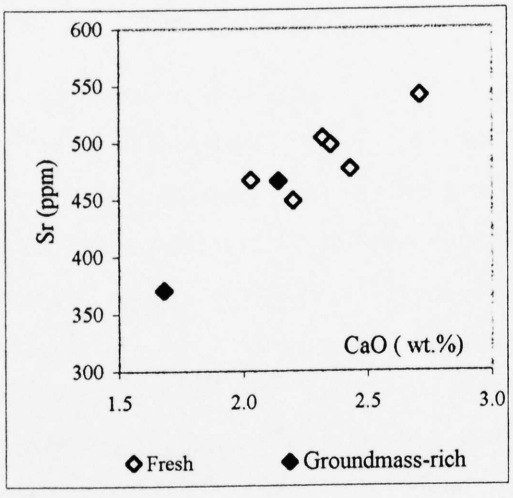


FIG. 2.16 Variation of Sr with CaO in whole rock samples of the feldspar porphyry.

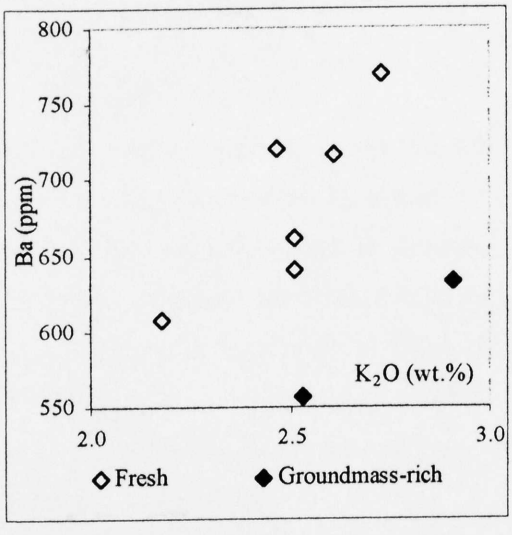


FIG. 2.17 Variation of Ba with K_2O in whole rock samples of the feldspar porphyry.

TABLE 2.3 Averaged compositions of the three groups of samples of the feldspar porphyry.

	Fresh	Early sericite	Phenocr't poor
SiO_2	66.39	67.15	65.19
Al_2O_3	16.67	16.46	16.76
FeO	3.69	3.26	4.57
MgO	1.30	1.17	1.57
CaO	2.34	1.31	1.91
Na_2O	4.28	3.81	4.45
K_2O	2.50	3.04	2.72
P_2O_5	0.19	0.16	0.19
TiO_2	0.44	0.38	0.47
MnO	0.03	0.02	0.04
LOI	1.65	1.91	1.89
Total	99.48	98.66	99.74
Ba	686	675	595
Sr	489	361	419
Cr	88	77	103
Cu	610	2160	1525
Ni	25	25	26
Zn	148	136	107
Zr	122	115	125
Mo	36	22	-

Aplite

The whole-rock compositions of three samples of aplite were determined. In comparison with the average composition of the magnetite-bearing samples of the monzogranite, the average composition of these three samples is depleted strongly in silica, and slightly in sodium and potassium, and is strongly enriched in iron, magnesium, titanium, calcium and phosphorous (Table 2.4). Barium and copper are somewhat depleted, while strontium and zinc are somewhat enriched.

TABLE 2.4 Averaged compositions of the aplite and magnetite-bearing samples of the monzogranite

	Aplite	Magnetite bearing
SiO_2	60.12	68.08
Al_2O_3	16.31	15.24
FeO	7.45	4.34
MgO	2.87	1.60
CaO	1.53	0.68
Na_2O	3.35	4.02
K_2O	3.22	3.60
P_2O_5	0.35	0.13
TiO_2	1.38	0.59
MnO	0.05	0.03
LOI	1.53	2.08
Total	99.84	98.70
Ba	359	598
Sr	173	139
Cr	93	102
Cu	1397	1635
Ni	29	22
Zn	258	209
Zr	203	227
Mo		39

2.4 Biotite geochemistry

2.4.1 Technique

The composition of primary biotite has been used to infer the activity of silica (Czamanske & Wones, 1973) and the relative oxidation state of melts (Ague & Brimhall, 1988; Scaillet *et al.*, 1995) while that of secondary biotite has been used to infer halogen fugacity in hydrothermal fluids (Munoz & Swenson, 1981) and as a geothermometer (Beane, 1974). Previous studies of secondary biotite in porphyry copper deposits are reviewed in section 4.1.1.

Primary biotite may continue to undergo re-equilibration at subsolidus temperatures, but iron, magnesium, fluorine, chlorine and hydroxyl are thought to reliably preserve high temperature equilibrium relationships (Ague & Brimhall, 1988). Titanium may be susceptible to low temperature re-equilibration. The presence of chlorite in biotite may indicate the action of deuteric alteration, but biotite altered in this manner should have substantially lower $\delta^{18}O$ values than fresh biotite (Nabelek *et al.*, 1983). This approach was used to confirm that biotite phenocrysts within the porphyry have not undergone deuteric alteration. A number of studies have observed that chlorite replacing biotite preserves the original ratio of magnesium to iron, so it is unlikely that variations in this ratio can be attributed to chloritisation in any case (e.g. Reynolds & Beane, 1985).

Biotite is the only ferromagnesian mineral present in all the lithologies at Quebrada Blanca. Biotite geochemistry was studied with three objectives: (1) To assess whether there was

variation in the chemistry of secondary biotite in potassically altered rocks which could be correlated with host-rock petrography/bulk geochemistry and hence could give an insight into the process by which potassic alteration took place. (2) To assess the character of primary and secondary biotite in the andesite dykes and that within the selvedges found on these dykes so that the three types of biotite could be compared. (3) To assess whether there was variation in the chemistry of primary igneous biotite within the feldspar porphyry which could give an insight into the magmatic history of this lithology.

The major element composition of biotite was determined by electron probe microanalysis (EPMA). A minimum of two analyses were made for each grain and averaged values are used. Results are summarised in Appendix A.3 with the operating conditions for the probe. Use of EPMA to determine biotite composition prohibits the collection of data relating to the valency of iron or the coordination of aluminium, without which unique substitution models for biotite cannot be defined (Hewitt & Abrecht, 1986).

2.4.2 Data

Monzogranite

Biotite occurs in the monzogranite as fine laths. In some instances these are clustered in such a manner that they appear to be replacing a phenocrystic phase while in others they have an interstitial character (Fig. 2.13). Both types may occur in the same sample. Biotite within the magnetite and sulphide-bearing groups occupy opposite ends of a trend of MgO vs. $FeO_{(total)}$, with the biotite in magnetite-bearing samples being richer in iron (Fig. 2.18). A line of best fit for the magnetite-bearing samples has a slightly more negative slope than the line for the sulphide only samples (Fig. 2.18). A plot of MgO/(MgO+FeO) vs. K_2O suggests that biotite in samples with magnetite has lower potassium than sulphide-bearing samples, though the difference is not great (Fig. 2.19).

Taking both groups together, the MgO/(MgO+FeO) of biotite exhibits a weak positive correlation with SiO_2 (Fig. 2.20) and a more pronounced negative correlation with chlorine (Fig. 2.21). Biotite in the samples containing magnetite shows well defined compositional variation: MgO/(MgO+FeO) is negatively correlated with TiO_2 (Fig. 2.22); TiO_2 is positively correlated with iron (Fig. 2.23). Collectively, the samples containing only sulphides appear to show trends opposite to these, but individually most of the samples show similar trends.

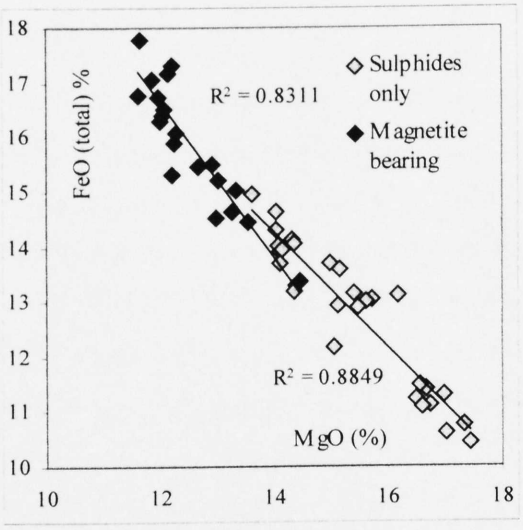


FIG. 2.18 Variation of MgO with $FeO_{(total)}$ in biotite from samples of the monzogranite.

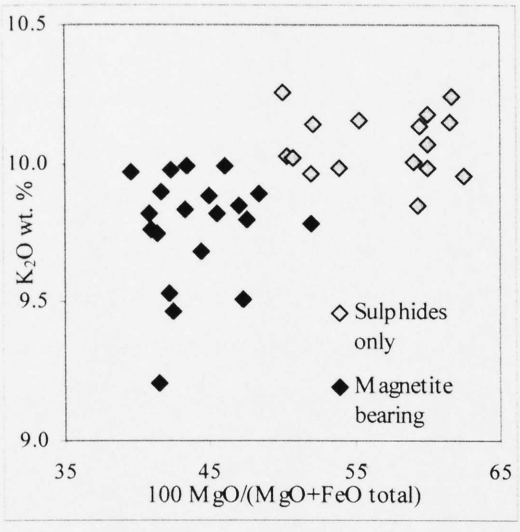


FIG. 2.19 Variation of K_2O with Mg# in biotite from samples of the monzogranite.

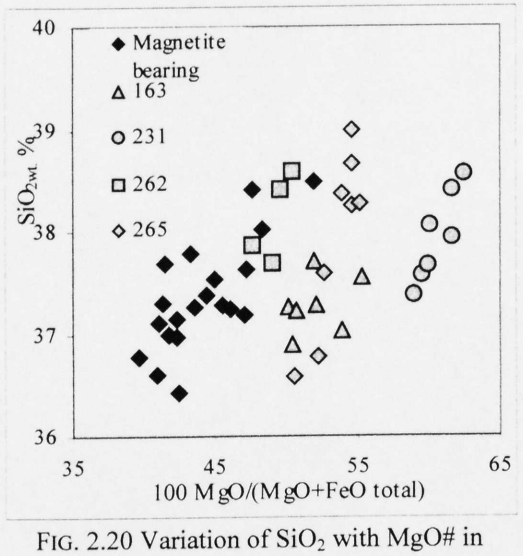


FIG. 2.20 Variation of SiO_2 with MgO# in biotite from samples of the monzogranite.

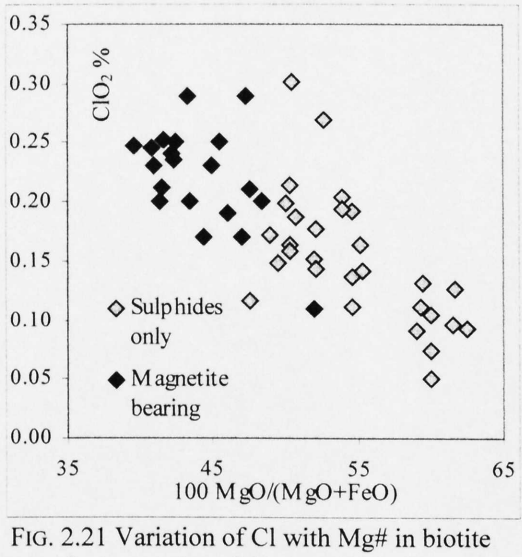


FIG. 2.21 Variation of Cl with Mg# in biotite from samples of the monzogranite.

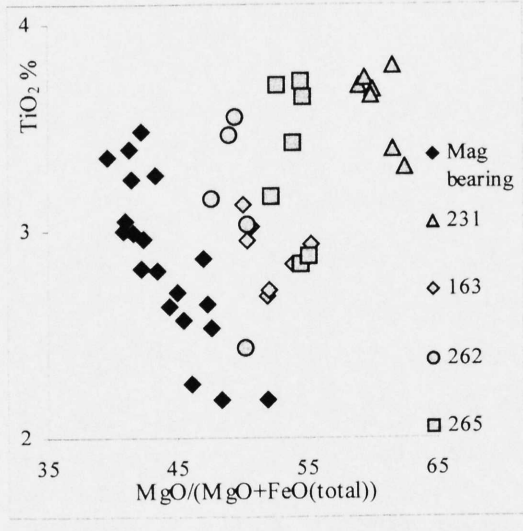


FIG. 2.22 Variation of TiO_2 with Mg# in biotite from samples of the monzogranite. Numbered samples are sulphide-only.

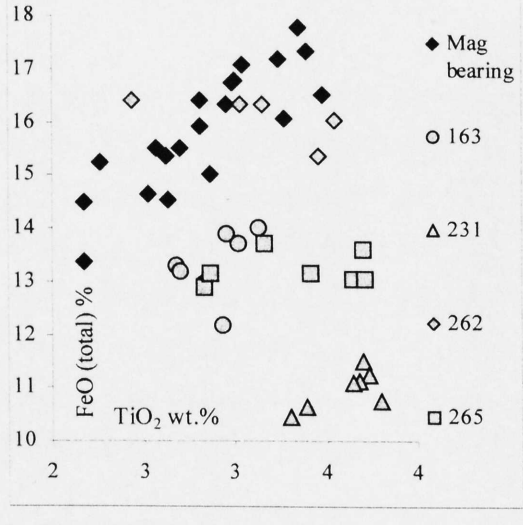


FIG. 2.23 Variation of $FeO_{(total)}$ with TiO_2 in biotite from samples of the monzogranite. Numbered samples are sulphide-only.

Andesite

Biotite compositions were only determined for the freshest sample of andesite and for four samples of the aphanitic selvedge material. In the andesite, biotite occurs as phenocrysts and as replacements after amphibole. Replacive biotite is iron-rich compared with phenocrystic biotite and on average has a higher titanium content (Figs. 2.24 & 2.25). Chlorite locally replaces phenocrystic biotite. Although hard to distinguish from secondary biotite optically, EPMA analyses of chlorite return low totals due to the high water content of this phase. Biotite in the selvedge material has a similar composition to the phenocrystic biotite within the andesite (Figs. 2.24 & 2.25).

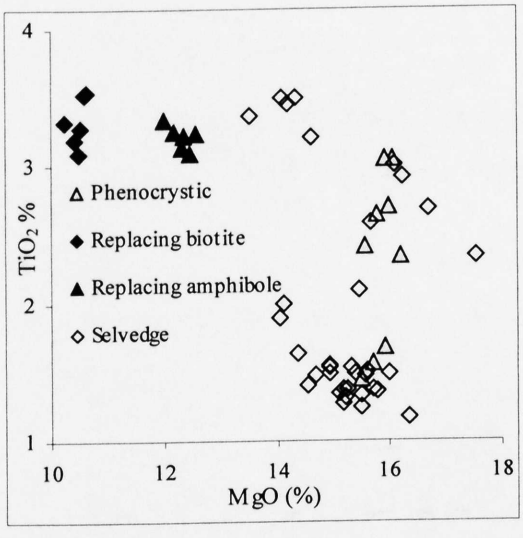


FIG. 2.24 Variation of TiO_2 with MgO in biotite from samples of the andesite.

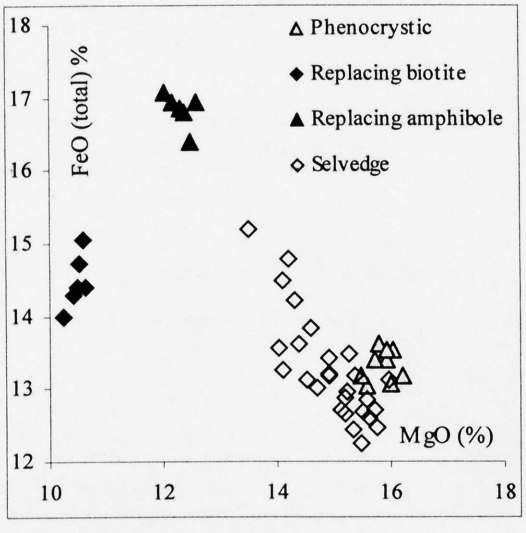


FIG. 2.25 Variation of FeO with MgO in biotite from samples of the andesite.

Feldspar Porphyry

Biotite occurs in two paragenetic stages within the feldspar porphyry; as phenocrysts and as replacements after amphibole. Neither type of biotite exhibits significant compositional variation. The MgO:(MgO+FeO) ratios of phenocrystic biotites appear to be normally distributed about a mode of 46, though there may be a slight negative skew (Fig. 2.26). These ratios exhibit a similar distribution in the replacive biotite (Fig. 2.26). The MgO/(MgO+FeO) ratios of phenocrystic biotite appear to vary independently of the other components, though there may be a weak correlation with SiO_2 (Fig. 2.27). Biotite within samples exhibiting early sericitisation is not compositionally distinct from that in fresh samples.

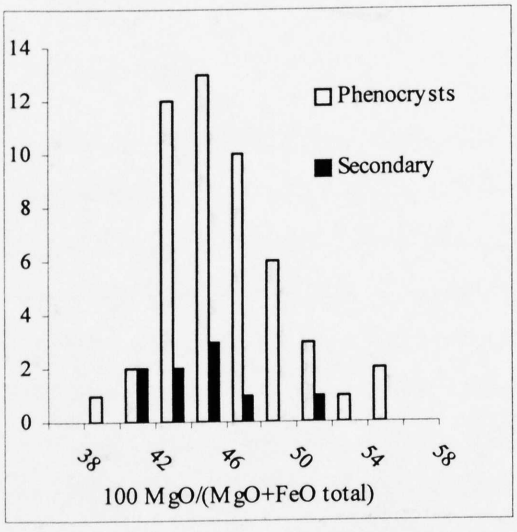


FIG. 2.26 Histogram of Mg# of biotite from the feldspar porphyry.

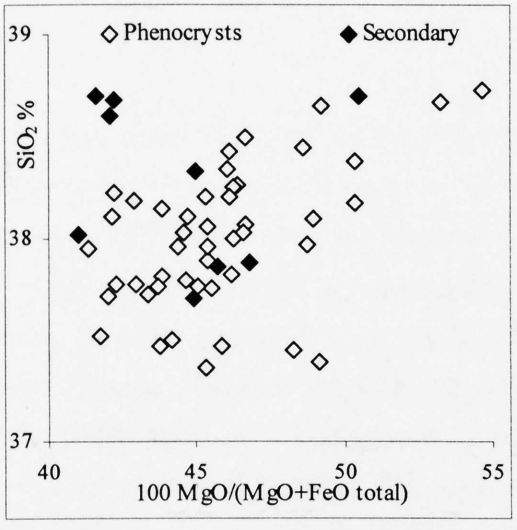


FIG. 2.27 Variation of SiO_2 with Mg# of biotite from the feldspar porphyry.

Aplite

The composition of biotite in one sample of aplite was determined. The composition of the biotite analysed overlaps with that of the biotite within the magnetite-bearing samples of the monzogranite.

2.5 Plagioclase zonation

2.5.1 Technique

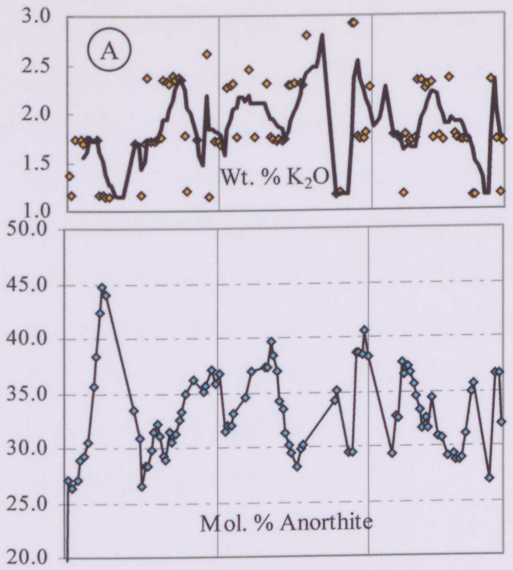
The stability and major element composition of plagioclase are dependent on the pressure, temperature and composition (P-T-X) of the melt from which it crystallises (Johannes, 1978; Tsuchiyama, 1985; Housh & Luhr, 1991). Changes in melt P-T-X will cause the composition of growing plagioclase to vary. Due to slow interdiffusion within feldspar crystals, episodes of growth are preserved as distinct zones, and the zonation displayed by a plagioclase phenocryst may record the chemical and physical evolution of the magma from which it grew (Anderson, 1984; Pearce *et al.*, 1987). In addition to the P-T-X properties of the surrounding melt, the composition of plagioclase is dependent upon kinetic factors such as rates of decompression (Nelson & Montana, 1992) and undercooling (Lofgren, 1980), and it is difficult to discriminate between different magmatic effects on the basis of binary compositional variations alone. Combination of major element abundances with data on the abundances of trace elements have been used to refine the discrimination (Blundy & Shimizu, 1991; Singer *et al.*, 1995).

During this study, EPMA transects across plagioclase phenocrysts from two samples of the feldspar porphyry were made, analysing for the major element composition of plagioclase (Si, Al, Na, Ca & K) and for strontium and iron, both of which may be present in plagioclase in minor to trace amounts (Singer *et al.*, 1995). Data are presented in Appendix A.4, together with the operating conditions for the probe. The feldspar porphyry was the only lithology to contain plagioclase considered fresh enough for application of this technique.

2.5.2 Zonation of plagioclase phenocrysts within the feldspar porphyry

Feldspar phenocrysts within the feldspar porphyry can be divided into two main groups: large (>2.5mm) and small (<2.0mm). Larger phenocrysts are commonly glomerophyric. They exhibit complex patterns of normal (decreasing anorthite) and reverse growth zoning, and sharp fluctuations in potassium content (Fig. 2.29). They have distinct rims and may have cores bounded by rounded surfaces which cross-cut compositional zonation. The composition of the plagioclase varies from An_{25} to An_{45}.

Small phenocrysts are euhedral and, like the larger phenocrysts, exhibit distinct cores and rims, the contrasting compositions of which allow the distinction of three subtypes (Blundy & Shimizu, 1991). The plateau subtype exhibits relatively little variation in anorthite content



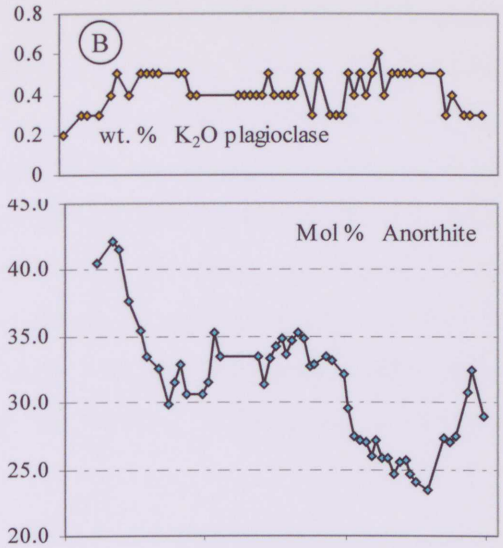
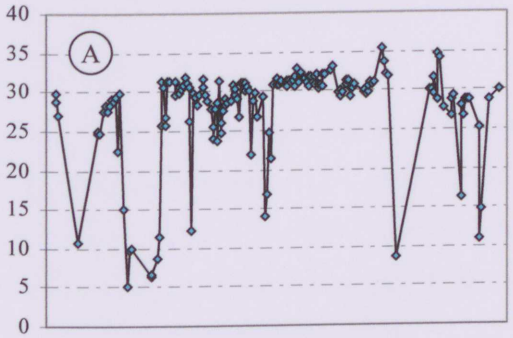
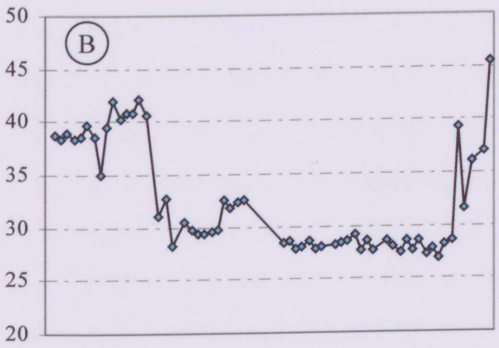


FIG. 2.29 (above) Variation in mol.% anorthite and wt.%K_2O along traverses across large feldspar phenocrysts from the feldspar porphyry (a) Sample 259.8, full width; K_2O trend is moving average (b) 259.9, half width.





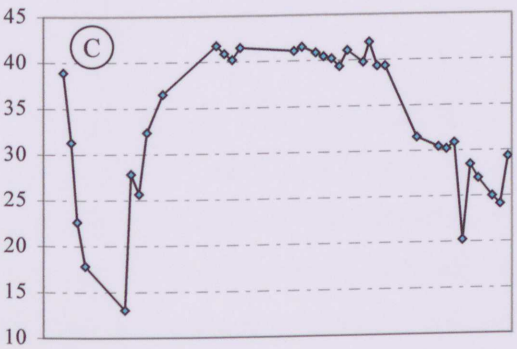


FIG. 2.30 (left) Variation in mol.% anorthite along traverses across small feldspar phenocrysts in the feldspar porphyry, all full widths. (a) Plateau subtype (b) Atoll subtype (c) Hiatal subtype.

FIG. 2.31 (Below) Photomicrograph of a small phenocryst in the feldspar porphyry exhibiting rounded surfaces (arrowed) interpreted to be the product of resorption.



between the core and the rim; both are typically An_{30} –An_{35} (Fig. 2.30a). The atoll subtype has a relatively anorthite-poor core and an anorthite-rich rim (Fig. 2.30b) while the hiatal subtype exhibits the opposite, having an anorthite-rich core and an anorthite-poor rim (Fig. 2.30c). Of the two examples of the atoll subtype analysed, one has a core of An_{25} and a rim of An_{30} while the other has a core of An_{30} and a rim of An_{40}. The single example of the hiatal subtype analysed has a core of An_{40} and a rim of An_{30}. The potassium contents of the phenocryst cores also appear to vary according to subtype; average K_2O contents are 0.38 %, 0.54 % and 0.22 % for the plateau, atoll and hiatal subtypes respectively. Cores in the plateau and atoll subtypes may be bounded by rounded surfaces which cross-cut compositional zonation (Fig. 2.31).

2.6 Hydrogen and oxygen isotope geochemistry

2.6.1 Technique

The D/H ratio of a magma may be approximated by the δD value of biotite with which it is in equilibrium (Nabelek *et al.*, 1983; Candela, 1994). During volatile exsolution, the D/H ratio of a magma is modified because deuterium is fractionated into water. As larger proportions of water are lost, the residual melt is characterised by more negative δD values (Taylor, 1988; Dobson *et al.*, 1989).

In this study, D/H values were measured on samples of two types: (1) Biotite, separated from samples of the feldspar porphyry, and powdered. The analysis requires ~40-50 mg of biotite, so it was not possible to measure the δD values of individual phenocrysts and each measurement represents an averaged value for a proportion of the phenocrysts within a given sample. Sampled phenocrysts vary in size though larger phenocrysts were easier to separate and probably make up the majority of each sample; (2) Powdered whole-rock material, representative of the andesite and the selvedges on the andesite dykes, which were too fine-grained to permit separation of individual phases for isotopic analysis. A listing of results is given in Appendix A.5.

A determination of $\delta^{18}O$ was made for a split of each of the samples analysed for δD, according to the method of Clayton and Mayeda (1963), following volatilisation of the sample by laser ablation. All data are quoted as parts per thousand (‰) deviation of the measured $^{18}O/^{16}O$ ratio relative to Vienna standard mean ocean water (VSMOW). A listing of results accompanies those for δD in Appendix A.5.

2.6.2 Data

Andesite

A sample of andesite (306) had a δD value of –79.0 ‰ and a $\delta^{18}O$ value of 6.6 ‰. A sample of the selvedge (292) had a δD value of –73.0 ‰ and a $\delta^{18}O$ value of 11.9 ‰.

Feldspar Porphyry

The δD and $\delta^{18}O$ values of biotite separates from seven samples of feldspar porphyry were determined (Table 2.5). Two samples from the same dyke differed in both $\delta^{18}O$ and δD values, by 0.7 ‰ and 6 ‰ respectively. These are not repeat analyses of the same separate. Fresh samples have similar $\delta^{18}O$ values, and δD values which range from –70 to –80 ‰. A sample representative of the groundmass-rich feldspar porphyry has a high δD of –55 ‰. Two samples exhibiting sericitic alteration have δD values of –65 and –71 ‰, and have higher $\delta^{18}O$ values than the fresh samples.

TABLE 2.5 $\delta^{18}O$ and δD values of biotite separates from samples of the feldspar porphyry

Sample	$\delta^{18}O$‰	δD ‰	Comment
211	5.2	-76	Fresh. Same dyke as 212
212	5.9	-70	Fresh. Same dyke as 211
239	5.9	-77	Fresh
259	5.8	-80	Fresh
267	6.1	-55	Groundmass-rich sample
177	7.0	-65	Sericitic alteration
296	7.3	-71	Sericitic alteration

2.7 Fluid inclusions

2.7.1 Technique

Fluid inclusions in two quartz phenocrysts from a sample of feldspar porphyry exhibiting early sericitisation were analysed by microthermometry. Details of this technique are described in section 3.4.1.

2.7.2 Fluid inclusions within quartz phenocrysts in the feldspar porphyry

Quartz phenocrysts contain inclusions which homogenise to liquid (type L), to vapour (type V) and to a critical condition (type C). A histogram of salinities suggests that type L inclusions fall into two groups, a lower salinity group with a mode between 16 and 20 wt % NaCl equiv. and a higher salinity group with a mode between 32 and 36 wt % NaCl equiv.

(Fig. 2.32). Type V inclusions have a mode between 8-12 wt % NaCl equiv. (Fig. 2.32), and there is overlap between the group of lower salinity type L inclusions and the type V inclusions in the range 12-20 wt % NaCl equiv. Type C inclusions appear to have a mode within this range (Fig. 2.32).

A plot of salinity vs. homogenisation temperature for all three types of inclusion shows considerable scatter (Fig. 2.33). However, the group of lower salinity type L inclusions have homogenisation temperatures which exhibit a similar range to the type V inclusions. The highest homogenisation temperatures are ~500°C. At this temperature, type L and type V inclusions with similar salinities are separated by type C inclusions with salinities intermediate between the two. The higher salinity group of type L inclusions have substantially lower homogenisation temperatures, in the range 325-375°C. Type C inclusions have homogenisation temperatures of ~500°C and salinity ~15 wt % NaCl equiv., and ~8.5 wt % NaCl equiv. and 450°C.

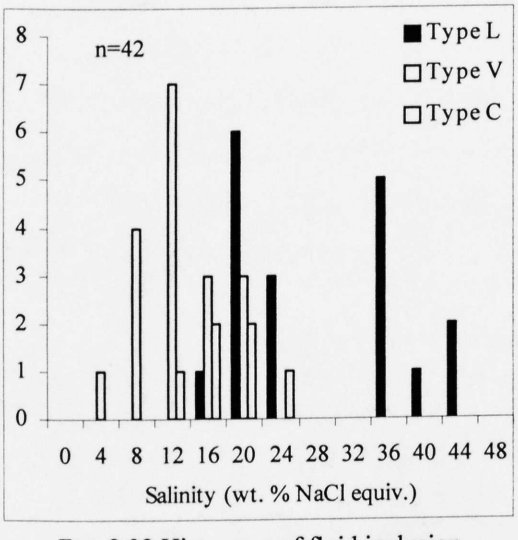


FIG. 2.32 Histogram of fluid inclusion salinities in quartz phenocrysts from the feldspar porphyry.

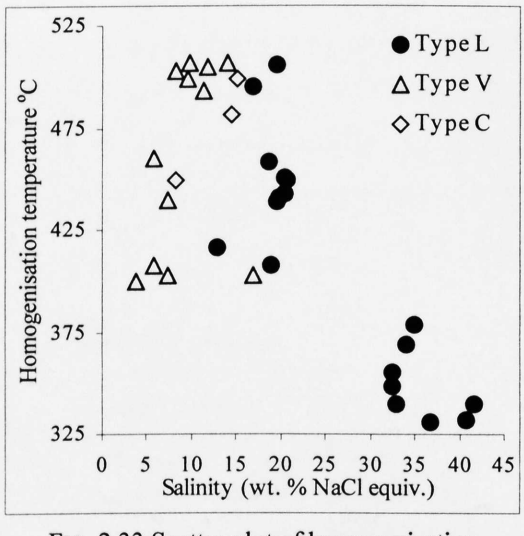


FIG. 2.33 Scatter plot of homogenisation temperature vs. salinity for fluid inclusions in quartz phenocrysts from the feldspar porphyry.

THE HYDROTHERMAL SYSTEM AT QUEBRADA BLANCA

3

At Quebrada Blanca, veins and breccias formed in response to the movement of hydrothermal fluids under brittle conditions of rock failure. This chapter presents data relating to these veins and breccias. Although volumetrically important, the breccias exhibit a strong overprint by supergene fluids which renders them of less use to this study than the veins, which are thought to record essentially single fluid events and can be constrained in time. Consequently, the data presented for the breccias is limited to their appearance in hand specimen and thin section and is given at the end of the chapter.

3.1 Vein classification

The morphology and mineralogy of the veins and the nature of the alteration associated with them as viewed in hand specimen enabled the distinction of six vein types. The criteria used for the identification of veins are described below and summarised in Table 3.1. Measurement of the length of individual veins was not possible because most of the observations were made on core.

TABLE 3.1. The vein paragenesis at Quebrada Blanca.

Stage	Type. Gangue/ore assemblage	Width (cm)	Alteration halo	Morphology
EARLY	1.Quartz + K-feldspar + Anhydrite ± Sulphides	0.3-5	± Potassic	Discontinuous – diffuse
	2. Quartz + Magnetite + K-feldspar ± Biotite ± Sulphides	0.2-0.8	± Sericitic	Sinuous with sharp boundaries
LATE	3. Quartz + K-feldspar ± Sulphides	0.5-1.0	± Potassic	Sinuous with sharp boundaries
	4. Quartz	0.5-1.0	± Potassic	Sinuous with diffuse boundaries
	5a. Quartz + Molybdenite	0.1-10	Halos absent or weakly sericitic	Sinuous with diffuse boundaries
	5b. As 5a but with cores of Pyrite + Quartz + Chalcedony	2.0-10.0	As 5a	Sinuous with diffuse boundaries
	6. Quartz + Chalcedony + Pyrite	0.6-10.0	Variable. Weak sericitic to strong phyllic	Sharp boundaries Sinuous or planar

Type 1. Veins of quartz, K-feldspar and anhydrite

These veins consist of translucent quartz grains and subhedral K-feldspar, which together comprise more than 90% of the vein volume. Chalcopyrite is present in slightly larger quantities than pyrite. Type 1 veins form branching networks which are difficult to distinguish from the host rock (Fig. 3.1), or discrete structures rich in quartz with cores of K-feldspar. The halos of type 1 veins are enriched in crystalline K-feldspar, biotite and anhydrite.

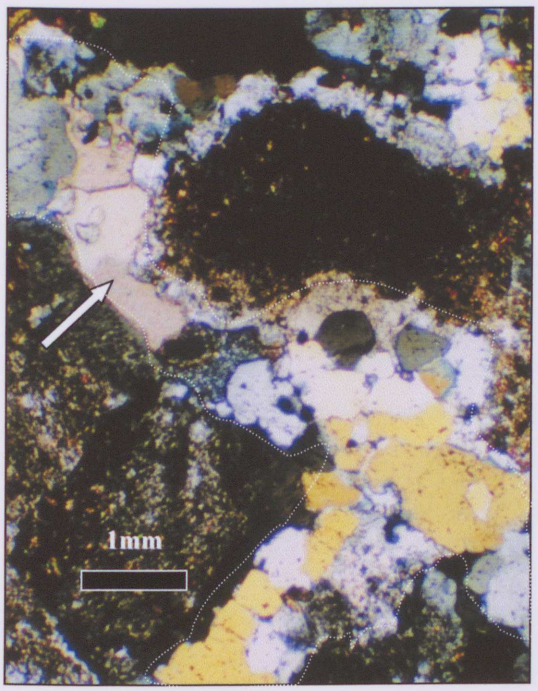


FIG. 3.1 Type 1 vein (outlined) in the monzogranite. Anhydrite arrowed.

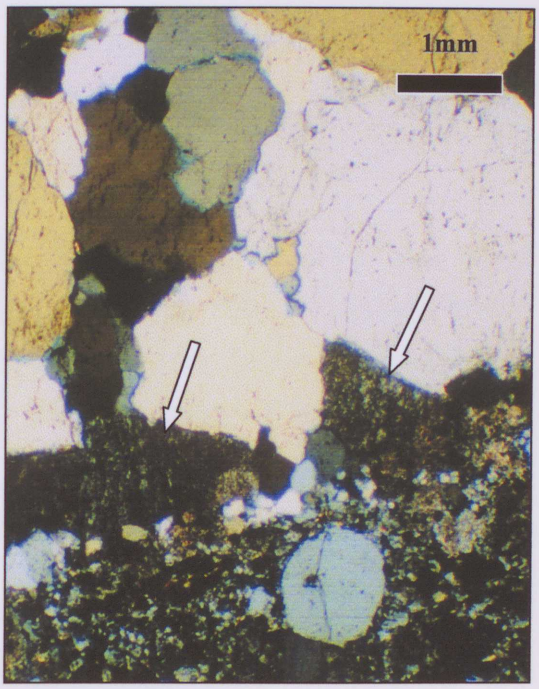


FIG. 3.2 Type 3 vein in the feldspar porphyry. Marginal K-feldspar arrowed.

Type 2. Veins of quartz, K-feldspar and magnetite

These veins comprise quartz, perthitic K-feldspar and magnetite. Some type 2 veins have diffuse margins; others have sharply defined contacts. Chalcopyrite and/or pyrite are present in all veins. Alteration associated with these veins sometimes leads to the introduction of biotite and K-feldspar, but sericitic halos are more common.

Type 3. Veins of quartz and K-feldspar lacking anyhdrite

Vein of this type have a similar mineralogy to type 1 veins but have a distinct morphology, internal structure and occurrence. Type 3 veins have sinuous but sharply defined boundaries and feldspar is consistently located on the margins (Fig. 3.2). The halos of type 3 veins are variably enriched in crystalline K-feldspar and biotite.

Type 4. Quartz-rich veins lacking appreciable sulphides

Type 4 veins appear internally zoned in hand specimen and have very sharply defined contacts with the wall rock. They are commonly sinuous and occasionally appear plastically deformed. They contain less than 1% sulphides by volume. Halos are are not always present, but where they are, they tend to be highly variable, ranging from potassic to sericitic. Potassic halos are probably most common, and consist of a thin but distinct zone of K-feldspar inside a thicker biotitic envelope. Wall rock within the alteration halos of these veins is depleted in disseminated opaques.

Type 5. Molybdenite bearing veins

These quartz-rich veins contain molybdenite which is invariably located in their outer margins and commonly lines the wall-rock. In some examples, flakes of molybdenite are only deposited on one side of the vein, but generally opaques are distributed symmetrically about the centre. The veins are clearly internally zoned, with pronounced cores and margins. Pyrite is present in the cores of a number of these veins, which are considered to be a subset of type 5 veins and will be referred to as type 5b.

Contacts with the wall rock are sharp and angular fragments of wall rock are present in some examples. Type 5a veins may be sinuous and occasionally appear plastically deformed. Type 5b veins are planar; plastically deformed examples have not been observed. Alteration halos are hard to distinguish and are absent in many cases. Where present, the wall-rock next to the vein is enriched in fine grained sericite and depleted in opaques.

Type 6. Quartz-pyrite veins

Veins of quartz and pyrite are abundant at Quebrada Blanca and show variation in pyrite:quartz ratios and in the nature of the alteration halo.

Quartz-dominated veins exhibit a thin selvedges of sericite and pronounced alteration halos which affect the host rock several decimetres from the margins. The wall-rock texture is enhanced due to the replacement of the groundmass by sericite. Biotite is bleached and feldspar sericitised in the zone immediately adjacent to the vein. Opaques may show a decrease in size and abundance in the halo, compared with the wall-rock outboard of the halo. Within these veins pyrite is located centrally or on one side of the vein.

Pyrite-dominated veins also exhibit thin selvedges of sericite but they are only locally developed. Vein boundaries are diffuse due to the vein quartz syntaxially overgrowing quartz in the wall rock. Halos are texturally destructive and initially enriched in sericite before grading into material in which quartz is enriched, sericite is interstitial and some phenocrysts remain unaltered. The opaques in the alteration halo are finer than in the fresher rock and are almost completely altered to covellite. Pyrite within these veins is also commonly filmed with covellite.

3.2 Vein paragenesis and spatial distribution

The spatial distribution of the vein types (Fig. 3.3) and the cross-cutting relationships between them allow two stages of vein development to be inferred. Together, vein types 1 and 2 form an early stage of vein development and are typically located at greater depth in the deposit relative to late stage veins. Type 1 veins were only found in the monzogranite, and were only well developed in a short interval of a single core. Cross-cutting relationships between type 1 veins and other veins were not observed.

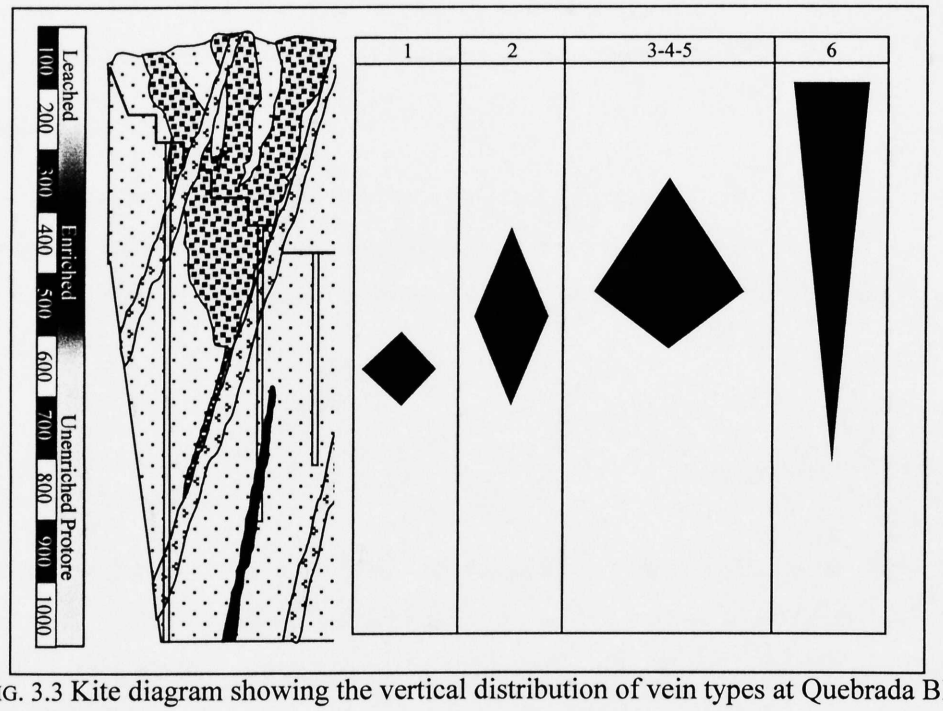


FIG. 3.3 Kite diagram showing the vertical distribution of vein types at Quebrada Blanca

The late stage comprises vein types 3, 4, 5 and 6, which are found higher in the deposit than early stage veins, in a zone overlapping the present base of enrichment (Fig. 3.3). Cross-cutting relations between these veins and type 2 veins are rare but, where observed, late stage veins clearly post-date type 2 veins. Veins within the late stage fail to show consistent cross-cutting relationships and it seems likely that they were approximately contemporaneous.

Type 3 veins are most commonly seen within dykes of the feldspar porphyry exhibiting early sericitic alteration. One specimen of a type 3 vein was seen to enclose material identical to the groundmass of the porphyry, with crystals of vein quartz terminating euhedrally into the core of material. Late stage veins appear to be contemporaneous with the development of the breccias; examples are seen both deformed by brecciation (commonly in a plastic fashion) and cross-cutting the breccia matrix. Vein types 4-6 are rare in the dykes of andesite and feldspar porphyry. Although type 6 veins decrease in abundance with depth (Fig. 3.3), their distribution may locally be structurally controlled; they are commonly associated with faults.

3.3 Petrography

Approximately one hundred and fifty veins were sectioned for petrographic examination. Samples most representative of each of the six vein types were then selected for analysis by fluid inclusion microthermometry. Detailed petrography was carried out on these samples using a combination of cathodoluminescence and electron probe microanalysis.

3.3.1 Techniques

Optical microscopy

All samples were subjected to a thorough examination using transmitted and reflected light. A preliminary assessment of the suitability of the sample for fluid inclusion analysis was made at this point, and samples considered to be representative of the six vein types were chosen.

Cathodoluminescence

The samples selected for microthermometric analysis were subject to a more detailed petrographic examination using cathodoluminescence (CL), as an appreciation of the growth history of vein minerals is essential for the correct interpretation of data obtained from any fluid inclusions they host. CL involves irradiation of the sample by an electron beam to encourage the emission of photons. Heterogeneities within the quartz, many of which are too subtle to be seen in polarised light, are revealed as variations in the colour and intensity of the resultant luminescence. Spectroscopic analysis allows quantification of these parameters but was not undertaken in this study. Consequently, all observations are somewhat subjective and luminescence cannot be easily compared between samples.

Samples were viewed using a Technosyn cold cathode system. System settings were approximately 15 kV with a current of 400-600 na. All samples exhibit weak, short-lived luminescence in the blue wavelength. This is characteristic of igneous quartz (Ramseyer *et al.*, 1988). Although the causes of luminescence in quartz are poorly understood (see D'Lemos *et al.*, 1997 for a review), variations in luminescence may reflect both structural and chemical heterogeneities. Both may result from variations in growth rate and/or mechanism, or from changes in the chemistry of the solution from which the quartz grew.

Electron probe micro-analysis (EPMA)

A number of studies have reported a correlation between aluminium content and the intensity of luminescence in quartz (D'Lemos *et al.*, 1997; Perny *et al.*, 1992). EPMA transects were carried out across a subset of the vein samples to determine whether relative variations in luminescence coincided with quantifiable variations in the trace element content of the quartz. Elements analysed for were aluminium, potassium, sodium, magnesium, iron, titanium, molybdenum and calcium. The raw data for the transects considered below can be found in Appendix B.1, along with the operating conditions and detection limits of the probe. Transects are presented in this chapter showing the variation of trace elements as weight percent oxide with distance along the transect. All transects were made normal to the vein margins and most veins were sectioned normal to their dips.

3.3.2 Data

Type 1 Veins of quartz, K-feldspar and anhydrite

The quartz of type 1 veins is subhedral to euhedral and overgrows wall-rock quartz in optical continuity. Wall-rock quartz has a dirty or dusty appearance due to an abundance of fluid and solid inclusions, while vein quartz appears relatively clean due to the diminished number of inclusions present. Igneous quartz and vein quartz are indistinguishable when viewed in CL. Quartz projecting into the vein forms euhedrally terminated crystals which exhibit a very subtle zonation only evident in CL. The feldspar present in these veins is observed to be perthitic and typically occupies the core of the vein. Uncleaved anhydrite is also present infilling vugs bounded by euhedral quartz faces. Biotite, ilmenite and zircon are accessory phases.

Type 2 Veins of quartz, K-feldspar and magnetite

In these veins, quartz displays very coarse to very fine anhedral mosaic textures. K-feldspar is intergrown with the quartz and exhibits a similar size range. Acicular biotite, typically altering to chlorite, is a minor constituent and is associated with the opaque phases. Magnetite has a granular appearance and may contain small blebs of ilmenite and/or chalcopyrite.

Type 3 Veins of quartz and K-feldspar lacking anhydrite

Quartz in type 3 veins forms a mosaic texture with grains being composed of distinct zones with subtly different extinction positions. These can be seen in both transmitted light and CL. The feldspar present in these veins is observed to be perthitic and is typically located on the vein margins.

Type 4 Quartz-rich veins lacking appreciable sulphides

Type 4 veins show variable quartz textures. Some examples consist entirely of a mosaic of coarse, equant crystals with smooth boundaries similar to the texture of the quartz in type 3 veins. In others, quartz at the margins forms a fine-grained, inequigranular mosaic, while that at the core is coarse and sometimes comb-like. EPMA transects across these veins indicate that the coarse comby cores are depleted in sodium, potassium and aluminium relative to the finer-grained, marginal quartz, and that the transition from one texture to another is marked by sharp inflections in total trace element content (Fig. 3.4). Veins consisting solely of coarse quartz fail to show any systematic variation in trace element content across their widths (Fig. 3.4).

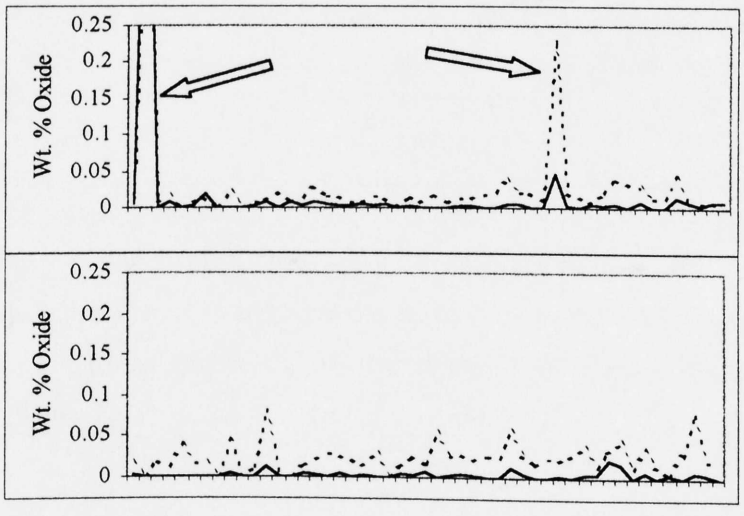


FIG. 3.4. EPMA transects across type 4 veins showing variation in Al_2O_3 (dashed line) and K_2O (solid line). Top (sample 151), vein showing core of coarse quartz and margin of finer-grained quartz. Arrows show the peaks in trace element content which correspond with the boundaries between the two textures. Bottom (sample 122), vein lacking textural variation and exhibiting an homogeneous EPMA trace.

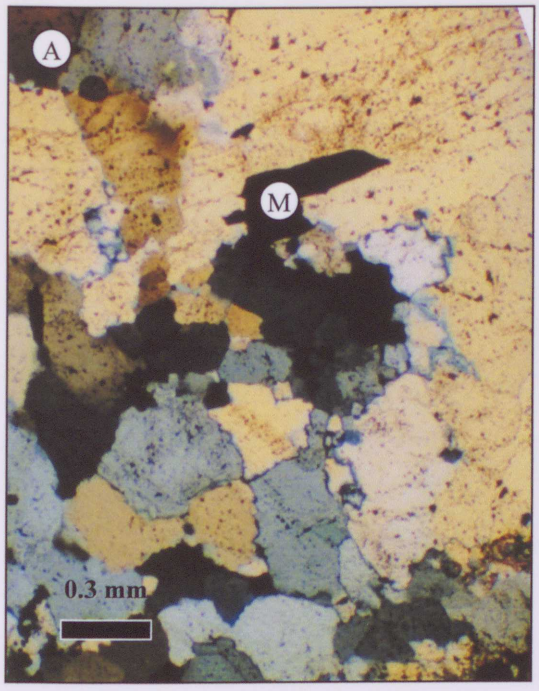
Compared with the marginal quartz, the core quartz is less intensely luminescent when viewed using CL. Small crystals with euhedral terminations are revealed on the vein margins when this technique is used. Successive overgrowths on these small crystals are increasingly rounded and usually coat more than one crystal. Bands of micro-inclusions (solid and liquid) cross-cut crystal boundaries and either parallel vein margins or are inclined to them at ~60°. Chalcopyrite and minor pyrite infill fractures with similar orientations. Clearly primary opaques are rare but include ilmenite and small blebs of chalcopyrite, locked in quartz.

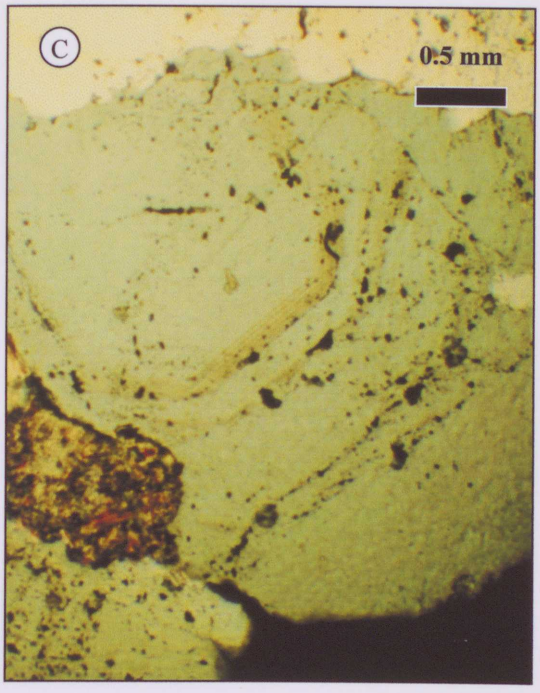
Type 5 Molybdenite bearing veins

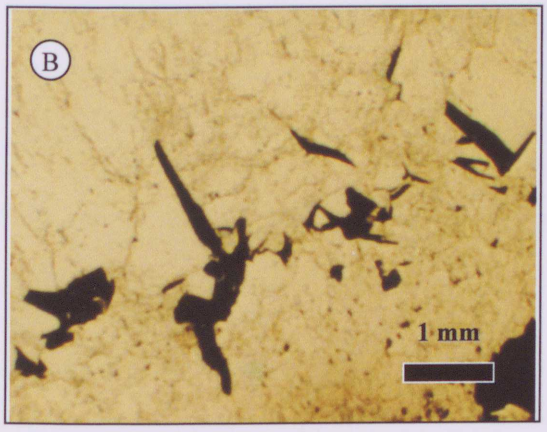
The texture and cathodoluminescent properties of the quartz in these veins are identical to those of the quartz in type 4 veins, though type 5 veins always exhibit a division between margin and core quartz. The transition from fine-grained to coarse-grained quartz is accompanied by the quartz changing from inclusion-rich to inclusion-poor (Fig. 3.5). Molybdenite tends to be located at the boundary between the two textures (Fig. 3.5). Some of the coarse crystals in the core show concentric growth rings while others show overgrowths defining stacked euhedral terminations into porosity. Both are defined by bands of micro-inclusions and can be seen in transmitted light (Fig. 3.5) as well as in CL. Coarse, subhedral crystals of quartz may be surrounded by discrete microcrystals or have irregularly sutured borders (Fig. 3.5). Molybdenite is the dominant opaque within type 5a veins but only represents 1-2% of the vein volume. It is usually associated muscovite. Lesser amounts of pyrite are present, in association with the molybdenite or enclosed by quartz.

The margins of type 5b veins have similar characteristics to those of type 5a veins though molybdenite is less abundant. Pyrite is observed to be deposited along the inside margins of the core quartz. The outer edge of the pyrite is intricately embayed while the inside edge is smoother. Mixtures of clean, inclusion-free quartz and chalcedony may be enclosed by the pyrite (Fig. 3.6). Chalcedony is poorly luminescent in CL. Plumose quartz (Dong *et al.*, 1995) is present locally (Fig. 3.6).

EPMA transects across type 5a veins reveal that the different types of quartz have distinct trace element contents. Relative to the finer grained margins, coarse grained quartz is depleted in potassium and aluminium (Fig. 3.7) and, in some cases sodium and magnesium (Fig. 3.8). The transition from one texture to the other is marked by abrupt changes in the total trace element content of the quartz.







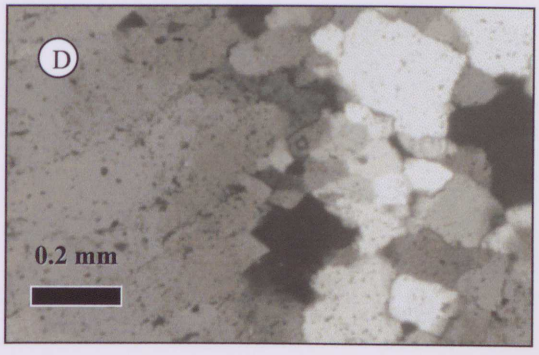


FIG. 3.5 Photomicrographs of type 5a veins. (a) Boundary between coarse, core quartz and finer grained marginal quartz. Note flake of molybdenite close to contact (M). (b) Boundary between core and marginal quartz showing inclusion-poor (above molybdenite flakes) and inclusion-rich nature (below molybdenite flakes) respectively. (c) Euhedral overgrowths on quartz crystal projecting into porosity (bottom right corner) defined by bands of solid and liquid inclusions. (d) Detail of a coarse quartz crystal from the core exhibiting a serrated margin surrounded by discrete microcrystals.

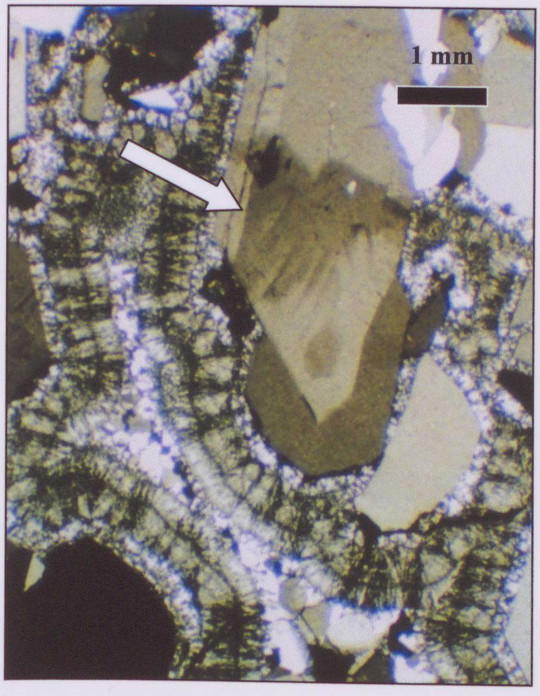


FIG. 3.6 (Right) Photomicrograph of quartz projecting into a pocket of chalcedony within a type 5b vein. Such mixtures are enclosed by pyrite (bottom left corner). Similar textures are also seen in type 6 veins. Large quartz crystal exhibits a plumose texture (arrowed).

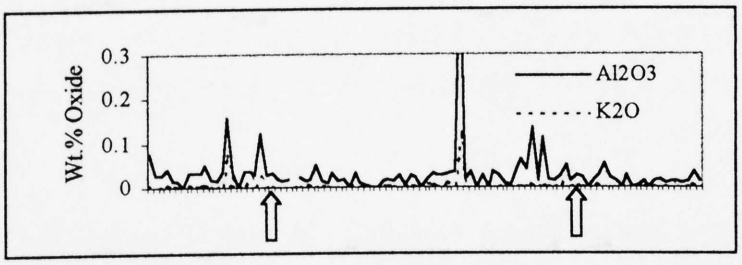


FIG. 3.7 EPMA transect across a type 5a vein (sample 92) showing variation in Al_2O_3 and K_2O. Arrows mark transition from fine, marginal quartz, to coarse, core quartz.

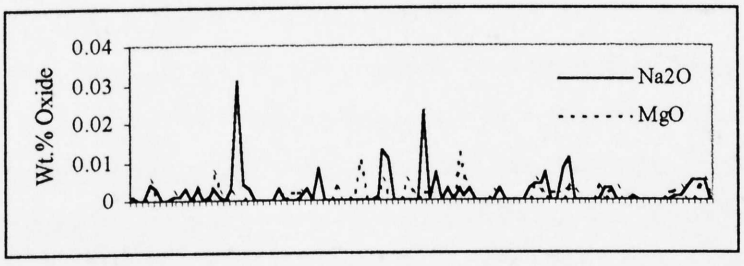


FIG. 3.8 As Fig. 3.7, but showing variation in Na_2O and MgO.

Type 6 Quartz-pyrite veins

The majority of the quartz in these veins is inclusion-free and associated with pockets of chalcedony, identical to those seen in type 5b veins. It forms a mosaic texture though is locally more euhedral where crystals project into residual porosity. The quartz-chalcedony mixture is poorly luminescent in CL. Pyrite has intricate margins and may be associated with ox-blood red rutile and/or acicular/fibrous muscovite. Rutile and tourmaline are observed associated with quartz and as late stage fracture fillings.

3.4 Fluid inclusion microthermometry

3.4.1 Technique

Following the detailed petrographic examination outlined above, fluid inclusion wafers 100μm thick were prepared from off-cuts of the respective vein samples, ensuring that microthermometric analyses were not carried out on material previously subjected to the high temperatures involved with the CL technique. Fluid inclusions are a direct means of determining the conditions of formation of a mineral in terms of the pressure, temperature and composition of the fluid from which it grew. Reviews of all aspects of fluid inclusion studies can be found in Roedder (1984) and Shepherd *et al.* (1985).

Although fluid inclusions are very useful, an appreciation of the limitations associated with the technique allows for more meaningful data interpretation. Only fluids that were trapped as the mineral grew (primary inclusions) and have not altered in any way since trapping will record growth conditions. Fluid inclusions commonly form during the fracture-seal cycle associated with brittle deformation of existing minerals and therefore do not record the

conditions at the time of mineral growth. These are termed secondary inclusions. Consequently, inclusions must be studied to determine their origin and whether they have altered since they were trapped.

Distinction between primary and secondary inclusions is made on the spatial relationship between the inclusions and structures within the host mineral, while post-entrapment changes to the inclusion and its contents can be identified by the presence of small inclusions "pinched" from larger ones, a process termed necking-down, and by wildly inconsistent thermometric properties of neighbouring inclusions. All data reported here are for inclusions thought to be primary, based largely on their random distribution and location away from planes or trails of inclusions. The distribution of inclusions has only been noted in the following vein descriptions where it is not random. The possibility of post-entrapment changes are considered more fully in section 6.2.2.

All fluid inclusions examined during this study lacked visible evidence for the presence of CO_2. All had a similar appearance with a vapour bubble surrounded by liquid. The relative proportions of vapour and liquid vary and are described by the degree of fill (the volumetric percentage of liquid). One or more solid phases were sometimes present. Such solids may be daughter minerals precipitated from the trapped solution as it cooled or may be trapped phases representing particulate matter insoluble in the fluid at the time of inclusion formation. Consistency in the phase proportions (liquid-vapour-solid) are used to suggest that solid phases are daughter minerals and not trapped particles.

Where two fluids coexist, one vapour-rich and one liquid-rich, varying proportions of the two fluids may be trapped in the same inclusion. Termed heterogeneous trapping, this produces a fluid that is not representative of either of the initial fluids. With the exception of type 5 veins (see below), all vein types hosted inclusions exhibiting a very scattered degree of filling varying between two endmembers, evidence for heterogeneous entrapment (Ramboz *et al.*, 1982). During microthermometry, emphasis was placed on the endmember compositions as indicated by consistency of phase proportions.

Fluid characteristics are determined by comparing the temperatures of phase changes recorded during freezing and heating of inclusions with those determined in experiments on simple systems. A Linkham THMS 600 stage was used for all measurements. A correction factor was applied to all temperatures noted following calibration of the heating/freezing stage using standards exhibiting phase changes of known temperature. Calibrations of this nature were made every four to six months and a number of correction factors were used.

The appropriate factors are given with the corrected microthermometric data in Appendix B.2, in which data are presented by vein type. The following phase changes are considered:

1. First melting (T_e). Following freezing of the entire contents of the inclusion, it is heated slowly. First melting of the frozen contents is often marked by an increase in the definition of ice crystals (sometimes seen as the apparently homogeneous ice becoming grainy) or by rounding of the vapour bubble. This temperature defines the main salts, such as NaCl, KCl and $CaCl_2$, present within the system. Only a very small amount of liquid forms initially, and this change can easily be confused with the freezing, during heating, of small portions of liquid that were metastable at lower temperatures, or with the subsolidus recrystallisation of ice or other phases stable at low temperature such as salt hydrates.

2. Ice melting (T_{mi}). Ice forms crystals which can be encouraged to recrystallise to form a single large grain by slow heating and cooling, so facilitating the recognition of final ice melting. The relief of ice crystals is high relative to saline solutions but low relative to other solid phases. The temperature of ice melting is largely a function of fluid salinity, higher salinity resulting in ice melting at cooler temperatures.

3. Daughter mineral dissolution (T_{md}). The temperature at which solid phases dissolve in a warmed solution can be used as an indicator of the salinity of that fluid. Some daughters may dissolve close to the homogenisation temperature (see below), indicating trapping of a fluid close to saturation with respect to that salt. Quite commonly, opaque phases do not dissolve before homogenisation of the liquid and vapour bubbles, if at all. Experimental evidence suggests that they could be daughters which are now insoluble due to changes in the redox state of the fluid in response to hydrogen migration out of the fluid following entrapment (Mavrogenes & Bodnar, 1994). In this study, consistency in the occurrence and volumetric proportions of opaque phases is used to infer that they do represent daughter minerals. Some inclusions encountered in this study homogenise by daughter mineral dissolution. These cases are rare and their relevance is discussed in Chapter 6.

4. Homogenisation (T_h). At a certain temperature, liquid and vapour homogenise so that the inclusion is filled with either a liquid-like or a vapour-like homogeneous fluid. Trapping of fluid at pressures greater than atmospheric calls for application of a positive correction to this temperature to determine the trapping temperature, as fluids of a given composition will homogenise at lower temperatures if trapped at higher pressures. The nature of homogenisation is used to define fluid inclusion type throughout this document. Type L inclusions homogenise into the liquid phase while type V inclusions homogenise into the

vapour phase. Type C inclusions homogenise by critical behaviour, observed as a fading of the bubble meniscus. This phenomenon is a result of the fluid being trapped close to its critical density.

These phase changes are related to fluid properties using a variety of methods. Using observed ice melting temperatures, the equation given by Hall *et al.* (1988) was used to determine the salinities of inclusions lacking salt daughters at room temperature and pressure (RTP). All undersaturated inclusions were treated as belonging to the pure $NaCl-H_2O$ system. Although other salts, notably KCl and $CaCl_2$ are almost certainly present (see below), the volume of hydrate forming in these dilute inclusions is too small to be seen and hydrate melting temperatures, giving an indication of the mole fractions of the various salts present, were not noted. The partitioning of salts between coexisting volatile phases is poorly understood and the salt composition of daughter bearing inclusions cannot be easily related to those of coexisting undersaturated inclusions (Sterner & Bodnar, 1986).

Inclusions saturated with respect to one or more salts at RTP invariably have first melting temperatures well below the eutectics of the $NaCl-H_2O$ or $NaCl-KCl-H_2O$ systems suggesting the presence of significant $CaCl_2$ (Shepherd *et al.*, 1986). The salinities of these inclusions were determined using the observed temperature of daughter dissolution and the equation given by Sterner *et al.* (1988) for the $NaCl-KCl-H_2O$ system. Due to the variable presence of sylvite in a given group of inclusions, the mol. fraction of NaCl was taken to be one, and all salinities are quoted as weight percent NaCl equivalent (wt. % NaCl equiv.)

In this chapter, fluid inclusion data are presented in two formats: as histograms showing single fluid inclusion parameters and as scatter plots comparing two fluid inclusion parameters. Pressure corrections have not been applied to homogenisation temperatures at this stage, and are considered in section 6.2.2. A summary of the average properties of the fluid types present in each sample analysed is tabulated at the end of the description of each vein type. These average values were obtained by considering only those inclusions thought to represent end-member compositions, as indicated by the histograms and scatter plots.

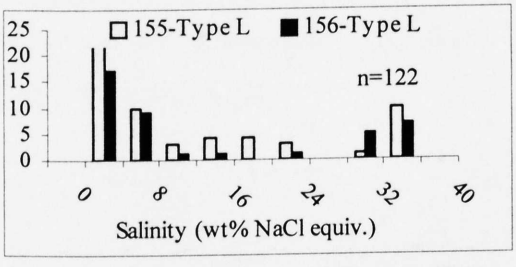
3.4.2 Data

Type 1 Veins of quartz, K-feldspar and anhydrite

These veins are the only type in which all inclusions are of type L (Table 3.2). Two samples, both occurring in monzogranite, have modes in fluid salinity at 0-8 wt% NaCl equiv. and 32-40 wt% NaCl equiv. (Fig. 3.9), though there is considerable scatter in the data. If the salinity data are compared with the homogenisation data (Fig. 3.11), it can be seen that the homogenisation temperatures of all the fluids are comparable. This is also evident in a histogram of homogenisation temperatures (Fig. 3.10).

TABLE 3.2. Summary of fluid inclusion properties for type 1 veins.

Sample number	Fluid type	T_e (°C)	Wt % NaCl equiv.	T_h (type)	Fill
155	1	-24	3.5	334 (L)	59
	2	-51	33	357 (L)	84
156	1	-	3.9	347 (L)	59
	2	-45	33	286 (L)	82



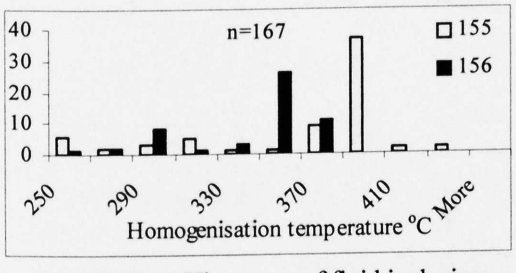


FIG.3.9 (Top) Histogram of fluid inclusion salinities in type 1 veins.

FIG.3.10 (Bottom) Histogram of fluid inclusion homogenisation temperatures in type 1 veins.

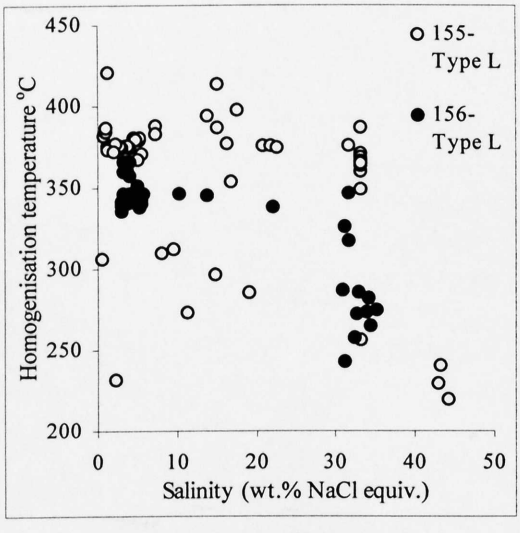


FIG.3.11 Scatter plot of homogenisation temperature vs. salinity for fluid inclusions in type 1 veins.

Inclusions of higher salinity in type 1 veins always contain halite and at least one opaque phase that can usually be identified as chalcopyrite. A second opaque phase is present in approximately half of these inclusions. Lower salinity inclusions do not consistently contain solid phases.

Type 2 Veins of quartz, K-feldspar and magnetite

A histogram (Fig. 3.12) showing the homogenisation temperatures of inclusions in four type 2 veins suggests that there are two populations of inclusions homogenising to liquid, one with a mode of 290 to 310°C and one with a mode of 370 to 390°C, and a single population of inclusions homogenising to vapour, mainly in the range 410 to 430°C. A comparison of homogenisation temperature with salinity (Fig. 3.13) shows that in two of the four samples most of the inclusions of lower salinity homogenise to vapour. In the remaining samples they homogenise to liquid. Inclusions of the more saline fluid homogenise to liquid by disappearance of the vapour bubble, and are responsible for the lower temperature population observed in Fig. 3.12.

TABLE 3.3. Summary of fluid inclusion properties for type 2 veins.

Sample number	Fluid type	T_e (°C)	Wt % NaCl equiv.	T_h (type)	Fill
93	1	-26	6	410 (V)	51
	2	-48	38	357 (L)	85
123	1	-29	4	350 (L)	63
	2	-47	33	286 (L)	81
247	1	-31	4	370 (L)	54
	2	-46	37	250 (L)	89
289	1	-	7	378 (V)	44
	2	-	33	316 (L)	84

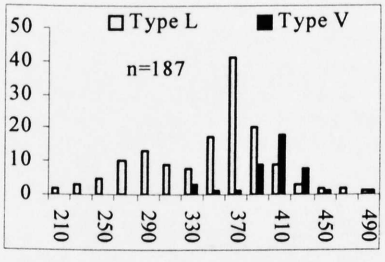


FIG. 3.12 (Above) Histogram of homogenisation temperatures for fluid inclusions in type 2 veins.

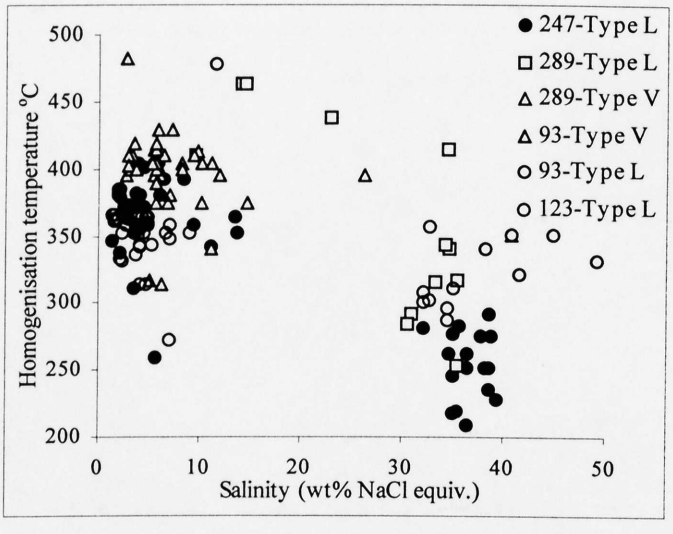


FIG. 3.13 (Right) Scatter plot of homogenisation temperature vs. salinity for fluid inclusions in type 2 veins.

Inclusions of the more saline fluid always contain halite which, on average, has an area equal to that of the bubble in plan view. Small daughters of sylvite are variably present. These saline inclusions always contain chalcopyrite and a second opaque that cannot be identified. Large flakes of hematite may be present and crystals of anhydrite are seen occasionally, but these are interpreted to be trapped phases. The less saline inclusions do not consistently contain solid phases.

Type 3 Veins of quartz and K-feldspar lacking anhydrite

A histogram of salinities (Fig. 3.14) shows that each sample of vein type 3 contains two groups of inclusions, one of low and one of high salinity. In samples 84 and 285, the low salinity inclusions are of type V and define a trend in which homogenisation temperature increases with salinity (Fig. 3.15). When these inclusions homogenise, they do so in a semi-critical manner, showing little change on heating before rapid expansion of the vapour bubble within 10-20°C of the final homogenisation temperature. The majority of type V inclusions contain a chalcopyrite daughter. In sample 273, many low salinity inclusions are type L. Inclusions within this sample exhibit a continuous spread in salinities and the distinct grouping seen in the other samples is not obvious (Fig. 3.15).

TABLE 3.4. Summary of fluid inclusion properties for type 3 veins.

Sample number	Fluid type	T_e (°C)	Wt % NaCl equiv.	T_h (type)	Fill
84	1	-25	2.7	399 (V)	50
	2	-52	33	321 (L)	85
273	1	-25	3.7	383 (L)	59
	2	-27	3.8	386 (V)	40
	3	-52	31	344 (L)	88
285	1	-	4.8	396 (V)	50

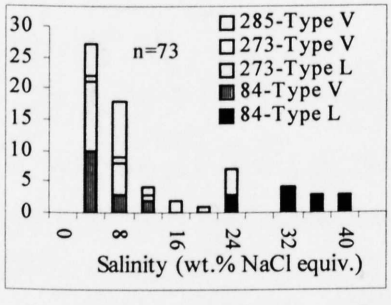


FIG. 3.14 (Above) Histogram of salinities for fluid inclusions in type 3 veins.

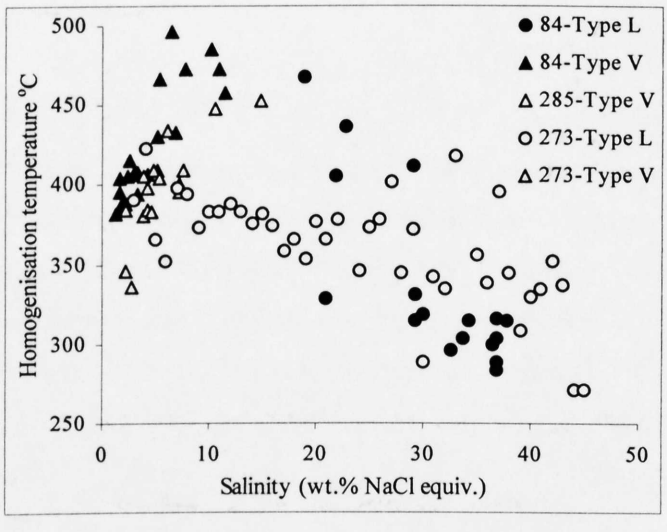


FIG. 3.15 (Right) Scatter plot of homogenisation temperature vs. salinity for fluid inclusions in type 3 veins.

Inclusions of the more saline fluid in these veins always contain halite and an opaque phase, usually identified as chalcopyrite. Two other translucent phases, possibly representing sylvite (KCl) and anhydrite, may be present, as may a second opaque phase. These are not considered to be true daughter salts as their presence is not consistent. Saturated inclusions were not suitable for microthermometric analysis in sample 285 as they all appeared to have necked. The saline inclusions in the two remaining samples have similar properties, with low first melting temperatures suggesting an important component of $CaCl_2$.

Within sample 84, the majority of type L inclusions with vapour-liquid homogenisation temperatures below 300°C homogenise by halite dissolution. A plot of temperature of vapour-liquid homogenisation versus temperature of halite dissolution (Fig. 3.16) shows that as the salinity of the inclusion increases (as indicated by the increasing temperature of halite dissolution) the liquid-vapour homogenisation temperature declines. These inclusions have been omitted from the calculation of the mean presented in Table 3.4.

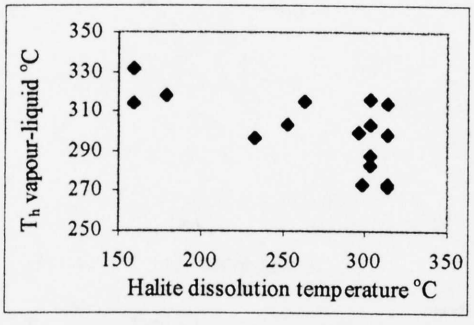


FIG. 3.16 Plot of vapour-liquid homogenisation vs. halite dissolution for saturated inclusions in type 3 veins.

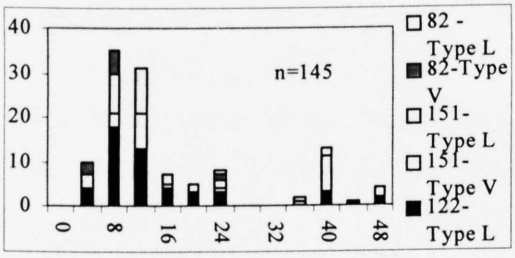
Type C inclusions in sample 84 fall into two groups; those with salinities of ~14 wt.% NaCl equiv. homogenise at ~490°C while those with lower salinities (~7 wt.% NaCl equiv.) homogenise at ~440°C. The higher salinity type C inclusions separate type V inclusions with salinities of ~10 wt.% NaCl equiv. from a scatter of type L inclusions with similar homogenisation temperatures.

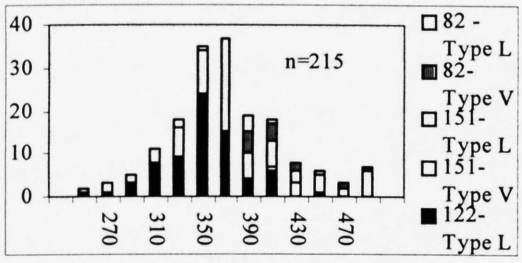
Type 4 Quartz-rich veins lacking appreciable sulphides

A histogram of salinities for fluid inclusions in type 4 veins (Fig. 3.17) shows modes at 4-8 and 36-40 wt% NaCl equiv. Inclusions of lower salinity fluid may be all of type L (sample 122), a mixture of types L and V (sample 151) or all of type V (sample 82; Table 3.5). As was noted for type 3 veins, type V inclusions within type 4 veins typically homogenise in a semi-critical manner. Homogenisation temperatures (Fig. 3.18) of type L inclusions in samples 122 and 151 show relatively normal distributions about modes falling in the ranges of 350-370 and 370-390°C respectively. The homogenisation temperatures for all inclusions have a well defined mode between 350-370°C (Fig. 3.18).

TABLE 3.5. Summary of fluid inclusion properties for type 4 veins.

Sample number	Fluid type	T_e (°C)	Wt % NaCl equiv.	T_h (type)	Fill
122	1	-28	5.7	349 (L)	71
	2	-	40.7	281 (L)	93
151	1	-25	6.0	318 (L)	61
	2	-31	9.2	446 (V)	47
	3	-49	39	331 (L)	85
82	1	-	7.2	411 (V)	48
	2	-	33	372 (L)	74





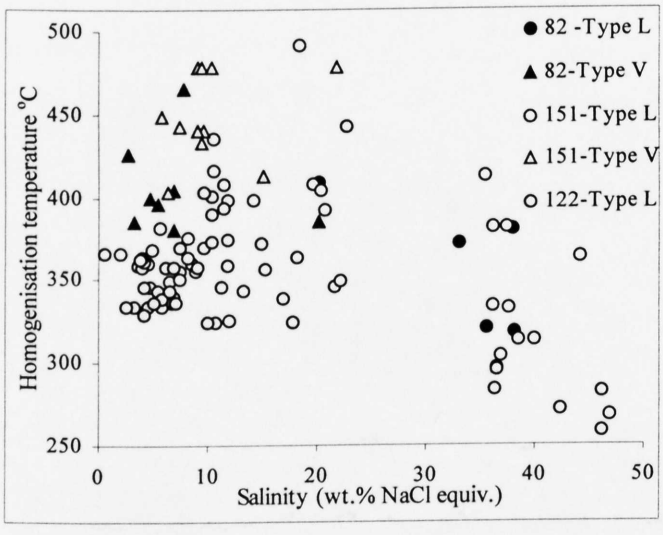


FIG. 3.17 (Above, left) Histogram of salinities for fluid inclusions in type 4 veins.

FIG. 3.18 (Above, right) Histogram of homogenisation temperatures for fluid inclusions in type 4 veins.

FIG. 3.19 (Left) Scatter plot of homogenisation temperature vs. salinity for fluid inclusions in type 4 veins.

A plot comparing salinity with homogenisation temperature (Fig. 3.19) shows there to be considerable scatter within the data set, with inclusions of salinity intermediate between the two apparent end-member fluids tending to homogenise at higher temperatures than the end members themselves. Saline inclusions with low homogenisation temperatures may homogenise by halite dissolution as seen in vein types 3 and 5. Halite is the only phase considered to be a daughter in the saline inclusions of these veins, though chalcopyrite and another opaque phase are commonly present. A single type C inclusion from sample 82 had a salinity of 9 wt.% NaCl equiv. and homogenised at 456°C.

Type 5 Molybdenite bearing veins

The appearance and properties of the fluid inclusions in samples of vein type 5 vary with the texture of quartz within which they are located. The fine grained marginal quartz has small but relatively well formed inclusions. Inclusions in the coarser core quartz are often streaked-out perpendicular to the edges of quartz grains and are clearly necked.

A scatter plot showing the variation of salinity with homogenisation temperature for inclusions from all samples (Fig. 3.20) suggests that the fine grained marginal quartz traps low salinity inclusions of type V and higher salinity inclusions of type L. As was seen in type 3 veins, inclusions within the higher salinity group with vapour-liquid homogenisation

temperatures below 300°C homogenise by halite dissolution. A plot of temperature of vapour-liquid homogenisation versus temperature of halite dissolution for these inclusions is similar to that presented for saturated inclusions in type 3 veins (Fig. 3.16). Solid phases within the inclusions in type 5 veins are identical to those in type 3 veins.

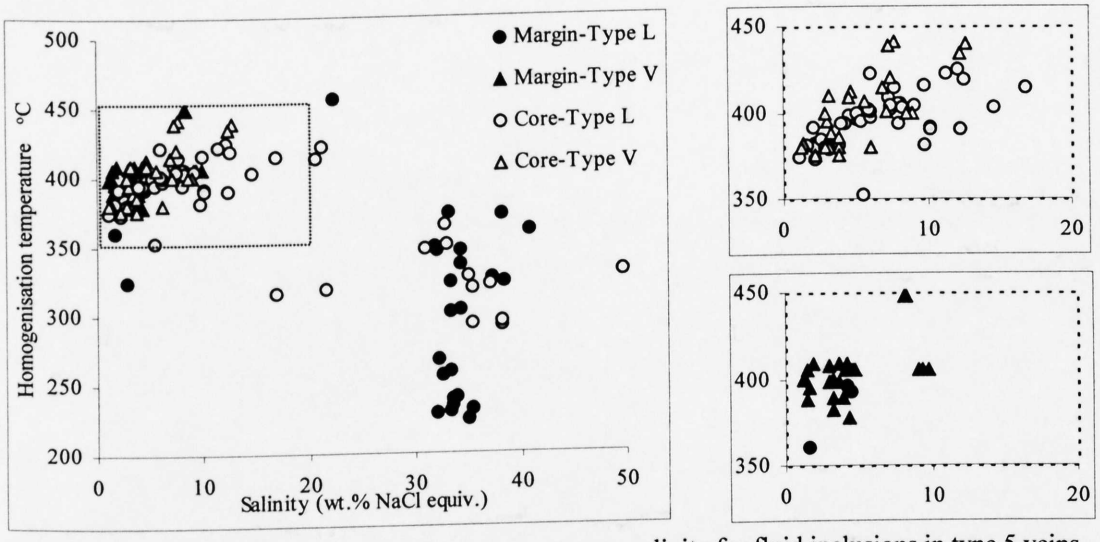


FIG. 3.20 Scatter plot of homogenisation temperature vs. salinity for fluid inclusions in type 5 veins. Area enclosed by hashed line is repeated in enlargements on the right to show overlap of fluid inclusion populations (symbols as main figure).

There is considerable overlap between inclusions of types L, V and C hosted in the coarse core quartz, particularly in the lower salinity region (Fig. 3.20), but it is probable that the fluids trapped in this region are the same as those trapped in the margins; a histogram of homogenisation temperatures for all samples, differentiating between inclusions of types L and V in both the core and marginal quartz (Fig. 3.21), shows that type V inclusions have similar properties regardless of their location, with the majority homogenising in the range 370-410°C. As was noted for vein types 3 and 4, type V inclusions within type 5 veins typically homogenise in a semi-critical manner.

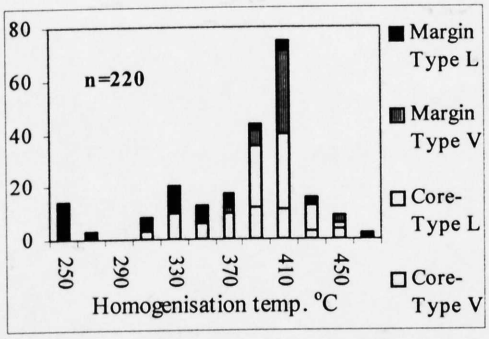


FIG. 3.21 Histogram of homogenisation temperatures for fluid inclusions in type 5 veins.

Type C inclusions trapped in the marginal quartz of type 5a veins have salinities of ~9 wt.% NaCl equiv. and homogenise at ~450°C, while those in the core have salinities of ~2 wt.% NaCl equiv. and homogenise at 385°C. Type C inclusions trapped in the marginal quartz of type 5b veins have salinities of ~2.5 wt.% NaCl equiv. and homogenise at ~395°C. A small group of type C inclusions trapped in quartz associated with pyrite in one of the two type 3b veins have very uniform properties, with a mean salinity of 4.5 wt.% NaCl equiv. and a

mean homogenisation temperature of 399°C (Table 3.6). These were the only inclusions to be found in quartz of this paragenetic stage. They do not contain solid phases.

TABLE 3.6. Summary of fluid inclusion properties for veins of type 5(a and b).

Sample number	Fluid type	T_e (°C)	Wt % NaCl equiv.	T_h (type)	Fill
5a	1	-27	4.3	398 (V)	46
	2	-50	27	353 (L)	83
5b core	1	-27	4.5	399 (C)	52

Type 6 Quartz-pyrite veins

Within type 6 veins, fluid inclusions are absent from the clean comby quartz associated with chalcedony but are abundant elsewhere. Of the three samples analysed, all contain type L inclusions (Table 3.7). One sample also contains a significant number of type C inclusions. Approximately half of all the inclusions contain a small triangular crystal of chalcopyrite.

A scatter plot comparing homogenisation temperature with salinity (Fig. 3.22) shows that each of the samples is dominated by a fluid of low salinity, and that for the group, the salinity of this fluid decreases as the homogenisation temperature decreases. The homogenisation interval of this fluid is distinct for each of the samples but the majority of inclusions homogenise between 340 and 400°C. Type C inclusions homogenise at the highest temperature (394°C) and are the most saline inclusions on the trend (~4.3 wt.% NaCl equiv.). Sample 74 contains a small population of inclusions which range in salinity from 8-16 wt% NaCl equiv. but have similar homogenisation temperatures to the lower salinity inclusions within this sample.

TABLE 3.7. Summary of fluid inclusion properties for type 6 veins.

Sample number	Fluid type	Wt % NaCl equiv.	T_h (type)	Fill
97	1	3.5	350 (L)	56
74	1	3.7	373 (L)	55
	2	12.6	379 (L)	60
103	1	4.3	389 (L)	54
	2	4.3	394 (C)	54

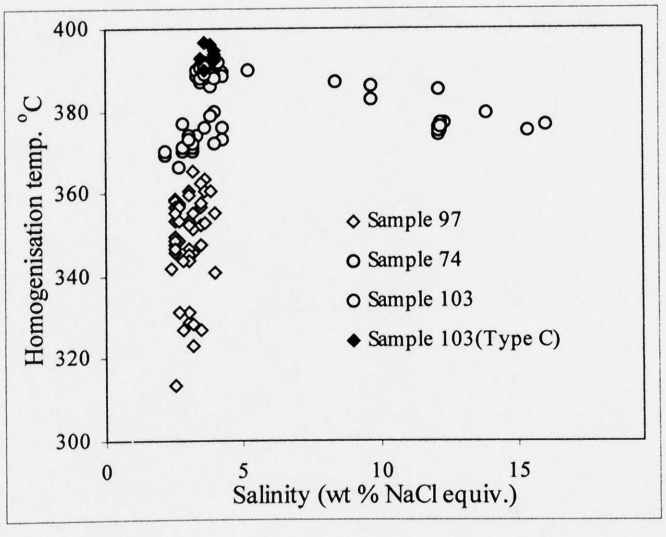


FIG. 3.22 Scatter plot of homogenisation temperature vs. salinity for fluid inclusions in type 6 veins. All inclusions are of type L with the exception of a group of type C inclusions in sample 103 (see key).

3.5 Light stable isotope geochemistry

3.5.1 Techniques

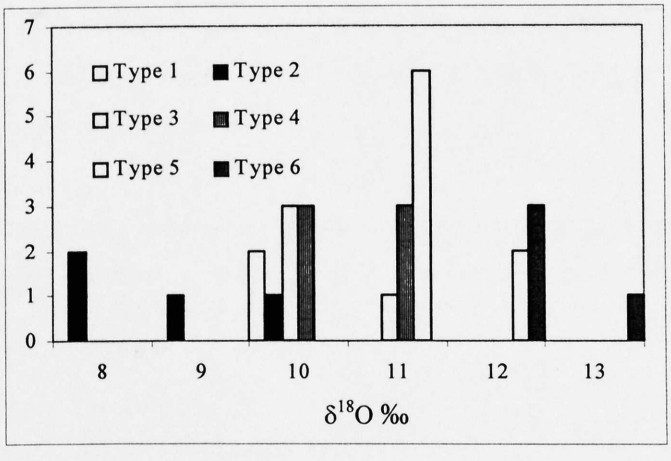
Separates from a selected number of samples were analysed for their light stable isotope compositions. Specifically these included: (1) Determination of the oxygen isotopic compositions of quartz and magnetite using the separation method of Clayton & Mayeda (1963) with ClF_3 instead of BrF_5 (Borthwick & Harmon, 1982) following laser ablation of the sample. The isotopic composition of the gas was measured using a VG Isogas Sira-10 mass spectrometer. Data are given in Appendix B.3. and are quoted as parts per thousand (‰) deviation of the measured $^{18}O/^{16}O$ ratio relative to Vienna standard mean ocean water (VSMOW); (2) Determination of the sulphur isotopic compositions of chalcopyrite, pyrite and molybdenite following the production of SO_2 by combustion (Robinson & Kusakabe, 1975) or by laser ablation (Kelley & Fallick, 1990). Isotopic composition of the gas was measured using a VG Isogas Sira-II mass spectrometer. Data are given in Appendix B.4. and are quoted as parts per thousand (‰) deviation of the measured $^{34}S/^{32}S$ ratio relative to Canyon Diablo Troilite (CDT).

3.5.2 Data

Oxygen

The measured $\delta^{18}O$ values of vein quartz from each vein type span a range of 2‰ and overlap to give a range of 8-12‰ (Fig. 3.23). In type 5a veins there is no distinction between marginal and core quartz, but while marginal quartz within type 5b veins has a similar value to the quartz in type 5a veins, the quartz-chalcedony mixtures enclosed by pyrite in these veins have markedly heavier values, averaging 17.8‰ (not shown). The isotopic values of the quartz become heavier moving through the paragenesis.

FIG. 3.23 Histogram of measured $\delta^{18}O$ values of quartz in each of the vein types occurring at Quebrada Blanca.



The measured $\delta^{18}O$ values of magnetite from two samples of type 2 veins were 2.9 ‰ and 2.2 ‰, giving $\Delta^{18}O_{quartz\text{-}magnetite}$ of 7.4 ‰ and 6.7 ‰ respectively. It was not possible to separate magnetite from the enclosing quartz in the remaining samples.

Sulphur

Of type 2 veins, only two veins yielded sufficient sulphides for isotopic analysis. Pyrite within sample 123 had an average $\delta^{34}S$ value of –2.6 ‰ (n=2) while chalcopyrite within sample 93 had a value of +3.0 ‰ (n=1). These contrast strongly with measured $\delta^{34}S$ values of sulphides from the other vein types, which cluster around 0.0 ‰. Measured $\delta^{34}S$ values of sulphides from vein types 1 and 3 are identical within experimental error; both chalcopyrite from a type 1 vein occurring in monzogranite and pyrite from a type 3 vein having values of 0.0 ‰. The $\delta^{34}S$ of the molybdenite from types 5a and 5b averaged +0.7 ‰ while the pyrite in type 5b veins averaged +0.6 ‰. Pyrite within type 6 veins had an average $\delta^{34}S$ of +0.8 ‰.

3.6 Data relating to breccias

Clasts within the breccias may be of monzogranite, andesite or feldspar porphyry. Intervals of breccia tend to consist of clasts of a single lithology and there is no evidence that clasts have been transported significant distances. Two distinct types of matrix are defined according to the dominant opaque phase present:

(1) Molybdenite-bearing matrix. Zones of breccia with a matrix consisting of quartz + molybdenite + sericite ± pyrite with a high porosity. Pyrite is irregularly distributed throughout these zones, where it tends to be located on the undersides of clasts. Zones of molybdenite-bearing matrix occur at greater depth than zones of pyrite-rich breccia.
(2) Pyrite-rich breccia. Zones of breccia with a matrix consisting of quartz + pyrite with lower porosities than the molybdenite-bearing zones. Where both molybdenite-bearing and pyrite-rich breccias are observed, the two are transitional.

Moderate to strong sericitic alteration occurs throughout the complex and appears to vary independently of the matrix. Blue-green, acicular tourmaline is present throughout the matrix of the breccia but not in abundance.

The texture of the breccia varies independently of the type of matrix and probably relates to the intensity of brecciation: areas marginal to zones of brecciation are characterised by a three-dimensional network of parallel-sided fractures. Zones of matrix-rich breccia are commonly separated by large expanses of this fractured, but relatively undisrupted, rock. As brecciation intensifies and the volume of matrix increases, tabular clasts are present (Fig. 3.24). These can be seen pulling away from the wall rock into the matrix in places. In parallel-walled cavities, these clasts may show foliation, though this is typically restricted to the smaller size fraction. There is some suggestion of sorting into bands, possibly indicating laminar flow (Fig. 3.25). Rare examples of packing suggest that there may have been some settling. As the volume of matrix increases further still, tabular clasts decline in abundance and isodiammetric clasts tend to predominate. These may be subangular to angular and display no evidence for sorting or foliation. Some clasts have fine protrusions and/or smoothly cuspate surfaces.

Hydrothermal breccias are seen to cross-cut all the lithologies present at Quebrada Blanca, though some dykes of andesite and of feldspar porphyry cut the breccias and are not brecciated. The igneous breccia occurs at greater depths than the hydrothermal breccia and the two may be transitional. This relationship is not clear, however, and the igneous and hydrothermal breccias often appear to form independently.



FIG. 3.24 Tabular clasts within the hydrothermal breccia. Sample has undergone supergene weathering. Same scale as photograph on right hand side.



FIG. 3.25 Suggestion of flow banding in molybdenite-bearing hydrothermal breccia. Sample has undergone minor supergene weathering.

A COMPARISON OF QUEBRADA BLANCA WITH OTHER PORPHYRY COPPER DEPOSITS

4

This chapter compares the observations presented in Chapters 2 and 3 with those reported from other porphyry copper deposits in order to see how representative of this type of deposit Quebrada Blanca is, in terms of the lithologies comprising the magmatic system and the veins comprising the hydrothermal system. This is not intended to be an exhaustive review, and concentrates on the more completely documented deposits for which a range of different types of data have been published. The majority of examples occur in the Cordillera of either North or South America.

The comparison follows the format of Chapters 2 and 3, commenting first on the field relations and petrography of the lithologies, and then on the data obtained from the veins. The relationship between the magmatic and hydrothermal systems is then considered. This chapter concludes with a summary of the characteristics of porphyry copper deposits in general.

4.1 Magmatic systems associated with porphyry copper deposits

4.1.1 The mineralised stock

At Quebrada Blanca mineralisation is hosted by a felsic stock of monzogranite to granodiorite composition. Mineralisation is associated with potassic alteration in which fine-grained biotite and K-feldspar and either magnetite or sulphides are added to the monzogranite. The composition of the fine-grained biotite varies with the nature of the opaque mineral assemblage. Propylitic alteration of the monzogranite is seen peripheral to the mineralised centre at Quebrada Blanca, where it may form two distinct zones (Hunt *et al.*, 1983).

Many porphyry copper deposits are hosted, at least in part, by a stock or pluton with a composition ranging from quartz monzonite/monzogranite to granodiorite. Such compositions are considered characteristic of this type of deposit (Creasey, 1977; Titley & Beane, 1981; Williams & Forrester, 1995). These stocks are typically composite, with

individual intrusions showing minor variations in texture and modal mineralogy. For example, at El Salvador early intrusives are equigranular and later intrusives are porphyritic (Cornejo *et al.*, 1997). At El Abra, intrusions display gradual transitions in modal quartz, K-feldspar or mafic phases (Ambrus, 1977). Contacts between intrusives are often gradational, as at Chuquicamata (Zentilli *et al.*, 1993).

Mineralisation in porphyry copper deposits is accompanied by potassic alteration which comprises two assemblages; biotite+K-feldspar+magnetite and biotite+K-feldspar+sulphides. The former typically occurs at greater depths than the latter (e.g. Lowell & Guilbert, 1970), and the magnetite-bearing assemblage is commonly overprinted by the sulphide bearing assemblage (Beane, 1982; Beane & Bodnar, 1985; Bowman *et al.*, 1987; Clark & Aranciba, 1993). Magnetite-rich alteration often includes amphibole and sodium feldspar, rather than biotite and K-feldspar, particularly in mafic lithologies (Clark & Aranciba, 1993; Heithersay & Walshe, 1995).

Previous studies of the composition of biotite associated with alteration in porphyry copper deposits have distinguished between primary, secondary and vein-associated biotite. All reported an increase in total MgO and Mg/(Mg+Fe) through this sequence (Moore & Czamanske, 1973; Mason, 1978; Jacobs & Parry, 1979; Preece & Beane, 1982; Reynolds & Beane, 1985). A single study reported that MgO and Mg/(Mg+Fe) increased towards the ore body (Ford, 1978). Some studies noted that TiO_2 contents show antithetic behaviour to MgO (Mason, 1978; Jacobs & Parry, 1979) and that Fe(III):Fe(II) increases in the transition from primary to secondary biotite (Jacobs & Parry, 1979).

4.1.2 The mineralising porphyry

At Quebrada Blanca the highest copper grades coincide with outcrops of feldspar porphyry. This lithology has a phenocryst assemblage comprising zoned plagioclase, resorbed quartz, amphibole replaced by biotite, primary biotite of homogeneous composition and magnetite. Sphene is present as an accessory phase. The phenocryst:groundmass ratio of the porphyry varies but is typically 1:1.

Porphyritic lithologies with an identical phenocryst assemblage to that of the porphyry at Quebrada Blanca have been documented at Potrerillos (Marsh *et al.*, 1997), Toquepala (Zweng & Clark, 1995), El Salvador (Gustafson & Hunt, 1975) and El Teniente (Camus, 1975), and it has been suggested that this may be a typical assemblage for a mineralising

porphyry (Marsh *et al.*, 1997). A similar assemblage, with altered sphene but lacking biotite, has been reported at El Abra (Ambrus, 1977). Groundmass to phenocryst ratios in such porphyritic lithologies range from 1:2 to 2:1 (Marsh *et al.*, 1997) and are commonly ~1:1 (Dilles, 1987; Zweng & Clark, 1995).

Resorbed quartz phenocrysts are ubiquitous in porphyritic lithologies associated with mineralisation, though the abundance of quartz is often reported as being highly variable within a single intrusive (Zweng & Clark, 1995; Marsh *et al.*, 1997). They are recorded as being present in each of the lithologies referred to in the preceding paragraph as well as at Chuquicamata (Lopez, 1939), Ely, Nevada (Fournier, 1967), and Yerington, Nevada (Dilles, 1987), to list but a few.

Plagioclase phenocrysts within the mineralising porphyry have been noted as displaying oscillatory zoning at a number of deposits (e.g. Marsh *et al.*, 1997) but have not been studied in detail. Neither have biotite phenocrysts; a single study has suggested that the magnesium number is positively correlated with the amount of aluminium replacing silica in biotite within intrusives associated with mineralisation, contrasting with a negative correlation in intrusives not associated with mineralisation (Mason, 1978). K-feldspar is usually absent from the phenocryst assemblage of porphyritic lithologies associated with mineralisation and, where present, may be megacrystic (Dilles, 1987), or may be restricted to the upper regions of dykes, suggesting that it could be a product of alteration (Camus, 1975).

4.1.3 Other intrusives

Dykes of andesite are present at depth within the felsic stock at Quebrada Blanca, but do not outcrop at surface. They appear to be contemporaneous with brecciation and with the intrusion of the porphyry dykes.

Mafic dykes of basaltic to andesitic composition are commonly present in porphyry copper deposits but are often interpreted as post-mineral and are rarely described in detail, despite the observation that many porphyry copper associated intrusives are accompanied by andesitic volcanism (Camus, 1975; Williams & Forrester, 1995). Large lenses of biotite-hornblende gabbro are reported to occur at depth within the felsic complex at Yerington and were interpreted to have been comagmatic with the felsic intrusives (Dilles, 1987). At El Salvador, the dacite porphyry which cross-cuts early alteration is accompanied by a mafic dacite/andesite porphyry (Gustafson & Hunt, 1975; Cornejo *et al.*, 1997). A trend in which

intrusives become progressively more mafic in composition has been noted at Chuquicamata and El Abra (Ambrus, 1977) and is well documented at El Salvador (Gustafson & Hunt, 1975; Cornejo *et al.*, 1997).

4.2 Hydrothermal systems associated with porphyry copper deposits

4.2.1 Vein paragenesis

A comparison of the vein paragenesis at Quebrada Blanca with parageneses reported for other porphyry copper deposits is presented in Table 4.1. It can be seen that veins with mineralogical assemblages similar to vein types 1, 2, 5 and 6 at Quebrada Blanca are reported for the majority of deposits. Veins with mineralogical assemblages similar to vein types 3 and 4 at Quebrada Blanca appear to be uncommon but this may reflect the difficulty distinguishing between vein types 1 and 3 and between sulphide-poor type 5 veins and type 4 veins, respectively, particularly in hand specimen. In contrast, vein types 1, 2, 5 and 6 are petrographically distinct. Studies which have included fluid inclusion analysis requiring detailed observation of the veins (e.g. El Salvador, Toquepala, Sierrita and Panguna) have generally made the distinction between veins of types 3 and 4.

TABLE 4.1. A comparison of the vein parageneses at various porphyry copper deposits.

	Quebrada Blanca Vein type and mineralogy	El Salvador	El Teniente	Collahuasi	Toquepala	Sierrita	Santa Rita	Bingham	Mines Gaspe	Island Copper	Panguna
EARLY	1 Qtz + K-spar + Anhy ± Sulph ± Potassic halo	✓	✓	✓	✓?	✓	✓			✓	
	2. Qtz + K-spar + Mag + Bio ± Sulph ± Sericitic halo	✓		✓	✓?	✓	✓?		✓	?✓	?✓
	3. Qtz + K-spar ± Sulph ± Potassic halo	✓			✓?			?✓			
	4. Qtz ± Potassic halo					✓					✓?
LATE	5. Qtz + MoS_2 ± Py Halos absent or weakly sericitic	✓	✓	✓	✓	✓?		?✓	✓	✓	
	6. Qtz + Py Weak sericitic to phyllic halo	✓	✓	✓	✓	✓	✓	✓		✓	✓?

✓ Signifies the occurrence of that vein type at an equivalent stage in the paragenesis. ✓? Signifies the occurrence of that vein type but not necessarily at that stage in the paragenesis. ?✓ Signifies the occurrence of a vein with similar but not identical mineralogy. Qtz- quartz, K-Spar- K-feldspar, Anhy- anhydrite, Sulph-sulphides, Mag-magnetite, Bio- biotite, Py- pyrite.

4.2.2 Morphology, internal structure and spatial distribution of vein types

Vein types 1 and 3

Veins with similar mineralogy to those of vein types 1 and 3 at Quebrada Blanca have been grouped together in previous studies. Type 1 veins are identical in composition and morphology to the A-type veins at El Salvador (Gustafson & Hunt, 1975). Gustafson & Hunt (1975) termed the internal structure of these veins as granular and noted that they were typically sinuous or discontinuous, both characteristics commented upon in other studies (Toquepala, Zweng & Clark, 1995; Collahuasi, Clark *et al.*, 1998). In their study of Sierrita, Preece & Beane (1982) noted that euhedral quartz was precipitated on vein margins and then overgrown by clear quartz and other phases, suggestive of open-space filling. This internal organisation was noted in type 1 veins at Quebrada Blanca. Gustafson & Hunt (1975) suggested that this vein type became progressively enriched in quartz with time, so that younger examples had less K-feldspar and sulphides and showed greater internal symmetry. Older and younger examples may correlate with the type 1 and 3 veins at Quebrada Blanca, respectively.

Type 2 veins

Early veins with magnetite similar to type 2 veins at Quebrada Blanca have been reported at depth at El Salvador (EB-type; Gustafson & Quiroga, 1995) and at Island Copper (Clark, 1993). In both these deposits, magnetite may be associated with actinolite and plagioclase, as well as or instead of K-feldspar. Sulphides are present in the EB veins at El Salvador and in the magnetite veins at Toquepala (Zweng & Clark, 1995).

Type 4 veins

Veins with a similar mineralogy to type 4 veins at Quebrada Blanca are not widely documented in the literature. At Sierrita, quartz veins lacking appreciable sulphide content (<1%) are reported to be the second most widely distributed type of vein after quartz-K-feldspar veins with or without magnetite (Haynes & Titley, 1980). Barren vitreous quartz veins occur at Santa Rita (Reynolds & Beane, 1985) and were grouped with K-feldspar-bearing veins. The sulphides in these veins were noted to fill microfractures, similar to the occurrence of the sulphides in type 4 veins at Quebrada Blanca.

Type 5 veins

Type 5 veins at Quebrada Blanca, characterised by the presence of molybdenite, are similar to the B-type veins described by Gustafson and Hunt (1975) at El Salvador. Anhydrite was noted in association with molybdenite at El Salvador but this phase is not seen in type 5 veins at Quebrada Blanca and its occurrence at El Salvador may be unusual; the only study considered here which specifically reports anhydrite in molybdenite-bearing veins is that of Toquepala (Zweng & Clark, 1995) and then only in small amounts. B-type veins at El Salvador do have a very similar internal structure to type 5 veins at Quebrada Blanca, comprising two textural variants of quartz, coarse-cockscomb and granular, and bands of sulphides paralleling the walls (Gustafson & Hunt, 1975). At Bingham, Roedder (1971) noted that the molybdenite in quartz-molybdenite veins lined the vein margins. He also noted the presence of small amounts of chalcedony coating vugs. Finally, Gustafson & Hunt (1975) noted that B-type veins are commonly reopened by pyrite veins. These veins would have the appearance of type 5b veins at Quebrada Blanca.

Type 6 veins

At Toquepala, Zweng & Clark (1995) distinguished between pyrite-rich quartz veinlets, pyrite-poor quartz veins, and veins consisting only of pyrite. All displayed sericitic-argillic alteration halos and all were grouped together into a late stage. A similar distinction was made for pyrite bearing veins at Panguna (Eastoe, 1978) but again, all were grouped together. Other studies reporting the presence of quartz-pyrite veins make no distinction between pyrite-rich and pyrite-poor.

At El Salvador, Gustafson and Hunt (1975) defined pyrite-quartz veins as D-type. They noted that D-type veins generally have feldspar-destructive halos from which chalcopyrite is leached, but do exhibit some variation in the nature of the halos. The D-type veins at El Salvador only have minor amounts of quartz, which is euhedral and typically free of inclusions. This is very similar to the quartz in pyrite-rich type 6 veins at Quebrada Blanca.

4.2.3 Fluid inclusions

In this study, the properties of primary fluid inclusions have been measured in veins classified according to their morphology and phase assemblage. A summary of the results is presented in Table 4.2. Although there have been many studies of the fluid inclusions in porphyry-copper deposits, it is difficult to correlate the results of the present study with those that have not used a similar classification scheme. For example, veins have been classified according to the alteration zone which they occupy (Bowman *et al.*, 1987) or by the nature of the fluid inclusions they contain (Eastoe, 1978). In many studies the small number of inclusions measured for each sample requires that sample sets have to be merged before the data can be considered significant, and the detail required to look at the processes determining the composition of the fluid inclusions in any given sample are lost.

TABLE 4.2. Summary of salinity and homogenisation temperature data for fluid inclusions in veins at Quebrada Blanca.

	Type L		Type V	
Vein type	Wt % NaCl equiv.	T_h	Wt % NaCl equiv.	T_h
1	3.5-3.9	334-347		
	33	286-347		
2	4	350-370	3-7	390-410
	35	270-290		
3	4	383	2.7-4.8	386-399
	31-33	321-344		
4	6	318-350	5.7-9.2	411-446
	33-41	281-372		
5	27	353	4.3	398
6	3.5-4.3	250-389		

Early veins with similar mineralogy to those of vein types 1, 2 and 3 at Quebrada Blanca have received the most attention during fluid inclusion studies. At Sierrita, homogenisation data for fluid inclusions in K-feldspar bearing veins, equivalent to vein types 1 and 3 at Quebrada Blanca, range between 250°C and 380°C (Haynes & Titley, 1980). Within this group, veins with sulphide display two distinct modes, one at 325°C and one at 360°C (Preece & Beane 1982). These may be analogous to the modes at 275-300°C and 350-400°C displayed by some of the type 1 veins at Quebrada Blanca. Veins lacking sulphide only have a mode at the lower temperature (Preece & Beane 1982). With the exception of some type V inclusions in K-feldspar bearing veins with anhydrite which homogenised at 420°C, inclusions either homogenised by vapour disappearance or by halite dissolution (Preece & Beane 1982). These are very similar to the characteristics of fluid inclusions in type 1 veins at Quebrada Blanca. Fluid inclusion data have been presented for K-feldspar bearing veins at Santa Rita by Ahmad and Rose (1980). Homogenisation temperatures for a set of 54 inclusions exhibit considerable spread, ranging up to 600°C, but have a mode at 320-340°C. The salinities of the inclusions have modes at 8-10 wt % NaCl equiv. and 42-44 wt % NaCl equiv.

Data for fluid inclusions in veins at Santa Rita with similar mineralogies to type 2 veins at Quebrada Blanca have been presented by Ahmad and Rose (1980). They identified the presence of inclusions with salinities of 0-3 wt % NaCl equiv. and halite-saturated inclusions, with the homogenisation temperatures of 156 inclusions having a mode between 320-340°C. These workers made no distinction between inclusions exhibiting different types of homogenisation.

Reynolds & Beane (1985) presented fluid inclusion data for what are described as vitreous quartz veins at Santa Rita. Homogenisation temperatures range up to 775°C for halite bearing inclusions (40-70 wt % NaCl equiv.) in which halite dissolved prior to liquid-vapour homogenisation and up to 520°C for inclusions which homogenised by halite dissolution (salinities 35-55 wt % NaCl equiv.). Liquid-vapour homogenisation temperatures in excess of 500°C were very rarely observed during the study of fluid inclusions at Quebrada Blanca. Low salinity type L inclusions homogenised between 260-360°C at Santa Rita. The absence of type V inclusions suggests that these vitreous veins are probably similar to type 1 veins at Quebrada Blanca, though their petrographic characteristics have more in common with type 4 veins.

At Mines Gaspe, veins similar to vein types 1, 2, and 5 at Quebrada Blanca were grouped together, and have similar fluid properties, with all inclusions, regardless of their nature, homogenising in the range 340-360°C (Shelton, 1983). This is a much more tightly grouped temperature range than displayed by the inclusions in vein types 1, 2 and 5 at Quebrada Blanca. Saturated inclusions in veins with properties similar to vein types 1 and 2 were reported to have daughter dissolution temperatures close to the temperature of liquid-vapour homogenisation, suggesting that the fluid was close to saturation with respect to NaCl at the time of trapping. This property is inferred for many of the fluids trapped in inclusions saturated with respect to NaCl at Quebrada Blanca.

Gustafson & Hunt (1975) noted the presence of low salinity inclusions in the youngest quartz lining drusy cavities in veins equivalent to type 5 veins at Quebrada Blanca. Fluid inclusions hosted in a molybdenite bearing vein at Toquepala had salinities between 10-16 and 33-46 wt % NaCl equiv. with homogenisation temperatures averaging 380°C (Zweng & Clark, 1995).

Despite being reported to be the second most abundant type of vein after veins with quartz and K-feldspar at Sierrita (Haynes and Titley, 1980), quartz veins lacking appreciable sulphide content (<1%), equivalent to type 4 veins at Quebrada Blanca, were not subjected to

fluid inclusion analysis. A barren quartz vein at Toquepala was reported to contain vapour-rich, liquid-rich and saturated inclusions, all of which showed similar homogenisation temperatures over the range 364-480°C (Zweng & Clark, 1995)

Reynolds & Beane (1985) presented evidence which suggested the primary inclusions in pyrite-bearing veins at Sierrita defined a trend of decreasing salinity with decreasing homogenisation temperature, very similar to that observed in type 6 veins at Quebrada Blanca. At El Salvador, Gustafson & Hunt (1975) noted that inclusions in pyrite-bearing veins had salinities of between 12-15 wt % NaCl equiv. and homogenisation temperatures of 300-350°C, similar to type 6 veins at Quebrada Blanca. Similar observations were reported for a pyrite vein at Toquepala, in which the salinity of fluid inclusions was 7-8 wt % and homogenisation temperatures ranged from 229 to 369°C. At Sierrita, Haynes and Titley (1980) reported homogenisation temperatures for inclusions in quartz-sulphide veins of 220-320°C. These temperatures are lower than those of inclusions in type 6 veins at Quebrada Blanca.

Studies which have characterised the fluids present within porphyry-copper systems rather than in specific veins have commonly noted the presence of two fluids, one dilute and one saline, as is the case for all veins at Quebrada Blanca with the exception of type 6. Primary inclusions at Sierrita (Preece & Beane, 1982) have modes in their salinity distribution at 8-10 and 38-40 wt % NaCl equiv., and salinity gaps have also been noted at Santa Rita (Ahmad & Rose, 1980) and at Mines Gaspe (Shelton, 1983). At Bingham, Roedder (1971) noted that fluids were grouped into salinities of 3, 20 and 40 wt % NaCl equiv.

4.2.4 Isotopes

Oxygen

The measured $\delta^{18}O$ values of quartz from veins at Quebrada Blanca range from 8.8-12.0‰ but cluster around 10.5‰. Later veins have higher $\delta^{18}O$ values. Isotopic proerties of quartz from veins similar to vein types 1 and 3 at Quebrada Blanca (which have averages of 9.5‰ and 9.9‰) were reported by Sheppard *et al.* (1980) for a number of deposits: 8-9‰ at Santa Rita, 9-10.5‰ at San Manuel and Ajo, and ~10‰ at Butte. At El Salvador (Sheppard & Gustafson, 1976), veins identical to type 1 veins at Quebrada Blanca had average values of 9.4‰, while veins with similar mineralogy to type 5 veins averaged 9.8‰. Pyrite veins at El Salvador had higher values, averaging 11.5‰. At El Teniente, quartz from veins with similar

mineralogy to vein types 1 and 5 at Quebrada Blanca had average $\delta^{18}O$ values of 8.8‰ and 9.7‰, respectively (Kusukabe *et al.*, 1984). At Bingham, the $\delta^{18}O$ values of vein quartz ranged from 8.3-9.7‰ in the potassic zone up to 11.2‰ in the transition zone between potassic and propylitic alteration, where the values were reported as being more variable (Bowman *et al.*, 1987).

Sulphur

Excluding sulphides in type 2 veins at Quebrada Blanca, which have values of +3‰ (chalcopyrite) and -3‰ (pyrite), all measured $\delta^{34}S$ values are close to 0‰. A narrow range of $\delta^{34}S$, usually 0±5‰, is typical of porphyry copper deposits associated with I-type granitoids in the western United States and in South America (Ohmoto & Goldhaber, 1997). At Quebrada Blanca, sulphides in later veins have slightly higher $\delta^{34}S$ values than those in earlier veins. A similar relationship was noted at Panguna (Eastoe, 1983), where veins identical to type 1 veins at Quebrada Blanca contained chalcopyrite which ranged in value from -1.6 to +0.9‰ and averaged 0.0‰ and sulphides in later quartz-pyrite veins ranged from +0.5 to +1.5‰ and averaged +1.0‰. Values reported for the deposits of El Salvador and El Teniente (Field & Gustafson, 1976; Kusukabe *et al.*, 1984) are more negative. At El Salvador, chalcopyrite in A-type veins ranged from -5.3‰ to -3.1‰, and averaged -4.2‰, while pyrite in quartz-pyrite veins ranged from -4.1‰ to -3.6‰ and averaged -3.6‰. A single sample of molybdenite from a molybdenite-bearing vein had a value of +0.82‰. This value is very similar to those measured on molybdenite at Quebrada Blanca. At El Teniente, $\delta^{34}S$ values of chalcopyrite and pyrite from veins with similar mineralogy to vein types 1 and 5 at Quebrada Blanca averaged -2.7‰ and -1.8‰ respectively.

4.2.5 Hydrothermal breccias

The breccias at Quebrada Blanca have not been studied in any detail. Large bodies of hydrothermal breccia with tourmaline are present in numerous porphyry-copper deposits in Chile and Peru (see Sillitoe, 1985, for a review) but are also found in areas unassociated with mineralisation and are considered characteristic of the central Andean orogen (Zweng & Clark, 1995).

4.3 Timing of mineralisation and magmatism

Hypogene mineralisation and alteration at Quebrada Blanca appears to have developed in two distinct stages; an early stage during which protore formed, comprising potassic alteration and chalcopyrite mineralisation, and a later stage in which quartz-rich, copper-poor veins and breccia bodies associated with sericitic alteration formed. Mineralisation/alteration associated with the early stage is predominantly disseminated, while that of the later stage is typically fracture hosted. The later stage of alteration and fracturing appears to have been contemporaneous with the intrusion of feldspar porphyry dykes, some of which exhibit intense alteration in which plagioclase is replaced by white mica and magnetite is replaced by sulphides.

Potassic alteration is commonly interpreted as occurring at a late magmatic stage. At El Abra, late magmatic alteration involved the addition of biotite and/or K-feldspar and quartz as interstitial grains, an addition indistinguishable from that associated with potassic alteration (Ambrus, 1977). A similar phenomenon has been noted in the felsic intrusives hosting mineralisation at El Teniente (Camus, 1975). At El Salvador, it was inferred that early potassic alteration took place in the presence of melt (Gustafson & Hunt, 1975).

Previous studies have reported a relationship between late intrusives and the development of quartz-rich veins. At El Teniente it was noted that molybdenum-bearing veins were commonly concentrated at the contacts between intrusive lithologies (Camus, 1975), suggesting that the fluids responsible for their deposition were introduced with later intrusives. Several authors have suggested that quartz-molybdenite veins may mark the onset of a more brittle style of deformation (e.g. Gustafson and Hunt, 1975) and some have gone as far as suggesting that the development of such veins may terminate hypogene copper mineralisation (Zweng & Clark, 1995). Previous studies have also reported a relationship between late intrusives and brecciation (Gustafson & Hunt, 1975; Ambrus, 1977; Zweng & Clark, 1995). The upper apophyses of porphyry dykes at El Abra were observed to be sericitically altered, contrasting with the rock surrounding them (Ambrus, 1977). This style of alteration may be analogous to the early sericitic alteration observed in some of the dykes of feldspar porphyry at Quebrada Blanca.

4.4 Summary

Porphyry copper deposits are characterised by distinctive intrusive lithologies, hydrothermal veins, and styles of alteration which exhibit consistent temporal relationships. Such deposits are typically centred upon a felsic intrusive complex varying in texture and mineralogy but generally of monzogranite to granodiorite composition. More mafic, primitive magmas are often present and may be contemporaneous with the felsic magmas.

Early, predominantly disseminated protore, comprising potassic alteration and chalcopyrite mineralisation, is hosted by the felsic complex and overprints magnetite-bearing alteration (Fig. 4.1a). Copper-bearing protore is typically cross-cut by porphyritic dykes with a phenocryst assemblage comprising plagioclase, resorbed quartz and biotite. Intrusion of these dykes appears to mark the onset of a more brittle style of deformation and the development of quartz-rich, copper-poor veins and breccias associated with sericitic alteration (Fig. 4.1b).

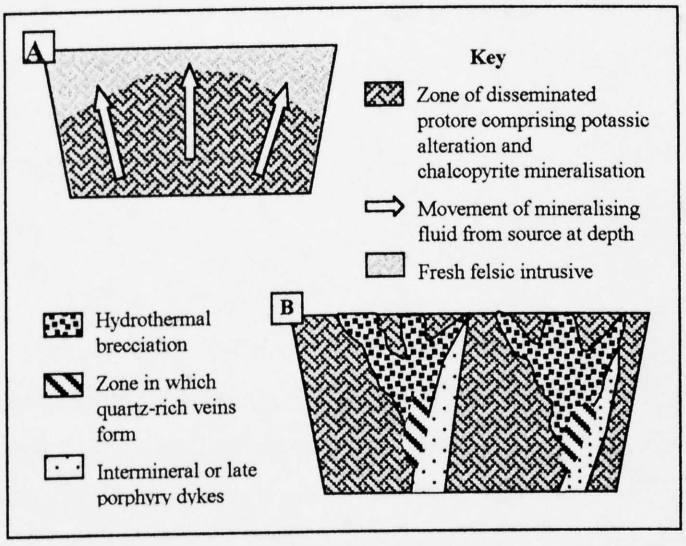


FIG.4.1 Diagram summarising the two stage development of hypogene mineralsisation in porphyry copper deposits (A) Disseminated protore (B) Overprinting by fracture-hosted assemblages associated with sericitic alteration.

The veins that form during the stage of development characterised by brittle deformation conform to a distinctive paragenesis in which veins containing K-feldspar and/or magnetite precede molybdenite-bearing veins, and molybdenite-bearing veins precede pyrite-bearing veins. The majority of veins comprising this paragenesis contain inclusions which trap two fluids of contrasting salinity, though paragenetically late veins often only contain a dilute fluid. Moving through the paragenesis, both the measured $\delta^{18}O$ values of vein quartz and the $\delta^{34}S$ values of vein sulphides become higher.

These distinctive components displaying their characteristic temporal relationships are present at Quebrada Blanca and it can be concluded that Quebrada Blanca is representative of porphyry copper deposits, particularly of those in the Andes.

EVOLUTION OF THE MAGMATIC SYSTEM AT QUEBRADA BLANCA

5

This chapter gives an interpretation of the data relating to the magmatic system at Quebrada Blanca which was presented in Chapter 2. Each lithology is discussed separately, with a view to determining the process(es) responsible for the petrography and geochemical variation displayed by the lithology and its constituent phases. This is followed by a brief consideration of the temporal relationships between lithologies.

5.1 Monzogranite

5.1.1 Petrography

Textural variation

The texture of the monzogranite changes from equigranular at the margins to weakly porphyritic in the core. Equigranular textures represent equilibrium textures achieved during slow cooling while porphyritic textures are the product of rapid cooling of a partially crystallised magma. This suggests that portions of the stock experienced different cooling histories and that crystallisation of the magma in the core of the intrusive may have been terminated by quenching prior to the attainment of an equilibrium texture. Additional evidence for rapid cooling of the internal zones of the intrusive are the septa of perthite seen separating optically continuous quartz; this crude granophyric texture is likely to be the product of rapid eutectic crystallisation (McBirney, 1984) and is commonly seen where interstitial melt is quenched (London *et al.*, 1989).

Mineralogical variation

The principal mineralogical variation observed within the monzogranite at Quebrada Blanca is the occurrence of some samples with the assemblage magnetite+chalcopyrite and others with the assemblage pyrite+chalcopyrite. Only a few samples in which magnetite is unaccompanied by chalcopyrite are observed. Characteristically in porphyry copper deposits it is the latter assemblage (magnetite without chalcopyrite or other sulphides) that is overprinted by the pyrite+chalcopyrite assemblage (e.g. Beane & Bodnar, 1995; Aranciba & Clark, 1996); for this reason, the magnetite+chalcopyrite assemblage observed at Quebrada

Blanca is assumed to represent an intermediate stage in the replacement of magnetite by sulphides. This may be a function of exposure; magnetite-rich zones are commonly present in the cores of porphyry copper deposits (e.g. Lowell & Guilbert, 1970) at depths which may not be exposed at Quebrada Blanca.

Both the magnetite+chalcopyrite and the pyrite+chalcopyrite assemblages are disseminated rather than fracture-related in the samples collected. This may imply that the assemblages developed in the presence of melt as well as hydrothermal fluid because in the absence of melt the movement of fluid might be expected to cause brittle failure of the rockmass, leading to fracture-hosted assemblages.

Initial water content

Initial water contents of felsic melts may be estimated by comparing the crystallisation sequence inferred from petrographic observations with experimentally determined crystallisation paths (Maaløe & Wyllie, 1975; Naney, 1983), though it is recognised that textural criteria do not reliably allow the determination of a crystallisation sequence and may permit contradictory interpretations (Ratajeski & Campbell, 1994). A comparison of the apparent crystallisation sequence of the monzogranite with experimental crystallisation sequences determined by Maaløe and Wyllie (1975) can be made because the composition and modal mineralogy of the experimental charge is similar to that of the monzogranite.

Such a comparison is necessarily restricted to the felsic components and biotite. Although there is evidence that some of the fine-grained biotite replaces phenocrysts of a preexisting mafic phase, there is no indication as to the identity of this phase. In the upper regions of the monzogranite, quartz is seen to form large rounded phenocrysts and clearly crystallises before biotite, which is interstitial. This suggests that the water content of the melt was less than 1.2wt.% (Maaløe & Wyllie, 1975).

Initial iron and magnesium contents

At Quebrada Blanca, samples in which both magnetite and sulphides are absent were not observed and it is not clear if the magnetite-bearing assemblage is a natural consequence of igneous crystallisation or is a product of the alteration acompanying mineralisation; some studies of mineralised felsic intrusives have suggested that mineralisation and alteration does not involve the addition of iron (Camus, 1975; Ford, 1978) while others have demonstrated

that a phase of iron-alkali metasomatism precedes the development of sulphide-bearing assemblages (Clark & Aranciba, 1995; Lang *et al.*, 1995). Although a phenocrystic mafic phase was probably present in the monzogranite at Quebrada Blanca prior to the addition of biotite during potassic alteration, it appears to have crystallised at a relatively late stage and is never present in amounts exceeding ~3%. This suggests that the initial iron (and magnesium) content of the monzogranite was low and, consequently, magnetite may be the product of iron metasomatism occurring at a late magmatic stage.

5.1.2 Whole-rock geochemistry

Samples containing only sulphides exhibit a compositional trend in which sodium and potassium are inversely related. This is consistent with the replacement of plagioclase by K-feldspar, for which there is clear petrographic evidence. Some magnetite-bearing samples may fall on this trend but there is considerable scatter in the data. Magnetite-bearing samples have a higher average ratio of $CaO/(Na_2O+K_2O)$ than samples containing only sulphides, suggesting that they have undergone less alkali metasomatism.

5.1.3 Biotite geochemistry

Biotite within the monzogranite exhibits two trends regardless of whether it occurs in magnetite- bearing or sulphide-only samples. The principal trend is variation of SiO_2 and TiO_2 with MgO/(MgO+FeO) and FeO. This suggests the action of the Ti-Tschermak substitution (Eqn. 5.1; Czamanske & Wones, 1973; Hewitt & Abrecht, 1988).

$$Ti^{4+} + 2Fe^{3+} \leftrightarrows Mg^{2+} + 2Si^{4+} \qquad (5.1)$$

The second trend is a negative correlation between MgO/(MgO+FeO) and chlorine. This is an intrinsic property of biotite which reflects the influence of Mg:Fe on the crystal lattice (Munoz & Swenson, 1981) rather than relating to extensive conditions such as the activity of chlorine in the melt or fluid with which the biotite equilibrated.

Since there is evidence that the sulphide-only assemblage represents an overprint of the magnetite-bearing assemblage, biotite within the samples containing only sulphides is inferred to originally have had a composition equivalent to that of the biotite accompanying magnetite. As such, the trend ascribed to the action of the Ti-Tschermak substitution which is displayed by biotite in both associations may reflect the initial development of fine-

grained biotite in the presence of magnetite. If this was the case, biotite precipitated in equilibrium with magnetite might be predicted to have evolved to more magnesium- and silica-rich compositions as titanium and iron were incorporated into magnetite.

Biotite in the sulphide-only samples of the monzogranite is distinguished from that in the magnetite-bearing samples by having a higher MgO:FeO ratio and potassium content. This suggests that changes in biotite composition during overprinting principally only involved iron, magnesium and potassium and that the magnesium:iron ratio and the activity of potassium were higher during the development of the sulphide-only assemblage than during the development of the magnetite-bearing assemblage.

The data appear to imply a change from the Ti-Tschermak substitution to a simpler substitution involving only iron and magnesium but it may be the case that both substitutions were operating concurrently; magnesium and iron are very well correlated in both groups of samples. In the absence of data concerning the iron(II):iron(III) ratio of the biotite, no definitive conclusion can be reached concerning the substitution mechanism. The gradational nature of the iron, magnesium and potassium contents of the biotite from magnetite-bearing to sulphide-only samples suggests that overprinting may have been the result of a continuous, rather than abrupt, change in the composition of the environment of formation. This change involved a decrease in the ratios of iron and titanium to magnesium and silica and an increase in the activity of potassium, consistent with the precipitation of iron followed by the fixation of potassium during the cooling of a hydrothermal fluid enriched in these elements (Whitney *et al*, 1985).

5.1.4 Summary

Textural variation within the monzogranite suggests that quenching of the core of the intrusive may have preserved heterogeneities produced during the hypogene development of the magmatic-hydrothermal system within the stock. These heterogeneities take the form of magnetite-bearing and sulphide-only assemblages which appear to record equilibration between partially crystalline magma and a cooling hydrothermal fluid. At higher temperatures, iron is fixed as magnetite and iron-rich biotite. As the fluid cools, potassium is fixed in the solid assemblage at the expense of sodium and calcium, and copper and iron bearing sulphides replace magnetite.

5.2 Andesite

5.2.1 Petrography

Within the andesite, textures such as highly elongate apatite and poikilitic quartz enclosing oligoclase laths indicate a period of rapid nucleation followed by steady crystallisation (Vernon, 1991). This could have been caused by sudden cooling of the melt before a return to equilibrium crystallisation (Hort, 1998). Such features are characteristic of synplutonic mafic dykes, which are thought to represent introduction of magma late in the crystallisation history of felsic chambers (Pitcher, 1991).

The aphanitic material seen as selvedges on the andesite dykes and as rare veins may be evidence that the andesite exsolved a volatile phase. Similar selvedges have been observed at the tips of basaltic dykes and were interpreted to have been precipitated from such a phase (Hoek, 1995). Both the selvedges on the basaltic dykes and those on the andesite at Quebrada Blanca consist largely of biotite. The selvedges on the basaltic dykes described by Hoek (1995) contained ilmenite. In contrast, the selvedges at Quebrada Blanca contain magnetite, indicative of a more oxidised state. Evidence has been presented suggesting that mafic-magma derived volatile phases present in magma chambers beneath some recent volcanoes were also relatively oxidised (Hattori, 1993; Matthews *et al.*, 1994a).

5.2.2 Whole-rock geochemistry

Samples of andesite exhibit a significant weight loss on ignition. This can most readily be attributed to the removal of water held in hydrous phases such as the chlorite observed replacing phenocrystic biotite. Such alteration may reflect either the action of a hydrothermal fluid sourced from outside the andesite or deuteric alteration associated with a fluid derived from the andesite itself (c.f. Nabelek et al., 1983).

If it is assumed that alteration was deuteric, the andesite appears to have been anomalously rich in copper; the average copper content of convergent margin andesites is typically 60-150 ppm (Gill, 1981). The high copper content of the andesite at Quebrada Blanca also contrasts with that of mafic lithologies of Eocene age in Chile, which are typically well below the average of 60-150ppm (Hammerschmidt *et al.*, 1992). The limited number of samples and the evident alteration of the andesite prohibit a more meaningful interpretation of its geochemistry.

The aphanitic material seen forming selvedges on the andesite dykes is strongly enriched in potassium relative to the dyke material. Experimental work suggests that volatile phases derived from andesitic magmas would be strongly enriched in potassium relative to the source magma (Sakuyama & Kushiro, 1979). The selvedge material is also strongly enriched in copper relative to the dyke material. Studies of arc lavas (Stanton, 1994) suggest that copper reaches a maximum within the melt at mafic compositions intermediate between basalt and andesite after which it decreases with increasing felsic character (Fig. 5.1). This significant depletion can best be explained by loss to a MVP; some depletion could be accounted for by the fractionation of magnetite and/or augite following the incorporation of copper into these phases but not in sufficient amounts to account for the magnitude of the observed variation (Eilenberg & Carr, 1981). Molybdenum exhibits a similar trend to copper (Fig. 5.1), as may gold, which follows copper closely (Stanton, 1994). These inferences are supported by the measurement of significant amounts of copper and gold in gases associated with andesitic volcanism (Table 5.1; Hedenquist, 1995).

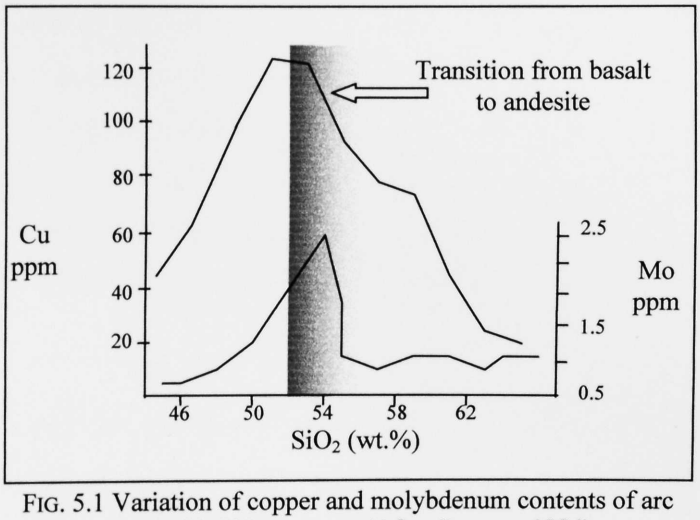


FIG. 5.1 Variation of copper and molybdenum contents of arc lavas with SiO_2 content. (After Stanton, 1994)

TABLE 5.1 Metal contents of volcanic exhalations (Hedenquist, 1995).

Volcano (Style of degassing)	Cu	Au	Mo
Augustine, Alaska (Explosive; 30 day duration)	12,000 tonnes	1,000 tonnes	No data
White Island, NZ (Passive)	>110 tonnes/ year	>36 kg/year	No data
Etna, Italy (Passive)	580 tonnes/ year	84 kg/year	84 tonnes/ year

5.2.3 Biotite geochemistry

Biotite occurs in two paragenetic stages within the andesite; as phenocrysts and as replacements after amphibole. Biotite is the principal component of the selvedge material and has a similar composition to the phenocrystic biotite within the andesite.

Biotite replacing amphibole has a higher titanium content than phenocrystic biotite, suggesting that secondary biotite developed in an environment in which the concentration of titanium was greater than during the precipitation of phenocrystic biotite. Such a situation could have developed in the residual melt of the andesite following the removal of a MVP depleted in titanium relative to the melt. Replacive biotite has a high iron:magnesium ratio compared with phenocrystic biotite. This trend is the opposite to that characteristically seen during potassic alteration in which the iron:magnesium ratio of biotite decreases (Moore & Czamanske, 1973; Mason, 1978; Jacobs & Parry, 1979; Preece & Beane, 1982; Reynolds & Beane, 1985). Removal of a MVP is unlikely to account for the enrichment of the residual melt in iron relative to magnesium because iron is preferentially concentrated in volatile phases.

Biotite in the selvedge material has a high magnesium:iron ratio. Although this could suggest that the medium from which this biotite precipitated was enriched in magnesium relative to iron, iron is preferentially concentrated in volatile phases relative to magnesium. An alternative explanation is that the high magnesium content of the biotite reflects its coprecipitation with magnetite.

5.2.4 Isotope geochemistry

The isotopic values determined for the andesite represent a whole-rock value. Although the $\delta^{18}O$ value (6.6‰) is within the range suggested for fresh andesites (Taylor, 1974), the high water content of the andesite, attributable in part to a high chlorite content, indicates that it has been altered. Chlorite fractionates isotopically light oxygen and samples in which biotite has been replaced by chlorite would be predicted to have more negative $\delta^{18}O$ values than unaltered samples (Nabelek et al., 1983). The δD value of the andesite (-79‰) is significantly below the initial value of -30‰ proposed for andesites (Giggenbach, 1992). This low δD value may be a product of degassing but could also reflect alteration.

The selvedges on the andesite dykes are composed almost entirely of biotite and the isotopic values measured on the selvedge material are assumed to be those of biotite. Field relations suggest that the selvedges may have been precipitated from a MVP. If this was the case, and equilibration between MVP and biotite is assumed, the measured $\delta^{18}O$ and δD values of the selvedge material can be related to $\delta^{18}O_{(fluid)}$ and $\delta D_{(fluid)}$ by temperature-dependent fractionation factors between biotite and fluid. The temperature at which the selvedges formed is not known but is considered to be within the range 800-1000°C. This temperature

range gives values of $\delta^{18}O_{(fluid)}$ of 10.7-11.7‰, according to the fractionation factor of Kyser (1987), and of $\delta D_{(fluid)}$ of -50 to -55‰, according to the fractionation factor of Suzuoki and Epstein (1976). The values of $\delta^{18}O_{(fluid)}$ are within the range of 10±3‰ proposed for volatile phases derived from andesites (Giggenbach, 1992), but the $\delta D_{(fluid)}$ values are very low compared with those predicted by empirical studies (Giggenbach, 1992).

The close spatial relationship between dykes and selvedges suggests that the MVP from which the selvedges are interpreted to have precipitated was probably derived from the andesite. Although the δD value of the MVP is 25-30‰ higher than that of the andesite and so would account for the δD value of the andesite becoming more negative, it is not clear that this episode of degassing was solely responsible for the large depletion in deuterium exhibited by the andesite; the andesite is clearly altered. Both the andesite and the postulated MVP have δD values which are very negative compared with those predicted by empirical studies. It is possible that these strong depletions reflect more than one stage of volatile loss but with so little data it is not realistic to consider the degassing history of the andesite in more detail.

5.2.5 Summary

The composition of the aphanitic material forming selvedges on the andesite dykes and veins is permissive evidence that it precipitated from a MVP derived from the andesite. The geochemistry of biotite within the andesite and the isotopic properties of the two components are consistent with this interpretation, though the full degassing history of the andesite is not clear. The MVP appears to have been rich in copper and the components of biotite and may have been relatively oxidised. Despite the evidence for separation of a copper-rich volatile phase from the andesite, it still retains an unusually high copper content. This could reflect incomplete separation of the volatile phase from the melt or an anomalously high initial copper content.

5.3 Feldspar porphyry

5.3.1 Petrography

Quartz

The rounded nature of the majority of the quartz phenocrysts in the feldspar porphyry at Quebrada Blanca may be the product of growth or destabilisation (for a review of this subject, see Donaldson & Henderson, 1988), but the silica-rich dissolution halos observed around the phenocrysts imply destabilisation rather than growth. A similar origin has been demonstrated for rounded quartz phenocrysts from the dacite porphyry at El Salvador (Watt *et al.*, 1997). The volume of phenocrystic quartz varies between samples, but there is little variation in the measured amount of SiO_2 from sample to sample. This suggests that there was little movement of crystals relative to melt once the dissolution process had initiated.

Destabilisation may reflect either chemical or thermal disequilibrium with the surrounding magma. Chemical disequilibrium may occur during volatile undersaturated, isothermal decompression of magmas which causes pH_2O to increase (Whitney, 1989). It is unlikely that the dykes were undersaturated with a volatile phase during dyke intrusion; the deep embayments seen in the phenocrysts at Quebrada Blanca most likely reflect the action of volatile bubbles (Donaldson & Henderson, 1988). As plagioclase phenocrysts at Quebrada Blanca also show resorption, the most likely driving mechanism for the destabilisation of quartz is increasing temperature (c.f. Whitney, 1989).

Sphene

Sphene, an accessory phase in the feldspar porphyry at Quebrada Blanca, is commonly seen where mafic and felsic magmas interact (Hibbard, 1991) and represents the addition of titanium to felsic melts in which it is only weakly soluble. The sphene at Quebrada Blanca is replaced by magnetite, which suggests that the oxidation state of the melt increased from between the nickel-nickel oxide and magnetite-hematite buffers (Drexler & Munoz, 1988), to close to the magnetite-hematite buffer.

A change in oxidation state of a magma requires that it behaves as an open system. Diffusive loss of hydrogen has commonly been proposed to be responsible for magmatic oxidation (Henley & McNabb, 1978; Eastoe, 1982). Work by Candela (1986), however, suggests that oxidation by hydrogen loss is only likely in very iron-poor melts (such as those associated with Climax-type molybdenum deposits) and in general cannot account for the extreme

oxidation observed in many systems. Calc-alkaline magmas may become more oxidised during interaction with more mafic magmas and/or their coexisting MVP (Matthews *et al.*, 1994a). During the process of thermal equilibration between two such melts, the mafic-derived MVP must cool, favouring the disproportionation of SO_2 (Eqn. 5.2). As a consequence, iron (II) within the more felsic magma can be oxidised to iron (III) (Eqn. 5.3).

$$SO_2 + H_2O \leftrightarrows H_2S + 3O^{2-} \tag{5.2}$$

$$O^{2-} + 2Fe_3O_4 \leftrightarrows 3Fe_2O_3 \tag{5.3}$$

If the crystallisation of sphene records interaction between the parental magma of the feldspar porphyry and a mafic MVP and replacement of this phase by magnetite indicates an increase in fO_2, it would appear that the increase in fO_2 was not instantaneous. This may suggest that introduction of the MVP occurred over a period of time during which fO_2 gradually increased.

Hornblende

The feldspar porphyry is the only lithology at Quebrada Blanca which contains significant amounts of hornblende, albeit now pseudomorphed by biotite. Compositional similarity between the biotite replacing hornblende and the phenocrystic biotite within the porphyry suggests that the alteration of amphibole may have been a magmatic process, possibly driven by increasing pH_2O or fO_2 (Speer, 1987; Scaillet *et al.*, 1995).

5.3.2 Whole-rock geochemistry

Fresh samples

The composition and modal mineralogy of the fresh feldspar porphyry is quite uniform and the small compositional differences between samples can be explained by minor variations in the proportions of the phenocrysts and in the ratio of phenocrysts to groundmass. For example, calcium and strontium are correlated in the fresh samples of feldspar porphyry because strontium partitions into the dominant calcium-bearing phase, the anorthite component of plagioclase.

Iron is seen to vary independently of other species but could be explained by varying amounts of oxyhornblende present within individual samples. Oxyhornblende with an iron to magnesium ratio of 3:1 contains ~20% iron, so a variation of ~1wt% iron in the whole rock analysis could be accounted for by varying the amount of oxyhornblende between 1 and 5 vol.%, similar to the variation seen in the samples. The variable content of oxyhornblende could suggest the action of crystal fractionation in the porphyry magma, but this phase is not present in the groundmass and may instead be xenocrystic.

Altered samples

Altered samples of the feldspar porphyry are enriched in potassium and copper relative to the fresh samples, suggesting that they may have equilibrated with a cooling volatile phase enriched in potassium and copper. Plagioclase is replaced either by K-feldspar or by white micas, replacements which would explain the trend in which calcium and strontium are depleted and potassium is enriched. The replacement of plagioclase by sericite was probably mediated by a fluid with a higher activity ratio of H^+:K^+ than the replacement of plagioclase by K-feldspar (Beane, 1982), and may have taken place at a lower temperature when acids, particularly HCl, would be more strongly dissociated.

Magnetite phenocrysts in samples of the groundmass-rich variant remain fresh while those in the samples exhibiting sericitic alteration have been sulphidised in a manner analogous to that observed in the sulphide-only samples of the monzogranite. This suggests that the activity of reduced sulphur increases as the fluid cools. This is most probably due to the disproportionation of SO_2.

5.3.3 Biotite geochemistry

The uniform composition of the biotite may suggest crystallisation under a relatively limited range of conditions (cf. Jacobs & Parry, 1979), but it could also just reflect rapid re-equilibration (c.f. Mason, 1978). Given that the other phenocrysts within the lithology appear to record changing melt characteristics, the latter interpretation is favoured.

5.3.4 Plagioclase zonation

Plagioclase phenocrysts within the feldspar porphyry can be divided into two groups, large and small. Small phenocrysts have been further subdivided into plateau, atoll and hiatal types, according to the nature of the zonation they display (c.f. Blundy & Shimizu, 1991).

The plateau type suggests crystallisation in a melt with a stable set of P-T-X properties. The atoll type develops in response to changes in the P-T-X properties of the melt such that the composition of plagioclase in equilibrium with the melt becomes more anorthitic, counter to the normal sequence of crystallisation. In contrast, the anorthite-rich core and anorthite-poor rim exhibited by phenocrysts of the hiatal type conform to the normal sequence of crystallisation, but the sharp break between core and rim indicates a period when the crystal was not growing. Phenocrysts of the hiatal type may represent the reintroduction of cumulate material into a more evolved melt (Blundy & Shimizu, 1991).

Comparison of the anorthite content of the cores and rims of the three types of phenocryst indicates that though the cores of each type of phenocryst are distinct, the rims are all of similar composition (~An_{35}). This suggests that each type of phenocryst initially crystallised from a melt of distinct P-T-X properties before a change to the system such that the equilibrium plagioclase composition became ~An_{35} and the rims crystallised. As the cores of each type possess distinct potassium contents, there is evidence for compositional variation within the system.

Since phenocrysts only record changes in the P-T-X properties of the melt that occurred while they were growing, the large plagioclase phenocrysts record longer periods in the evolution of the melt than the small phenocrysts. Additionally, rims commonly represent the crystallisation of interstitial melt and so may not record equilibrium growth (Blundy & Shimizu, 1991; Singer *et al.*, 1995). As such, they cannot be used to reliably infer changes in melt chemistry.

Of the two large plagioclase phenocrysts studied, one (259.9) exhibits successive zones with compositions of An_{25}, An_{30-35} and An_{40}, and a rim of >An_{40}. The progressive increase in anorthite content in the core is significant because it echoes the trend observed in the smaller phenocrysts. This suggests that the sharp changes in composition at the core-rim boundary observed in the smaller phenocrysts may reliably record changing melt properties. The other large phenocryst studied has a core exhibiting a series of sharp oscillations from An_{30} –An_{40}

(259.8), suggesting fluctuation in the properties of the melt with which this crystal was in equilibrium.

Assuming equilibrium crystallisation, the concentration of non-binary components in plagioclase can be related to their concentrations in the melt by means of a partition coefficient. Although the thermal and compositional dependencies of the partitioning behaviour of potassium between melt and plagioclase are not known, a suitable expression to describe this partitioning in dacitic melts is $D_K^{plag\text{-}melt} = 0.09$ (Singer *et al.*, 1995). Using this expression, the average measured values of K_2O in the cores of the small phenocrysts are calculated to correspond with melt potassium concentrations of 2.4% (hiatal), 6.0% (atoll) and 4.2% (plateau). Although the poor precision of the measurements of plagioclase potassium content limits the calculation of absolute concentrations of potassium within the melt, the relative changes are considered to be significant.

A similar exercise cannot be performed on one of the large phenocrysts studied (259.8) because the anorthite and potassium contents of the plagioclase show coincident, jagged trends; this strongly suggests the accumulation of potassium, an incompatible element in plagioclase, in the boundary layer of melt around the crystal during rapid crystallisation. In such cases the melt of the boundary layer and the bulk melt are not in equilibrium and inferences about the composition of the bulk melt cannot be made.

Certain zones of the other large phenocryst studied (259.9) are suitable for application of this technique. Six distinct zones are evident within the crystal and are termed A-F, from the core to the rim (Fig. 5.2). Zone A is normally zoned from An_{32} to An_{23}, and appears to have grown from a melt with a potassium content of ~3.5%. Zone B exhibits reverse zonation from An_{23} to An_{28}, and grew from a melt with a potassium content of ~5.5%. The transition from zone A to B is sharp, suggesting an abrupt change in potassium content of the melt. Zone C is characterised by a sharp change in anorthite content and so may reflect disequilibrium growth. The potassium content of the plagioclase in this zone cannot be reliably used to infer the potassium content in the bulk melt. Following a period of fluctuation at the start of zone D, the composition of the plagioclase and the concentration of potassium in the melt appear to settle at ~An_{34} and 4.5%, respectively. Zone E is characterised by a rise in the anorthite content of the plagioclase and a small increase in the potassium content of the melt to 5.5%. The rise in anorthite content persists in the rim (zone F) but the concentration of potassium in the melt appears to show a gradual decrease down to ~2%.

The calculated potassium content of the melt in equilibrium with zones A, B and D of the large plagioclase phenocryst are similar to the contents calculated from the cores of the hiatal (2.4%), atoll (6.0%) and plateau (4.2%) types of the group of smaller phenocrysts respectively. The cores of the smaller phenocrysts may represent nuclei that grew at the same time as the corresponding zone of the larger phenocryst.

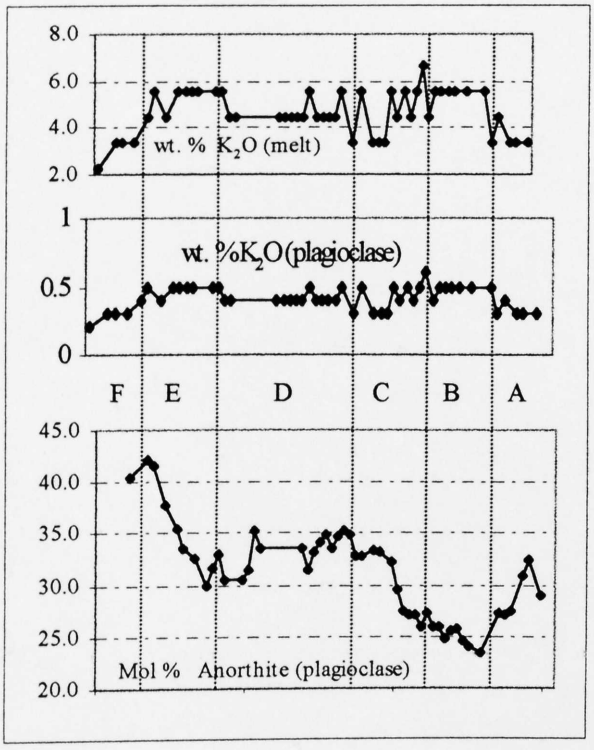


FIG. 5.2 Plot showing transects across plagioclase phenocryst 259..9 showing variation in anorthite content (bottom), measured K_2O in the plagioclase (middle) and calculated K_2O in the melt (top). See text for details.

In summary, the cores of plagioclase phenocrysts appear to record three distinct stages in the evolution of the magma chamber: an early stage during which the plagioclase composition changed from An_{40} to An_{25} and the potassium content of the melt increased from ~2.4% to ~3.5%; a transitory stage during which the plagioclase composition changed abruptly to An_{35-40}, accompanied by a rise in melt potassium to ~5.5-6%; and a final stage of stability during which the composition of plagioclase was An_{30-35} and the melt potassium content was 4.2-4.5%. Coincidence of a reversal in zonation and a sharp increase in the calculated potassium concentration of the melt suggests a causal relationship between the two.

The trend towards more anorthitic compositions could be explained by an increase in calcium on mixing with a more calcic melt of higher temperature, but the distinctive sieve-textured overgrowths produced when albite-rich plagioclase reacts with such melts (Tsuchiyama, 1985) were not observed during this study, suggesting that mixing did not occur. However, the rounded surfaces observed truncating compositional zonation in some of the phenocrysts, previously interpreted as resorption surfaces produced by simple dissolution (Tsuchiyama, 1985), do suggest heating of the magma.

Alternatively, the increasingly anorthitic equilibrium composition of plagioclase could be a response to an increasing H_2O concentration in the melt; this variable is thought to be the principal control of plagioclase composition in calc-alkaline magmas (Housh & Luhr, 1991).

Melt H_2O might be expected to increase in response to the crystallisation of anhydrous phases, but this would produce a gradual change in feldspar composition and is unlikely to have produced the atoll textures observed. Furthermore, it does not account for the abrupt shift to higher potassium concentrations within the melt, nor the increase in temperature suggested by the resorption surfaces. An alternative explanation for an increasing H_2O concentration in the melt would be the addition of a MVP from a hotter underplated magma. This could produce the sharp changes observed, account for the shift in melt potassium and explain the increasing temperature.

If it is assumed that that the introduction of a MVP was responsible for the changes observed, the three stages of melt evolution recorded by the plagioclase phenocrysts can be interpreted as follows:

(1) An early stage, representing closed system evolution of a magma, during which the anorthite content of plagioclase decreased while the potassium content of the melt increased from 2.5% to 3.5%. This would require the crystallisation of approximately 40% of the melt, with the crystallising assemblage excluding significant amounts of a potassium-bearing phase. K-feldspar is not present within the porphyry and biotite is only present in minor amounts, consistent with this interpretation.

(2) A transitory stage, representing the introduction of a MVP from an underplated magma, during which melt water and potassium contents rose sharply causing a reversal in the crystallisation sequence and the growth of anorthitic plagioclase rich in potassium.

(3) A third stage, characterised by stable conditions during which melt water and potassium contents appear to have remained constant. The apparent constancy of melt water and potassium contents during the third stage may imply the existence of a buffer for these species. A volatile phase would be an ideal buffer, since both water and potassium would partition into it. By inference, this capacity to buffer melt water and potassium contents was not present during the earlier stages of the evolution of the magma.

5.3.5 Isotope geochemistry

Fresh samples

The δD values of the biotite phenocrysts from samples of fresh feldspar porphyry are all similar, ranging from -70 to -80 ‰ (Table 2.4). These values are towards the depleted end of those normally found in granitic rocks (Nabelek *et al.*, 1983) and may indicate the feldspar porphyry magma underwent degassing. Variation in the δD value of biotite separated from different areas of the same dyke may suggest that different parts of dykes underwent different amounts of degassing.

Altered samples

Biotite within one of the samples of the groundmass-rich variant, all of which exhibit potassic alteration, has a higher δD value than biotite occurring in the fresh samples (-55‰ compared with an average of -76‰), but a similar $\delta^{18}O$ value. Biotite within samples exhibiting sericitisation has δD values slightly lower (average -68‰) than those of biotite within fresh samples, but displays markedly higher $\delta^{18}O$ values (average of 7.2‰ compared with an average of 5.7‰). The higher δD values of the altered samples compared with the fresh samples suggests that the altered samples equilibrated with a cooling fluid phase, consistent with their geochemistry.

Variation in $\delta^{18}O$ and δD values between the two groups of altered samples could be explained by the groundmass-rich samples having equilibrated with a single phase fluid and the samples exhibiting sericitic alteration having equilibrated with the brine component producted during phase separation of the same single phase fluid. During phase separation, isotopically heavy oxygen would partition into the brine (Truesdell, 1974; Horita *et al.*, 1995) explaining the higher $\delta^{18}O$ values of the sericitised samples, while deuterium would fractionate into the vapour (Horita *et al.*, 1995), thereby causing the δD value of the brine to decrease, and so explaining the lower δD values of the sericitised samples.

5.3.6 Fluid inclusions within the quartz phenocrysts

The presence of inclusions of type L and V, separated in salinity by type C inclusions but having similar homogenisation temperatures, suggests very strongly that the phenocrysts trap a supercritical fluid on the point of separation into a less saline vapour and a more saline brine. The salinity of the fluid before separation appears to have been ~15wt.% NaCl equiv.

Fluids of magmatic origin are typically thought to have such salinities (Rye, 1993; Hedenquist *et al.*, 1998).

If the fluid was undergoing separation, the measured homogenisation temperatures approximate the temperatures at which the inclusions were trapped. These temperatures (~400-500°C) are too low for the fluid to have been in equilibrium with melt. No evidence to indicate that melt was present at the time of fluid trapping, such as melt inclusions and/or devitrified glass (Ratajeski & Campbell, 1994) was found. It is therefore concluded that the inclusions have a secondary origin and are not primary as was initially thought. Previous studies of fluid inclusions in igneous quartz (e.g. Konnerup-Madsen, 1979; John, 1989; Ratajeski & Campbell, 1994) have also been hampered by an inability to determine primary and secondary inclusions due to the absence of growth zones and fracture planes.

In a fluid undergoing phase separation, homogenisation temperatures of type C inclusions define fluid pressure because the point of intersection of the critical isochore for a fluid of known salinity with the boundary of the two phase field has a unique pressure. Using the method of Knight & Bodnar (1989) for the NaCl-H_2O system, type C inclusions trapped within quartz phenocrysts indicate trapping pressures of 550-425 bars.

5.3.7 Summary

Although the feldspar porphyry exhibits little geochemical variation, the phenocrysts it contains appear to record changes in melt properties. These include heating, an increase in water and potassium contents and an increase in fO_2, all of which are consistent with the introduction of a MVP derived from a mafic magma. Evidence suggests that this MVP may have been introduced over a period of time during which the porphyry magma itself eventually became saturated with a volatile phase.

During dyking, the feldspar porphyry appears to have undergone varying degrees of equilibration with cooling volatiles: fresh samples are interpreted not to have equilibrated with a cooling volatile phase; groundmass-rich samples may have equilibrated with a single phase fluid; samples exhibiting sericitisation may record equilibration with the brine component of a volatile phase that underwent phase separation. Quartz phenocrysts within samples exhibiting sericitic alteration do trap fluids indicative of phase separation. Samples exhibiting sericitisation are significantly enriched in copper compared with the fresh porphyry dykes, suggesting that the fluids they equilibrated with were copper-rich.

5.4 Aplite and igneous breccia

5.4.1 Petrography

Aplite dykes with a texture and mineralogy equivalent to those at Quebrada Blanca occur in the Adamello Massif and were interpreted as representing interstitial melt, squeezed from an incompletely crystalline magma and focussed into dilatant fractures during the application of strain (John & Blundy, 1993; John & Stunitz, 1995). A similar origin for aplites has been proposed by many authors (see Vigneresse *et al.*, 1996, for a review). Aplite dykes at Quebrada Blanca cross-cut almost completely solidified monzogranite in which magnetite had been precipitated. As the crude graphic texture of the quartz and K-feldspar within magnetite-bearing samples is suggestive of the quenching of interstitial melt which appears to have been immobile, it follows that if it was interstitial melt which accumulated to form the aplite dykes, it must have been derived from a less-crystallised, more internal part of the chamber.

At Quebrada Blanca aplite dykes are commonly observed closely associated with the andesite dykes. It is possible that, rather than representing remobilised interstitial material, the aplite is a product of the efflux of volatiles from the andesite into the host monzogranite at high fluid:rock ratios. The introduction of heat and volatiles could have produce localised melting amd remobilisation of the monzogranite. The tongues of aplitic material observed may represent small diapirs of fluid-fluxed magma. Further from the contact zone the volatiles may be responsible for the pronounced potassic halos seen associated with the aplite; there is evidence to suggest that volatiles sourced from the andesite were extremely rich in potassium.

5.4.2 Biotite geochemistry

If the aplitic material does represent interstitial melt derived from a deeper part of the chamber than the samples of monzogranite bearing magnetite and this melt equilibrated with the same hydrothermal fluid as the magnetite-bearing samples, it follows that the aplitic material may record the effects of interaction between monzogranite and hydrothermal fluid at higher temperatures than in-situ samples occurring higher in the system. Biotite within the aplite has a similar composition to that in the magnetite-bearing samples of the monzogranite.

5.4.3 Summary

The aplitic material may represent interstitial melt derived from the monzogranite and remobilised during the application of strain. Alternatively, aplitic dykes could represent portions of the monzongranite which have interacted with volatiles derived from the andesite dykes as they intruded.

5.5 Relationships between lithologies

Convolute to flame-like contacts, entrainment and flow alignment of phenocrysts derived from the monzogranite within the andesite dykes and backveining of the dykes by the monzogranite all suggest contemporaneity of the andesite and monzogranite melts. The style of interaction suggests that at the level at which andesite dykes are observed, the monzogranite had a low melt fraction at the time of dyke intrusion (Pitcher, 1991). Such interaction represents mingling, in which magmas are brought into physical contact but remain distinct (Bateman, 1985).

Recent models of magma chamber crystallisation have predicted that chambers establish a stable stratification during equilibrium cooling, in which an upper layer of almost completely solid magma is separated from a lower layer of almost completely liquid magma by a thin crystallisation interval (e.g. Marsh, 1988). The feldspar porphyry may represent a sample of this liquid layer; similar dykes are considered to have sampled magma chambers concealed at depth in other studies (e.g. Shinohara & Hedenquist, 1997). The phenocryst assemblage of the feldspar porphyry records changes in melt properties which are consistent with it having originated as a felsic magma into which a MVP derived from a mafic magma was introduced, and exhibits evidence which suggests that, although it was initially undersaturated with respect to a volatile phase at the time the mafic-derived MVP was introduced, it became saturated at some point thereafter.

The absence of cross-cutting relationships between andesite and porphyry dykes could imply that they were intruded at the same time, an inference supported by the apparent contemporaneity of both these lithologies with the development of the breccias. Simultaneous hypabyssal dyking of two magmas of contrasting composition may suggest evacuation of a compositionally layered magma chamber (Cornejo *et al.*, 1997). It is conceivable that the andesite, perhaps pooled at the base of the felsic chamber, may have been the source of the volatiles supplied to the magma from which the dykes of feldspar porphyry crystallised (c.f. Eichelberger, 1980; Thomas *et al.*, 1993). Exsolution of volatiles

from mafic magmas pooled in felsic chambers has been seen by some as a prelude to mixing (Huppert *et al.*, 1982) while others have suggested that it may initiate eruption (e.g. Sparks *et al.*, 1977; Eichelberger, 1980; Tait & Jaupart, 1990). There is no textural evidence for mixing at Quebrada Blanca. Eruption, on the other hand, may preclude hypogene mineralisation (Hedenquist, 1995).

It is proposed that a period of time elapsed between introduction of the andesite magma to the monzogranite chamber and chamber evacuation. During this period, the dominantly liquid magma at the base of the chamber became saturated with respect to a fluid phase as volatiles were supplied to it from the andesitic magma. Following saturation, volatiles could pass from the hybridised layer into the dominantly solid portions of the monzogranite chamber. This latter supply of volatiles may have been responsible for the development of disseminated mineralisation.

Eventually, the build up of volatile pressure may have caused the dominantly solid portions of the chamber to rupture, allowing the more liquid portions and the andesitic magma to ascend as dykes. Dyking of the andesite and feldspar porphryry may have induced strain in the monzogranite, prompting the remobilisation of interstitial melt and thereby accounting for the intrusion of the aplite dykes and the formation of the igneous breccia. Alternatively, volatiles escaping from the ascending andesite dykes may have caused localised melting and mobilisation of the monzogranite where the two came into contact. Evacuation of the chamber is likely to have led to decompression of the system which may have caused the quenching evident within the monzogranite.

5.6 Summary

Variation within each of the three main lithologies at Quebrada Blanca, the monzogranite, the andesite and the feldspar porphyry, appears to be the result of varying styles of interaction between partially crystalline magma and one or more fluid phases.

1. Variation within the monzogranite can be attributed to equilibration between partially crystallised magma and a fluid rich in iron, potassium and copper. Samples from greater depths within the monzogranite appear to have equilibrated with this fluid at higher temperatures than those at shallower depths. Enrichment of the monzogranite in iron and magnesium at a late stage in its crystallisation suggests that this fluid was externally sourced, rather than derived in-situ as a result of crystallisation.
2. Evidence indicates that the andesite underwent degassing as it ascended as dykes through the monzogranite. Isotopic evidence is permissive for this stage of volatile loss having been the last event of a prolonged degassing history.

3. The feldspar porphyry may have interacted with two fluids of differing origin; the phenocryst assemblage of the feldspar porphyry records changes in melt properties which are consistent with the introduction of a fluid derived from a mafic magma, while differences between samples of the porphyry can be explained by varying degrees of interaction between the porphyry magma and cooling fluid following dyking.

A sequence of events, commencing with the introduction of a volatile-rich mafic magma to the base of a monzogranite chamber, has been proposed to account for the variation displayed by the three main lithologies and for the relationships between them. This is discussed in more detail in Chapter 7.

EVOLUTION OF THE HYDROTHERMAL SYSTEM AT QUEBRADA BLANCA

6

In this chapter, data presented in Chapter 3 relating to the veins and breccias comprising the hydrothermal system at Quebrada Blanca are interpreted. Before looking at the data for the various hydrothermal assemblages occurring at Quebrada Blanca, some of the general processes which may effect fluids following their exsolution from a melt are briefly reviewed.

6.1 Processes influencing the evolution of the MVP

6.1.1 Regimes of fluid flow associated with porphyry-copper deposits

When a melt becomes saturated with respect to a fluid phase bubbles of fluid are exsolved resulting in a mixture of two discrete phases. For this fluid phase to become concentrated sufficiently to produce the fracture-hosted hydrothermal assemblages associated with porphyry-type deposits, movement of the fluid phase relative to the melt is required: if the bubbles fail to migrate relative to the melt as the system cools, the fluid phase becomes trapped where it may later produce disseminated alteration/mineralisation when the system cools sufficiently below its solidus (Candela, 1991).

Previous studies have suggested that movement of the fluid phase relative to the melt only occurs at relatively high volatile fractions, either by the migration of large bubbles (Shinohara & Kazahaya, 1995) or by advection of fluid through coalesced bubble volumes, termed spanning clusters (Candela, 1991). In either case, the transfer of fluid to the boundary between the melt-present and subsolidus parts of the chamber is thought to be episodic, reflecting the time required to accumulate bubble volume.

At temperatures above 400°C, the approximate temperature of the brittle-ductile transition (Fournier, 1992), the subsolidus parts of the chamber and any country rock overlying the intrusion behave in a plastic fashion with a rheology dependent on the rate at which strain develops. The pulses of fluid from the magma chamber may induce strain sufficiently rapidly to cause this plastic material to fail in a brittle manner, allowing the formation of fractures. Fractures which propagate through the brittle-ductile transition may vent to the surface and mineral assemblages will develop in a hydrostatic pressure regime.

6.1.2 Phase relations in evolving magmatic fluids

Fluids of magmatic origin typically have salinities of 10-15 wt.% NaCl equiv. (Rye, 1993; Hedenquist *et al.*, 1998) and so will exist as supercritical, vapour-rich fluids at magmatic temperatures and pressures greater than ~550bars (Sourirajan & Kennedy, 1962). As the fluid ascends, it may undergo both cooling and decompression. Cooling causes the vapour-rich fluid to increase in density until it passes through its critical isochore and becomes liquid-rich, a process that is commonly, and will hereafter be, referred to as condensation (Path C; Fig. 6.1). Decompression causes the vapour-rich fluid to undergo separation into a more dilute vapour and a more saline brine (Path B; Fig. 6.1). Although strictly termed condensation, this process will be referred to as phase separation. The term boiling is used only for the separation of a liquid-rich fluid into a more dilute vapour and a more saline brine.

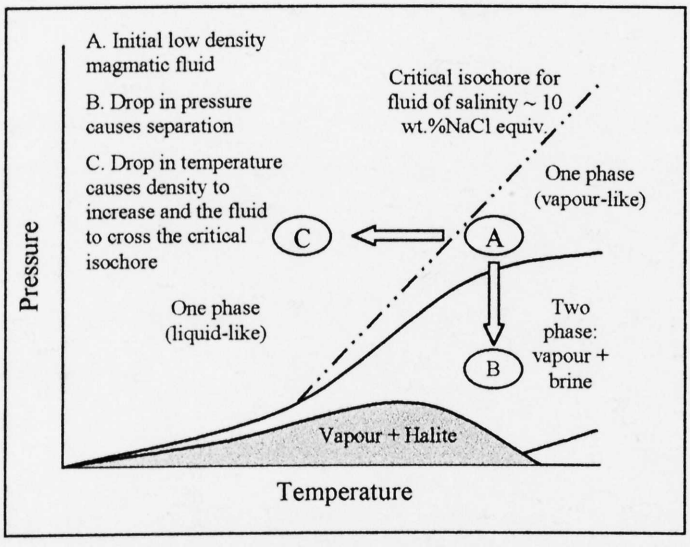


FIG. 6.1 Schematic pressure-temperature diagram showing phase relations in an evolving magmatic fluid (after Bodnar, 1995).

6.2 Early stage veins

6.2.1 Petrography

Type 1 veins

With their branched nature, diffuse margins and quartz-K-feldspar composition, type 1 veins are comparable with descriptions of fluid-rich interstitial melt focussed in fractures at a submagmatic stage (Hibbard, 1980). Alternatively, type 1 veins may represent an incipient stage in the development of a spanning cluster (Candela, 1991), a development perhaps halted by a failure to achieve sufficient fluid volume. The accumulated fluids would become trapped *in-situ* where they would deposit their mineral content as the rockmass surrounding them cooled.

Preservation of anhydrite in these veins suggests that they do represent closed pockets of fluid because anhydrite exhibits retrograde solubility (Rimstidt, 1997) and is best preserved

where it is isolated from subsequent fluid flow. Anhydrite solubility decreases with pressure, but it is unlikely that type 1 veins experienced abrupt decompression during their formation; the zonal texture of the quartz in these veins suggests that they developed in a stable environment from a fluid only slightly saturated with respect to silica (Dong *et al.*, 1995). Anhydrite may have precipitated in response to rising sulphate concentrations produced by the disproportionation of SO_2 as the trapped fluid cooled.

Type 2 veins

The morphology of type 2 veins suggests that they formed entirely within the brittle regime. The precipitation of K-feldspar in these veins may suggest that they experienced a sharp drop in confining pressure (Eqn. 6.1; Shinohara, 1991).

$$\underset{\text{High pressure}}{KAl_3Si_3O_{10}(OH)_2} + 6SiO_2 + 2KCl \leftrightarrows \underset{\text{Low pressure}}{3KAlSi_3O_8} + 2HCl \qquad (6.1)$$

6.2.2 Fluid inclusions

Type 1 veins

Type 1 veins contain two groups of type L inclusions, one saline and one dilute, which homogenise at similar temperatures. The absence of type V inclusions suggests that the inclusions in these veins do not represent trapping of a fluid undergoing phase separation but it is possible that they trapped two fluids previously produced by phase separation at greater depth, with the dilute inclusions representing a vapour condensate. Mixing between brine and condensate would account for inclusions with salinities intermediate to those of the two groups lacking elevated homogenisation temperatures.

Fluid inclusion temperatures are inconsistent with the hypothesis that type 1 veins represent pockets of fluid initially accumulated at near magmatic temperatures; they are too low. Such pockets of fluid may have long cooling histories compared with veins, however, and it may be that inclusions were only trapped in the latter stages of mineral precipitation. The trend to lower temperatures at almost constant salinity exhibited by the saline inclusions in these veins implies that the brine cooled and decompressed simultaneously. This would be consistent with a protracted period of cooling.

Type 2 veins

Type 2 veins contain two groups of inclusions, one saline and one dilute. In some veins the dilute inclusions are of type V but in others they are of type L. Dilute type V inclusions homogenise at higher temperatures than dilute type L inclusions and all dilute inclusions homogenise at higher temperatures (>50°C) than the saline inclusions with which they coexist. The presence of type V inclusions of similar salinity but higher homogenisation temperature than type L inclusions strongly suggests the trapping of a vapour and a vapour condensate respectively. The coexistence of saline inclusions with either vapour or vapour condensate suggests trapping of a fluid that has undergone phase separation at some point in its evolution but was not necessarily doing so at the time of trapping.

These observations are consistent with type 2 veins having formed in a thermal plume-like environment (Henley & McNabb, 1978). Where conduits occupied by vapour-brine mixtures are open to the surface, they may act as reflux columns; vapour that ascends to the cooler parts of the system condenses and the condensate drains back down the conduit where it may mix mechanically with the residual brine and/or with fresh influxes of vapour-rich fluids (Fig. 6.2).

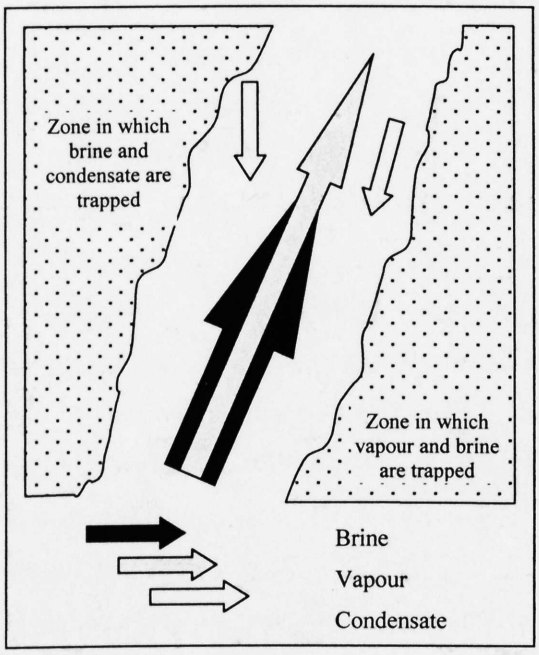


FIG. 6.2 Schematic diagram showing the proposed environment of formation of type 2 veins (after Henley & McNabb, 1978).

6.2.3 Oxygen isotopes

Type 1 veins

Previous studies have noted that the $\delta^{18}O$ values of quartz in veins with characteristics similar to type 1 veins at Quebrada Blanca and located within the potassic zone were similar to those of igneous quartz, suggesting equilibration between fluid and wall-rock (Sheppard & Gustafson, 1976; Bowman *et al.*, 1987). Equilibration with the wall-rock makes it impossible to determine the initial isotopic composition of the fluid in these veins and so draw comparisons between these fluids and subsequent fluids which may not have been buffered isotopically by the surrounding rock.

Type 2 veins

The measured $\delta^{18}O$ values of the quartz in type 2 veins range from 8.7‰ to 10.3‰ and average 9.5‰. Magnetite separates from two samples average 2.5‰. If quartz and magnetite are assumed to have coprecipitated, $\Delta^{18}O_{quartz\text{-}magnetite}$ can be related to the temperature at which they formed. Using average values, $\Delta^{18}O_{quartz\text{-}magnetite}$=7‰, a temperature of ~590°C is calculated, according to the fractionation equation of Zheng (1995). If this temperature is used for the fractionation between fluid and quartz, the calculated fluid composition is ~8.0‰ (Matsuhisa, 1979).

The isotopic temperature is ~200°C higher than the homogenisation temperature of the fluid inclusions in these veins. These inclusions are not thought to trap a boiling fluid and the homogenisation temperatures represent minimum trapping temperatures; the true temperature of trapping could be substantially higher. A trapping temperature of 590°C would indicate a minimum trapping pressure of ~1.3 kbar for a fluid with a salinity of ~7wt.% NaCl equiv. (Zhang & Franz, 1987), a depth of ~5km under lithostatic conditions. Late stage veins are seen to cross-cut type 2 veins and record substantially lower pressures (see below). Although the removal of 3-4 km of overburden between the development of type 2 and late stage veins is possible, it seems more probable that quartz and magnetite were not precipitated in equilibrium. This may reflect rapid precipitation or precipitation at different times. If the fluid inclusion temperature (average ~375°C) is used for the fractionation between fluid and quartz, the calculated fluid composition is ~5.0‰ (Matsuhisa, 1979).

6.2.4 Sulphur isotopes

Type 1 veins

Sulphides in type 1 veins have $\delta^{34}S$ values close to 0.0‰, similar to those seen in late stage veins. Previous studies of sulphides in veins with properties similar to those of type 1 veins have suggested that the $\delta^{34}S$ values of the sulphides these veins contain reflect varying degrees of equilibration between sulphide and sulphate following SO_2 disproportionation (Field & Gustafson, 1976; Shelton & Rye, 1982; Kusukabe *et al.*, 1984). It is possible, therefore, that the measured value of type 1 vein sulphide at Quebrada Blanca is not related to $\delta^{34}S_{(fluid)}$ by an equilibrium fractionation and consequently cannot be compared with $\delta^{34}S_{(fluid)}$ calculated for other vein types.

Type 2 veins

Chalcopyrite in one of the type 2 veins (93) has a $\delta^{34}S$ value of +3.0‰ while pyrite in another (123) has a $\delta^{34}S$ value of -2.6‰. Both sulphides are in intimate association with magnetite. The higher value may be explained by the precipitation of chalcopyrite prior to the disproportionation of SO_2 and the production of isotopically light H_2S. The light pyrite may have been produced during the sulphidation of magnetite, a process which has been suggested to occur in magnetite veins within other deposits (Zweng & Clark, 1995). This process may have occurred after the disproportionation of SO_2, incorporating sulphur derived from the low $\delta^{34}S_{(H2S)}$ reservoir, a process consistent with the temperatures recorded by fluid inclusions.

Disproportionation is driven by cooling and so its effects on the sulphur reservoir might be expected to be more pronounced within examples of type 2 veins in which the vapour phase is interpreted to have condensed. This seems to be the case; the sample with isotopically heavy sulphide (93) contains inclusions which trap vapour and brine while the sample with isotopically light sulphide (123) contains inclusions interpreted to trap condensate and brine.

6.2.5 Evolution of early stage hydrothermal assemblages

Environment of formation

The nature of type 1 veins at Quebrada Blanca is consistent with them having initiated in an environment in which melt was present. It is possible that they represent pockets of accumulated fluid that failed to migrate to more brittle portions of the chamber before their host rocks cooled and they became trapped. Type 2 veins may have been precipitated from fluids which ascended sufficiently rapidly to induce fracturing in the plastic material and then breach the brittle-ductile transition. Such fluids are likely to decompress quickly relative to the rate at which they cool, promoting phase separation.

Relationships between early stage hydrothermal assemblages

The two vein types comprising the early stage of vein development at Quebrada Blanca do not appear to share a common mode of formation. Although there is no evidence to suggest that the two vein types represent different stages in the evolution of a single fluid, it is possible that they did precipitate from fluids of similar composition; type 1 veins may have precipitated from a static fluid while type 2 veins clearly precipitated from a migrating fluid.

6.3 Late stage hydrothermal assemblages

6.3.1 Petrography

Breccias

The predominant texture of the hydrothermal breccia at Quebrada Blanca (tabular/cuspate clasts showing little movement relative to each other) strongly suggests that it formed in response to decompressive shock (Fletcher, 1977). This condition develops when volatile-rich fluids escape from overpressured zones (Norton & Cathles, 1973).

The earliest assemblage to be precipitated in the hydrothermal breccia consists of quartz and molybdenite. Experimental evidence suggests that molybdenum is not complexed by sulphur or halides in solution (Candela & Holland, 1984; Tingle & Fenn, 1984) occurring instead as molybdate (e.g. H_2MoO_4; Bernard *et al.*, 1990). The solubilities of other salts of oxyanions such as sulphates (Dickson *et al.*, 1963) and tungstates (Polya, 1990) have been shown to exhibit a positive pressure dependency and molybdate might be expected to behave in a similar manner. Consequently, the deposition of molybdenite may have been triggered by a drop in fluid pressure, consistent with the textural evidence relating to the mode of brecciation.

The assemblage quartz+pyrite appears to post-date the quartz+molybdenum assemblage. The transitional nature of the two assemblages suggests that they were precipitated from an evolving fluid. Pyrite precipitation is unlikely to be a response to decompression (Hemley & Hunt, 1992), but decompression may trigger phase separation and the loss of acid volatiles, promoting the fixation of iron in solid phases (Whitney *et al.*, 1985). The tourmaline seen to accompany sulphides in the breccia matrix is also unlikely to have precipitated in response to sudden decompression (London & Manning, 1995) and it has been postulated that its deposition may reflect the addition of aluminium to the evolving magmatic fluid during acid leaching (Zweng & Clark, 1995). The sericitic alteration of the clasts in the breccia suggests the presence of an acid-rich fluid.

Acid leaching is likely to have been responsible for the formation of the quartz-dominated assemblage seen in the uppermost exposures of the breccia column. This has the characteristics of vuggy silica zones formed by acid leaching seen both in modern hot spring environments, where the acidity is generated by the near-surface oxidation of H_2S, and in high sulphidation epithermal deposits, where the acidity is produced by the disproportionation of SO_2 of magmatic origin (Stoffregen, 1987; Hedenquist *et al.*, 1994). In

HSE deposits, vuggy silica breccias are thought to form within 500m of the surface and may have vertical extents of several hundred metres. Vuggy breccias formed in the near surface environment typically have thicknesses of less than 50m (Stoffregen, 1987). The true thickness of the vuggy silica at Quebrada Blanca is not known.

Vein types 3, 4 and 5a

Vein types 3, 4 and 5a exhibit similar morphologies; they have sharply defined margins but are commonly plastically deformed. This suggests that the veins formed under conditions of brittle failure but were later subjected to more distributed strain, a situation only likely to develop in material below the brittle-ductile transition.

Quartz in vein types 3, 4 and 5a has a mosaic texture, a common texture in the porphyry environment (Dowling & Morrison, 1990). In type 3 veins and some type 4 veins, mosaic quartz is coarse but in other type 4 veins and all type 5a veins both fine-grained and coarse-grained mosaic quartz is present. Where fine-grained quartz is present, it occupies the vein margins. The banding that results is similar in appearance to the crustiform texture produced during multiple fracture-seal events (Dong *et al*, 1995) and suggests the occurrence of two phases of quartz deposition.

The presence of subgrains at the contacts between coarse quartz grains in the cores of type 5a veins may be evidence of annealing. During experimental studies of quartz annealing, it has been observed that fine grains recrystallise on coarser grains to form large, optically continuous crystals (Masuda *et al.*, 1997). Consequently, the coarse quartz in the cores of vein types 4 and 5 could be the product of annealing of finer-grained quartz. Subgrains may not have been preserved in type 4 veins; they are dominated by coarse, equant grains exhibiting 120° triple boundaries, an equilibrium texture which suggests annealing may have been more complete.

During annealing, fine grained quartz dissolves in intergranular fluid before being reprecipitated. Impurities in the dissolved quartz become concentrated in the intergranular fluid and may eventually inhibit annealing by preventing quartz dissolution (Tullis & Yund, 1982). The precipitation of these impurities from the intergranular fluid at some later stage would account for the presence of opaque phases at the grain boundaries within type 4 veins. This characteristic has been noted in other veins thought to have annealed (Williams & Bauer, 1995).

EPMA traverses across veins of types 4 and 5a reveal that coarse-grained quartz has a low concentration of trace elements compared with fine-grained quartz and that the transition between the two textures is marked by a sharp increase in trace element content. Such variation is consistent with impurities in fine-grained primary quartz being removed during the annealing process and concentrated at annealing fronts (Fig. 6.3), but could also be the product of the deposition of minute amounts of a mineral phase (perhaps a mica) at the boundary between the two types of quartz.

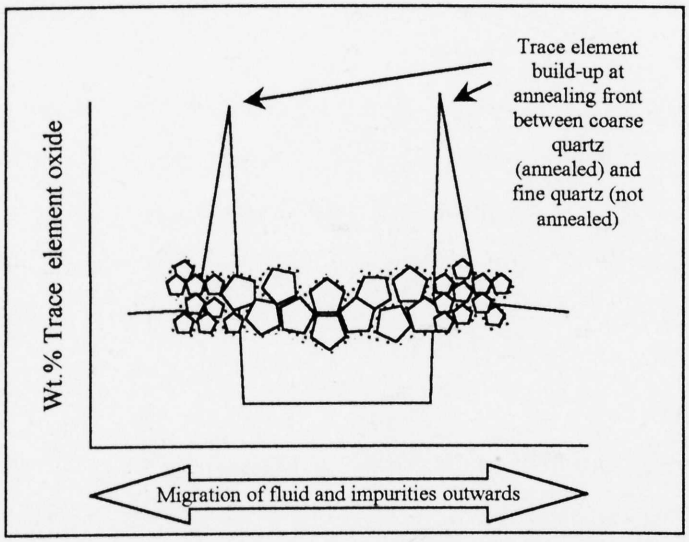


FIG. 6.3 Schematic EPMA trace across a vein exhibiting a core of coarse quartz and margins of fine quartz, interpreted to be the product of annealing and representative of the primary, and depositional texture respectively.

K-feldspar is present as a gangue phase in addition to quartz in type 3 veins. As noted for type 2 veins, the precipitation of K-feldspar may be a response to declining pressure. Although K-feldspar is observed in both types of early stage vein, it is not seen in any of the other late stage veins. This may suggest that type 3 veins have a mode of formation which is more similar to that of early stage veins than that of late stage veins.

Wall-rock fragments in type 5 veins may suggest that abrupt decompression accompanied vein formation (cf. Cooke & Bloom, 1990) in a manner analogous to that proposed for the breccias. The presence of molybdenite at the boundary between the two quartz textures in type 5 veins is also consistent with the veins having undergone decompression (see section 6.3.1). A large drop in pressure may significantly decrease quartz solubility, despite the high temperatures of the fluids from which these veins are thought to precipitate (Fournier, 1985; Herrington & Wilkinson, 1993). Rapidly precipitated quartz would be fine grained and an ideal substrate for annealing (Masuda *et al.*, 1997).

Vein types 5b and 6

Vein types 5b and 6 are not observed to be plastically deformed and may have formed entirely within the brittle region. Type 5b veins have margins of fine-grained mosaic quartz

identical to those seen on type 5a veins but have cores filled with a mixture of pyrite, quartz and chalcedony. Type 6 veins have an identical mineralogy and texture to the cores of type 5b veins, though chalcedony is not seen in all samples.

Quartz within vein types 5b and 6 locally exhibits interpenetrating grain boundaries which suggest it may have recrystallised from a non-crystalline precursor (Saunders, 1990), a process which is favoured by time and temperature and not specifically pressure (Fournier, 1985). The transition from margins of fine grained quartz to cores which contain chalcedony, as displayed by type 5b veins, suggests precipitation of silica from a solution increasingly supersaturated with respect to silica.

Type 6 veins in which the quantity of quartz exceeds that of pyrite display selvedges of sericite. These are not observed on the type 6 veins in which the quantity of pyrite exceeds that of quartz. In this latter subtype the small amounts of quartz that are present overgrow wall-rock quartz. Both subtypes exhibit sericitic alteration halos, suggesting the fluids they precipitated from were acidic. Increasing acidity may be responsible for the transition between the two subtypes since it inhibits quartz precipitation (Muntean *et al.*, 1990).

6.3.2 Reliability of fluid inclusion data

Vein types 3, 4 and 5a

Care must be taken when interpreting fluid inclusions present in quartz which is thought to have annealed; inclusions only preserve the density of the fluid from which their host mineral precipitated if their volume remains constant, and grain boundary migration during annealing has been found to destroy pre-existing inclusions and lead to the formation of new ones (Johnson & Hollister, 1992). In such cases, fluid densities may reflect the conditions of annealing rather than primary precipitation. Inclusions containing the grain boundary fluid which facilitates recrystallisation might also form during annealing.

Petrographic observations suggest that the quartz in the cores of type 5a veins may have annealed; that on the margins probably did not. Both regions of quartz host type V inclusions with similar properties, suggesting that these inclusions are unaffected by annealing. This may be because these inclusions are trapped close to their critical volume (Table 6.1); only a slight increase in density, or mixing with a small amount of saline liquid, would be required to force these inclusions to change their mode of homogenisation from type V to type L. Consequently, where there is evidence that type V inclusions trapped a fluid close to its

critical volume, these inclusions are considered to preserve the composition and density of the fluid from which the quartz grew, regardless of the presence of textural evidence for annealing.

Type L inclusions with similar properties to those of the type V inclusions in type 5a veins may be the product of annealing rather than of condensation or heterogeneous entrapment. Petrographic observations suggest that type 4 veins are also variably annealed. Samples of this vein type exhibit variation in the homogenisation nature of the low salinity inclusions they contain, from solely type V, through a mix of types L and V, to solely type L. The vein hosting the low salinity inclusions which are all of type L is one of those which, according to its EPMA trace, appears to have annealed completely (122) suggesting that annealing may have been responsible for the changes. Entrapment of a condensate of the vapour-phase present in type V inclusions cannot be ruled out for the samples in which low salinity type L inclusions have a similar salinity to these type V inclusions but generally homogenise at substantially lower temperatures.

TABLE 6.1 Critical temperatures of fluids trapped in type V inclusions within late stage veins.

Vein type	Sample number	wt % NaCl equiv	T_h (°C)	Critical point (°C)	Density g/cc
3	273	3.8	386	409	0.54
	285	4.8	396	419	0.54
4	151	9.2	446	459	0.50
	82	7.2	411	441	0.55
5	average	4.3	398	414	0.52

Vein types 5b and 6

Petrographic characteristics suggest that some of the quartz present in vein types 5b and 6 may have recrystallised from a metastable precursor, another process which may influence fluid inclusion properties. Sander & Black (1988) contested that fluid inclusions within zones arising from the recrystallisation of chalcedony do not accurately reflect conditions of primary silica deposition. However, Kamilli & Ohmoto (1990) found that there was no difference in the homogenisation temperatures or calculated salinities of inclusions in plumose and adjacent non-plumose quartz. They did note that recrystallisation would tend to homogenise distinct fluid populations, though evidence of necking would be expected to be preserved as an indicator of this process. Saunders (1990) found that quartz that had recrystallised generally lacked fluid inclusions and, for this reason, quartz hosting fluid inclusions in vein types 5b and 6 is thought to have precipitated as quartz. The chalcedony observed in these veins is inclusion-free.

6.3.3 Fluid inclusions

Vein types 3, 4 and 5a

Fluid inclusions in vein types 3, 4 and 5a share similar properties. Two groups of inclusions are present, one saline and one dilute. In some veins the dilute inclusions are of type V but in others they are of type L. Both may contain chalcopyrite daughters. Type V inclusions have properties similar to coexisting type C inclusions and typically exhibit semi-critical homogenisation. Dilute type V inclusions homogenise at slightly higher temperatures than dilute type L inclusions and all dilute inclusions homogenise at higher temperatures (>50°C) than the saline inclusions with which they coexist. Saline inclusions may homogenise either by vapour disappearance or by halite dissolution and there is an overlap in temperature between the two styles of homogenisation.

Amongst the saline inclusions, overlap of the lowest temperatures of daughter dissolution with the range of liquid-vapour homogenisation temperatures suggests heterogeneous trapping of a saturated solution undergoing phase separation (Ramboz *et al.*, 1982). The presence of both type L and type V inclusions also suggests that fluid trapped in vein types 3, 4 and 5a may have undergone phase separation. Saline inclusions in vein types 3, 4 and 5a typically have salinities of ~30 wt.% NaCl equiv. and homogenisation temperatures of ~350°C. According to published data on the P-T-X properties of NaCl-H_2O fluids (Sourirajan & Kennedy, 1962; Bodnar *et al.*, 1985), the salinity of the vapour in equilibrium with such saline fluids should be negligible, which is clearly not the case (Table 6.1).

Although type V inclusions in these veins could be the product of the heterogeneous entrapment of dilute vapour and saline brine, a common occurrence where fluids are undergoing phase separation (Ramboz *et al.*, 1982), and one which would account for the elevated homogenisation temperatures of the type V inclusions, type V inclusions in vein types 3, 4 and 5 all appear to be trapped close to their critical points (Table 6.1). The consistent nature of this relationship argues against these fluids having been heterogeneously trapped.

The phenomenon of type V inclusions trapped close to their critical points and with homogenisation temperatures greater than those of coexisting type L inclusions has been noted at other porphyry-associated deposits (e.g. Ahmad & Rose, 1980). Fluid inclusion data presented for a molybdenite-bearing vein at Bingham (Roedder, 1971), similar to those of vein types 3, 4 and 5a at Quebrada Blanca, were interpreted by Bodnar (1995) to record the trapping of a vapour-rich fluid both before and after it had intersected the two-phase field

boundary (Fig. 6.1). He suggested that inclusions trapped in the one-phase field near the critical isochore would exhibit semi-critical homogenisation and so be distinct from type V inclusions produced by phase separation in the two-phase field.

Type V inclusions within vein types 3, 4 and 5a typically exhibit a semi-critical style of homogenisation and so, following Bodnar (1995), are proposed to have been trapped in the one phase field close to their critical isochore. The presence of chalcopyrite daughter minerals in these inclusions may indicate that they trap a magmatic fluid that has failed to undergo separation; it has been suggested that such a fluid is much more likely to contain daughter minerals than low-density fluids produced by phase separation (Bodnar, 1995).

Saline type L inclusions in vein types 3, 4 and 5a may trap the brine phase produced during phase separation of a single-phase low density fluid. Mass balance suggests that the products of such separation will be dominated volumetrically by the low salinity phase (e.g. Shinohara & Hedenquist, 1997), but this dilute vapour does not appear to have been trapped. This could reflect the differing wetting properties of the two fluids (Hedenquist *et al.*, 1992). Alternatively, it is possible that the dilute vapour mixed with magmatic vapour that had failed to undergo phase separation, producing the trend defined by type V inclusions within vein types 3, 4 and 5a in which salinity decreases with homogenisation temperature (Fig. 6.4). This is discussed further in section 6.3.6.

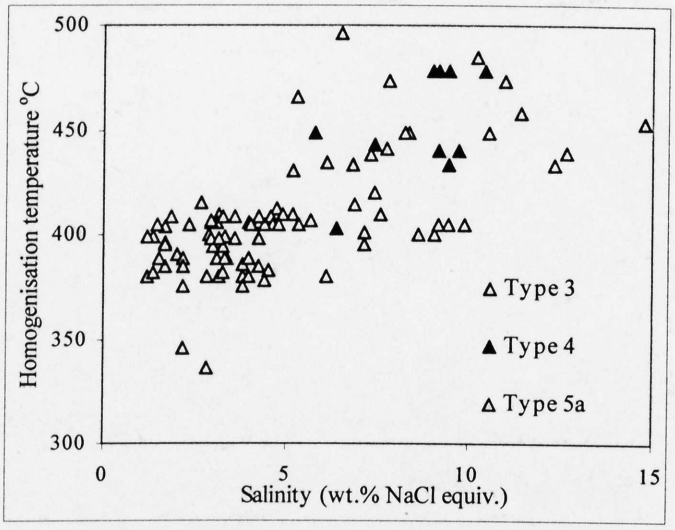


FIG. 6.4 Scattter plot of homogenisation temperature vs. salinity for type V inclusions in vein types 3, 4 and 5a.

Petrographic evidence suggests that veins of types 4 and 5 may have experienced abrupt decompression. Type C fluid inclusions are common in the late stage veins at Quebrada Blanca and can be used to infer trapping pressures. In a fluid undergoing phase separation, homogenisation temperatures of type C inclusions define fluid pressure because the point of intersection of the critical isochore for a fluid of known salinity with the boundary of the two phase field has a unique pressure. Fluid inclusion evidence suggests that type C inclusions in late stage veins at Quebrada Blanca may have been trapped as a low-density fluid passed from a vapour-like state through its critical isochore into a liquid-like state. As such, type C

inclusions may not have coexisted with a boiling fluid and so the pressure they indicate is strictly a minimum pressure.

Using the method of Knight & Bodnar (1989) for the $NaCl-H_2O$ system and the properties of type C inclusions, minimum formation pressures of the late stage veins have been calculated (Table 6.2). The calculated pressures range from 500 bars in type 3 veins to 250 bars in type 5a veins, and generally decrease through the paragenesis. The presence of type C inclusions indicating different pressures in individual veins supports the concept of veins forming in an environment in which the fluid pressure fluctuated. Petrographic evidence suggests that some of these veins formed in the ductile regime so P_{fluid} approximates $P_{lithostatic}$. Taking an average rock density of 2.6-2.7 g/cc, the pressures recorded by late stage veins suggests that they formed over a depth range of ~1-2 km. There is insufficient stratigraphic information available at Quebrada Blanca to indicate the depth, and hence pressure, at which the system formed, and so corroborate these estimates.

TABLE 6.2. Minimum formation pressures of late stage veins.

Vein type	Wt % NaCl equiv.	T_h (°C)	Pressure (bars)[1]
3	14	488	500
	7	438	385
4	9	456	440
5a margin	9	448	415
Core	2	386	250
5b margin	2.5	395	265
Core	4.5	399	275
6	4.3	394	270

[1] Subject to an error of ~20 bars (Knight & Bodnar, 1989)

Vein types 5b and 6

Fluid inclusions hosted in the marginal quartz of type 5b veins have properties identical to those trapped in type 5a veins. Fluid inclusions within the cores of type 5b veins are identical to the dilute type V inclusions present in type 5a veins and are interpreted to have had a similar origin, i.e. they trap a low density fluid in the one phase field close to its critical isochore.

Neither highly saline nor type V inclusions are present in type 6 veins. Low salinity inclusions in these veins define a trend in which salinity decreases with homogenisation temperature. The most saline inclusions on this trend are type C inclusions, the properties of which overlap with those of type C inclusions in vein types 5a and 5b. This trend could be the result of the vapour-rich fluid seen in vein types 5a and 5b having passed from a vapour-like state through its critical isochore into a liquid-like state (Fig. 6.1). Dilution of the magmatic fluid appears to have continued following this change of state.

6.3.4 Oxygen isotopes

The measured isotopic composition of vein quartz can be related to the isotopic composition of the fluid from which it precipitated by a temperature dependent fractionation factor. Calculated isotopic compositions of water in equilibrium with late stage veins are given in Table 6.3. Using the quartz-water fractionation of Matsuhisa (1979), compositions were calculated at the temperatures recorded by fluid inclusions in each vein. Where two fluids of differing temperatures were present, two compositions were calculated. The two values determined represent a range of possible values of $\delta^{18}O_{(fluid)}$.

TABLE 6.3. Calculated $\delta^{18}O$ of fluids in equilibrium with vein quartz.

Vein Type	$\delta^{18}O$ Measured	$\delta^{18}O_{(fluid)}$‰ calculated using: Min. fluid temperature	Max. fluid temperature
3	9.9	4.5	6.0
4	10.0	4.5	6.2
5a/b (margin)	10.5	5.4	6.5
5a (core)	10.5	5.4	6.5
5b (core)	17.8	6.2 [1]	13.7 [2]
6	11.5	6.8	

[1] Temperature of chalcedony precipitation (Arribas *et al.*, 1995)
[2] Temperature of type C inclusions

The range of $\delta^{18}O_{(fluid)}$ calculated for vein types 3 and 4 are very similar and overlap with that of type 5 veins. The almost identical measured $\delta^{18}O$ values of quartz from the margins and cores of type 5a veins (Table 6.3) suggests that the two regions of quartz were precipitated from a fluid of similar temperature. Vein types 5b and 6 continue a general trend in which $\delta^{18}O_{(fluid)}$ becomes higher moving through the paragenesis.

In contrast with type 5a veins, the $\delta^{18}O$ values of chalcedony from the cores of 5b veins are much higher and suggest final equilibration between quartz and fluid at a temperature of ~200°C, assuming the fluid had the same isotopic value as that from which the margins were precipitated (Fig. 6.5). This is close to the temperature at which chalcedony is thought to begin to precipitate (Fournier, 1985; Muntean *et al.*, 1990; Arribas *et al.*, 1995).

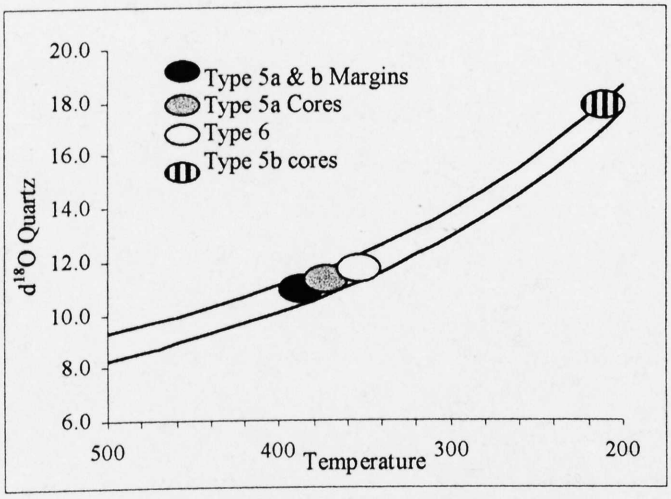


FIG 6.5 Schematic graph of measured $\delta^{18}O_{(quartz)}$ vs. temperature (°C) for veins types 5 and 6. Curves show equilibrium $\delta^{18}O_{(fluid)}$ values of 6‰ (lower) and 7‰ (upper).

For such an extreme enrichment in isotopically heavy oxygen to develop, an efficient mechanism to remove isotopically light oxygen must have been present. Boiling followed by the removal of a low-density phase would be a mechanism to extract isotopically light oxygen because vapours are enriched in isotopically light oxygen relative to the residual brines (Truesdell, 1974; Horita *et al.*, 1996). Fluid inclusion evidence suggests that such a process may have occurred. The quartz margins seen to jacket the cores of type 5b veins may have acted as a barrier to any diffusion of isotopically light oxygen from the wall-rock.

6.3.5 Sulphur isotopes

Sulphur isotope fractionation between H_2S in solution and molybdenite and pyrite is almost identical (Ohmoto & Goldhaber, 1997) so the $\delta^{34}S$ values of the sulphides should be comparable if it is assumed that both sulphides precipitated at the same temperature. With the exception of pyrite from a type 3 vein which has a $\delta^{34}S$ value of 0.0‰, pyrite and molybdenite from vein types 5a, 5b and 6 have identical values of +0.6‰ within error. This suggests the existence of a stable $\delta^{34}S$ reservoir during precipitation of these veins.

Fluid inclusions trapped in late stage veins appear to record the dilution of a single-phase low-density fluid. The diluent must either have had a similar $\delta^{34}S$ to the fluid being diluted, or have had an insignificant sulphur content; otherwise the $\delta^{34}S$ values would show more variation between veins that have undergone differing degrees of dilution.

6.3.6 Evolution of late stage hydrothermal assemblages

Environment of formation

Hydrothermal breccias at Quebrada Blanca record the abrupt decompression of an overpressured, fluid-bearing zone. Vein types 3, 4 and 5 also record fluctuating pressure conditions. It is proposed that the late stage hydrothermal assemblages at Quebrada Blanca precipitated from fluid of magmatic origin which failed to ascend to the surface and, for a period of time, became trapped in the zone of material below the brittle-ductile transition at depths of 1-2km. A sequence of events is envisaged as follows:

1. A pulse of fluid from the magma chamber induces strain sufficiently rapidly to fracture the plastic material below the brittle-ductile transition. The fluid undergoes decompression, initiating phase separation and quartz precipitation. The products of phase separation become physically separated due to their differing densities. The vapour ascends to higher levels than the brine where it encounters increasingly cooler wall-rocks, upon which it condenses. Condensation results in a decrease in fluid volume and hence a decrease in fluid pressure. As the fluid pressure drops below the sum of the lithostatic pressure plus the tensile strength of the material, fracture propagation ceases.

2. Fluid introduced to the existing fracture system during subsequent pulses may undergo phase separation but the preceding flows of hot fluid will have warmed the material such that condensation of the vapour-rich phase does not occur. In the absence of condensation, ascent of the vapour phase should cause an increase in fluid pressure as the vapour attempts to expand (Shmulovich *et al.*, 1995). As horizontal connectivity is likely to equal or exceed vertical connectivity in material below the brittle-ductile transition (Fournier, 1992), any localised increase in pressure may quickly be distributed, leading to an overpressured zone charged with fluids. As the pressure increases, quartz precipitation is inhibited and new additions of magmatic fluid may cease to undergo phase separation.

3. Prolonged residence of the magmatic fluid below the brittle-ductile transition enables the various batches of fluid to equilibrate with each other and with the wall-rock. Due to their similar physical properties, late batches of fluid that have failed to undergo phase separation may mix with the vapour-rich phase produced during phase separation of earlier batches to form an homogeneous fluid. Although still single-phase and of low density, the fluid produced will be less saline than the initial fluid exsolved from the magma.

4. Eventually, the overpressured zone is likely to rupture, releasing the evolved magmatic fluid into material above the brittle-ductile transition. If the fluid has cooled sufficiently, it may fail to intersect its solvus as the fluid pressure switches to a hydrostatic regime and so remain unseparated (Meinert *et al.*, 1997; Shinohara & Hedenquist, 1997; Hedenquist *et al.*, 1998). Dilution may reinforce this effect. Contact of this fluid with the cool wall-rocks above the brittle-ductile transition causes it to condense and become liquid-like. Cooling also leads to acid dissociation. Decompression triggers the precipitation of quartz which traps the diluted magmatic fluid, both in low density and higher density (condensed) states, and brine brought from depth entrained in the flow of volatiles (Rye, 1993).

5. Following decompression and fluid migration, fluid-filled fractures below the brittle-ductile transition are likely to be sealed, both by the precipitation of quartz and in response to the fluid pressure falling below the lithostatic pressure (Fournier, 1992). Rapidly precipitated quartz present within these veins is liable to annealing due to its fine grain size and the high confining pressure which increases the solubility of quartz in the grain boundary fluid (Fournier, 1985; Rimstidt, 1997).

This sequence of events accounts for veins exhibiting plastic deformation and two distinct phases of quartz deposition. It also explains the dilution the magmatic fluid appears to have undergone, and for the conservation of $\Sigma\delta^{34}S_{(fluid)}$ during this process. This magmatic fluid existed in a vapour-like state at higher temperatures and in a liquid-like state at lower temperatures. As it cooled and condensed, dissociation caused the acidity of the fluid to increase.

Relationships between late stage hydrothermal assemblages

The properties of the fluids that type 4 veins trap overlap with those of the fluids trapped by type 5a veins but, on average, the low density fluid appears to have undergone less dilution and has a higher temperature in type 4 veins. This suggests that if vein types 4 and 5 do represent points along the evolution of a single fluid, type 4 veins record an earlier stage than type 5a veins (Fig. 6.6). Type 5b veins contain identical fluids to those in type 5a veins and are interpreted to be slightly lower pressure equivalents of type 5a veins, as suggested by the calculated formation pressures. Precipitation of an iron-bearing phase from the fluids that deposited type 5a veins is consistent with the high iron contents of fluids reported in a quartz-molybdenum vein at Bingham (~28,000 ppm; Anderson *et al.*, 1989). Type 6 veins are interpreted to represent lower temperature equivalents of type 5b veins, consistent with the fluid inclusion evidence (Fig. 6.6).

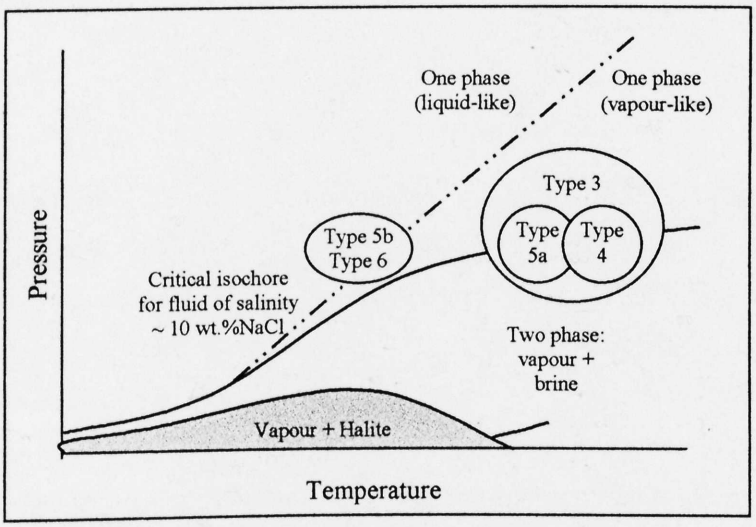


FIG. 6.6 Schematic pressure-temperature diagram showing conditions at which the various types of late stage veins are thought to have formed.

The succession from a breccia in which molybdenite is the dominant sulphide to one in which pyrite is dominant suggests that the breccias may be analogous to vein types 5 and 6. The increasingly acidic style of alteration encountered moving up the breccia column suggests that the breccias may record the evolution of the magmatic fluid to lower temperatures than the veins, when acid dissociation would be more pronounced.

Type 3 veins are slightly anomalous, sharing characteristics of both early and late stage veins. The salinity of the low density fluid which type 3 veins trap varies from ~10 wt.% NaCl equiv., similar to that observed in type 4 veins, down to ~2 wt.% NaCl equiv., similar to that observed in type 5 veins. Consequently, type 3 veins do not appear to record a stage of fluid evolution distinct from those recorded by vein types 4 and 5 (Fig. 6.6). Of all the vein types, type 3 veins are most clearly associated with dykes of the feldspar porphyry, typically being hosted by this lithology. The origin of type 3 veins is discussed further in Chapter 7.

6.3.7 Summary

Petrographic and fluid inclusion evidence suggests that late stage veins formed in an environment in which the pressure fluctuated, resulting in fluids supersaturated with respect to silica. Following the cessation of fluid flow, annealing of fine grained quartz appears to have occurred, modifying the primary texture of the veins. Despite this textural modification, fluid inclusions in vein types 4, 5a, 5b and 6 appear to record the progressive evolution of a single phase, relatively low density fluid of magmatic origin. Type 3 veins also appear to trap this fluid but their relationship with the other late stage veins is not clear.

6.4 Summary

Type 1 veins appear to have precipitated from static fluid initially trapped in melt-present parts of the chamber. Type 2 veins may have been precipitated from fluid migrating from zones of accumulation in the melt-present parts of the chamber through the brittle-ductile transition. Late stage veins are interpreted to trap fluids which failed to migrate past the brittle-ductile transition before they had cooled substantially. It is proposed that all the veins observed at Quebrada Blanca were precipitated from fluids which shared a common origin and initial composition and that the differences between the veins reflect variation in the environment through which this fluid flowed.

A MODEL FOR THE DEVELOPMENT OF HYPOGENE MINERALISATION IN PORPHYRY COPPER DEPOSITS

7

This chapter derives a model for the development of hypogene mineralisation in porphyry copper deposits, taking into account the characteristics of the components of the magmatic-hydrothermal system and their relationships at Quebrada Blanca and, by reference to the summary concluding Chapter 4, the characteristics of this type of deposit in general.

7.1 Introduction

7.1.1 Previous models

Previous theoretical models for the hypogene development of porphyry copper mineralisation have been constructed assuming that magmatic fluids are the product of magma chamber degassing as proposed by Burnham (1979). Most such models have examined how magmatic variables such as composition, crystallinity, initial water content and depth of intrusion influence the chemical composition of the MVP, and have concluded that progressive degassing of a magma could produce variation in the exsolved MVP (Burnham & Ohmoto, 1980; Candela & Holland, 1986; Candela, 1989; Cline & Bodnar, 1991; Cline 1995).

Chapter 4 concluded that the hypogene evolution of porphyry copper deposits comprises two distinct stages; an early stage during which potassic alteration and chalcopyrite mineralisation develop, and a later stage in which quartz-rich fracture fills associated with sericitic alteration form. Although it has been suggested that fluids responsible for the late stage of alteration may be largely meteoric in origin (Reynolds & Beane, 1985), many workers consider both early and late stage fluids to be magmatically-derived (e.g. Gustafson & Hunt, 1975; Zentilli *et al.*, 1993; Shinohara & Hedenquist, 1997).

Shinohara and Kazahaya (1995) proposed a model to explain the transition from potassic to sericitic alteration which assumed that all fluids were derived from a single magma chamber. Using this model, the compositions of fluids responsible for alteration and mineralisation at the Far South East deposit have been related to the evolution of the associated magma chamber (Shinohara & Hedenquist, 1997).

At the Far South East deposit, dating indicated a period of only ~100,000 years between early potassic and late sericitic alteration (Shinohara & Hedenquist, 1997). Similarly short intervals between the two stages of evolution have been inferred for other deposits (Clarke, 1993; Marsh *et al.*, 1997; Clarke *et al.*, 1998). At Chuquicamata, however, K/Ar dating determined a gap of ~3My between early potassic and late sericitic alteration, and it was suggested that an epizonal magma chamber would have solidified well within this period, necessitating a second intrusion to source the sericitic fluid (Zentilli *et al.*, 1993). Contemporaneity of late stage assemblages with the intrusion of porphyritic dykes has lead others to this conclusion (e.g. Gustafson & Hunt, 1975), but the ubiquity of the early and late stages of alteration/mineralisation and the consistency of their temporal relationship argues for them being related by some process within an evolving magmatic-hydrothermal system.

7.1.2 Relationships between magmatic and hydrothermal events at Quebrada Blanca

At Quebrada Blanca, the morphology of type 1 veins suggests that they may represent zones of fluid accumulation and may have precipitated from static fluid. Type 2 veins are proposed to have precipitated from fluid which migrated rapidly from depth and transected the brittle-ductile transition. The fluid(s) from which vein types 1 and 2 precipitated may have been derived either from the monzogranite or from some deeper source concealed at depth.

Given the spatial and temporal relationship between late stage veins and late porphyritic intrusives at Quebrada Blanca, it would at first appear that these late intrusives were the source of the magmatic fluid from which these veins precipitated. Theoretical studies have suggested that dykes do not lose volatiles they have exsolved to the wall-rock until they intersect the brittle-ductile transition (Eichelberger *et al.*, 1986; Jaupart & Allegre, 1991), however, and the morphology of vein types 4 and 5a at Quebrada Blanca clearly indicates that some late stage veins formed below this rheological boundary.

The array of fluid inclusion data collected for the late stage veins at Quebrada Blanca is also hard to reconcile with a fracturing event taking place above the brittle-ductile transition. An alternative explanation, proposed in section 6.3.6, is that late stage hydrothermal assemblages precipitated from fluid which initially failed to ascend to the surface and became trapped in the zone of material below the brittle-ductile transition. As with the early stage veins this fluid may have been derived either from the monzogranite or from some deeper source concealed at depth.

The trapped fluids are interpreted to have subsequently escaped upwards following a further episode of pressure release. It is proposed that the feldspar porphyry dykes acted as localised low-pressure zones within the system through which the fluid trapped below the brittle-ductile transition could flow following decompression of the dykes as they intersected the brittle-ductile transition and lost their volatile content. The magnitude of decompression would be greater in the fractures more proximal to the dykes than in the more distal fractures. Precipitation of quartz in response to decompression would tend to choke the proximal fractures, preventing the low-pressure zones extending far from the dykes. This pattern of events could explain why molybdenite-bearing veins are spatially associated with late intrusives; as discussed earlier, molybdenum solubility may be highly pressure-dependent, and the drop in pressure may only be sufficient to trigger molybdenite precipitation in the contact zones of the late intrusives.

Type 3 veins occur in dykes of feldspar porphyry exhibiting sericitic alteration. These are interpreted to have acted both as conduits for fluids supplied from the magma chamber as it underwent decompression and second-boiling and as channels for fluids that were initially stalled below the brittle-ductile transition. It is proposed that this latter flow of fluid was responsible for the sericitic alteration of the dykes. Similarity between the fluid inclusions in type 3 veins and those in late stage veins of types 4 and 5 suggests that type 3 veins may also record the passage of fluids that were formerly trapped below the brittle-ductile transition.

7.1.3 This model

In the remainder of this chapter, the sequences of events outlined in sections 5.5 and 7.1.2 for the development of the magmatic-hydrothermal system at Quebrada Blanca are discussed in more detail. This development is divided into five discrete stages: (1) Establishment of a physically stratified felsic magma chamber. (2) Introduction of mafic magma into the felsic chamber and exchange of components. (3) Production of a layer of volatile saturated magma. (4) Fluid flow, leading to the development of protore and fracture related assemblages. (5) Chamber evacuation. (6) Degassing of the evacuated magma(s) and decompression of the system.

7.2 Stage 1: Establishment of a stratified felsic magma chamber

7.2.1 Physical stratification

Physical properties of magmas such as density and viscosity can be related to the volume and composition of crystalline material they contain. The model of magma chamber crystallisation that this study uses is based upon that proposed by Shinohara & Kazahaya (1995), who followed earlier studies by Marsh (1988, 1989) and Brandeis & Jaupart (1987). They suggested that felsic chambers are split into three regions: an upper region of solidified magma; an intermediate region of magma with a rheology reflecting interaction between solids; and a lower region dominated by melt in which solids are held in suspension (Fig. 7.1).

Shinohara & Kazahaya (1995) suggested that the intermediate region was divided into two layers: a rigid crust and a mush. The rigid crust contained 99-50% crystals and the mush 50-25% crystals. The lower limit of crystallinity of the mush was determined by calculating the crystallinity of the magma with a viscosity of 3-10 times that of its liquidus viscosity and was dependent on magma composition. They suggested that the intermediate region was thin (<10% of the chamber thickness) for much of the cooling history of the chamber.

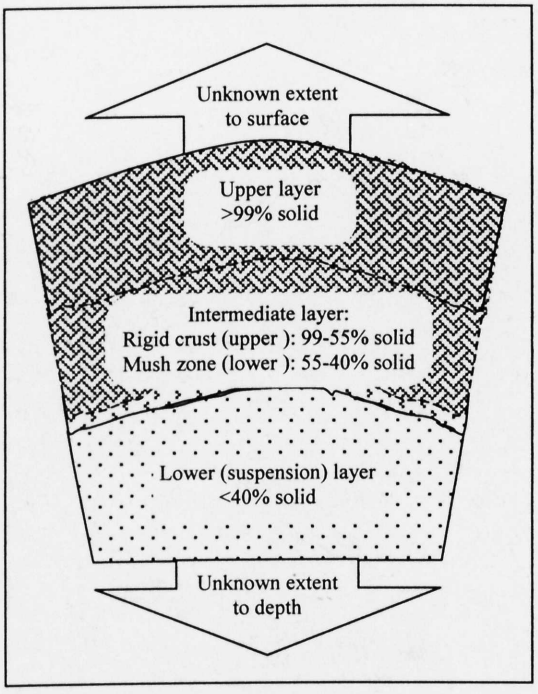


FIG. 7.1 Stratification of the modelled magma chamber (after Shinohara & Kazahaya, 1995)

In the model proposed here, the boundary between rigid crust and mush is considered to occur at crystallinities of 55%, the crystallinity at which it has been proposed that a framework capable of supporting hydrostatic stress is established (Vigneresse *et al.*, 1996). Recent work has suggested that crystal effects only dominate magma viscosity at volume fractions greater than 40% (Lejeune & Richet, 1995; Scaillet *et al.*, 1997), higher than those determined in earlier studies (e.g. van der Molen & Paterson, 1979) and, in this model, the lower limit of the mush corresponds with crystallinities of ~40%. Shinohara & Kazahaya (1995) suggested that the underlying suspension layer was transitional to a fourth layer free of crystals. In this model, crystal content is assumed to grade continuously from 40%-0%.

7.2.2 Rheological variations in the magma chamber

The upper solid region of the chamber is divided into zones characterised by brittle and ductile deformation, split by a transition at temperatures of ~370-400°C (Fournier, 1992). In the intermediate layer, material with a crystallinity of >55% is assumed to deform as a solid while material with a crystallinity of 40-55% behaves as an extremely viscous liquid. In this model, movement of melt relative to the crystal framework is considered to be possible in material with crystallinities of 55-70%.

7.2.3 Variation in melt composition within the magma chamber

In conjunction with melt fraction diagrams, experimentally determined phase diagrams can be used to approximate the crystallisation history of natural intrusives of known or assumed initial water content. The composition and volume of crystalline material can then be related to the composition of the residual melt.

Volatile content

Like many studies of fluid inclusions in porphyry copper deposits (Burnham, 1979), this study did not find evidence for CO_2. This suggests either that CO2 was not a significant component of the volatile phase associated with the development of mineralisation. Two possible explanations for the small quantities of CO_2 are the removal of a CO_2-H_2O fluid from the melt prior to the formation of porphyry style mineralisation, or evolution of an initial CO_2-rich fluid to a water dominated fluid on cooling. Lost CO_2-H_2O fluids may be responsible for the propylitic halos which commonly surround porphyry copper deposits; this alteration is essentially isochemical except for the addition of small volumes of H_2O and CO_2 (Beane, 1982). The model presented here is developed assuming that CO_2 contents were insignificant in any of the magmas present, and that water was the dominant volatile.

Although the large volume of volatiles associated with silicic extrusives (Anderson, 1992) is evidence for exsolution during magmatic decompression, as predicted by recent models (Shinohara & Kazahaya, 1995), the evidence for crystallisation-induced exsolution in such magmas is not clear (Lowernstern, 1993). Such intrusives, for example obsidian, are often erupted with no crystal content (Eichelberger, 1995). Whatever the initial water content of the felsic melt at Quebrada Blanca, the content during much of the crystallisation period was unlikely to have been significant (section 5.1.1) and a value of 1% will be used as an estimate of the water content at the start of crystallisation.

A phase diagram for the monzogranite

Following petrographic observation, sample 164, one of the magnetite-bearing samples of the monzogranite, was considered to be the least altered example of the felsic intrusive at Quebrada Blanca. The normalised composition of this sample (Table 7.1) is similar to the R5 composition of Whitney (1975b; Table 7.1). A similar Na_2O:K_2O ratio in both compositions should mean that the phase diagram predicts the boundary between plagioclase and alkali feldspar for the monzogranite and so the phase diagram for this composition at 2 kbar is used for illustrative purposes in the development of the model. Melt fractions have not been presented for composition R5, so have been estimated from Whitney (1989) and are approximate. The phase diagram assumes crystallisation in the absence of iron and magnesium. Iron and magnesium are not thought to have been present in large amounts in the felsic magma at Quebrada Blanca prior to fluid-mediated alteration (section 5.1.1), but if they were, their presence would not alter the topology of the phase diagram significantly (Naney, 1983).

TABLE 7.1 Normalised composition and modal mineralogy of samples 164 and R5.

	164	R5[1]
SiO_2	73.55	70.34
Al_2O_3	16.74	18.00
CaO	1.33	3.97
Na_2O	4.84	4.37
K_2O	3.54	3.32
	100.00	
Qtz	30.6	23.1
Or	21.6	19.8
Ab	42.4	37.3
An	5.4	19.8

[1]=Whitney (1975)

Figure 7.2, an enlargement of the area of interest on the phase diagram, shows the cooling trajectory the melt will follow. According to this diagram, plagioclase should be the only stable phase in both the suspension and mush layers and is only joined by quartz in the rigid crust when crystal contents rise to ~55%. The magma will become saturated with respect to a

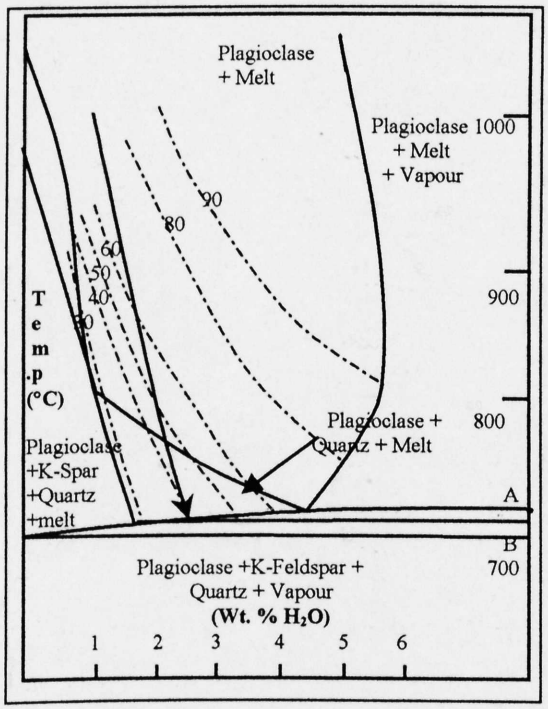


FIG. 7.2 Enlargement of a portion of the theoretical phase diagram for the monzogranite at 2 kbar (after Whitney, 1975b). Dashed lines are contours of percentage melt and are approximate. Arrow denotes cooling trend assuming no loss of vapour. Field below A is Plagioclase+Quartz+Melt+Vapour. Field above line labelled B (the solidus) is Plagioclase+K-Spar+Quartz+Melt+Vapour.

vapour phase at a crystal content of 60% and K-feldspar will join plagioclase+quartz on the liquidus with further cooling. The solidus temperature is ~700°C (Whitney, 1975b).

Compositions of the residual melt at the boundary conditions for the individual layers can be calculated by subtracting the composition of the crystalline assemblage (Table 7.2). Plagioclase is assumed to have a composition of An_{30}. When quartz joins plagioclase on the liquidus, they are assumed to crystallise in equal amounts until there is no sodium left. This occurs at a melt fraction of ~40%, coinciding with volatile saturation and the onset of alkali feldspar crystallisation. K-feldspar with the composition of stoichiometric orthoclase and quartz are then considered to crystallise in equal amounts, until all the melt has crystallised.

TABLE 7.2 Normalised composition of the residual melt and modal mineralogy of the solid assemblage at the boundaries between layers in the felsic magma chamber.

	Residual melt composition					
SiO_2	70.34	74.78	78.93	78.66	78.37	0
Al_2O_3	18.00	13.62	10.15	9.91	9.97	0
CaO	3.97	2.42	1.17	0.94	1.04	0
Na_2O	4.37	2.14	0.33	0	0	0
K_2O	3.32	5.44	7.22	8.09	8.12	0
H_2O	1	1.6	2.2	2.5	2.5	0
	100.00					
	Solid phase assemblage					
Plag	0	40	55	57.5	57.5	57.5
Quartz	0	0	0	2.5	7.5	22.5
K-Spar	0	0	0	0	5	20
Total	0	40	55	60	70	100
T(°C)		875	775	725	~700	~700

7.2.4 Magma chamber processes

Although assimilation and processes of igneous differentiation which act to separate the crystallised component of magmas from the melt component, such as fractional crystallisation and boundary layer fractionation (Baker & McBirney, 1985; Mahood & Cornejo, 1992), are thought to be common during the crystallisation of bodies of felsic magma, they are disregarded in the model.

7.3 Stage 2: Introduction of mafic magma and exchange of components

7.3.1 Effects of magma juxtaposition

In this model, it is envisaged that mafic magma invades the felsic chamber relatively late in its crystallization history and, due to its greater density, pools at the base of the chamber (Fig. 7.3). Evidence from volcanic emissions indicates that many basaltic to andesitic magmas saturate with a MVP at depths greater than 6km (Sisson & Lange, 1993; Giggenbach, 1996), and the mafic magma may or may not be saturated when it intersects the felsic chamber. Volatile loss from the mafic magma during invasion of the felsic chamber would cause the liquidus temperature to drop sharply, but studies suggest that the melt would quickly re-equilibrate by rapid crystallisation, with little or no cooling (Hort, 1998). Loss of heat from the mafic melt to the overlying suspension layer would promote crystallisation and volatile exsolution (Eichelberger, 1980; Huppert *et al.*, 1982).

A large temperature gradient is likely to exist across the suspension layer, from the liquidus temperature of the underlying mafic magma to the solidus temperature of the dominantly crystalline felsic material. This may promote turbulent convection. The dykes of feldspar porphyry are interpreted to be samples of the suspension layer at Quebrada Blanca. Stripping of the mush layer from the base of the rigid crust by convective action may explain the presence of quartz in the porphyry, which should not be on the liquidus at crystal fractions of ~40% (Table 7.2), and the welded nature of some of the large plagioclase phenocrysts. Convection would also explain the homogeneity of the porphyry.

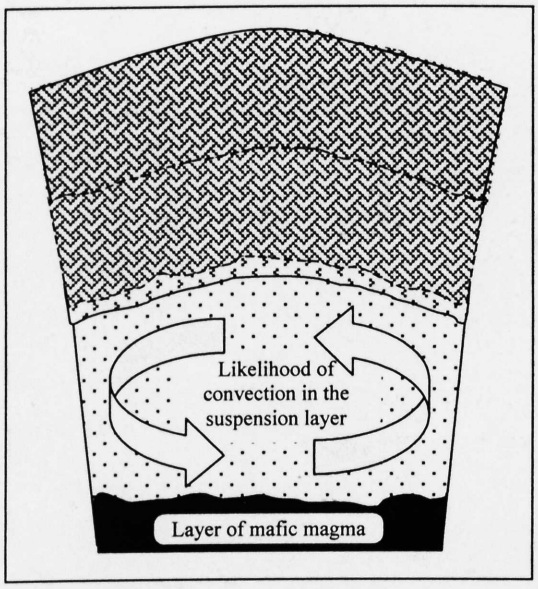


FIG. 7.3 The modelled felsic chamber following introduction of mafic magma. Strata

7.3.2 Nature of material exchange

Mixing between juxtaposed magmas is thought to occur when they are in thermal equilibrium and then only if their viscosities are of the same order of magnitude (Poli *et al*, 1996). Material exchange by diffusion prior to thermal equilibrium is unlikely to be significant due to the much greater diffusivity of heat than chemical species in magmas.

Evidence for material exchange between the andesite and monzogranite magmas at Quebrada Blanca is recorded by the porphyry but textural evidence for mixing is lacking (section 5.3.1). In the absence of physical or chemical mixing, the volatile phase exsolved from the mafic magma may transfer material and heat to the felsic magma.

Experimental simulation of volatile transfer between adjacent layers indicates two regimes (Thomas *et al.*, 1993): when the viscosities of the two layers are similar, bubbles are transferred across the interface individually (homogeneous bubbling regime); where the upper layer is more viscous, bubbles coalesce at the interface before rising as plumes of volatiles + melt + crystals (plume regime). Coalescence of bubbles at the interface encourages the development of a foam layer, which may fragment into the overlying magma, forming mafic enclaves (Eichelberger, 1980). These may be disaggregated and their constituents disseminated throughout the more felsic magma as xenocrysts (Stimac & Pearce, 1992).

At Quebrada Blanca, hornblende in the feldspar porphyry is present either as oxyhornblende or replaced by biotite and there is no evidence that hornblende was ever stable in the suspension layer. One possible explanation is that all the hornblende originated in the andesite and was introduced to the suspension layer as xenocrysts during volatile pluming. Subsequent oxidation resulted in the more magnesium-rich hornblende being replaced by biotite, while the more iron-rich hornblende remained stable but was converted to oxyhornblende. This is permissive evidence for the initial transfer of volatiles from the andesite to the suspension layer at Quebrada Blanca having taken place in the plume regime.

7.3.3 Limits on the volume of volatiles introduced

It has been proposed that interaction between mafic and felsic magmas may cause overpressuring of magma chambers, initiating extrusion (e.g. Sparks *et al.*, 1977; Eichelberger, 1980; Tait & Jaupart, 1990). This topic has recently been the subject of a theoretical study (Pyle & Pyle, 1995) which found that if bubbles are assumed not to interact with the melt, the pressure increase due to their volume is proportional to the height that they rise. Where bubble rise is slow relative to the rate of water diffusion within the melt, however, this assumption is invalid and water in the bubbles may dissolve into the melt, resulting in a decline in bubble volume. If the magma into which the bubbles are introduced is convecting turbulently, the bubble ascent velocity will be zero because convection rates are rapid compared with those of bubble rise (Pyle & Pyle, 1995). Turbulent convection will

ensure that bubbles equilibrate with melt and, if the magma remains undersaturated with respect to water following equilibration, there will be no change in pressure.

Equilibrium between bubbles and melt is assumed to have been the case at Quebrada Blanca. During equilibration, the amount of mafic volatiles that could dissolve in the suspension layer before it too became volatile-saturated would be determined by the solubility of water in this layer. The solubility of water in the porphyry melt at 2 kbar and 800°C is ~5.0 wt.%, assuming the magma was completely molten (calculated according to the method of Burnham, 1994, Appendix C.1). In fact, the magma contains ~47% crystals, so the solubility of water in the porphyry magma, consisting of approximately equal quantities of melt and crystals, is ~2.7 wt.%. Assuming the concentration of water in the magma prior to interaction can be approximated by that present in the theoretical suspension layer (1.6 wt. %; Table 7.2), the suspension layer can dissolve an additional ~1wt.% water, before it too becomes volatile-saturated.

7.3.4 Composition of the mafic MVP

The selvedges on the andesite dykes are interpreted to have precipitated from a MVP initially in equilibrium with the andesitic magma (section 5.2.2). It is suggested that MVPs derived from mafic melts are qualitatively enriched in the components of biotite (i.e. rich in iron, magnesium, potassium and silica, and poor in calcium and sodium); the selvedge material on the andesite at Quebrada Blanca and the selvedges seen on basalt dykes (Hoek, 1995) are composed almost entirely of this phase.

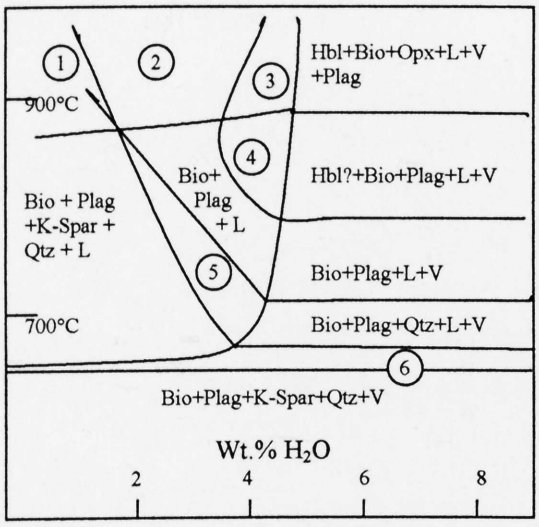
7.3.5 Effects of MVP transfer

Experiments were carried out by Naney (1983) to determine how adding biotite to the iron- and magnesium-free granodiorite composition used by Whitney (1975b) modified the phase diagram. From the modified phase diagram (Fig. 7.4), it is apparent that the assemblage biotite+plagioclase+quartz occurs over a restricted temperature range which is inconsistent with the temperature proposed for the suspension layer (~875°C; Table 7.2). Although incorporation of cooler material from the mush zone might be expected to lower the average temperature somewhat, orthopyroxene should be stable and quartz should be absent at temperatures of 800-850°C. The absence of orthopyroxene may reflect the very low contents of calcium in the melt when iron and magnesium were added (c.f. Naney, 1983), but it is also possible that the phase assemblage observed is metastable.

FIG. 7.4 Illustrative phase diagram for the monzogranite following the addition of the components of biotite (after Naney, 1983).

1. Opx+Plag+K-Spar+Qtz+L
2. Opx+Bio+Plag+L
3. Hbl+Bio+Opx+Plag+L
4. Hbl ?+Bio+Plag+L
5. Bio+Plag+Qtz+L
6. Bio+Plag+K-Spar+Qtz+L+V

Opx- orthopyroxene, Plag- plagioclase, K-Spar- K-feldspar, Qtz- quartz, Bio- biotite, Hbl- hornblende, L- melt, V- vapour.



Although porphyritic textures are preserved by quenching, they are produced when crystallisation is dominated by growth rather than by nucleation. Naney & Swanson (1980) suggested that the presence of iron or magnesium in granitic liquids would inhibit nucleation due to their disruptive influence on the framework structures within the melt that form the nuclei to these phases. Water and alkalis have a similar effect (Hess *et al.*, 1995; Hess & Dingwell, 1996). Increasing fO_2 would exacerbate the effect of the other species by increasing the ratio of non-bonding:bonding oxygen in the melt. Under these conditions, it would be predicted that those phases present in the suspension layer following equilibration with the mafic MVP would grow, while the nucleation of new phases would be inhibited.

The suspension layer at Quebrada Blanca is interpreted to have received an influx of iron, magnesium and alkalis during the transfer of volatiles from the mafic magma, and to have undergone an increase in fO_2 as a result of this exchange, conditions ideal for the inhibition of nucleation. Quartz is interpreted to have been a metastable phase in the porphyry at Quebrada Blanca. The hexagonal bipyramidal morphology displayed by some of the quartz phenocrysts prior to rounding suggests that they grew in a melt that was only slightly undercooled (MacLellan and Trembath, 1991), consistent with conditions inferred within the suspension layer. Furthermore, unstable crystals would dissolve very rapidly in convecting magma (Kerr, 1995). The metastable persistence of quartz would be favoured where the crystallisation of biotite and magnetite, both phases undersaturated with respect to silica, was increasing the activity of silica in the melt.

7.4 Stage 3: Generation of a MVP in equilibrium with the suspension layer

Following equilibration with the initial pulse of volatiles from the andesite, the viscosity of the suspension layer may decrease by several orders of magnitude in response to the depolymerisation effect of the added volatiles and alkalis (Hess *et al.*, 1995; Hess & Dingwell, 1996). This decreases the viscosity contrast between the adjacent layers and homogeneous bubbling may occur. In this regime, bubbles do not coalesce at the interface between magmas. Consequently, they are likely to be small and ascend slowly, and so equilibrate with the suspension layer. Eventually, the suspension layer will itself become saturated and will exsolve a volatile phase.

7.4.1 Composition of the melt in the suspension layer

Once the suspension layer has become saturated with a volatile phase, species may partition between the melt and the volatile phase. Due to the slow diffusion of chemical species in solids, it is assumed that crystalline phases play no part during this partitioning. The melt composition of the suspension layer at Quebrada Blanca can be determined by subtracting a phenocryst assemblage totalling 47% of the bulk composition, comprising 40% plagioclase (An_{30}), 5% quartz and 2% magnetite (Appendix C.1, Table 7.3). The K_2O content of the melt so determined (Table 7.3) is in very good agreement with that indicated by the potassium concentration of the plagioclase interpreted to have crystallised under volatile saturated conditions (4.2-4.5 wt %; section 5.3.1). This suggests that despite the approximate nature of the potassium contents determined in plagioclase and the uncertainty of the partition coefficient $D_K^{plag\text{-}melt}$, the variation in melt potassium content suggested by this method may be of significance.

TABLE 7.3 Composition of melt and relative composition of fluid within the suspension layer.

	Suspension layer melt (wt. %)	Ratio in melt[1]	Ratio in fluid[1]
SiO_2	67.49		
Al_2O_3	12.85		
FeO	4.22	1:1	1:2
MgO	2.39	1:2	1:8
CaO	0.00	0	0
Na_2O	2.23	1:2	1:2
K_2O	4.60		
P_2O_5	0.35		
TiO_2	0.81		
MnO	0.06		
H_2O-	5.00		
Total	100.00		

[1] ratios are wt.% element: wt.% potassium

7.4.2 The MVP in equilibrium with the suspension layer

Nature of the volatile phase

Depending on the bulk salinity of the MVP, it may exist either as a supercritical fluid or as a mixture of low density vapour and high density brine. At temperatures of 800°C and pressures of 2 kbar, the conditions assumed for the suspension layer, fluids of salinity <30 wt.% NaCl equiv. will be supercritical (Bodnar *et al.*, 1985). It is proposed that the salinity of the fluid in equilibrium with the suspension layer was well below this value; the bulk salinity of fluids exsolved from felsic magmas is thought to be 2-10 wt.% NaCl equiv. (Hedenquist *et al.*, 1998). Fluids at Quebrada Blanca are interpreted to have evolved from a single supercritical fluid. The highest salinity determined for inclusions exhibiting semi-critical or critical homogenisation is ~14 wt.% NaCl equiv. (inclusions trapped within the quartz phenocrysts). Although these inclusions are probably secondary, they may be indicative of the salinity of the magmatic fluid at Quebrada Blanca.

Major element composition

Variation in the potassium content of the plagioclase phenocrysts in the feldspar porphyry suggests that the potassium content of the melt peaked at ~6.0 wt % K_2O before falling to ~4.2wt % K_2O. It is believed that this drop reflects partitioning of potassium between melt and MVP. If so, the partition coefficient $D_K^{vapour\text{-}melt}$ is ~0.43, which is not in very good agreement with the experimentally determined value for $D_K^{vapour\text{-}melt}$ of 0.74±.06 (high silica rhyolite, 770-880°C, 1.4-2.4 kbar; Holland, 1972). Given the presence of such an iron-rich melt (Candela & Holland, 1984), it is doubtful whether experimentally determined partition coefficients can be used to describe the absolute distribution of potassium or other species between melt and MVP at Quebrada Blanca. However, some predictions about the relative concentrations of the major species in the MVP can be made, given a number of assumptions with regard to partition coefficients as outlined below.

Partitioning coefficients have not been determined for iron or sodium, but it has been suggested that iron may equal the amount of calcium in fluids in equilibrium with melt containing plagioclase and magnetite, and that the ratio of sodium to potassium in the fluid should be approximately that of the melt, regardless of the presence of $CaCl_2$ or $FeCl_2$ (Burnham & Ohmoto, 1980). Consequently, iron and sodium are assumed to have similar partition coefficients to calcium and potassium respectively, and the ratios Fe:Ca or Na:K within the residual melt are assumed to be equivalent to the ratios in the volatile phase. The

experimentally determined value of the partition coefficient for calcium is half that determined for potassium while that for magnesium is only a quarter (Holland, 1972), and it follows that the ratios K:Ca or K:Fe in the volatile phase should be twice that in the melt, while the ratio K:Mg should be four times that in the melt. This results in a volatile phase in equilibrium with the melt in which iron and sodium are present in approximately equal amounts, and together equal the concentration of potassium; the iron:magnesium ratio is 4:1, and there is negligible calcium (Table 7.3). Partitioning data are not available for silica and aluminium, but it is likely that they are insignificant components of high pressure volatile phases (Kilinc & Burnham, 1972).

Although the composition of fluids associated with tin mineralisation have been analysed by a number of workers for several different deposits (see Heinrich, 1995, for a review), the composition of fluids associated with mineralisation in porphyry copper deposits has not been nearly so well studied, and there are no data with which the predictions of the previous paragraph can be compared.

Copper content

Experimentally determined partition coefficients indicate that copper should partition very strongly into a chlorine-bearing volatile phase, where it may be enriched by a factor of ~20 relative to the melt (Candela & Holland, 1984). In the absence of sulphides, it is assumed that all of the copper in the feldspar porphyry will be in the melt and so available to partition into the volatile phase. This suggests that the copper content of the volatile phase in equilibrium with the feldspar porphyry melt may have been as high as 23,000 ppm. Copper contents of fluids associated with mineralisation in porphyry copper deposits are typically thought to be on the order of several hundred to a few thousand parts per million (Bodnar, 1995).

Sulphur speciation

Sulphur speciation in the melt will exert a significant control on sulphur speciation in the MVP. At fO_2 values greater than the fayalite-magnetite-quartz buffer plus 2.2 log units, anhydrite may replace Fe-sulphide as the major sulphur-bearing condensed phase (Caroll & Webster, 1994). This phase has been observed in lavas thought to have been produced by interaction between magmas of contrasting composition (Matthews *et al.*, 1994a). Anhydrite

stability in the melt will lead to an enrichment of the MVP in reduced sulphur relative to oxidised sulphur (Burnham & Ohmoto, 1980).

There is no evidence for anhydrite saturation in the porphyry at Quebrada Blanca, despite fO_2 approaching values of the magnetite-hematite buffer (section 5.3.1). This may reflect insufficient quantities of calcium in the melt to stabilise anhydrite. In the absence of a sulphur-bearing condensed phase to modify the speciation of the sulphur partitioning into the MVP, the ratio SO_2:H_2S would be determined by the oxidation state of the magma. At conditions of 2 kbar, 800°C and fO_2 values slightly below the magnetite-hematite buffer, the molar ratio SO_2:H_2S would be ~45:1 (Westrich & Gerlach, 1992).

7.5 Stage 4: Fluid flow

Following saturation of the suspension layer, a steady state system, in which volatiles are supplied to the suspension layer from the mafic magma before being transferred to the dominantly solid-portions of the chamber, may be established (Fig. 7.5). Disseminated protore is thought to develop in response to the small-scale movement of fluid through the dominantly solid-portions of the chamber. Accumulations of fluid which achieve sufficient volume may migrate from these regions into the rigid crust where they may deposit veins.

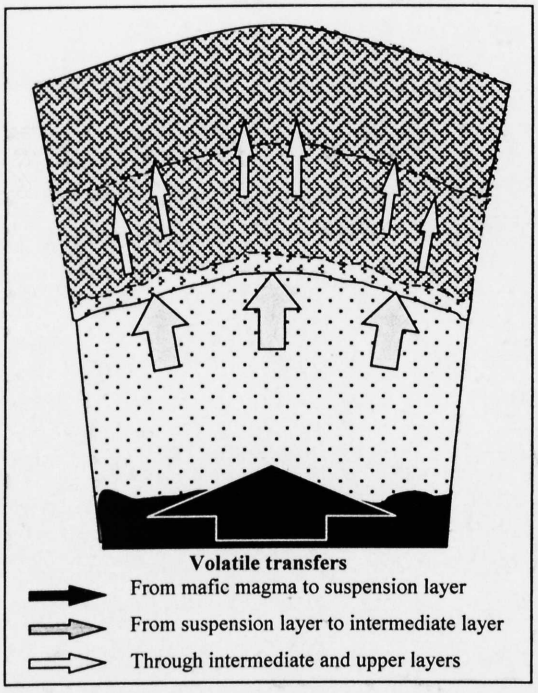


FIG. 7.5 Volatile flows within the magma chamber during the development of protore. Strata as Fig. 7.1.

7.5.1 Disseminated mineralisation and alteration

Disseminated protore mineralisation at Quebrada Blanca appears to have developed in the presence of both melt and fluid. In this model, the volatile phase sourced from the suspension layer is responsible for iron-alkali-copper metasomatism, the character of which is dependent upon the temperature at which final equilibration occurs. Experimental studies suggest that first iron then potassium precipitates from a cooling iron- and potassium-rich

solution (Whitney *et al.*, 1985). Iron may be incorporated by magnetite and biotite. Potassium may be hosted by the potassium-rich alkali-feldspar seen to replace plagioclase.

The development of the sulphide-bearing assemblage suggests that the activity of reduced sulphur increased. Disproportionation of SO_2 is a likely mechanism to bring about this increase and may be a response either to cooling or to the consumption of oxygen by magnetite formation. The common presence of anhydrite in the sulphide-bearing protore suggests that cooling, leading to the development of sulphate, may be the driving mechanism in many deposits. Magnetite may be an essential precursor to chalcopyrite because precipitation of copper, present primarily as Cu^+ in solution, requires reduced sulphur and oxidised iron (Eqn. 7.1; Ohmoto & Goldhaber, 1997).

$$\underset{\text{in solution}}{Cu^+} + \underset{\text{in magnetite}}{Fe^{3+}} + \underset{\text{in solution}}{2S^{2-}} \leftrightarrows CuFeS_2 \qquad (7.1)$$

At Quebrada Blanca, biotite in the magnetite-bearing samples of the monzogranite has a high iron:magnesium ratio. This may reflect the high iron:magnesium ratio predicted for the fluid derived from the suspension layer (~4:1; Table 7.3). During overprinting of the magnetite-bearing assemblage by the sulphide-bearing assemblage, the potassium content of the biotite and of the whole-rock increases, consistent with increased potassium fixation during cooling.

7.5.2 Fracture related mineralisation

Veins with a mineralogy similar to type 1 veins at Quebrada Blanca are responsible for the introduction of large amounts of copper at El Salvador (Gustafson & Hunt, 1975) and it is generally accepted that the majority of copper mineralisation in porphyry copper deposits is concomitant with the precipitation of early veins associated with potassic alteration. Although this may be typical of porphyry copper deposits in general, copper-bearing phases are not always restricted to this stage of the paragenesis; at deposits such as Toquepala (Zweng & Clark, 1995), Rio Blanco-Los Bronces (Warnaars *et al.*, 1985) and many of the deposits of British Columbia (Clark, 1993) the bulk of copper mineralisation accompanies molybdenite in veins which lack alteration halos.

Type 1 veins are rare at Quebrada Blanca and can account for little of the hypogene copper mineralisation at the level of observation. Nor are copper-bearing minerals observed in significant quantities within the phase assemblages of vein types 4, 5 or 6. Although this could be a product of low copper concentrations in the fluids at Quebrada Blanca, two lines

of evidence suggest that the fluids responsible for the precipitation of the late stage veins contained significant amounts of copper. Firstly, chalcopyrite is seen as daughter minerals in inclusions thought to trap magmatic fluid that has failed to undergo separation within late stage veins. Secondly, samples of feldspar porphyry exhibiting sericitisation, interpreted to have equilibrated with evolved fluids initially trapped below the brittle-ductile transition, are significantly enriched in copper compared with fresh samples.

It is possible that the copper contained in fluids initially trapped below the brittle-ductile transition may have remained in solution until the fluids migrated to higher regions of the system following decompression of the fluid-pressured zone. The occurrence of the dominant phase of copper precipitation in late veins with sericitic halos is rare but has been documented at the deposits of Butte (Brimhall, 1979), Cuajone (Clark, 1993) and Park Premier (John, 1989). The precipitation of chalcopyrite is thought to postdate that of pyrite in the later stages of porphyry-copper mineralisation (Hemley & Hunt, 1992), and it may be that at Quebrada Blanca, copper was precipitated in the lower temperature equivalent of type 6 veins. Unfortunately, this portion of the system has been eroded at Quebrada Blanca and it is not possible to verify this assertion.

7.6 Stage 5: Chamber evacuation

It is proposed that protore mineralisation develops in a period of time bracketed by the introduction of mafic magma into the felsic chamber and evacuation of the magma chamber. The suggestion that the intrusion of porphyry dykes and the onset of sericitic alteration may terminate hypogene copper mineralisation in the porphyry environment has been made previously (Zweng & Clark, 1995).

Dyke initiation may be a response to the action of an external process on the system, such as a new influx of mafic melt or tectonic activity, but is also commonly thought to reflect opening of a conduit by a volatile phase; the low density and viscosity of the volatile phase make it an effective medium for transmitting reservoir pressure upward to shallow depth (Eichelberger, 1995; Rubin, 1995). This mechanism is considered to be responsible for dyke initiation in this model, and is predicted to occur when the flux of volatiles to the base of the rigid crust exceeds the flux of volatiles away from this layer (Fig. 7.5), causing the chamber pressure to increase. The increase in pressure is constrained by the strength of the country rock and fracturing is likely when the volume of the chamber increases by >0.1% (Pyle & Pyle, 1995).

The characteristic nature of the porphyry dykes associated with porphyry copper deposits suggests regulation by a magmatic process. Judging from the ubiquity of resorbed quartz phenocrysts in porphyritic dykes associated with mineralisation (section 4.1.2), a process that is occurring at the point of dyke initiation is quartz resorption; preservation of resorbed quartz phenocrysts indicates that magma was removed from the chamber shortly after the onset of this process, as unstable crystals dissolve rapidly in chambers where they move relative to melt (Kerr, 1995). In contrast, quartz dissolution is likely to be minimal in dykes, as they ascend on timescales that are rapid compared with the diffusivity of silica within the melt (c.f. Kerr, 1995). This accounts for the preservation of dissolution halos around the quartz phenocrysts.

In the undersaturated field, quartz dissolution may be a response to increasing temperature or increasing water content, and the phenocrysts may simply record the increase in volatile pressure associated with dyke initiation. In the saturated field, however, dissolution is more likely to represent increasing temperature (Fig. 7.4). If this is the case, quartz dissolution may be indirectly responsible for the increased supply of volatiles to the base of the rigid crust; by increasing the ratio of Si:Ca+Na+K in the suspension layer, it causes the solubility of water in the melt to decline (e.g. Bagdassarov & Dorfman, 1998).

As the suspension layer is evacuated from the chamber, the mafic magma may move upwards to take its place (c.f. Pyle & Pyle, 1995). Ascent of this magma in fractures through the crystalline parts of the chamber may produce the dykes observed at high levels in the system (Fig. 7.6). It is proposed that it was at this stage that the andesite dykes observed in core exposures developed at Quebrada Blanca. The absence of this lithology from the higher parts of the system may reflect exsolution induced freezing, or a reduced overpressure in this magma due to expansion into the volume vacated by the suspension layer.

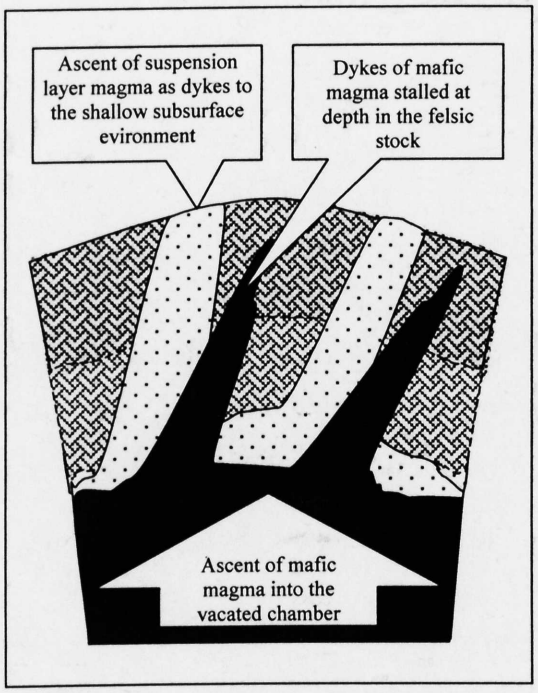


FIG.7.6 Evacuation of the chamber and ascent of the magmas as dykes. Strata as Fig. 7.1.

7.7 Stage 6: Dyke degassing

7.7.1 Behaviour of volatiles during dyke ascent

The behaviour of volatile phases in volcanic conduits has been the subject of several studies (Eichelberger *et al.*, 1986, Vergniolle & Jaupart, 1986, Jaupart & Allegre, 1991) which provide a useful framework for understanding the degassing of the dykes of andesite and feldspar porphyry. Two processes act to remove the MVP from the magma forming the dykes; flow separation and loss of the MVP to the host rock. Flow separation occurs when the MVP flows upwards faster than the magma, and is favoured by a low initial value of chamber overpressure (Jaupart & Allegre, 1991). A low initial chamber overpressure would be predicted where the build up of pressure was gradual, as hypothesised in this model.

The presence of selvedges on the andesite dykes at Quebrada Blanca is good evidence that they began to undergo flow separation during ascent. Of the dykes of feldspar porphyry, fresh dykes and those exhibiting sericitic alteration are interpreted to have degassed efficiently. Dykes exhibiting potassic alteration may have degassed inefficiently and equilibrated with volatiles supplied from the magma chamber as it underwent second boiling.

7.7.2 Loss of the volatile phase from the dykes

Volatile loss to the wall rock is promoted in the brittle regime as the permeability increases (Eichelberger *et al.*, 1986) and because, unlike aqueous fluids, magma cannot perfectly wet intricate/rough channels (Jaupart & Allegre, 1991). If volatile loss does not occur until dykes intersect the brittle-ductile transition, the volatiles present in the magma at the initiation of dyking may buffer magma pressure during dyke ascent, decompression being countered by expansion of the volatile phase or by further volatile exsolution (c.f. Rubin, 1995). Dyke ascent to the brittle-ductile transition may thus be isobaric, consistent with the requirement for high fluid pressures at the leading edges of propagating dykes (Rubin, 1995).

7.7.3 Decompression of the system

Loss of volatiles from the dykes results in decompression of the magma. If the dykes are still connected with the magma chamber at depth, this drop in pressure will be transmitted downwards, and may trigger second boiling. It seems probable that fluid exsolved from the magma remaining in the chamber at depth during this episode of degassing will utilise the dykes as conduits to the surface rather than forming new fractures. If vented efficiently at the surface, these late exsolved fluids may not have had time to precipitate their ore-elements.

7.8 Summary

The model described above accounts for many of the observations made at Quebrada Blanca, including the apparent contemporaneity of mafic and felsic magmas and the characteristics displayed by the feldspar porphyry. This is not the first study to suggest that interaction between magmas of contrasting composition may encourage the development of mineralisation. Magma mixing has been seen as a mechanism to enrich felsic-dominated systems in metals, chlorine and sulfur (Whitney, 1989; Clark, 1993; Matthews *et al.*, 1995; Cornejo *et al.*, 1997) while quenching of mafic magma during mingling is thought to promote volatile saturation, leading to the direct production of a mineralizing fluid phase (Eichelberger, 1980; Keith *et al.*, 1997). The model proposed here is distinct because material transfer between magmas is mediated by a mafic-derived MVP (i.e. mixing does not occur), and because mineralisation is produced by a second MVP exsolved from the felsic magma that was enriched in ore elements and water by the initial transfer.

Compared with other models for the hypogene development of porphyry copper deposits, this model accounts more completely for the occurrence and nature of the characteristic veins that comprise the hydrothermal systems associated with these deposits and, perhaps more significantly, their temporal relationships. Rather than the different vein types within the paragenesis having precipitated from compositionally distinct fluids, it is proposed that the variation the veins display reflects differences in the rate at which batches of fluid of unique composition ascend.

APPLICATIONS AND IMPLICATIONS OF THE MODEL

8

The model detailed in Chapter 7 is consistent with observations of the magmatic-hydrothermal system at Quebrada Blanca which, it is suggested (Chapter 4), has the characteristics typical of porphyry copper deposits, particularly those occurring in the Andes. As such, it may be a reasonable empirical model for this style of mineralisation. The strength of a genetic model for porphyry-copper mineralisation, however, lies in its ability to predict the variation displayed by deposits of this type. The first two parts of this chapter examine how the model proposed in Chapter 7 may account for some of the more pronounced variations displayed by porphyry copper deposits, and the implications it has for exploration in arc environments. During the course of this study, a number of areas for further research have been identified. These are discussed in the third part of this chapter.

8.1 Variations on a theme

8.1.1 Barren systems with evidence of mafic-felsic magma interaction

Variation in the proportions of mafic and felsic magmas interacting

The most significant stage in the model is the introduction of mafic magma into the shallow crustal felsic chamber, a process which the geologic record suggests has been, and continues to be, a very common process, particularly in arcs above subduction zones (see Matthews *et al.*, 1994b, for a review). Following juxtaposition of magmas, there are a number of ways in which the system may respond. Interaction may initiate extrusion, which precludes the development of porphyry-style mineralisation (Hedenquist, 1995; this study). Eruption initiation would be predicted where the transfer of volatiles from the mafic magma to the suspension layer produces an increase in the chamber pressure which exceeds the strength of the wall-rock. This could reflect a high mafic:felsic ratio or a high water content in the suspension layer prior to interaction.

Conversely, introduction of the mafic magma into a dominantly liquid chamber would favour mixing and the production of a layered chamber in which all compositions show a degree of hybridisation (e.g. Bateman, 1985). Dilution of ore forming components would be greater, rendering them less amenable to concentration by any subsequently exsolved MVP.

Ideal conditions for mineralisation then, can be viewed as intermediate between mixing and extrusion (Fig. 8.1).

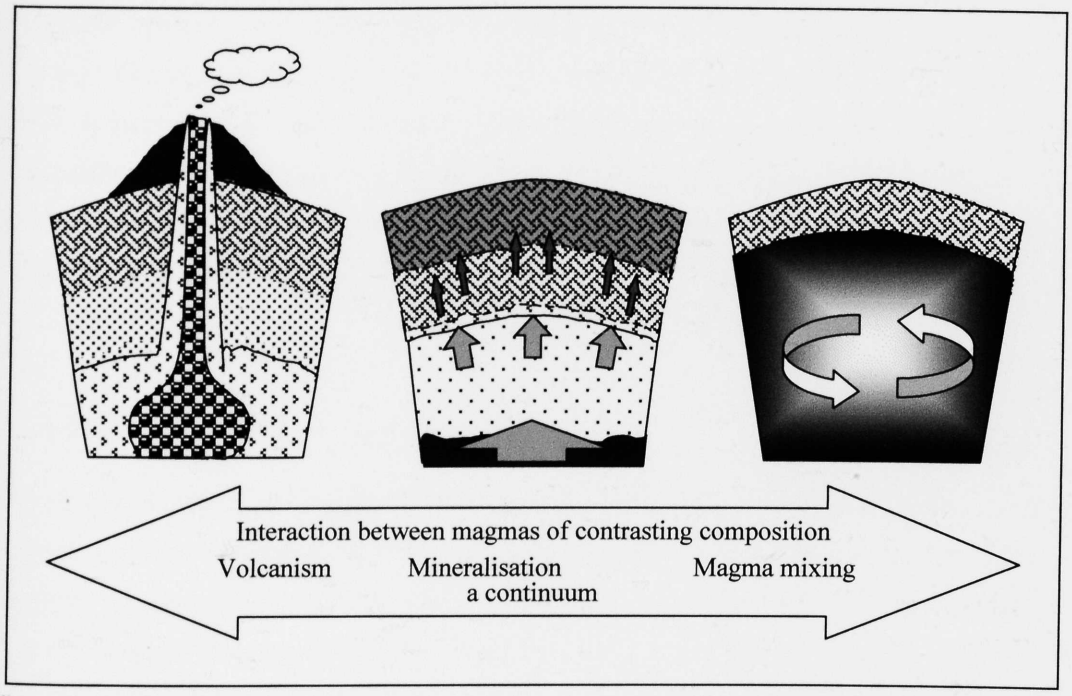


FIG. 8.1 Mineralisation as an intermediate condition between volcanism and magma mixing.

Variation in the composition of the mafic MVP

At Quebrada Blanca evidence suggests that the mafic-derived MVP was enriched in copper, but this need not be the case for all such volatile phases. A likely source region for highly oxidised, potassic magmas in continental arc settings is pyroxenite in the lithospheric mantle, which may be enriched in copper during metasomatism of the mantle wedge by fluids released by the subducting plate (see Keith *et al.*, 1997, and Muller & Groves, 1997, for reviews). Due to their high sulphur contents, these magmas are liable to fractionate ore-bearing sulphides and, in order to maximise the amount of ore forming components available to the MVP, it is important that these magmas ascend rapidly from their source regions to depths at which they become volatile-saturated. Large transcrustal structures may facilitate magma ascent, explaining the location of the major porphyry-copper deposits of Chile on the Sierra Castillo-Domeyeko-West Fissure fault system.

Systems exhibiting evidence of interaction between magmas of contrasting composition but lacking significant copper mineralisation may result where ore-metal bearing phases have fractionated. However, transfer of volatiles may still have very significant petrogenetic implications; it has been suggested that the genesis of oxidised- and reduced-type granites

can be attributed to a difference in the absolute abundance of SO_2 in the magmas, oxidised magmas forming where SO_2 is >250ppm (Takagi & Tsukimura, 1997). The principal distinction between the two geochemically similar types is the presence of magnetite, which in many cases is considered to be the product of late stage alteration (Takagi & Tsukimura, 1997). It may be that such alteration reflects equilibration of a hydrothermal fluid with dominantly crystalline magma as predicted by the model proposed in Chapter 7, and that fluid-mediated interaction between mafic and felsic magmas plays a part in the genesis of oxidised-type (magnetite-series) granites.

8.1.2 Contrasting styles of hypogene alteration

The model presented in this thesis suggests that the volatile phase which effects protore mineralisation and alteration was derived from the suspension layer, of which the feldspar porphyry is a sample, and that the composition of the mineralising fluid reflects equilibration with the melt of this layer (section 7.4.3). Consequently, variation in the composition of the melt should cause the fluid composition to vary, the evidence for which may be preserved in the alteration assemblages accompanying mineralisation.

A style of hypogene alteration that is not observed at Quebrada Blanca but has been recorded in a number of porphyry-copper deposits is calc-potassic alteration (Lang *et al.*, 1995). Like the iron-alkali stage of hypogene alteration at Quebrada Blanca (section 7.4.5), this alteration is typically pervasive and leads to enrichment in iron and titanium, though these elements are hosted by andradite garnet, and magnetite is absent (Lang *et al.*, 1995). In contrast to the alteration at Quebrada Blanca, however, calcium is enriched and not depleted, implying a higher activity ratio of calcium to potassium in the fluid phase. According to this model, this implies a higher activity ratio of calcium to potassium in the melt of the suspension layer, which would be predicted where a potassium-bearing phase was crystallising. Evidence presented by Lang *et al.* (1995) indicates that the porphyritic intrusives

TABLE 8.1 Composition of the melt and equilibrium MVP of the porphyritic intrusives at Yerington, Nevada.

	Bulk[1]	Melt	Ratio in melt[2]	Ratio in fluid[2]
SiO_2	68.1	64.87		
Al_2O_3	15.6	15.51		
FeO	2.42	4.44	1.8:1	0.9:1
MgO	0.98	1.80	0.75:1	1:5
CaO	2.84	4.12	1.7:1	0.85:1
Na_2O	4.32	3.86	1.6:1	1.6:1
K_2O	3.35	2.45		
P_2O_5	0.14	0.26		
TiO_2	0.37	0.68		
MnO	0.0	0.00		
H_2O^-	1.1	2.02		
Total	99.2	100		

[1] Analysis GPD Y-781 (Dilles, 1987)
[2] relative to potassium

sourcing the mineralising fluids in the deposits exhibiting calc-potassic alteration were crystallising potassium bearing phases such as K-feldspar and leucite (Lang *et al.*, 1995), consistent with this hypothesis.

The deposits exhibiting calc-potassic alteration are associated with magmas of alkalic rather than calc-alkaline affinity (Lang *et al.*, 1995), and it could be argued that this distinction is responsible for the different style of hypogene mineralisation. Calcium-rich hypogene alteration is also present at Yerington, however, which is of calc-alkaline affinity (Dilles & Einaudi, 1992). Using the phenocryst assemblage and the whole-rock composition of the porphyritic lithology associated with mineralisation (Dilles, 1987), the composition of the residual melt was calculated (Appendix C.4, Table 8.1). Following the method used in section 7.4.3, the composition of the fluid in equilibrium with this melt was also estimated (Table 8.1). It can be seen that the calculated ratio of Ca:K in the fluid is considerably higher than in the fluid at Quebrada Blanca (Table 7.3).

8.2 Implications for mineral exploration

Given that most of the major mineral deposits found in the circum-Pacific within the period 1970-1995 owe their discovery to events which "defy rational analysis and categorisation" (Sillitoe, 1995b) it is debatable whether any model for deposit genesis can have universal application in the search for new mineral deposits. The model presented here, however, indicates a fundamental role for mafic magmas in the genesis of porphyry copper mineralisation which has not previously been stressed. Evidence for volcanism of strongly contrasted composition, particularly that showing a strong spatial relationship with district scale faults, should be viewed favourably, as it is indicative of the occurrence of a process which in lithologies of a similar age and association, may have produced mineralisation.

8.3 Areas for further research

8.3.1 Validation of the model

In the model presented in Chapter 7 the characteristic components of porphyry copper deposits are linked by processes that are consistent with observations made at Quebrada Blanca. These processes are not inconsistent with observations made during a study of the magmatic system beneath the porphyry copper deposits of Yerington (Dilles, 1987). As noted in Chapter 1, the study of Yerington is the only study tackling the full spectrum of

magmatic and hydrothermal processes in such systems to be published. Clearly, more magmatic systems associated with porphyry copper mineralisation need to be investigated in detail.

Two particular areas for further research are apparent. Firstly, a more detailed understanding of the late stages in the evolution of the magmatic system is required. It has been demonstrated during this study that plagioclase phenocrysts in the porphyritic lithology spatially associated with mineralisation appear to record the evolution of the magma chamber at depth. With sufficient data about variation in plagioclase composition, it should be possible to trace the compositional evolution of the melt, and hence the compositional evolution of the fluid in equilibrium with the melt. Secondly, the role of mantle-derived mafic lithologies in the hypogene evolution of porphyry-copper deposits needs to be defined. A number of techniques for assessing this role are discussed below.

Lead isotopes

Lead isotopes reflect the geochemical behaviour of ore metals but, unlike the light stable isotopes, are not measurably fractionated during redox reactions in solution or by fluid-mineral reactions. Consequently lead isotopic compositions should reflect their source (McFarlane & Petersen, 1990). A lead isotope study of porphyry copper deposits in the Lachlan Fold Belt of Australia (Carr *et al.*, 1995) presented evidence suggesting that although ore elements in the deposits may have originated in enriched lithospheric mantle, the lead isotope characteristics were dominated by a crustal signature which may have been acquired either during crustal assimilation or during contamination at the hydrothermal stage.

The results of the study of the Lachlan Fold Belt (Carr *et al.*, 1995) highlight some of the problems encountered when using lead isotopes to examine interaction between mantle and crust: (1) Crustal rocks have a much higher concentration of lead than mantle melts so lead isotopes are highly insensitive to mantle contributions to the crust (Miller & Wooden, 1994). (2) Lead isotopes, like strontium isotopes, probably reequilibrate very rapidly during magma mingling (Lesher, 1994), so preservation of mafic material with a primary signature is unlikely. (3) Lead is mobile under most hydrothermal conditions (Richards *et al.*, 1991) and so is liable to be reworked during overprinting by meteoric fluids, homogenising the values within a deposit and the surrounding country rock.

Rhenium-osmium isotopes

The rhenium-osmium system is likely to be of use when examining interaction between mantle and crust since it is a very good indicator of such processes (Freydier *et al.*, 1996). At present, the system is poorly documented, especially with application to the magmatic-hydrothermal environment, but it may be of use in the future.

Helium isotopes

Helium is an attractive tracer of mantle volatiles due to the large variations in $^4He/^3He$ between the atmosphere, the crust and the upper mantle. Helium and argon isotopes have been used to investigate the mantle input into fluids associated with tungsten-molybdenum mineralisation where they appeared to indicate an input of unfractionated mantle noble gases to the crust (Stuart *et al.*, 1995). Consequently, this technique could be applied to the study of fluid source in porphyry copper deposits. The very high content of radiogenic helium in the crust is liable to dominate any signature the fluids may have, since isotopic equilibration is likely to be very rapid. If the method is to be successful, very precise measurement are required. Mantle-derived melts that have undergone any equilibration with the crust are unlikely to retain their initial isotopic signature, particularly if they have undergone degassing (Hilton *et al.*, 1993), so it is unlikely that the mafic magmas associated with porphyry copper deposits could be correlated with mineralising fluids using this technique.

CO_2-Cl-He-Ar-N_2 ratios

Geothermal fluids contain a number of species (CO_2, Cl, He, Ar, and N_2) which may of magmatic origin and are thought to be conserved during fluid evolution (see Giggenbach, 1995, for a review). Different source regions have distinct ratios of these species such that if the composition of a fluid can be determined, its source area may be predicted (Giggenbach, 1995). These species may all be measured in fluids using quadrupole mass spectrometry, either by bulk analysis or by analysis of individual inclusions (see Graney & Kesler, 1995, for a review). Of all the techniques outlined in this section, this may be the most promising for evaluating the role of mantle-derived fluids in porphyry-copper mineralisation.

8.3.2 The model as a framework

The model presented in Chapter 7 provides a framework which relates hydrothermal components to each other. With an understanding of these relationships, it should be possible to test some of the predictions made by experimental studies concerning the partitioning of metals and other species of interest in melt-fluid and vapour-brine systems. This would require a knowledge of the composition of the fluids trapped in fluid inclusions and the melt with which they equilibrated. A number of techniques exist to analyse the composition of fluid inclusions including ICP-AES/MS (Wilkinson *et al.*, 1994), proton-induced X-ray (PIXE) and gamma-ray (PIGE) emission (e.g. Heinrich *et al*, 1992; Anderson *et al.*, 1989) and synchrotron X-ray fluorescence (SXRF; see Bodnar, 1995, for a review).

CONCLUSIONS

9

1 Andean porphyry copper deposits are characterised by distinctive intrusive lithologies, hydrothermal veins, and styles of alteration which exhibit consistent temporal relationships and together record the evolution of a magmatic-hydrothermal system. Such deposits are centered upon felsic intrusive complexes varying in texture and mineralogy but generally of monzogranite to granodiorite composition. More mafic, primitive magmas are often present and they and the felsic magmas may be comtemporaneous. Predominantly disseminated protore, comprising potassic alteration and chalcopyrite mineralisation, is hosted by the felsic complex and may overprint precursor magnetite alteration. This protore is cross-cut by porphyritic dykes with a phenocryst assemblage comprising plagioclase, resorbed quartz and biotite. These dykes are contemporaneous with the development of quartz-rich veins and breccias which are associated with sericitic alteration.

These distinctive components displaying their characteristic temporal relationships are present at Quebrada Blanca which can therefore be considered representative of Andean porphyry copper deposits.

2 The consistent nature of the temporal relationships displayed by the components that characterise porphyry copper deposits indicates the action of a process or processes common to the evolution of the magmatic-hydrothermal systems associated with deposits of this type. Analysis of data relating to the components that comprise the magmatic-hydrothermal system at Quebrada Blanca suggests that evolution of the system was driven by a series of processes occurring in a sub-volcanic environment:

1. Introduction of mafic magma, rich in volatiles and copper, into the base of a physically stratified felsic magma chamber residing at a shallow level within the crust.
2. Transfer of species from the mafic magma to a layer of felsic magma at the base of the chamber by means of a volatile phase derived from the mafic magma.
3. Saturation of the layer of felsic magma with respect to a volatile phase rich in potassium, iron and copper and with a high ratio of SO_2:H_2S.
4. Transfer of this volatile phase into the dominantly crystalline regions of the chamber and into the material below the brittle-ductile transition.
5. Equilibration of the cooling volatile phase with its surroundings.
6. Dyking of the layer of felsic magma at the base of the chamber upwards through the dominantly crystalline regions of the chamber and ascent of the mafic magma into the evacuated chamber.
7. Decompression-driven degassing of the felsic and mafic magmas.

3 The model proposed accounts more completely for the nature and interrelationships of the characteristic components of magmatic-hydrothermal systems associated with porphyry copper deposits than previous genetic models.

REFERENCE LIST

AGUE, J.J. & BRIMHALL, G.H. 1988. Regional variations in bulk chemistry, mineralogy and the composition of mafic and accessory minerals in the batholiths of California. *Geological Society of America Bulletin* **100** 891-911.

AHMAD, S.N. & ROSE, A.W. 1980. Fluid inclusions in porphyry and skarn ore at Santa Rita, New Mexico. *Economic Geology* **75** 229-250.

AMBRUS, J. 1977. Geology of the El Abra porphyry copper deposit, Chile. *Economic Geology* **72** 1062-1085.

ANDERSON, A.J., CLARK, A.H., MA, X-P., PALMER, G.R., MACARTHUR, J.D. & ROEDDER, E. 1989. Proton induced x-ray and gamma-ray emission of unopened fluid inclusions. *Economic Geology* **84** 924-939.

ANDERSON, A.T. 1984. Probable relations between plagioclase zoning and magma dynamics, Fuego Volcano, Guatemala. *American Mineralogist* **69** 660-676.

ANDERSON, A.T. 1992. Subvolcanic degassing of magma. In Hedenquist, J.W. (Ed) *Magmatic contributions to hydrothermal systems*. Geological Society of Japan Report 279 12-15.

ARANCIBA, O.N. & CLARK, A.H. 1996. Early magnetite-amphibole-plagioclase alteration-mineralisation in the Island Copper porphyry Cu-Mo-Au deposit, British Columbia. *Economic Geology* **91** 402-438.

ARRIBAS, A. 1995. Characteristics of high sulphidation epithermal deposits, and their relation to magmatic fluid. In Thompson, J.F.H. (Ed) *Magmas, fluids and ore deposits*. MAC Short Course Vol. 23 419-454.

ARRIBAS, A., CUNNINGHAM, C.G., RYTUBA, J.J., RYE, R.O., KELLY, W.C., MCKEE, E.H., PODWYSOCKY, M.H. & TOSDAL, R.M. 1995a. Geology, geochronology, fluid inclusions and isotope geochemistry of the Rodalquilar Au-Alunite deposit, Spain. *Economic Geology* **90** 795-822.

ARRIBAS, A., HEDENQUIST, J.W., ITAYA, T., OKADA, T., CONCEPCION, R.A. & GARCIA, J.S. 1995b. Contemporaneous formation of adjacent porphyry and epithermal Cu-Au deposits over 300 ka in northern Luzon, Philippines. *Geology* **23** 337-340.

BAGDASSAROV, N. & DORFMAN, A. 1998. Granite rheology: magma flow and melt migration. *Journal of the Geological Society London* **155** 863-872

BAKER, B.H. & MCBIRNEY, A.R. 1985. Liquid fractionation. III Geochemistry of zoned magmas and the compositional effects of liquid fractionation. *Journal of Volcanology and Geothermal Research* **24** 55-81.

BATEMAN, R. 1985. Progressive crystallisation of a granitoid diapir and its relationship to stages of emplacement. *Journal of Geology* **93** 645-662.

BEANE, R.E. 1974. Biotite stability in the porphyry copper environment. *Economic Geology* **69** 241-256.

BEANE, R.E. 1982. Hydrothermal alteration in silicate rocks. In Titley, S.R. (Ed) *Advances in the geology of porphyry copper deposits, southwestern North America*. Univ. Ariz. Press, Tucson 117-137.

BEANE, R.E. & BODNAR, R.J. 1995. Hydrothermal fluids and hydrothermal alteration in porphyry copper deposits. In Pierce, F.W. & Bolm, J.G. (Eds) *Porphyry copper deposits of the American Cordillera.* Arizona Geological Society Digest 20 83-93.

BLUNDY, J.D. & SHIMIZU, N. 1991. Trace element evidence for plagioclase recycling in calc-alkaline magmas. *Earth and Planetary Science Letters* **102** 178-197.

BODNAR, R.J. 1995. Fluid-inclusion evidence for a magmatic source for metals in porphyry copper deposits. In Thompson, J.F.H. *Magmas, fluids and ore deposits*. MAC Short Course Vol 23 139-152.

BODNAR, R.J., BURNHAM, C.W. & STERNER, S.M. 1985. Synthetic fluid inclusions in natural quartz. III. Determination of phase equilibrium properties in the system H_2O-NaCl to 1000°C and 1500 bars. *Geochimica et Cosmochimica Acta* **49** 1861-1873.

BORTHWICK, J. & HARMON, R.S. 1982. A note regarding ClF_3 as an alternative to BrF_5 for oxygen isotope analysis. *Geochimica et Cosmochimica Acta* **46** 1665-1668.

BOWMAN, J.R., PARRY, W.T., KROPP, W.P. & KRUER, S.A. 1987. Chemical and isotopic evolution of hydrothermal solutions at Bingham, Utah. *Economic Geology* **82** 395-428.

BRANDEIS, G. & JAUPART, C. 1987. The kinetics of nucleation and crystal growth and scaling laws for magmatic crystallisation. *Contributions to Mineralogy and Petrology* **26** 24-34

BURNHAM, C.W. 1979. Volatiles in magmas. In Barnes, H. (Ed) *Geochemistry of hydrothermal ore deposits*, 2nd Edition, Wiley. 71-136.

BURNHAM, C.W. 1981. Physicochemical constraints on porphyry mineralisation. In Dickinson, W.R. & Payne, W.D. (Eds) *Relations of tectonics to ore deposits in the southern cordillera*. Tucson, Arizona Geological Society Digest 14 71-77.

BURNHAM, C.W. 1994. The Burnham model for water solubility in silicate melts. In Caroll, M.R. & Holloway, J. (Eds) *Volatiles in magmas*. Reviews in Mineralogy 30, Mineralogical Association of America, 231-280.

BURNHAM, C.W. 1997. In Barnes, H. (Ed) *Geochemistry of hydrothermal ore deposits*, 3rd Edition, Wiley.

BURNHAM, C.W. & OHMOTO, H. 1980. Late stage processes of felsic magmatism. In Ishihara, S. & Takenouchi, S. (Eds) *Granitic magmatism and related mineralisation.* Mining Geology Special Issue 8 1-11.

CAMUS, F. 1975. Geology of the El Teniente orebody with emphasis on wall-rock alteration. *Economic Geology* **70** 1341-1372.

CANDELA, P.A. 1986. The evolution of aqueous vapour from silicate melts: effect on oxygen fugacity. *Geochimica et Cosmochimica Acta* **50** 1205-1211.

CANDELA, P.A. 1989. Magmatic ore-forming fluids; Thermodynamic and mass transfer calculations of metal concentrations. In Whitney, J.A. & Naldrett, A.J. (Eds) *Ore deposition associated with magmas*. Reviews in Economic Geology 4, Economic Geology Publishing Co., El Paso. 223-233.

CANDELA, P.A. 1991. Physics of aqueous phase exsolution in plutonic environments. *American Mineralogist* **76** 1081-1091.

CANDELA, P.A. 1994. Combined chemical and physical model for plutonic devolatilisation: A non-Rayleigh fractionation algorithm. *Geochimica et Cosmochimica Acta* **58** 2157-2167.

CANDELA, P.A. & HOLLAND, H.D. 1984. The partitioning of copper and molybdenum between silicate melts and aqueous fluids. *Geochimica et Cosmochimica Acta* **48** 373-380.

CANDELA, P.A. & HOLLAND, H.D. 1986. A mass transfer model for copper and molybdenum in magmatic hydrothermal systems; the origin of porphyry type ore deposits. *Economic Geology* **81** 1-19.

CAROLL, M.R. & WEBSTER, J.D. 1994. Solubilities of sulphur, noble gases, nitrogen, chlorine and fluorine in magmas. In Caroll, M.R. & Holloway, J. (Eds) *Volatiles in magmas*. Reviews in mineralogy 30, Mineralogical Association of America, 231-280.

CARR, G.R., DEAN, J.A., SUPPEL, D.W. & HEITHERSAY, P.S. 1995. Precise lead isotope fingerprinting of hydrothermal activity associated with Ordovician to Carboniferous metallogenetic events in the Lachlan Fold Belt of New South Wales. *Economic Geology* **90** 1467-1505.

CLARK, A.H. 1993. Are outsize porphyry copper deposits either anatomically or environmentally distinctive? In Whiting, B. H., Hodgson, C.J. & Mason, R. (Eds) *Giant ore Deposits*. Economic Geology Special Publication 2, 213-284.

CLARK, A.H. & ARANCIBA, O.N. 1995 The occurrence, paragenesis and implications of magnetite-rich alteration and mineralisation in calc-alkaline porphyry copper deposits. In Clark, A.H. (Ed) *Giant ore deposits II* QminEx, Department of Geological Sciences, Queen's University, Kingston, Ontario. 146-181.

CLARK, A.H., ARCHIBALD, D.A. LEE, A.W. FARRAR, A.W. & HODGSON, C.J. 1998. Laser probe $^{40}Ar/^{39}Ar$ ages of early- and late-stage alteration assemblages, Rosario porphyry copper-molybdenum deposit, Collahuasi District, I Region, Chile. *Economic Geology* **93** 326-337.

CLAYTON, R.N. & MAYEDA, T.K. 1963. The use of bromine pentafluoride in the extraction of oxygen from oxides and silicates for isotopic analysis. *Geochimica et Cosmochimica Acta* **27** 43-52.

CLINE, J.S. 1995. Genesis of porphyry copper deposits: the behaviour of water, chloride and copper in crystallising melts. In Pierce, F.W. & Bolm, J.G. (Eds) *Porphyry copper deposits of the American Cordillera*. Arizona Geological Society Digest 20 69-82.

CLINE, J.S. & BODNAR, R.J. 1991. Can economic porphyry copper mineralisation be generated by a typical calc-alkaline melt? *Journal of Geophysical Research* **96** B5 8113-8126.

CORNEJO, P., TOSDAL, R.M., MPODOZIS, C., TOMLINSON, A.J., RIVIERA, O AND FANNING, C.M. 1997. El Salvador, Chile, Porphyry copper revisited: Geologic and Geochronologic framework. *International Geology Review* **39** 22-54.

CYGAN, G.L. & CANDELA, P.A. 1995. Preliminary study of gold partitioning among pyrrhotite, pyrite, magnetite and chalcopyrite in gold-saturated chloride solutions at 600 to 700°C, 140 MPa (1400 bars). In Thomson, J.F.H. (Ed) *Magmas, fluids and ore deposits*. MAC Short Course 23. 129-138.

CZAMANSKE, G.K. & WONES, D.R. 1973. Oxidation during magmatic differentiation, Finnmarka complex, Oslo area, Norway. Part II Mafic silicates. *Journal of Petrology* **14** 349-380.

D'LEMOS, R.S., KEARSLEY, A.T., PEMBROKE, J. W., WATT, G. R. & WRIGHT, P. 1997. Complex quartz growth histories in granite revealed by scanning cathodoluminescence techniques. *Geological Magazine* **134** 549-552.

DELL'ANGELO, L.N. & TULLIS, J. 1988. Experimental deformation of partially melted granitic aggregates. *Journal of Metamorphic Geology* **6** 495-515.

DICKSON, F. W., BLOUNT, C. W. & TUNELL, G. 1963. Use of hydrothermal solution equipment to determine the solubility of anhydrite in water from 100-275°C and from 1 bar to 1000 bars pressure. *American Journal of Science* **261** 61-78.

DILLES, J.H. 1987. Petrology of the Yerington Batholith, Nevada; Evidence for evolution of porphyry copper ore fluids. *Economic Geology* **82** 1750-1789.

DILLES, J.H. & EINAUDI, M.T. 1992. Wall rock alteration and hydrothermal flow paths about the Ann-Mason porphyry copper deposit, Nevada - A 6 km vertical reconstruction. *Economic Geology* **87** 1963-2001

DOBSON, P.F., EPSTEIN, S. & STOLPER, E.M. 1989. Hydrogen isotope fractionation between coexisting vapor and silicate glasses and melts at low pressure. *Geochimica et Cosmochimica Acta* **53** 2723-2730.

DONALDSON, C.H. & HENDERSON, C.M.B. 1988. A new interpretation of round embayments in quartz crystals. *Mineralogical Magazine* **52** 27-33.

DONG, G., MORRISON, G. & SUBHASH, J. 1995. Quartz textures in epithermal veins, Queensland- classification, origin and implication. *Economic Geology* **90** 1841-1856.

DOWLING, K. & MORRISON, G. 1990. Application of quartz textures to the classification of gold deposits using North Queensland examples. In Keays, Ramsey & Groves (Eds) *The geology of gold deposits.* Economic Geology Monograph 6.

DREXLER, J.W. & MUNOZ, J.L. 1988. Highly oxidised pyrrhotite-anhydrite bearing silicic magmas from the Julcani Ag-Cu-Bi-Pb-Au-W district, Peru: Physicochemical conditions of a productive magma. In R. Taylor, R. & Strong, D. (Eds) *Recent advances in the geology of granite related ore deposits.* Canadian Institute of mining and metallurgy Special Volume 39 72-79.

EASTOE, C.J. 1978. A fluid inclusion study of the Panguna Porphyry copper deposit, Bougainville, Papua New Guinea. *Economic Geology* **73** 721-748.

EASTOE, C.J. 1982. Physics and chemistry of the hydrothermal system at Panguna porphyry copper deposit, Bougainville, Papua New Guinea. *Economic Geology* **77** 127-153.

EASTOE, C.J. 1983. Sulphur isotope data and the nature of the hydrothermal systems at the Panguna and Frieda River porphyry copper deposits, Papua New Guinea. *Economic Geology* **78** 201-213.

EICHELBERGER, J.C. 1980. Vesiculation of mafic magma during replenishment of silicic magma reservoirs. *Nature* **288** 446-450.

EICHELBERGER, J.C. 1995. Silicic volcanism: Ascent of viscous magmas from crustal reservoirs. *Anniversary Reviews in Earth and Planetary Science* **23** 41-63.

EICHELBERGER, J.C., CARRIGAN, C.R., WESTRICH, H.R. & PRICE, R.H. 1986. Non-explosive silicic volcanism. *Nature* **323** 598-602.

EILENBERG, S. & CARR, M.J. 1981. Copper contents of lavas from active volcanos in El Salvador and adjacent regions in Central America. *Economic Geology* **76** 2246-2248.

FIELD, C.W. & GUSTAFSON, L.B. 1976. Sulphur isotopes in the porphyry copper deposit of El Salvador, Chile. *Economic Geology* **71** 1533-1548.

FORD, J.H. 1978. A chemical study of alteration at the Panguna porphyry copper deposit, Bougainville, Papua New Guinea. *Economic Geology* **73** 703-720.

FOURNIER, R.O. 1967. The porphyry copper deposit exposed in the Liberty pit mine near Ely, Nevada, I: Syngenetic formation. *Economic Geology* **62** 57-81.

FOURNIER, R.O. 1985. Silica minerals as indicators of conditions during gold deposition. *USGS Bulletin* **1646**, 15-26.

FOURNIER, R.O. 1992. The influences of depth of burial and the brittle-ductile transition on the eveolution of magmatic fluids. In Hedenquist, J.W. (Ed) *Magmatic contributions to hydrothermal systems*. Geological Society of Japan Report 279 57-59.

FREYDIER, C., RUIZ, J., CHESLEY, S.T., MCCANDLESS, T.E., MUNIZAGA S. & PUIG, A. 1996. Re-Os isotope systematics on sulphides: preliminary results on base metal porphyry mineralisation in Chile. *Geological Society of America Abstracts with programs* **28** 154.

GIGGENBACH, W.F. 1992. Isotopic shifts in waters from geothermal and volcanic systems along convergent plate boundaries and their origin. *Earth and Planetary Science Letters* **113** 495-510.

GIGGENBACH, W.F. 1995. Composition of magmatic components in hydrothermal fluids. In Thomson, J.F.H. (Ed) *Magmas, fluids and ore deposits*. MAC Short Course 23 247-262.

GIGGENBACH, W.F. 1996. Chemical composition of volcanic gases. In Scarpa, R. & Tilling, R.I. (Eds) *Monitoring and mitigation of volcano hazards*. Springer-Verlag, Berlin. 221-256.

GRANEY, J.R. & KESLER, S.E. 1995. Gas composition of inclusion fluid in ore deposits: Is there a relation to magmas? In Thomson, J.F.H. (Ed) *Magmas, fluids and ore deposits*. MAC Short Course 23 221-246.

GUSTAFSON, L.B. 1978. Some major factors of porphyry copper genesis. *Economic Geology* **73** 600-607.

GUSTAFSON, L.B. & HUNT, J.P. 1975. The porphyry copper deposit at El Salvador, Chile. *Economic Geology* **70** 857-912.

GUSTAFSON, L.B. & QUIROGA, J. 1995. Patterns of mineralisation and alteration below the porphyry copper orebody at El Salvador, Chile. *Economic Geology* **90** 2-16.

HALL, D.L., STERNER, S.M. & BODNAR, R.J. 1988. Freezing point depression of NaCl-KCl-H_2O solutions. *Economic Geology* **83** 197-202.

HAMMERSCHMIDT, K., DOBEL, R. & FRIEDRICHSEN, H. 1992. Implication of $^{40}Ar/^{39}Ar$ dating of early Tertiary volcanic rocks from the north-Chilean Precordillera. *Tectonophysics* **202** 55-81.

HATTORI, K. 1993. High sulfur magma, a product of fluid discharge from underlying mafic magma; evidence from Mt Pinatubo, Phillippines. *Geology* **21** 1083-1086.

HAYASHI, K.I. & OHMOTO, H. 1991. Solubility of gold in NaCl- and H_2S-bearing aqueous solutions at 250-350°C. *Geochimica et Cosmochimica Acta* **55** 2111-2126.

HAYNES, F.M. & TITLEY, S.R. 1980. The evolution of fracture related permeability within the Ruby Star Granodiorite, Sierrita Porphyry Copper deposit, Pima County, Arizona. *Economic Geology* **75** 673-683.

HEDENQUIST, J.W. 1995. The ascent of magmatic fluid: Discharge versus mineralisation. In Thompson, J.F.H. (Ed) *Magmas, fluids and ore deposits*. MAC Short Course Vol 23 263-290.

HEDENQUIST, J.W., ARRIBAS, A., REYNOLDS, T.J. 1998. Evolution of an intrusion centered hydrothermal system: Far South East-Lepano porphyry and epithermal Cu-Au deposits, Philippines. *Economic Geology* **93** 373-404.

HEDENQUIST, J.W., REYES, A.G., SIMMONS, S.F. & TAGUCHI, S. 1992. The thermal and geochemical structure of geothermal and epithermal systems. A framework for interpreting fluid inclusion data. *European Journal of Mineralogy* **4** 989-1015.

HEINRICH, C.A. 1995. Geochemical evolution and hydrothermal mineral deposition in Sn(-W-base metal) and other granite-related ore systems: Some conclusions from Australian examples. In Thomson, J.F.H. (Ed) *Magmas, fluids and ore deposits*. MAC Short Course 23. 203-220.

HEINRICH, C.A., RYAN, C.G., MERNAGH, T.P. & EADINGTON, P.J. 1992. Segregation of ore metals between magmatic brine and vapour. A fluid inclusion study using PIXE microanalysis. *Economic Geology* **87** 1566-1583.

HEITHERSAY, P.S. & WALSHE, J.L. 1995. Endeavour 26 North: A porphyry copper-gold deposit in the late Ordovician shoshonitic Goonumbla Volcanic Complex, New South Wales, Australia. *Economic Geology* **90** 1506-1532.

HEMLEY, J.J. & HUNT, J.P. 1992. Hydrothermal ore-forming processes in the light of studies in rock-buffered systems: II. Some general geologic applications. *Economic Geology* **87** 23-43

HENLEY, R.W. & MCNABB, A. 1978. Magmatic vapour plumes and ground water interaction in porphyry copper emplacement. *Economic Geology* **73** 1-20.

HERRINGTON, R.J & WILKINSON, J.J. 1993. Colloidal gold and silica in mesothermal vein systems. *Geology* **21** 539-542.

HESS, K. -U. & DINGWELL, D.B. 1996. Viscosities of hydrous leucogranitic melts: A non-Arrhenian model. *American Mineralogist* **81** 1297-1300.

HESS, K. -U., DINGWELL, D.B. & WEBB, S.L. 1995. The influence of excess alkalis on the viscosity of a haplogranitic melt. *American Mineralogist* **80** 297-304.

HEWITT, D.A. & ABRECHT, J. 1988. Experimental evidence on the substitution of titanium in biotite. *American Mineralogist* **73** 1275-1284.

HIBBARD, M.J. 1980. Indigenous source of late stage dykes and veins in granitic plutons. *Economic Geology* **75** 410-423.

HIBBARD, M.J. 1991. Texural anatomy of twelve magmamixed granitoid systems. In Didier & Barbarin (Eds) *Enclaves and granite petrology*, Elsevier, Amsterdam. 431-444.

HILTON, D.R., HAMMERSCHMIDT, K., TEUFEL, S. & FRIEDRICHSEN, H. 1993. Helium isotopic characteristics of Andean geothermal fluids and lavas. *Earth and Planetary Science Letters* **120** 265-282.

HOEK, J.D. 1995. Dyke propogation and arrest in proterozoic tholeiitic dykes swarms, Westfold Hills, East Antartica. In Baer & Heimann (Eds) *Physics and chemistry of dykes*, Balkema, Rotterdam, 79-93.

HOLLAND, H.D. 1972. Granites, solutions and base metal deposits. *Economic Geology* **67** 281-301.

HORITA, J., COLE, D.R. & WESOLOWSKI, D.J. 1995. The activity-composition relationship of oxygen and hydrogen isotopes in aqueous salt solutions: III. Vapour-liquid water equilibration of NaCl solutions to 350°C. *Geochimica et Cosmochimica Acta* **59** 1139-1151.

HORT, M. 1998. Abrupt change in magma liquidus temperature because of volatile loss or magma mixing: effects of nucleation, crystal growth and thermal history of the magma. *Journal of Petrology* **39** 1063-1076.

HOUSH, T.B. & LUHR, J.F. 1991. Plagioclase-melt equilibria in hydrous systems. *American Mineralogist* **76** 477-492.

HUNT, J.P., BRATT, J.A., & MARQUARDT, J.C. 1983. Quebrada Blanca, Chile: An enriched porphyry copper deposit. *Mining Engineering* **35** 636-644.

HUPPERT, H.E., SPARKS, R.S.J. & TURNER, J.S. 1982. Effects of volatiles on mixing in calc-alkaline magma systems. *Nature* **297** 554-557.

ISHIHARA, S., ULRIKSEN, C.E., SATO, K., TERASHIMA, S., SATO, T. & ENDO, Y. 1984. Plutonic rocks of north-central Chile. *Bulletin of the Geological Society of Japan* **35** 503-536.

JACOBS, D.C. & PARRY, W.T. 1979. Geochemistry of biotite at the Santa Rita porphyry copper deposit, New Mexico. *Economic Geology* **74** 860-897.

JAUPART, C. & ALLEGRE, C.J. 1991. Gas content, eruption rate and instabilities of eruption regime in silicic volcanoes. *Earth and Planetary Science Letters* **102** 413-429.

JOHANNES, W. 1978. Melting of plagioclase in the system albite-anorthite-H2O and Quartz-Albite-Anorthite-H_2O at pH_2O=5kbar, an equilibrium problem. *Contributions to Mineralogy and Petrology* **66** 295-303.

JOHN, B.E. & BLUNDY, J.D. 1993. Emplacement-related deformation of granitoid magmas, southern Adamello Massif, Italy. *Geological Society of America Bulletin* **105** 1517-1541.

JOHN, B.E. & STUNITZ, H. 1995. Evidence for magmatic fracturing and small-scale melt segregation during pluton emplacement. In Brown, J. & Piccoli, P. (eds) *The origin of granite and related rocks*. USGS Circular 1129 75-76.

JOHNSON, E. L. & HOLLISTER, L.S. 1992. Grain boundary migration in quartz and its effects on the interpretation of fluid inclusion data from metamorphic rocks. *Geological Society of America Abstracts with programs* **24** 322.

JOLIFF, B.L., PAPIKE, J.J. & SHEARER, C.K. 1986. Tourmaline as a recorder of pegmatite evolution, Bob Ingersoll pegmatite, Black Hills, South Dakota. *American Mineralogist.* **71** 472-500

KAMILLI, R. J. & OHMOTO, H. 1988. A discussion on "Crystallisation and recrystallisation of growth zoned vein quartz crystals from epithermal systems; implications for fluid inclusion studies" Sander, M.V. & Black, J.E. *Economic Geology* **85** 1084-1085.

KEITH, J.D., WHITNEY, J.A., HATTORI, K., BALLANTYNE, G.H., CHRISTIANSEN, E.H., BARR, D.L., CANNAN, T.M. & HOOK, C.J. 1997. The role of magmatic sulphides and mafic alkaline magmas in the Bingham and Tintic Mining districts, Utah. *Journal of Petrology* **38** 1679-1690.

KELLEY & FALLICK, A. 1990. High precision spatially resolved analysis of $\delta^{34}S$ in sulphides using a laser extraction technique. *Geochimica et Cosmochimica Acta* **54** 883-888.

KERR, R.C. 1995. Convective crystal dissolution. *Contributions to Mineralogy and Petrology* **121** 237-246.

KILINC, I.A. & BURNHAM, C.W. 1972. Partitioning of chloride between a silicate melt and coexisting aqueous phase from 2 to 8 kilobars. *Economic Geology* **67** 231-235.

KNIGHT, C.L. & BODNAR, R.J. 1989. Synthetic fluid inclusions: IX. Critical PVTX properties of $NaCl-H_2O$ solutions. *Geochimica et Cosmochimica Acta* **53** 3-8.

KUSUKABE, M., NAKAGAWA, S., HORI, M., MATSUHISA, Y., OJEDA, J.M. & SERRANO, L. 1984. Oxygen and sulphur isotopic compositions of Quartz-anhydrite and sulphide minerals from the El Teniente and Rio Blanco porphyry copper deposits, Chile. *Bulletin of the Geological Society of Japan* **35** 583-614.

KYSER, T.K. 1987. Equilibrium fractionation factors for stable isotopes. In Kyser, T.K. (Ed) *Stable isotope geochemistry*. Mineralogical Association of Canada Short Course 13, 45-72.

LANG, J.R., STANLEY, C.R., THOMPSON, J.F.H & DUNNE, K.P.E. 1995. Na-K-Ca Magmatic-hydrothermal alteration in alkalic porphyry Cu-Au deposits, British Colombia. In Thomson, J.F.H. (Ed) *Magmas, fluids and ore deposits*. MAC Short Course 23 339-366.

LEJEUNE, A. & RICHET, P. 1995. Rheology of crystal-bearing silicate melts: An experimental study at high viscosities. *Journal of Geophysical Research* **100** B3 4215-4229.

LESHER, C.E. 1994. Kinetics of Sr and Nd exchange in silicate liquids: Theory, experiments and applications to uphill diffusion, isotopic equilibration and irreversible mixing of magmas. *Journal of Geophysical Research* **99** 9585-9604.

LOFGREN, G.E. 1980. Experimental studies on the dynamic crystallisation of silicate melts. In Hargraves, R.B. (Ed) *Physics of magmatic processes*, Princeton University Press, Princeton, New Jersey, 487-551.

LONDON, D. & MANNING, D.A.C. 1995. Chemical variation and significance of tourmaline from Southwest England. *Economic Geology* **90** 495-519.

LONDON, D., MORGAN, G.B. & HERVIG, R.L. 1989. Vapour undersaturated experiments with Macusani glass and water at 200 MPa and the internal differentiation of granitic pegmatites. *Contributions to Mineralogy and Petrology* **102** 1-17.

LOPEZ, V.M. 1939. The primary mineralisation at Chuquicamata, Chile. *Economic Geology* **34** 674-711.

LOWELL, J.D. & GUILBERT, J.M. 1970. Lateral and vertical alteration-mineralisation zoning in porphyry ore deposits. *Economic Geology* **65** 373-408.

LOWERNSTERN, J.B. 1993. Evidence for a copper bearing fluid in magma erupted at the Valley of Ten Thousand Smokes, Alaska. *Contributions to Mineralogy and Petrology* **114** 409-421.

MAALOE, S. & WYLLIE, P.J. 1975. Water content of a granite magma deduced from the sequence of crystallisation determined experimentally with water undersaturated conditions. *Contributions to Mineralogy and Petrology* **52** 175-191.

MACLELLAN, H. E. & TREMBATH, L.T. 1991. The role of quartz crystallisation in the development and preservation of igneous texture in granitic rocks: Experimental evidence at 1 kbar. *American Mineralogist* **76** 1291-1305.

MAHOOD, G.A. & CORNEJO, P.C. 1992. Evidence for ascent of differentiated liquids in a silicic magma chamber found in a granitic pluton. *Transactions of the Royal Society of Edinburgh Earth Sciences* **83** 63-69.

MAKSAEV, V. & ZENTILLI, M. 1988. Metallogenic framework of the large porphyry copper deposits of the Andes of northern Chile. *Actas V Congreso Geologico Chileno*, vol. **1** B181-B212.

MARSH, B.D. 1988. Crystal capture, sorting and retention in convecting magma. *Geological Society of America Bulletin* **100** 1720-1737.

MARSH, B.D.1989. Magma chambers. *Anniversary Reviews in Earth and Planetary Science* **17** 439-474.

MARSH, B.D. & MAXEY, M.R. 1983. On the distribution and settling of crystals in a convecting magma. *Journal Volcanology and Geothermal Research* **24** 95-150.

MARSH, T.M., EINAUDI, M.T. & MCWILLIAMS, M. 1997. $^{40}Ar/^{39}Ar$ geochronology of Cu-Au and Au-Ag mineralisation in the Potrerillos District, Chile. *Economic Geology* **92** 784-806.

MASON, D.R. 1978. Compositional variation in ferromagnesian minerals from porphyry copper generating and barren intrusions of the Western Highlands, Papua New Guinea. *Economic Geology* **73** 878-890.

MASUDA, T., MORIKAWA, T., NAKAYAMA, Y., & SUZUKI, S. 1997. Grain boundary migration of quartz during annealing experiments at high temperatures and pressures, with implications for metamorphic geology. *Journal of Metamorphic Geology* **15** 311-322.

MATSUHISA, Y. 1979. Oxygen isotopic fractionation in the system quartz-albite-anorthite-water. *Geochimica et Cosmochimica Acta* **43** 1131-1140.

MATSUHISA, Y. 1992. Origin of magmatic waters in subduction zones: stable isotope constraints. In Hedenquist, J.W. (Ed) *Magmatic contributions to hydrothermal systems.* Geological Society of Japan Report 279 104-109

MATTHEWS, S., JONES, A., & BEARD, A. 1994a. Buffering of melt oxygen fugacity by sulphur redox reactions in calc-alkaline magmas. *Journal of the Geological Society of London.* **151** 815-823.

MATTHEWS, S., JONES, A., & GARDEWEG, M. 1994b. Lascar Volcano, Northern Chile; Evidence for steady state disequilibrium. *Journal of Petrology* **35** 401-432.

MATTHEWS, S.J., SPARKS, R.S.J. & GARDEWEG, M.C. 1995. The relationships between magma mixing and volatile behaviour in the Lascar volcano (23°22'S, 67°44'W) northern Chile: Significance for the formation of copper sulphide and magnetite-apatite orebodies. In Clark, A.H. (Ed) *Giant ore deposits II* QminEx, Department of Geological Sciences, Queen's University, Kingston, Ontario. 146-181.

MAVROGENES, J.A. & BODNAR, R.J. 1994. Experimental evidence and geologic imolications of hydrogen movement into and out of fluid inclusions in quartz. *Geochimica et Cosmochimica Acta* **58**, 141-148.

MCBIRNEY, A.R. 1984. *Igneous petrology*. Oxford University Press, 504pp.

MCFARLANE, A.W. & PETERSEN, U. 1990. Pb isotopes of the Hualgayoc Area, N.Peru: Implications for metal provenance and genesis of a Cordilleran polymetallic mining district. *Economic Geology* **85** 1303-1327.

MEINERT, L.D., HEFTON, K.K., MAYES, D. & TASIRAN, I. 1997. Geology, zonation and fluid inclusion evidence of the Big Gossan Cu-Au skarn deposit, Ertsberg District, irian Jaya. *Economic Geology* **92** 509-526.

MILLER, C.F. & WOODEN, J.L. 1994. Anatexis, hybridisation and the modification of ancient crust: Mesozoic plutonism in the Old Woman Mountains area, California. *Lithos* **32** 111-133.

MOORE, W.J. & CZAMANSKE, G.K. 1973. Composition of biotites from unaltred and altred monzonitic rocks in the Bingham mining district, Utah. *Economic Geology* **68** 269-280.

MULLER, D. & GROVES, D.I. 1997. *Potassic igneous rocks and associated copper-gold mineralisation*. (second edition) Springer, Berlin. 238 pp.

MUNOZ, J.L. & SWENSON, A. 1981. Chloride-hydroxyl exchange in biotite and estimation of relative HCl/HF activities in hydrothermal fluids. *Economic Geology* **76** 2212-2221.

MUNTEAN, J. L., KESLER, S.E., RUSSELL, N. & POLANCO, J. 1990. Evolution of the Monte Negro Acid Sulfate Au-Ag deposit, Pueblo Viejo, Dominican Republic: Important factors in grade development. *Economic Geology* **85** 1738-1758.

NABELEK, P.I., O'NEIL, J.R. & PAPIKE, J.J. 1983. Vapour phase exsolution as a controlling factor in hydrogen isotope variation in granitic rocks. The Notch Peak granitic stock, Utah. *Earth and Planetary Science Letters* **66** 137-150.

NANEY, M.T. 1983. Phase equilibria of rock-forming ferromagnesian silicates in granitic systems. *American Journal of Science* **283** 993-1033.

NANEY, M.T. & SWANSON, S.E. 1980. The effects of Fe and Mg on crystallisation in granitic systems. *American Mineralogist* **65** 639-653.

NELSON, S.T. & MONTANA, A. 1992. Sieve-textured plagioclase in volcanic rocks produced by rapid decompression. *American Mineralogist* **77** 1242-1249.

NORTON, D.L. 1978. Sourcelines, source regions, and pathlines for fluids in hydrothermal systems related to cooling plutons. *Economic Geology* **73** 21-28.

OHMOTO, H. & GOLDHABER, M.B. 1997. Sulphur and carbon isotopes. In Barnes, H. (Ed) *Geochemistry of hydrothermal ore deposits* (third edition) Wiley & Sons, New York. 517-612.

PERNY, B., EBERHARDT, P. RAMSEYER, K., MULLIS, J. & PANKRATH, R. 1992. Microdistribution of Al, Li, and Na in α-quartz: Possible causes and correlation with short-lived cathodoluminescence. *American Mineralogist* **77** 534-544.

PITCHER, W.S. 1991. Synplutonic dykes and mafic enclaves. In Didier & Barbarin (eds) *Enclaves and granite petrology*, Elsevier, Amsterdam. 383-392.

POLI, G. TOMMASINI, S. & HALLIDAY, A.N. 1996. Trace element and isotopic exchange during acid-basic magma interaction processes. *Transactions of the Royal Society of Edinburgh* **87** 225-232.

POLYA, D, A. 1990. Pressure dependence of wolframite stability for hydrothermal vein formation. *Transactions of the Institute of Mining and Metallurgy* **99** B120-124.

PREECE, R.K. & BEANE, R.E. 1982. Contrasting evolutions of hydrothermal alteration in quartz monzonite and quartz diorite wall rocks at the Sierrita porphyry copper deposit, Arizona. *Economic Geology* **77** 1621-1641.

PYLE, D.M. & PYLE, D.L. 1995. Bubble migration and the initiation of volcanic eruptions. *Journal Volcanology and Geothermal Research* **67** 227-232.

RAMBOZ, C., PICHAVANT, M. & WEISBROD, A. 1982. Fluid immiscibility in natural processes: use and misuse of fluid inclusion data. *Chemical Geology* **37** 29-48.

RAMSEYER, K., BAUMANN, J., MATTER, A. & MULLIS, J. 1988. Cathodoluminescence colours of α-quartz. *Mineralogical Magazine* **52** 669-678.

RATAJESKI, K. & CAMPBELL, A.R. 1994. Distribution of fluid inclusions in igneous quartz of the Capitan pluton, New Mexico, USA. *Geochimica et Cosmochimica Acta* **58** 1161-1174.

REUTTER, K-J., SCHEUBER, E. & CHONG, G. 1996. The Precordilleran fault system of Chuquicamata, Northern Chile: Evidence for reversals along arc-parallel strike-slip faults. *Tectonophysics* **259** 213-228.

REUTTER, K-J., SCHEUBER, E. & HELMCKE, D. 1991. Structural evidence of orogen-parallel strike-slip displacements in the Precordillera of Northern Chile. *Geol. Rundsch.* **80** 135-153.

REYNOLDS, T.J. & BEANE, R.E. 1985. Evolution of hydrothermal fluid characteristics at the Santa Rita, New Mexico, porphyry copper deposit. *Economic Geology* **80** 1328-1347.

RICHARDS, J.P., MCCULLOCH, M.T., CHAPPELL, B.W. & KERRICH, R. 1991. Sources of metals in the Porgera Gold deposit, Papua New Guinea: Evidence from alteration, isotope and noble metal geochemistry. *Geochimica et Cosmochimica Acta* **55** 565-580.

RIMSTIDT, J.D. 1997. Gangue mineral transport and deposition. In Barnes (Ed) *Geochemistry of hydrothermal ore deposits* (third edition) Wiley & Sons, New York.

ROBINSON, B.W. & KUSUKABE, M. 1975. Quantitative preparation of sulphur dioxide, for $^{34}S/^{32}S$ analyses, from sulphides by combustion with cuprous oxide. *Analytical Chemistry* **47** 1179-1181.

ROEDDER, E. 1971. Fluid inclusion studies on the porphyry type ore deposits at Bingham, Utah, butte, Montana, and Climax, Colorado. *Economic Geology* **66** 98-120.

ROEDDER, E. 1984. *Fluid inclusions*. Reviews in mineralogy 12, Mineralogical Society of America.

RUBIN, A.M. 1995. Getting granite dykes out of their source region. *Journal of Geophysical Research* **100** 5911-5929.

SAKUYAMA, M. & KUSHIRO, I. 1979. Vesiculation of hydrous andesitic melt and transport of alkalis by separated vapour phase. *Contributions to Mineralogy and Petrology* **71** 61-66.

SANDER, M.V. & BLACK, J.E. 1988. Crystallisation and recrystallisation of growth zoned vein quartz crystals from epithermal systems; implications for fluid inclusion studies. *Economic Geology* **83** 1052-1060.

SAUNDERS, J.A. 1990. Colloidal transport of gold and silica in epithermal precious metal systems: evidence from the Sleeper deposit, Nevada. *Geology* **18** 757-760.

SCAILLET, B., PICHAVANT, M. & DALL'AGNOL, R. 1995. Effects of fO2 on phase equilibria in granitic systems. Conditions of stability and compositional variation of biotite and

amphibole. In Brown, M. & Piccoli, P. (eds) *The origin of granite and related rocks*. USGS Circular 1129 135-136.

SCAILLET, B., HOLTZ, F. & PICHAVANT, M. 1997. Rheological properties of granitic magmas in their crystallisation range. In Boucher (Ed) *Granite from segregation of melt to emplacement fabrics*. Kluwer, Amsterdam. 34-56.

SHELTON, K.L. 1983. Composition and origin of ore-forming fluids in a carbonate–hosted porphyry copper and skarn deposit: A fluid inclusion and stable isotope study of Mines Gaspe, Quebec. *Economic Geology* **78** 387-435.

SHELTON, K.L. & RYE, D.M. 1982. Sulphur isotopic composition of ores from Mines Gaspe, Quebec. An example of sulphate-sulphide disequilibrium in ore forming fluids with applications to other porphyry-type deposits. *Economic Geology* **77** 1688-1709.

SHEPHERD, T.J., RANKIN, A.H. & ALDERTON, D.H.M. 1986. *A practical guide to fluid inclusions*. London, Blackie, 239p.

SHEPPARD, S.M.F. & GUSTAFSON, L.B. 1976. Oxygen and hydrogen isotopes in the porphyry copper deposit of El Salvador, Chile. *Economic Geology* **71** 1549-1559.

SHEPPARD, S.M.F., NIELSON, & TAYLOR. 1980. Oxygen and hydrogen isotope ratios of clay minerals from porphyry copper deposits. *Economic Geology* **64** 755-777.

SHINOHARA, H. & HEDENQUIST, J.W. 1997. Contraints on magma degassing beneath the Far South East Porphyry Cu-Au deposit, Philippines. *Journal of Petrology* **38** 1741-1752.

SHINOHARA, H. & KAZAHAYA, K. 1995. Degassing processes related to magma chamber crystallisation. In Thompson, J.F.H. (Ed) *Magmas, fluids and ore deposits*. MAC Short Course Vol 23 47-70.

SHMULOVICH, K.I., TKACHENKO, S.I. & PLYASUNOVA, N.V. 1995. Phase equilibria in fluid systems at high pressures. In Shmulovich, K., Yardley, B. & Gonchar, G. (Eds) *Fluids in the crust*. Chapman & Hall, London, 193-214.

SILLITOE, R.H. 1985. Ore-related breccias in volcano-plutonic arcs. *Economic Geology* **80** 1467-1514.

SILLITOE, R.H. 1988. Epochs of intrusion-related copper mineralisation in the Andes. *Journal of South American Earth Science* **1** 89-108.

SILLITOE, R.H. 1995a. The influence of magmatic-hydrothermal models on exploration strategies for volcano-plutonic arcs. In Thompson, J.F.H. *Magmas, fluids and ore deposits*. MAC Short Course Vol 23 511-525.

SILLITOE, R.H. 1995b. *Exploration and discovery of base- and precious-metal deposits in the circum-Pacific region during the last 25 years.* Resource Geology Special Issue 19, Society of Resource Geology, Japan, 119p.

SILLITOE, R.H. 1997. Characteristics and controls of the largest porphyry copper-gold and epithermal gold deposits in the circum-Pacific region. *Australian Journal of Earth Science* **44** 373-388.

SINGER, B.S., DUNGAN, M.A., & LAYNE, G.D. 1995. Textures and Sr, Ba, Mg, Fe, K and Ti compositional profiles in volcanic plagioclase: Clues to the dynamics of calc-alkaline magma chambers. *American Mineralogist* **80** 776-798.

SISSON, T.W. & LANGE, G.D. 1993. Water in basalt and basaltic-andesite glass inclusions from subduction related volcanics. *Earth and Planetary Science Letters.* **117** 619-635.

SOURIRAJAN, S. & KENNEDY, G.C. 1962. The system H2O-NaCl at elevated temperatures and pressures. *American Journal of Science* **260** 115-141.

Sparks, R.S.J. et al. 1977 *Nature* **267** 315-318.

SPEER, J.A. 1987. Evolution of magmatic AFM mineral assemblages in granitoid rocks: The hornblende +melt=biotite reaction in the Liberty Hill pluton, South Carolina. *American Mineralogist* **72** 863-878.

STANTON, R.L. 1994. *Ore elements in arc lavas.* Oxford University Press, Oxford, 391p.

STERNER, S.M., HALL, D.L. & BODNAR, R.J. 1988. Synthetic fluid inclusions. V. Solubility relations in the system NaCl-KCl-H2O under vapor-saturated conditions. *Geochimica et Cosmochimica Acta* **52** 989-1005.

STIMAC, J. A. & PEARCE, T.H. 1992. Textural evidence of mafic-felsic magma interaction in dacite lavas, Clear Lake, California. *American Mineralogist* **77** 795-809.

STOFFREGEN, R. 1987. Genesis of acid-sulphate alteration and Au-Cu-Ag mineralisation at Summitville, Colorado. *Economic Geology* **82** 1575-1592.

STUART, F. M., BURNARD, P.G., TAYLOR, G. & TURNER, G. 1995. Resolving mantle and crustal contributions to ancient hydrothermal fluids: He-Ar isotopes in fluid inclusions from Dae Hwa W-Mo mineralisation. *Geochimica et Cosmochimica Acta* **59** 4663-4673.

SUZUOKI, T. & EPSTEIN, S. 1976. Hydrogen isotope fractionation between OH-bearing minerals and water. *Geochimica et Cosmochimica Acta* **40** 1229-1240.

TAIT, S. & JAUPART, C. 1990. Physical processes in the evolution of magmas. In Nicholls, J. & Russell, J.K. (Eds) *Modern methods of igneous petrology*. Reviews in Mineralogy 24, Mineralogical Society of America.

TAKAGI, T. & TSUKIMURA, K. 1997. Genesis of oxidised and reduced type granites. *Economic Geology* **92** 81-86.

TAYLOR, B.E. 1988. Degassing of rhyolitic magmas: hydrogen isotope evidence and implications for magmatic-hydrothermal ore deposits. In Taylor, R.P. & Strong, D.F. (Eds) *Recent advances in the geology of granite related mineral deposits*. Canadian Institute of Mining and Metallurgy Special Volume 39 33-49.

TAYLOR, H.P. 1974. The application of O and H isotope studies to problems of hydrothermal alteration and ore deposition. *Economic Geology* **69** 843-883.

THOMAS, N., TAIT, S. & KOYAGUCHI, T. 1993. Mixing of stratified liquids by the motion of gas bubbles: application to magma mixing. *Earth and Planetary Science Letters* **115** 161-175.

TITLEY, S.R. & BEANE, R.E. 1981. Porphyry copper deposits. *Econ. Geol. 75th Anniversary volume* 214-269.

TRUESDELL, A.H. 1974. Oxygen isotope activities and concentration in aqueous salt solutions at elevated temperatures: Consequences for isotope geochemistry. *Earth and Planetary Science Letters* **23** 387-396.

TSUCHIYAMA, A. 1985. Dissolution kinetics of plagioclase in the melt of the system diopside-albite-anorthite, and origin of dusty plagioclase in andesites. *Contributions to Mineralogy and Petrology* **89** 1-16.

TULLIS, J. & YUND, R.A. 1982. Grain growth kinetics of quartz and calcite aggregates. *Journal of Geology* **90** 301-318.

VAN DER MOLEN, I. & PATERSON, M.S. 1979. Experimental deformation of partially melted granite. *Contributions to Mineralogy and Petrology* **70** 299-318.

VERGNIOLLE, S. & JAUPART, C. 1986. Separated two-phase flow and basaltic eruptions. *Journal of Geophysical Research* **91** B12 12,842-12860.

VERNON, R.H. 1991. Interpretation of microstructures in microgranitoid enclaves, in Didier & Barbarin (Eds) *Enclaves and granite petrology*, Elsevier, Amsterdam. 277-291.

VIGNERESSE, J.L., BARBEY, P. & CUNEY, M. 1996. Rheological transitions during partial melting and crystallisation with application to felsic magma segregation and transfer. *Journal of Petrology* **37** 1579-1600.

VILA, T. & SILLITOE, R.H. 1991. Gold-rich porphyry systems in the Maricunga belt, northern Chile. *Economic Geology* **86** 1238-1260.

WATT, G.R., WRIGHT, P., GALLOWAY, S. & MCLEAN, C. 1997. Cathodoluminescence and trace element zoning in quartz phenocrysts and xenocrysts. *Geochimica et Cosmochimica Acta* **61** 4337-4348.

WESTRICH, H.R. & GERLACH, T.M. 1992. Magmatic gas source for the stratospheric SO_2 cloud from the June 15, 1991, eruption of Mount Pinatubo. *Geology* **20** 867-870.

WHITNEY, J.A. 1975a. Vapour generation in a quartz-monzonite magma. A synthetic model with application to porphyry copper deposits. *Economic Geology* **70** 346-358.

WHITNEY, J. A. 1975b. The effects of pressure, temperature and *X*H2O on phase assemblage in four synthetic rock compositions. *Journal of Geology* **83** 1-27.

WHITNEY, J.A. 1989. Origin and evolution of silicic magmas. In Whitney, J.A. & Naldrett, A.J. (Eds) *Ore deposition associated with magmas*. Reviews in Economic Geology 4 183-201.

WHITNEY, J.A., HEMLEY, J.J. & SIMON, F.O. 1985. The concentration of iron in chloride solutions equilibrated with synthetic granite compositions: the sulfur-free system. *Economic Geology* **80** 444-460.

WILKINSON, J.J., RANKIN, A.H., MULSHAW, S.C., NOLAN, J. & RAMSEY, M.H. 1994. Laser ablation-ICP-AES for the determination of metals in fluid inclusions: An application to the study of magmatic ore fluids. *Geochimica et Cosmochimica Acta* **58** 1133-1146

WILLIAMS, S.A. & FORRESTER, J.D. 1995. Characteristics of porphyry copper deposits. In Pierce, F.W. & Bolm, J.G. (Eds) *Porphyry copper deposits of the American Cordillera*, Arizona Geological Society Digest 20 21-34.

WILLIAMS, M.L. & BAUER, P.W. 1995. The Copper hill Cu-Ag-Sb deposit, Picuris range, New Mexico; retrograde mineralisation in a brittle ductile trap. *Economic Geology* **90** 1994-2005.

ZENG, Y. 1995. Oxygen isotope fractionation in magnetites: Structural effect and oxygen inheritance. *Chemical Geology* **121** 309-316.

ZENTILLI, M., GRAVES, M., LINDSAY, D., OSSANDON, G. & CAMUS, F. 1993. Recurrent mineralisation in the Chuquicamata porphyry copper system: restrictions on genesis from mineralogical, geochronological and isotopic studies. In Whiting, B. H., Hodgson, C.J. & Mason, R. (Eds) *Giant ore Deposits*. Economic Geology Special Publication 2, 86-100.

ZHANG, Y. & FRANZ, J.D. 1987. Determination of the homogenisation temperature and densities of supercritical fluids in the system NaCl-KCl-$CaCl_2$-H_2O using synthetic fluid inclusions. *Chemical Geology* **64** 335-350.

ZWENG, P.L. & CLARK, A.H. 1995. Hypogene evolution of the Toquepala porphyry copper molybdenum deposit, Moquegua, Southeastern Peru. In Pierce, F.W. & Bolm, J.G. (Eds) *Porphyry copper deposits of the American Cordillera*. Arizona Geol. Soc. Digest 20 566-611.

A1. Preparation of samples for whole-rock analysis

1. The moisture content (H_2O^-) and loss on ignition (LOI) of samples is determined by fusion.
2. % H_2O^- is determined by heating the sample, about 4g, overnight at 110°C.
3. After the H_2O^- has been determined, 0.2500 g of the dried sample is weighed into a clean porcelain crucible.
4. Remainder of powder is reweighed. The %LOI is then determined by heating this sample from room temperature to 950°C in a muffle furnace and keeping at this temperature overnight. Sample is allowed to cool for ~3 hours before reweighing and determining LOI.
5. The 0.25g aliquote is mixed with 0.7500g of Spectroflux 100B (fluxing agent) and placed in a pre-ignited graphite crucible before being fused in a muffle furnace for 20 minutes at 1000°C.
6. After fusion, the molten bead is poured into a beaker containing 25 ml 2N HNO_3 and 150 ml H_2O.
7. The bead is dissolved in the beaker using a magnetic stirrer for 30 minutes. The contents are then transferred to a 250 ml volumetric flask, the beaker rinsed and the rinsings also added to the flask.
8. The flask is diluted to volume, shaken well, and then the contents are filtered through a Whatman No.41 filter paper into a plastic bottle. The bottle is sealed with a piece of plastic beneath the cap. This solution is 1000ppm sample and is ready for analysis.

Samples of the monzogranite
Samples with magnetite

Sample #	164	176	220	233	250	286
SiO2	66.74	66.39	68.86	67.84	70.55	
Al2O3	15.19	15.18	15.42	14.71	14.89	16.05
FeO	5.29	5.48	2.91	2.71	3.23	6.42
MgO	1.49	1.82	1.39	0.99	1.2	2.72
CaO	1.21	0.36	0.32	0.23	0.52	1.44
NaO	4.39	3.72	4.32	4.08	4.5	3.11
K2O	3.21	3.39	3.46	4.62	3.81	3.1
P2O5	0.22	0.07	0.08	0.09	0.09	0.21
TiO2	0.73	0.66	0.57	0.49	0.51	
MnO	0.04	0.04	0.01	0.01	0.02	0.05
H2O-	1.21	2.09	1.84	1.52	1.01	1.2
	99.72	99.2	99.18	97.29	100.33	
Ba	580	482	584	729	698	516
Sr	161	137	76	118	161	179
Cr	75	95	119	103	120	101
Cu	1555	2305	828	1384	736	3000
Ni			21	28	17	
Zn	100	76	587	199	94	198
Zr	247	174	255	236	225	
Mo	39	55				22

Samples of the monzogranite
Samples with sulphides only

Sample #	163	168	231	236	248	258	262
SiO2	70.39	70.41	72.31	68.94	68.67	70.58	67.6
Al2O3	14.95	14.98	13.47	14.58	14.6	14.69	14.57
FeO	2.8	3.07	1.36	3.86	3.78	2.6	3.44
MgO	1.06	1	0.99	1.32	1.44	1.04	1.31
CaO	0.49	0.4	0.4	0.46	0.36	0.31	0.25
NaO	5.44	4.57	2.98	3.76	4.69	4.2	2.43
K2O	2.34	3.83	6.83	5.11	3.56	3.73	7.29
P2O5	0.13	0.07	0.09	0.13	0.15	0.07	0.15
TiO2	0.52	0.51	0.37	0.5	0.52	0.51	0.5
MnO	0.02	0.02	0.01	0.04	0.02	0.01	0.02
H2O-	1.64	1.15	0.77	0.86	1.66	1.84	1.31
	99.78	100.01	99.58	99.56	99.45	99.58	98.87
Ba	379	791	879	798	609	644	1223
Sr	107	142	136	146	104	110	153
Cr	140	120	159	149	146	138	123
Cu	1154	878	1811	2255	1100	1777	3199
Ni			35	20	25	16	23
Zn	106	102	32	120	88	69	108
Zr	225	244	173	240	248	240	212
Mo	41.5	34.28					

Samples of the monzogranite

	Samples of the monzogranite Samples with sulphides only							
Sample #	265	287	290	295	299	300	303	305
SiO2								
Al2O3	14.1	14.23	14.42	15.61	13.95	14.12	14.31	13.06
FeO	2.57	2.46	2.79	3.6	3	3.03	2.76	3.33
MgO	1.26	1.08	0.99	1.46	0.86	0.88	1.13	0.91
CaO	0.31	0.39	0.49	0.64	0.24	0.22	0.31	0.7
NaO	4.21	4.76	4.61	4.25	3.84	3.57	4.35	3.92
K2O	4.47	3.25	3.72	3.48	3.67	3.77	3.83	4.04
P2O5	0.06	0.06	0.17	0.16	0.05	0.04	0.05	0.15
TiO2	0.28							
MnO	0.02	0.01	0.01	0.02	0.01	0.01	0.01	0.03
H2O-		0.4	0.3	1.2	0.6	0.7	0.1	0.1
Ba	589	558	546	601	670	675	752	684
Sr	138	136	113	246	85	85	99	132
Cr	98	100	109	56	126	115	115	138
Cu	3941	6347	2073	3773	525	973	2161	963
Ni								
Zn	60	117	53	182	121	97	64	50
Zr								
Mo	90	39		17	7	5	65	23

	aplite		
Sample #	283	216	253
SiO2		57.11	63.13
Al2O3	16.12	16.7	16.12
FeO	7.22	9.2	5.92
MgO	2.27	2.98	3.37
CaO	1.26	1.75	1.58
NaO	3.18	3.76	3.1
K2O	3.36	3.72	2.58
P2O5	0.34	0.46	0.24
TiO2		1.53	1.23
MnO	0.03	0.06	0.05
H2O-		2.08	2.79
		99.35	100.11
Ba	573	259	246
Sr	173	155	190
Cr	83	83	112
Cu	502	1986	1704
Ni		34	24
Zn	168	413	194
Zr		200	206
Mo	2		

Samples of the andesite dykes and their selvedges

Sample #	304	256	213	306	280	292	301
SiO2		54.81	48.34	47.48	49.8	42.81	42.22
Al2O3	16.5	18.3	17.94	18.86	17.41	16.32	17.33
FeO	8.21	7.73	11.64	10.37	11.53	17.33	14.43
MgO	2.65	5.66	8.12	7.88	7.7	10.28	12.12
CaO	2.59	0.79	0.7	0.68	0.16	0.07	0.07
NaO	3.75	3.44	2.66	3.06	0.75	0.31	0.3
K2O	2.17	4.59	6.27	7.09	7.08	8.74	8.58
P2O5	0.25	0.14	0.17	0.15	0.07	0.06	0.04
TiO2	0.57	0.97	1.16	1.33	0.89	0.9	1.02
MnO	0.04	0.05	0.1	0.09	0.08	0.08	0.12
H2O-	0.4	2.89	2.5	1.98	3.53	1.87	2.38
Total		99.37	99.6	98.97	99	98.77	98.61
Ba	344	548	364	375	280	293	237
Sr	248	204	102	92	41	18	13
Cr	75	167	99	372	259	569	709
Cu	423	1117	1651	2973	1728	579	2484
Ni		79	46	68	85	132	204
Zn	71	183	237	96	187	107	152
Zr		145	99	105	102	79	61
Mo			6				

	Samples of the feldspar porphyry							
	Fresh						Groundmass-rich	
Sample #	172	212	239	259	272	273	261	267
SiO2	67.05	65.4	67.12	66.49		65.87	63.81	66.57
Al2O3	16.98	16.61	16.88	16.88	15.74	16.92	17.16	16.36
FeO	3.41	4.42	3	3.58	3.59	4.14	5.11	4.02
MgO	1.3	1.38	1.35	1.41	1.09	1.28	1.58	1.55
CaO	2.2	2.03	2.43	2.32	2.35	2.71	2.14	1.68
NaO	4.03	4.61	4.23	4.55	3.96	4.3	4.49	4.4
K2O	2.73	2.51	2.18	2.51	2.47	2.61	2.91	2.53
P2O5	0.18	0.23	0.18	0.17	0.19	0.18	0.2	0.18
TiO2	0.45	0.48	0.49	0.44	0.33	0.43	0.51	0.43
MnO	0.03	0.05	0.04	0.03	0.02	0.03	0.04	0.04
H2O-	1.88	1.9	2.11	1.75	0.9	1.33	1.78	1.99
Total	100.24	99.62	100.01	100.13		99.8	99.73	99.75
Ba	770	640	607	661	720	716	632	557
Sr	449	467	477	504	498	541	466	371
Cr	36	83	101	97	61	151	96	110
Cu	916	380	703	119	753	789	1998	1052
Ni		23	28	24		26	28	23
Zn	67	332	59	109	161	160	99	114
Zr	113	122	137	119		117	123	127
Mo	67				5			

	Early sericitic alteration					
Sample #	177	260	296	297	309	310
SiO2	65.72	68	67.74			
Al2O3	17.43	16.13	17.29	15.72	15.76	16.4
FeO	4.27	2.65	2.81	3.47	3.35	3.03
MgO	1.24	1.24	1.09	1.29	1.26	0.9
CaO	1.77	1.65	1.27	0.74	1.16	1.25
NaO	3.15	4.3	3.51	4.91	3.4	3.57
K2O	3.19	3.38	2.48	2.81	4.06	2.3
P2O5	0.18	0.16	0.08	0.2	0.14	0.18
TiO2	0.49	0.37	0.46	0.3	0.32	0.32
MnO	0.02	0.03	0.02	0.02	0.01	0.01
H2O-	2.65	1.83	3.6	1.2	1.4	0.8
Total	100.11	99.74	100.35			
Ba	733	801	695	488	587	743
Sr	416	422	368	235	254	468
Cr	41	131	107	58	95	31
Cu	1400	1033	1152	1265	3069	5040
Ni		28	21			
Zn	104	115	155	167	104	173
Zr	109	101	135			
Mo	28			16	21	23

Accuracy of whole-rock analyses

	W-2			BE-N			JR-2		SY-2	
Sample	M	M	Stand.	M	M	Stand.	M	Stand.	M	Stand.
SiO2	52.58	52.43	52.44	38.81	38.54	38.20	75.44	75.65	60.23	60.11
Al2O3	15.32	15.28	15.35	10.10	10.07	10.07	12.65	12.82	12.05	12.04
Fe2O3	11.12	11.09	10.74	13.27	13.14	12.84	0.81	0.86	6.45	6.31
MgO	6.33	6.32	6.37	13.11	13.08	13.15	0.16	0.05	2.69	2.69
CaO	10.89	10.88	10.87	14.32	13.95	13.87	0.52	0.45	7.97	7.96
Na2O	2.33	2.31	2.14	3.14	3.26	3.18	4.07	4.03	4.35	4.31
K2O	0.68	0.64	0.63	1.33	1.36	1.39	4.59	4.45	4.58	4.45
P2O5	0.14	0.13	0.13	1.03	1.04	1.05	0.02	0.01	0.43	0.43
TiO2	1.06	1.06	1.06	2.63	2.61	2.61	0.07	0.09	0.14	0.15
MnO	0.16	0.16	0.16	0.20	0.20	0.20	0.11	0.11	0.31	0.32
Ba	171	172	182	1023	1018	1025	31	39	449	460
Sr	192	193	194	1374	1371	1370	9	8	269	271
Cr	129	123	93	385	376	360	25	3	47	10
Cu	93	98	103	77	72	72	14	2	12	5
Ni	90	90	70	287	278	267	14	1	31	10
Zn	76	75	77	122	123	120	27	30	259	248
Zr	92	92	94	266	266	265	86	102	295	280

	Difference between standard and measured						Mean diff.	measure mean	%diff
SiO2	0.14	-0.01	0.61	0.34	-0.21	0.12	0.16	53.0038	0.31
Al2O3	-0.03	-0.07	0.03	0.00	-0.17	0.01	-0.04	12.5807	0.29
Fe2O3	0.38	0.35	0.43	0.30	-0.05	0.14	0.26	9.31328	2.77
MgO	-0.04	-0.05	-0.04	-0.07	0.11	0.00	-0.01	6.94928	0.20
CaO	0.02	0.01	0.45	0.08	0.07	0.01	0.11	9.75573	1.10
Na2O	0.19	0.17	-0.04	0.08	0.04	0.04	0.08	3.24308	2.46
K2O	0.05	0.02	-0.06	-0.03	0.14	0.13	0.04	2.19521	1.80
P2O5	0.00	0.00	-0.02	-0.01	0.01	0.00	0.00	0.46457	0.52
TiO2	0.00	0.00	0.02	0.00	-0.02	-0.01	0.00	1.26199	0.11
MnO	0.00	0.00	0.00	0.00	0.00	-0.01	0.00	0.19002	0.87
Ba	0.14	-0.01	-2.13	-6.57	-8.21	-10.98	-4.63	477.269	0.97
Sr	-1.94	-0.77	3.85	0.75	1.12	-1.77	0.21	568.041	0.04
Cr	36.38	30.03	25.47	15.71	22.18	36.94	27.79	180.952	15.36
Cu	-9.86	-5.03	5.44	0.12	11.91	7.33	1.65	61.1522	2.70
Ni	20.48	19.87	19.68	10.71	12.54	20.88	17.36	131.527	13.20
Zn	-0.86	-1.99	2.37	2.85	-3.19	11.48	1.78	113.776	1.56
Zr	-2.31	-2.25	0.51	0.56	-16.48	14.56	-0.90	182.433	0.46

Detection limits

	BLK1	BLK2	BLK3	BLK4	Mean	stdev	detection Limit
SiO2		0.19641			0.049		0.05 wt%
Al2O3	0.05796	0.11717	0.07031	0.05715	0.076	0.028	0.10 wt%
Fe2O3	0.03406	0.03806	0.02521	0.02791	0.031	0.006	0.04 wt%
MgO	0.1126	0.12043	0.11215	0.11566	0.115	0.004	0.12 wt%
CaO	0.02234				0.006		0.01 wt%
Na2O	0.02596	0.05327	0.03244	0.03413	0.036	0.012	0.05 wt%
K2O	0.0517	0.07977	0.0252	0.01904	0.044	0.028	0.07 wt%
P2O5					0.000		0.00 wt%
TiO2	0.01049	0.01222	0.0106	0.0116	0.011	0.001	0.01 wt%
MnO					0.000		0.00 wt%
Ba	3.49198	6.93229	5.39359	5.46876	5.322	1.411	7 ppm
Sr	1.23956	1.67741	1.3742	1.70685	1.500	0.229	2 ppm
Co	3.53839	3.38381	5.10994	5.42215	4.364	1.052	5 ppm
Cr	3.31178	10.3863	6.82037	9.07387	7.398	3.097	10 ppm
Cu	7.18306	61.7756	68.4626	11.4357	37.214	32.384	70 ppm
Ni	8.9118	13.8807	10.8195	13.865	11.869	2.441	14 ppm
Zn					0.000		0 ppm
Zr	12.3103	16.9455	13.1498	39.076	20.370	12.632	33 ppm

EPMA analysis of biotite

All values are weight % oxide of the element. Each set of values represents the average of either two or three repeats - samples that failed to produce a repeat have been excluded as have samples with low totals. With the exception of Mn, Ca and Cl, all elements are effectively majors and well above detection limits. All quoted values of Cl are above detection limit except where prefixed by a minus. The operating conditions of the probe were 15 Kv potential with 100 second livetime.

Phenocrystic biotite from the feldspar porphyry

	Sample 166			Sample 172					Sample 17
Oxide	N7	N3	N5	N7	N8	N2	N3	N5	N1
Si	38.185	37.493	37.992	38.255	38.488	37.807	38.026	37.824	37.724
Ti	4.196	4.067	3.485	3.952	3.798	4.455	4.173	4.319	3.916
Al	15.599	15.333	15.8	15.46	15.989	15.381	15.377	14.968	15.905
Fe	16.742	16.253	15.813	15.931	15.438	16.537	16.517	15.825	17.935
Mn	0.204	0.211	0.222	0.12	0.216	0.154	0.134	0.212	0.251
Mg	12.583	12.862	13.613	13.782	13.495	12.901	13.27	13.601	11.522
Ca	0.046	0.038	0.085	0.086	0.075	0.064	0.015	0.075	0.009
Na	0.545	0.456	0.605	0.627	0.528	0.495	0.581	0.633	0.408
K	9.211	9.073	9.248	9.207	9.18	9.227	9.092	8.909	9.207
Cl	0.258	0.282	0.242	0.159	0.208	0.196	0.211	0.207	0.104
Total	97.569	96.068	97.105	97.579	97.415	97.217	97.396	96.573	96.981

Oxide	N4	N6	N3	N6	211 1 1	211 2 1	211 3 1	211 4 1	239B 1 1
Si	37.77	37.716	38.06	38.197	38.09	37.89	37.47	37.96	38.25
Ti	3.751	3.932	3.917	4.054	3.85	4.35	3.92	4.2	2.7
Al	15.442	15.729	15.419	15.573	14.68	14.34	14.7	14.79	15.72
Fe	16.888	16.948	15.641	16.2	14.79	15.44	15.67	15.67	14.78
Mn	0.233	0.139	0.129	0.172	0.07	0.13	0.23	0.21	0.08
Mg	12.727	12.286	13.685	13.424	14.19	12.84	12.21	12.51	12.73
Ca	0.036	0.103	0.046	0.055	0.04	0.06	0.02	0.01	0.05
Na	0.533	0.562	0.66	0.502	0.54	0.45	0.53	0.51	0.33
K	9.015	8.933	8.902	9.171	9.22	9.32	8.96	9.29	9.43
Cl	0.297	0.274	0.214	0.168	0.16	0.18	0.19	0.2	0.16
Total	96.692	96.622	96.673	97.516	95.63	95	93.9	95.35	94.23

Oxide	239B 2 1	239B 3 1	239B 4 1	257 1 1	257 2 1	257 3 1	257 4 1	257 5 1	261 1 1
Si	37.45	38.02	38.17	38.666	37.38733	38.722	38.3765	39.0815	37.75
Ti	3.85	2.81	3.78	3.2885	3.563	3.645667	3.6715	3.1585	3.81
Al	14.77	15.92	14.91	15.5055	14.91	15.337	15.464	16.2045	14.94
Fe	14.49	14.73	13.76	12.898	14.09467	12.76833	14.006	13.279	15.56
Mn	0.18	0.23	0.19	0.188	0.127667	0.178	0.1755	0.098	0.19
Mg	13.54	12.85	13.97	14.6965	13.636	15.39	14.224	14.2795	13.01
Ca	-0.1	0.06	0.04	0.1035	0.089	0.103667	-0.0135	0.0265	-0.02
Na	0.67	0.36	0.45	0.4915	0.442333	0.581	0.6345	0.588	0.49
K	9.39	9.81	9.34	9.5805	9.181	9.541333	9.618	9.888	9.54
Cl	0.18	0.16	0.18	0.17	0.195	0.168	0.2355	0.15	0.25
Total	94.42	94.95	94.79	95.588	93.626	96.435	96.392	96.7535	95.52

Oxide	261 2 1	261 3 1	261 4 1	267 1 1	267 3 1	267 4 1	267 5 1	267 6 1	267 7 1
Si	37.76	37.36	37.47	38.22267	38.1435	38.10433	38.057	37.514	37.97033
Ti	3.88	3.75	4.12	2.927	4.1705	3.521333	3.9625	3.334333	3.569333
Al	14.7	14.56	14.97	15.51833	14.3905	15.53533	14.5655	15.573	14.53433
Fe	15.76	15.64	15.59	16.40867	16.5215	15.39233	15.8545	16.37033	14.52667
Mn	0.32	0.21	0.26	0.430333	0.54	0.519333	0.6805	0.543333	0.587333
Mg	12.91	12.97	13.19	11.99067	12.8775	12.43967	13.1665	11.74	13.827
Ca	0.09	-0.01	0.04	0.088667	0.0925	0.110667	0.028	-0.030667	0.123667
Na	0.28	0.49	0.57	0.168	0.1515	0.167667	0.071	0.231667	0.219
K	9.55	9.37	9.51	9.77	9.4885	8.726333	9.5635	9.923	9.309667
Cl	0.25	0.3	0.24	0.228	0.192	0.212333	0.23	0.201	0.175667
Total	95.5	94.64	95.96	95.75233	96.568	94.72933	96.179	95.4	94.843

Oxide	Phenocrystic biotite from the feldspar porphyry								
Si	285 5 1	296 1 1	296 2 1	296 3 A1	296 3 B1	296 2 A1	296 2 B1	296 1 A1	296 6 1
Ti	38.58675	38.10267	38.4425	38.341	37.942	38.6445	37.722	37.757	37.7755
Al	4.1685	3.511667	4.412	4.5795	4.5555	4.4175	4.0395	3.6965	4.401
Fe	14.83025	15.31933	14.198	14.162	14.6145	14.3745	14.585	14.8155	14.6155
Mn	12.20175	16.407	15.135	15.6885	17.3445	14.7905	16.18	16.3605	16.41
Mg	0.1645	0.511667	0.449	0.3975	0.5055	0.639	0.42	0.504	0.457
Ca	15.44275	11.97067	14.3225	13.3785	12.2385	14.3235	12.398	12.684	12.04
Na	0.1265	0.153333	0.07	0.155	0.111	0.074	0.0385	0.1285	0.1565
K	0.55525	0.173	0.2055	0.3015	0.2445	0.227	0.1855	0.206	0.2445
Cl	9.37475	8.681	9.452	9.2095	9.279	9.4315	9.4115	9.1075	8.6035
Total	0.21675	0.225	0.2665	0.2365	0.1785	0.2685	0.252	0.265	0.2935
	95.66775	95.05533	96.953	96.4495	97.0135	97.1905	95.232	95.5245	94.997

Oxide	297 1 1	297 2 1	297 3 1	297 4 1	297 5 1
Si	38.202	38.4275	37.95667	36.586	37.79
Ti	3.513	3.56	3.486	4.898667	3.496
Al	15.7975	15.5895	15.753	15.41133	15.575
Fe	15.359	15.193	15.334	15.65667	15.494
Mn	0.254	0.2055	0.218333	0.168333	0.247
Mg	13.1345	13.018	12.74733	11.86267	12.498
Ca	0.091	0.049	0.094	0.164667	0.106
Na	0.614	0.4465	0.416667	0.608667	0.5555
K	9.5935	9.64	9.306333	8.782333	9.302
Cl	0.2285	0.2075	0.202333	0.236	0.2035
Total	96.787	96.3365	95.51467	94.37533	95.267

Secondary biotite pseudomorphing hornblende in the feldspar porphyry

	Sample 166			Sample 172		S'ple 177			
Oxide	N6	N2	N1	N1	N4	N2	285 2 1	285 7 1	
Si	38.677	38.014	38.604	38.698	37.705	37.874	38.69867	37.85875	
Ti	2.605	3.897	2.845	2.88	4.101	3.653	2.828333	3.282	
Al	16.961	16.074	17.106	17.065	15.395	15.327	16.001	15.3435	
Fe	16.283	17.137	16.922	16.235	15.856	15.571	13.63633	15.57625	
Mn	0.082	0.168	0.28	0.155	0.308	0.063	0.246667	0.2745	
Mg	11.893	11.913	12.303	11.569	12.927	13.688	13.9	13.1165	
Ca	0.112	0.108	0.046	0.043	0.138	0.121	0.068	0.00775	
Na	0.556	0.592	0.598	0.432	0.655	0.563	0.432667	0.41125	
K	9.301	8.865	9.51	9	8.733	8.859	9.456333	9.27975	
Cl	0.148	0.307	0.218	0.166	0.241	0.214	0.206667	0.23125	
Total	96.618	97.075	98.432	96.243	96.059	95.933	95.47467	95.3815	0

Sulphides only samples of the monzogranite

Oxide	163-C	163-G	163-A	163-B	163-D	163-E	163-F	155-A	155-B
Si	36.894	37.255	37.037	37.544	37.7035	37.2785	37.2215	38.8645	39.2955
Ti	2.956	3.129	2.832667	2.932	2.6835	2.707	3.017	3.7465	3.5045
Al	17.221	17.0855	16.95733	17.347	17.125	17.7205	17.2845	15.143	15.529
Fe	13.9065	14.014	12.941	12.1755	13.3	13.1805	13.7055	11.4185	11.301
Mn	0.229	0.1405	0.195333	0.0935	0.148	0.1245	0.0795	0.134	0.0815
Mg	14.103	14.079	15.12267	15.0445	14.372	14.3625	14.1135	16.684	16.999
Ca	0.095	0.0045	0.076	0.147	0.026	0.075	0.141	0.059	0
Na	0.5275	0.5885	0.665333	0.375	0.623	0.4555	0.628	0.4795	0.5455
K	10.025	10.257	9.985	10.1555	9.9605	10.141	10.0215	9.8495	10.174
Cl	0.1635	0.199	0.203	0.142	0.152	0.177	0.1865	0.1115	0.0745
Total	96.1205	96.752	96.01533	95.956	96.0935	96.222	96.3985	96.49	97.5045

Sulphides only samples of the monzogranite

Oxide	231 1 1	231 2 1	231 3 1	231 4 1	231 5 1	231 6 1	231 7 1	262 5 1	262 2 1
Si	38.4	37.94333	38.5705	37.37267	37.5795	38.054	37.6795	37.75667	37.87
Ti	3.8015	3.391	3.307	3.705333	3.7385	3.6805	3.6525	2.435667	3.1565
Al	15.601	15.413	15.826	15.75967	16.3	15.5585	16.076	16.39733	16.3185
Fe	10.76	10.618	10.4445	11.501	11.241	11.138	11.086	14.12933	14.9705
Mn	0.117	0.197667	0.2145	0.157333	0.1835	0.1985	0.148	0.111667	0.0925
Mg	17.3275	17.01833	17.4235	16.55933	16.502	16.7535	16.61	14.29833	13.6075
Ca	-0.004	0.122667	0.027	0.015333	0.0215	0.086	0.024	0.059	0.067
Na	0.5515	0.460333	0.616	0.468	0.579	0.589	0.486	0.467	0.389
K	10.2395	10.14767	9.957	10.00333	10.1345	9.98	10.071	9.801667	10.165
Cl	0.1265	0.096667	0.092	0.091	0.1305	0.104	0.051	0.158667	0.116
Total	96.9205	95.40867	96.478	95.633	96.41	96.142	95.884	95.61533	96.7525

Sulphides only samples of the monzogranite

Oxide	262 3 2	262 4 1	262 1 1	265-A	265-D	265-B	265-C	265-E	265-F
Si	38.582	37.69675	38.412	36.7765	38.2535	36.573	38.992	38.361	38.655
Ti	3.0295	3.46625	3.5485	3.161	3.6485	4.556	3.718	3.42	2.8355
Al	16.32	15.348	16.0225	16.3005	15.2025	16.2505	15.158	15.314	15.6235
Fe	13.934	14.62875	14.306	13.6995	13.027	14.0655	13.014	13.153	12.8825
Mn	0.151	0.0935	0.0985	0.153	0.183	0.239	0.297	0.18	0.2095
Mg	14.1515	14.037	14.041	14.9675	15.7055	14.3665	15.628	15.4	15.4715
Ca	0.0185	0.0235	0.005	0.285	0.054	0.054	0.097	0.0315	0.0145
Na	0.6775	0.52425	0.492	0.563	0.5845	0.4705	0.512	0.607	0.493
K	10.052	9.90625	9.9745	9.927	9.893	10.0005	9.418	10.0035	9.9965
Cl	0.213	0.17125	0.148	0.1425	0.1915	0.3005	0.137	0.193	0.111
Total	97.129	95.8955	97.048	95.9755	96.743	96.876	96.971	96.663	96.2925

Sulphides only samples of the monzogranite

Oxide	265-H	265-G
Si	38.2775	37.5945
Ti	2.8715	3.6985
Al	15.034	15.3215
Fe	13.1225	13.6
Mn	0.2235	0.1525
Mg	16.1835	15.169
Ca	0.0335	0.0535
Na	0.5655	0.633
K	9.8685	9.9675
Cl	0.1625	0.2695
Total	96.3425	96.4595

Magnetite bearing samples of the monzogranite

Oxide	220 1 1	220 2 1	220 3 1	220 4 1	220 5 1	233 1 1	233 2 1	233 3 1	233 4 1
Si	38.41	37.64	37.25	37.28	38.02	37.37	37.53	38.48	37.18
Ti	2.53	2.64	2.26	2.57	2.18	2.63	2.7	2.18	2.87
Al	16.99	17.12	17.96	17.54	17.54	16.47	16.78	16.69	16.73
Fe	14.62	14.51	15.22	15.5	14.47	15.33	15.48	13.35	15.02
Mn	0.1	0.22	0.19	0.07	0.15	0.08	0.2	0.09	0.18
Mg	13.27	12.99	13	12.92	13.55	12.22	12.66	14.44	13.32
Ca	0.07	0.08	0.09	-0.02	-0.02	0.02	0.1	0.02	0.06
Na	0.42	0.53	0.47	0.35	0.41	0.46	0.41	0.51	0.34
K	9.8	9.51	9.99	9.82	9.89	9.68	9.88	9.78	9.85
Cl	0.21	0.29	0.19	0.25	0.2	0.17	0.23	0.11	0.17
Total	96.41	95.54	96.62	96.29	96.39	94.44	95.97	95.65	95.73

Magnetite bearing samples of the monzogranite

Oxide	233 5 1	250-A	250-B	250-C	250-D	250-E	250-F	250-G	286 1 1
Si	37.26	37.3015	36.7725	37.6925	37.1425	36.983	36.6075	37.0975	37.79
Ti	2.81	3.3935	3.357	3.2465	2.813	2.994	3.0045	3.0475	3.27
Al	16.96	16.3165	16.4505	16.419	16.8985	16.27	16.2225	16.345	16.37
Fe	15.91	17.3285	17.7695	17.178	16.3975	16.7365	16.783	17.0745	16.07
Mn	0.24	0.1545	0.246	0.1835	0.182	0.1675	0.13	0.166	0.17
Mg	12.24	12.1945	11.6415	12.157	12.022	11.955	11.597	11.848	12.28
Ca	-0.03	0.053	0.0595	0.088	0.0095	0.01	0.0385	0.043	-0.01
Na	0.36	0.508	0.3145	0.588	0.298	0.5995	0.5435	0.423	0.58
K	9.99	9.7465	9.967	9.209	9.977	9.8955	9.82	9.762	9.83
Cl	0.2	0.2005	0.247	0.2115	0.2355	0.253	0.2465	0.2305	0.29
Total	95.93	97.197	96.825	96.973	95.9755	95.864	94.993	96.037	96.64

Magnetite bearing samples of the monzogranite

Oxide	286 2 1	286 3 1
Si	36.43	36.98
Ti	2.96	3.48
Al	15.74	15.39
Fe	16.3	16.51
Mn	0.33	0.2
Mg	12	12.08
Ca	0.07	0.08
Na	0.43	0.39
K	9.47	9.53
Cl	0.25	0.24
Total	93.98	94.89

Aplite

Oxide	253 5 1	253 2 1	253 4 1	253 1 1	253 6 1	253 3 1
Si	37.8505	38.355	38.2435	37.739	37.883	37.349
Ti	2.837	2.842	2.957	2.9685	3.1555	2.234667
Al	16.48	16.2665	15.9225	16.3915	16.359	16.51
Fe	15.6605	13.5565	15.133	14.232	15.551	14.517
Mn	0.1965	0.103	0.1265	0.143	0.23	0.138667
Mg	12.7035	14.27	13.658	13.5985	12.901	13.29367
Ca	0.068	0.0685	0.1045	0.009	0.061	0.068
Na	0.4995	0.65	0.552	0.647	0.6255	0.535
K	9.944	9.5705	9.495	9.64	9.7395	9.537667
Cl	0.1995	0.226	0.1995	0.228	0.248	0.203333
Total	96.439	95.908	96.3915	95.5965	96.7535	94.387

Phenocrystic biotite from the mafic material

	A	A2	B	C	C2	D	E1	E2	F
Oxide	39.015	39.726	38.865	39.635	39.502	39.6	39.433	38.319	39.682
Si	2.64	1.676	2.341	2.412	3.045	1.453	2.696	1.562	3.047
Ti	15.055	15.308	15.227	16.451	14.882	15.597	15.019	16.631	14.929
Al	13.596	13.39	13.184	13.036	13.529	13.182	13.056	13.397	13.535
Fe	0.212	0.236	0.186	0.204	0.256	0.178	0.262	0.268	0.245
Mn	15.78	15.938	16.197	15.564	16.048	15.483	15.998	15.71	15.919
Mg	0.147	0.165	0.156	0.089	0.084	0.22	0.105	0.21	0.094
Ca	0.608	0.431	0.573	0.512	0.546	0.508	0.51	0.414	0.573
Na	8.231	7.643	7.361	7.581	8.384	7.584	8.352	7.115	8.638
K	0.119	0.12	0.065	0.083	0.164	0.047	0.114	0.073	0.135
Cl	95.403	94.633	94.155	95.567	96.44	93.852	95.545	93.699	96.797
Total									

Biotite replacing biotite in the mafic material

Oxide	A1	A2	B1	B2	C	D1	D2
Si	39.759	39.739	39.068	40.008	40.053	40.295	38.812
Ti	3.187	3.285	3.093	3.521	3.096	3.534	3.318
Al	16.029	15.654	15.751	15.77	16.531	15.783	15.334
Fe	14.282	14.736	14.35	15.066	14.408	14.389	13.987
Mn	0.061	0.055	0.097	0.203	0.084	0.098	0.028
Mg	10.418	10.54	9.978	10.599	10.48	10.632	10.254
Ca	0.442	0.469	0.347	0.188	0.416	0.475	0.369
Na	0.359	0.409	0.303	0.385	0.474	0.424	0.343
K	7.848	7.59	7.452	8.211	7.53	7.397	7.515
Cl	0.255	0.196	0.247	0.242	0.208	0.238	0.229
Total	92.64	92.673	90.686	94.193	93.28	93.265	90.189

Replacing amphibole Biotite replacing amphibole in the mafic material

Oxide	A	B	C	E	F	H
Si	38.071	37.811	38.464	37.849	37.451	37.65
Ti	3.086	3.253	3.232	3.219	3.34	3.136
Al	16.829	17.508	17.478	17.023	16.77	17.112
Fe	16.397	16.948	16.938	16.81	17.066	16.852
Mn	0.183	0.153	0.151	0.156	0.217	0.232
Mg	12.482	12.19	12.59	12.377	12.02	12.326
Ca	0.039	0.067	0.022	0.083	0.053	0.053
Na	0.404	0.454	0.487	0.483	0.389	0.462
K	9.323	9.509	9.493	9.357	9.183	9.501
Cl	0.21	0.263	0.273	0.267	0.256	0.262
Total	97.024	98.156	99.128	97.624	96.745	97.586

Oxide	292 1 1	292 2 1	292 3 1	292 4 1	292 5 1	292 6 1	301		
Si	37.45	37.3	38.19	38.21	37.95	38.84	39.262	37.986	37.61
Ti	1.89	2	1.53	1.64	1.41	1.55	1.485	1.529	1.499
Al	17.49	17.32	18.05	17.52	17.3	17.32	18.065	17.364	17.927
Fe	13.55	13.26	13.42	13.6	13.13	13.21	13.105	12.449	12.593
Mn	0.18	0.12	0.12	0.15	0.16	0.11	0.172	0.114	0.067
Mg	14.05	14.12	14.92	14.37	14.53	14.92	15.982	15.33	15.603
Ca	0.03	-0.02	0.02	-0.01	-0.01	0.09	0.059	0.036	0.05
Na	0.41	0.26	0.6	0.26	0.32	0.4	0.605	0.478	0.681
K	9.97	10.01	10.24	10.12	9.89	10.02	10.48	9.67	9.995
Cl	0.23	0.21	0.22	0.18	0.22	0.24	0.137	0.103	0.152
Total	95.24	94.58	97.3	96.04	94.91	96.71	99.352	95.059	96.177
Oxide									
Si	36.337	38.555	39.303	38.124	38.682	37.232	36.737	37.695	37.819
Ti	1.471	1.24	1.172	1.326	1.363	1.368	1.496	1.472	1.491
Al	17.894	16.644	15.878	17.757	16.535	17.834	17.661	17.403	17.779
Fe	13	12.257	11.856	12.681	12.47	13.462	13.162	12.833	13.16
Mn	0.277	0.133	0.056	0.186	0.148	0.138	0.244	0.212	0.091
Mg	14.685	15.491	16.326	15.51	15.765	15.265	14.919	15.562	15.378
Ca	0.044	0.019	0.037	-0.009	0.051	0.101	-0.032	0.065	0.073
Na	0.526	0.703	0.562	0.664	0.559	0.682	0.662	1.035	0.764
K	9.769	9.349	9.292	10.042	9.381	9.58	8.226	9.983	9.771
Cl	0.117	0.163	0.141	0.116	0.149	0.166	0.126	0.059	0.117
Total	94.12	94.554	94.623	96.397	95.103	95.828	93.201	96.319	96.443
Oxide									
Si	38.169	37.639	37.453	37.547	38.055				
Ti	1.37	1.351	1.269	1.323	1.37				
Al	17.124	17.424	17.693	17.165	17.285				
Fe	12.668	12.708	12.872	12.941	12.704				
Mn	0.216	0.219	0.253	0.138	0.286				
Mg	15.181	15.11	15.196	15.216	15.717				
Ca	0.11	0.024	0.038	0.087	0.015				
Na	0.465	0.87	0.697	0.701	0.767				
K	9.777	10.031	9.409	9.504	9.754				
Cl	0.114	0.162	0.143	0.135	0.146				
Total	95.194	95.538	95.023	94.757	96.099				

Plagioclase analyses

Samples 259 and 239B. Analyses performed on automated run. Zero value signifies value below detection limit. Blank signifies poor total (given). Operating conditions were current of 2nA with a potential of 15 kV. Live time of 100 seconds.

Analysi	Total	Na20	Al2O3	SiO2	K2O	CaO	FeO	SrO	%Anorthite	%Albite
TWO	104.61									
2	103.13									
3	89.02									
4	102.96									
5	96.67									
6	104.50									
7	101.27	7.90	24.40	62.10	0.30	6.00	0.00	0.50	28.68	68.32
8	101.07	7.70	24.40	62.60	0.30	6.10	0.00	0.00	29.91	68.33
9	99.79	7.90	23.30	62.80	0.40	5.50	0.00	0.00	27.13	70.52
10	91.67									
11	74.11									
12	75.94									
13	78.08									
14	85.75									
15	80.24									
16	72.67									
17	3.16									
18	72.83									
19	48.89									
20	83.35									
21	81.22									
22	71.76									
23	81.83									
24	98.91	9.40	20.60	66.20	0.17	2.10	0.00	0.50	10.72	86.86
25	100.76									
26	100.71									
27	100.22									
28	85.02									
29	80.49									
30	96.55									
31	98.32									
32	85.09									
33	80.62									
34	65.94									
35	72.81									
36	77.00									
37	99.93	8.20	23.30	62.10	0.50	5.20	0.00	0.70	24.75	70.62
38	99.94	8.10	23.20	62.90	0.30	5.10	0.30	0.00	25.06	72.03
39	99.14	8.20	23.00	61.90	0.40	5.10	0.00	0.60	24.59	71.55
40	94.00									
41	86.00									
42	99.32	7.90	23.40	61.40	0.30	5.70	0.00	0.60	27.57	69.14
43	98.53	7.70	23.40	61.40	0.40	5.70	0.00	0.00	28.34	69.29
44	99.92	7.70	23.70	61.20	0.40	5.90	0.20	0.70	28.30	66.85
45	99.50	7.70	23.60	61.10	0.40	5.70	0.40	0.60	27.47	67.16
46	98.82	7.80	23.40	61.10	0.40	5.80	0.20	0.00	28.23	68.69
47	99.19	7.80	23.40	60.90	0.40	5.90	0.00	0.70	28.27	67.63
48	98.84	7.50	23.40	61.00	0.40	5.90	0.00	0.60	29.10	66.95
49	99.76	7.50	23.70	61.90	0.40	5.80	0.00	0.50	28.83	67.46
50	10.92									

51	100.89	7.80	24.10	61.90	0.30	6.10	0.00	0.60	29.19	67.55
52	99.52	8.50	22.70	63.20	0.40	4.60	0.00	0.00	22.49	75.19
53	99.29	7.60	23.80	61.60	0.30	6.00	0.00	0.00	29.84	68.39
54	88.00									
55	61.00									
56	70.00									
57	98.98	9.30	21.50	64.90	0.21	3.00	0.00	0.00	14.94	83.81
58	99.14									
59	100.73	9.40	19.60	67.20	2.80	1.10	0.00	0.60	5.05	78.14
60	99.67	9.90	20.40	66.20	0.20	2.00	0.00	0.90	9.69	86.80
61	99.24									
62	101.12	8.90	19.30	71.10	0.00	1.80	0.00	0.00	10.05	89.95
63	97.00									
64	100.32									
65	100.69									
66	101.19									
67	99.97									
68	99.72									
69	99.67									
70	97.00									
71	99.03									
72	100.84									
73	98.00									
74	100.37									
75	94.00									
76	99.46	9.20	19.40	67.60	1.60	1.30	0.00	0.40	6.48	82.95
77	100.73	2.70	6.20	88.40	0.60	0.50	1.40	0.90	6.51	63.62
78	102.00									
79	99.87									
80	100.52									
81	99.22	10.00	20.20	66.30	0.19	1.80	0.00	0.80	8.76	88.04
82	99.67	9.60	20.90	66.60	0.30	2.30	0.00	0.00	11.48	86.73
83	99.65	8.10	23.40	62.70	0.30	5.20	0.00	0.00	25.72	72.51
84	100.01	7.40	24.40	61.10	0.20	6.40	0.00	0.60	31.44	65.79
85	99.04	7.40	24.00	60.60	0.30	6.20	0.00	0.60	30.58	66.05
86	98.87	8.00	23.30	61.50	0.30	5.50	0.20	0.00	26.84	70.65
87	99.50	8.10	23.30	62.00	0.30	5.30	0.00	0.40	25.81	71.39
88	99.56	7.40	23.80	60.70	0.30	6.50	0.00	0.90	31.35	64.58
89	98.49	7.30	24.00	59.90	0.20	6.30	0.00	0.60	31.39	65.81
90	95.00									
91	97.00									
92	97.00									
93	99.53	7.30	24.40	60.00	0.30	6.50	0.30	0.80	31.35	63.71
94	100.16	7.60	24.10	61.10	0.30	6.10	0.00	0.90	29.47	66.45
95	91.00									
96	100.21	7.50	24.30	61.10	0.30	6.30	0.00	0.60	30.65	66.03
97	99.89	7.60	24.10	60.90	0.30	6.20	0.20	0.60	29.82	66.15
98	99.93	7.50	24.10	60.90	0.30	6.30	0.00	0.90	30.41	65.51
99	99.47	7.60	24.20	61.30	0.20	6.20	0.00	0.00	30.71	68.11
100	99.81	7.50	24.30	61.30	0.30	6.50	0.00	0.00	31.82	66.43
101	96.00									
102	99.69	7.50	24.30	60.50	0.30	6.40	0.00	0.50	31.07	65.88
103	98.19	7.30	23.90	59.80	0.30	6.20	0.00	0.80	30.69	65.40
104	98.98	8.10	23.30	61.60	0.30	5.40	0.30	0.00	26.15	70.99
105	98.90	9.90	21.00	65.50	0.00	2.50	0.00	0.00	12.25	87.75
106	95.00									
107	99.78	7.70	23.70	61.20	0.30	6.20	0.00	0.60	29.78	66.94
108	100.80	7.90	24.20	61.80	0.20	6.10	0.00	0.50	29.18	68.39
109	98.90	7.70	23.50	61.40	0.30	5.70	0.20	0.00	28.29	69.16
110	94.00									
111	99.61	6.40	23.10	59.00	0.40	5.20	0.00	0.60	29.57	65.87
112	91.00									
113	100.03	7.40	24.20	61.60	0.40	6.40	0.00	0.00	31.58	66.07
114	100.22	7.60	24.30	61.70	0.30	6.20	0.00	0.00	30.53	67.71

115	100.46	7.60	24.00	61.50	0.40	6.20	0.00	0.90	29.64	65.75
116	99.95	7.90	23.90	61.80	0.40	6.00	0.00	0.00	28.88	68.82
117	96.09									
118	98.00									
119	98.87	7.80	23.30	60.70	0.30	5.80	0.20	0.70	27.88	67.84
120	99.94	8.10	23.30	62.50	0.30	5.20	0.00	0.50	25.38	71.55
121	101.68	8.10	23.00	64.40	0.50	5.00	0.40	0.40	24.06	70.53
122	100.38	7.90	23.90	61.70	0.30	5.80	0.20	0.50	27.78	68.47
123	99.36	7.60	23.30	61.60	0.40	5.80	0.00	0.60	28.50	67.57
124	99.52	8.30	22.70	62.80	0.40	4.90	0.00	0.50	23.71	72.68
125	99.17	8.30	22.10	61.40	0.40	7.10	0.00	0.00	31.42	66.47
126	99.44	8.20	22.80	62.40	0.30	5.10	0.00	0.60	24.73	71.96
127	100.59	7.50	23.60	63.00	1.20	5.30	0.00	0.00	26.11	66.85
128	101.16	8.00	23.90	63.10	0.40	5.70	0.00	0.00	27.60	70.10
129	100.44	7.80	24.20	62.20	0.30	5.90	0.00	0.00	28.96	69.29
130	100.30	7.70	23.70	62.10	0.30	5.80	0.00	0.70	28.33	68.07
131	99.24	7.70	23.50	61.90	0.30	5.70	0.00	0.00	28.51	69.70
132	88.00									
133	99.31	7.50	23.50	60.90	0.50	5.90	0.00	0.90	28.70	66.03
134	82.00									
135	99.39	7.40	24.10	61.40	0.30	6.10	0.00	0.00	30.73	67.47
136	100.05	7.70	24.00	61.10	0.40	6.20	0.00	0.70	29.54	66.39
137	99.01	7.40	23.80	60.50	0.30	6.20	0.00	0.80	30.42	65.70
138	99.06	7.70	23.60	60.30	0.30	6.10	0.00	1.00	29.14	66.57
139	85.00									
140	99.77	8.10	23.50	62.40	0.30	5.50	0.00	0.00	26.81	71.45
141	99.43	7.40	24.00	60.40	0.30	6.40	0.00	0.90	31.01	64.89
142	99.80	7.60	24.30	61.20	0.30	6.40	0.00	0.00	31.20	67.05
143	99.11	7.50	23.80	60.20	0.30	6.30	0.30	0.80	30.15	64.95
144	99.97	7.40	24.20	61.50	0.30	6.30	0.20	0.00	31.18	66.28
145	100.00	7.60	24.40	61.50	0.30	6.20	0.00	0.00	30.53	67.71
146	99.61	7.80	24.30	61.10	0.20	6.20	0.00	0.00	30.17	68.68
147	96.00									
148	98.61	8.50	22.50	63.00	0.20	4.40	0.00	0.00	21.98	76.83
149	93.00									
150	97.41	7.40	23.40	59.50	0.80	5.90	0.00	0.50	28.76	65.28
151	99.00	7.60	23.70	60.20	0.30	6.20	0.30	0.60	29.71	65.90
152	98.12	7.80	23.00	60.80	0.40	5.50	0.00	0.70	26.87	68.95
153	92.00									
154	89.00									
155	98.00									
156	99.22	7.80	23.90	59.70	0.30	6.30	0.00	1.20	29.41	65.89
157	96.00									
158	100.36	9.60	21.60	65.60	0.24	2.90	0.00	0.40	13.96	83.62
159	99.03	9.30	21.40	64.30	0.14	3.50	0.00	0.50	16.85	81.04
160	87.00									
161	99.19	8.20	22.70	62.20	0.14	5.10	0.00	0.90	24.77	72.06
162	98.70	8.60	22.60	62.20	0.11	4.40	0.00	0.80	21.44	75.82
163	98.00									
164	99.97	7.50	24.10	60.90	0.40	6.40	0.00	0.70	30.73	65.17
165	98.00									
166	99.98	7.60	24.20	60.80	0.30	6.40	0.00	0.60	30.72	66.01
167	100.00	7.50	24.30	61.10	0.20	6.50	0.00	0.50	31.58	65.95
168	99.01	7.50	24.00	60.90	0.30	6.20	0.00	0.00	30.80	67.42
169	99.53	7.60	24.10	61.10	0.30	6.40	0.00	0.00	31.20	67.05
170	100.27	7.50	24.20	61.20	0.30	6.50	0.00	0.50	31.40	65.57
171	97.00									
172	98.00									
173	99.84	7.50	23.60	60.30	0.40	6.50	0.00	0.50	31.22	65.19
174	99.56	7.50	24.10	60.40	0.40	6.40	0.20	0.70	30.50	64.68
175	99.09	7.60	24.20	60.40	0.40	6.50	0.00	0.00	31.36	66.35
176	97.86									
177	99.65	7.60	24.10	60.50	0.30	6.50	0.00	0.70	30.97	65.52
178	100.20	7.60	24.30	60.70	0.30	6.60	0.00	0.60	31.38	65.38

179	98.64	7.30	23.90	60.10	0.30	6.50	0.00	0.50	31.96	64.95
180	99.49	7.40	24.00	60.40	0.40	6.40	0.30	0.70	30.65	64.13
181	98.59	7.10	24.10	60.60	0.30	6.50	0.00	0.00	32.99	65.20
182	99.46	7.40	24.20	60.90	0.30	6.30	0.30	0.00	31.06	66.02
183	99.19	7.50	24.00	60.20	0.30	6.60	0.00	0.50	31.73	65.25
184	98.79	7.20	24.10	60.50	0.30	6.50	0.30	0.00	32.31	64.76
185	99.97	7.30	24.50	60.90	0.30	6.40	0.00	0.50	31.62	65.27
186	98.73	7.40	24.00	60.10	0.30	6.40	0.00	0.50	31.34	65.58
187	98.78	7.10	23.90	60.10	0.30	6.40	0.30	0.70	31.65	63.55
188	99.41	7.50	24.20	60.60	0.30	6.40	0.30	0.00	31.12	66.00
189	98.92	7.80	23.90	60.70	0.20	6.30	0.00	0.00	30.50	68.34
190	99.34	7.60	24.20	60.60	0.30	6.60	0.00	0.00	31.87	66.41
191	99.41	7.40	24.10	61.20	0.30	6.40	0.00	0.00	31.76	66.46
192	99.05	7.40	23.90	60.30	0.30	6.40	0.20	0.50	31.11	65.08
193	98.73	7.60	23.90	60.70	0.30	6.30	0.00	0.00	30.87	67.38
194	98.70	7.40	23.90	60.60	0.30	6.40	0.00	0.00	31.76	66.46
195	99.26	7.20	24.20	60.40	0.30	6.50	0.00	0.60	32.16	64.47
196	99.37	7.50	23.70	60.60	0.30	6.30	0.20	0.70	30.34	65.36
197	98.71	7.60	23.80	60.10	0.30	6.40	0.00	0.50	30.80	66.18
198	99.01	7.60	24.00	60.90	0.30	6.30	0.00	0.00	30.87	67.38
199	99.33	7.50	23.90	60.50	0.20	6.30	0.20	0.60	30.60	65.91
200	98.91	7.10	24.20	60.00	0.30	6.50	0.00	0.90	32.19	63.63
201	98.93	7.30	24.00	60.10	0.30	6.60	0.00	0.60	32.21	64.46
202	98.00									
203	98.00									
204	98.00									
205	98.98	7.40	24.20	60.60	0.20	6.60	0.00	0.00	32.63	66.20
206	94.00									
207	98.80	7.20	24.40	60.00	0.30	6.70	0.20	0.00	33.10	64.37
208	98.00									
209	96.00									
210	98.00									
211	98.90	7.50	23.90	60.30	0.20	6.10	0.00	0.90	29.91	66.54
212	98.64	7.70	23.60	60.30	0.30	6.10	0.00	0.70	29.37	67.09
213	100.22	7.90	24.00	61.60	0.20	6.30	0.20	0.00	30.01	68.11
214	98.69	7.50	23.70	61.00	0.30	6.00	0.20	0.00	29.87	67.57
215	95.00									
216	100.09	7.30	24.30	60.30	0.30	6.40	0.30	1.10	30.77	63.52
217	98.62	7.30	24.00	60.20	0.20	6.30	0.00	0.60	31.39	65.81
218	98.70	7.40	24.10	60.00	0.30	6.40	0.00	0.60	31.26	65.41
219	99.46	7.70	24.10	60.20	0.20	6.40	0.20	0.60	30.40	66.19
220	98.69	7.60	23.70	60.10	0.30	6.10	0.00	1.00	29.40	66.28
221	98.70	7.70	23.70	60.10	0.30	6.30	0.00	0.50	30.20	66.79
222	98.71	7.50	23.60	60.10	0.30	6.40	0.00	0.90	30.74	65.20
223	98.00									
224	97.00									
225	97.00									
226	91.00									
227	96.00									
228	81.00									
229	100.49	7.60	24.00	61.50	0.40	6.20	0.00	0.80	29.72	65.92
230	98.72	7.40	23.60	60.40	0.40	6.10	0.00	0.70	29.98	65.82
231	99.81	7.30	23.80	61.30	0.50	6.00	0.00	0.80	29.65	65.27
232	99.43	7.60	23.80	60.80	0.40	6.20	0.00	0.60	29.87	66.27
233	98.74	7.50	23.80	60.70	0.30	6.20	0.20	0.00	30.56	66.91
234	99.66	7.30	24.00	60.80	0.40	6.40	0.30	0.50	31.08	64.15
235	99.45	7.40	24.00	60.80	0.40	6.30	0.00	0.60	30.74	65.35
236	98.60	7.20	23.70	60.10	0.30	6.30	0.20	0.70	31.16	64.43
237	96.00									
238	79.00									
239	75.00									
240	84.00									
241	81.00									
242	83.00									

243	99.18	7.00	24.70	59.30	0.30	7.30	0.00	0.50	35.45	61.51
244	99.83	7.20	24.70	60.50	0.30	6.90	0.30	0.00	33.62	63.49
245	100.67	7.50	24.60	61.60	0.30	6.60	0.00	0.00	32.15	66.11
246	99.80	7.50	24.30	60.30	0.40	6.70	0.00	0.60	31.79	64.40
247	103.00									
248	52.00									
249	103.00									
250	85.00									
251	102.00									
252	83.00									
253	99.47	9.70	20.20	67.10	0.13	1.70	0.00	0.60	8.62	88.95
254	104.00									
255	82.00									
256	72.00									
257	29.00									
258	83.00									
259	82.00									
260	108.00									
261	103.00									
262	102.00									
263	102.00									
264	101.28									
265	102.00									
266	101.00									
267	100.59									
268	98.00									
269	80.00									
270	83.00									
271	81.00									
272	90.00									
273	98.68									
274	82.00									
275	100.01									
276	97.00									
277	99.73	7.60	24.00	61.90	0.20	6.00	0.00	0.00	30.01	68.80
278	100.02	7.80	24.10	61.70	0.20	6.20	0.00	0.00	30.17	68.68
279	99.42	7.70	24.00	60.80	0.30	6.10	0.00	0.60	29.45	67.26
280	99.84	7.50	24.30	61.40	0.20	6.40	0.00	0.00	31.67	67.15
281	87.00									
282	100.02	7.90	24.30	61.70	0.20	5.90	0.00	0.00	28.87	69.96
283	98.54	7.10	24.50	59.70	0.30	7.00	0.00	0.00	34.64	63.59
284	99.06	7.30	24.60	59.90	0.20	7.00	0.00	0.00	34.23	64.60
285	98.00									
286	95.00									
287	98.50	7.10	23.30	62.10	0.12	5.20	0.30	0.50	27.81	68.72
288	97.00									
289	93.00									
290	98.00									
291	89.00									
292	100.49	8.10	24.00	62.50	0.40	5.50	0.00	0.00	26.65	71.04
293	99.46	7.80	23.90	60.90	0.30	6.00	0.00	0.60	28.85	67.87
294	99.19	7.80	23.70	60.40	0.30	6.20	0.30	0.50	29.28	66.65
295	97.00									
296	98.00									
297	97.00									
298	98.00									
299	98.96	9.10	21.90	64.30	0.30	3.30	0.00	0.00	16.40	81.83
300	99.10	8.00	23.30	61.00	0.20	5.90	0.00	0.70	28.10	68.96
301	99.37	7.90	23.50	61.50	0.30	5.50	0.00	0.60	26.86	69.81
302	98.00									
303	98.96	7.70	23.70	60.30	0.30	6.00	0.00	1.10	28.73	66.71
304	99.92	7.90	23.90	60.70	0.30	6.20	0.30	0.70	28.88	66.60
305	99.74	7.70	23.60	61.40	0.20	5.90	0.00	0.80	28.77	67.95
306	92.00									

307	97.00									
308	97.00									
309	91.00									
310	96.00									
311	97.00									
312	99.52	8.20	23.20	62.70	0.30	5.10	0.00	0.00	25.13	73.11
313	99.45	9.70	21.10	66.20	0.25	2.20	0.00	0.00	10.97	87.54
314	98.96	9.30	21.40	64.70	0.54	3.00	0.00	0.00	14.65	82.21
315	86.00									
316	96.00									
317	98.00									
318	96.00									
319	97.00									
320	98.50	7.80	23.50	60.60	0.20	5.90	0.00	0.50	28.75	68.77
321	97.00									
322	94.00									
323	91.00									
324	96.00									
325	89.00									
326	98.00									
327	98.79	7.60	23.60	60.00	0.30	6.30	0.30	0.70	29.97	65.42
328	98.00									
329	98.00									
330	96.00									
331	89.00									
332	92.00									
FOUR										
2	99.27	6.50	25.30	58.10	0.40	8.10	0.20	0.70	38.80	56.35
3	99.50	6.70	25.20	58.70	0.30	8.00	0.00	0.60	38.45	58.27
4	99.18	6.50	25.40	58.40	0.40	8.00	0.00	0.50	39.01	57.35
5	99.12	6.60	25.30	58.60	0.40	7.90	0.30	0.00	38.44	58.11
6	99.60	6.70	25.50	59.00	0.40	7.90	0.00	0.00	38.54	59.14
7	99.89	6.50	25.50	58.30	0.30	8.30	0.00	0.90	39.70	56.26
8	98.65	6.60	25.30	57.80	0.40	8.00	0.00	0.60	38.56	57.57
9	98.60	7.00	24.60	59.10	0.40	7.30	0.30	0.40	34.94	60.63
10	99.52	6.50	25.60	58.20	0.30	8.20	0.00	0.80	39.51	56.68
11	98.84	6.40	25.70	57.90	0.30	8.60	0.00	0.00	41.87	56.39
12	99.66	6.60	25.90	58.10	0.40	8.50	0.30	0.00	40.18	56.46
13	99.68	6.30	25.70	58.80	0.40	8.30	0.20	0.00	40.82	56.07
14	99.42	6.40	25.80	57.60	0.30	8.60	0.30	0.50	40.87	55.04
15	98.80	6.00	25.70	57.90	0.40	8.40	0.00	0.40	42.10	54.42
16	99.13	6.20	25.60	58.90	0.40	8.00	0.00	0.00	40.62	56.96
17	98.00									
18	99.43	7.20	24.00	60.90	0.50	6.30	0.00	0.60	31.11	64.34
19	98.80	7.20	24.40	60.10	0.40	6.60	0.00	0.00	32.83	64.80
20	98.55	6.80	24.00	60.00	4.00	6.80	0.00	0.50	28.17	50.98
21	96.00									
22	98.69	7.30	23.60	60.00	0.50	6.30	0.00	1.10	30.43	63.81
23	99.39	7.40	23.90	61.60	0.50	5.90	0.00	0.00	29.67	67.34
24	99.44	7.60	23.60	61.60	0.60	6.00	0.00	0.00	29.31	67.19
25	98.65	7.50	23.70	61.00	0.50	5.90	0.00	0.00	29.40	67.63
26	98.62	7.40	23.60	60.60	0.50	6.00	0.00	0.50	29.62	66.11
27	99.79	7.50	23.70	61.40	0.50	6.10	0.00	0.50	29.70	66.08
28	98.95	7.20	23.70	60.90	0.50	6.60	0.00	0.00	32.63	64.42
29	98.80	7.40	23.70	60.60	0.50	6.50	0.00	0.00	31.73	65.37
30	99.72	7.20	24.20	61.30	0.50	6.50	0.00	0.00	32.30	64.74
31	98.62	7.00	23.70	60.00	0.40	6.60	0.30	0.60	32.51	62.39
32	98.00									
33	98.00									
34	98.00									
35	97.00									
36	97.00									
37	99.53	7.60	23.40	61.30	0.60	5.90	0.00	0.70	28.44	66.29
38	98.90	7.70	23.30	61.50	0.60	5.90	0.00	0.00	28.71	67.81

39	99.69	7.50	23.60	61.60	0.60	5.70	0.20	0.60	27.85	66.31
40	98.61	7.70	23.10	61.50	0.60	5.70	0.00	0.00	28.01	68.48
41	99.50	7.40	23.60	61.80	0.50	5.70	0.00	0.50	28.56	67.10
42	99.45	7.50	23.30	61.50	0.60	5.70	0.30	0.50	27.82	66.23
43	98.88	7.80	23.00	61.70	0.60	5.80	0.00	0.00	28.12	68.42
44	97.00									
45	100.77	7.90	23.60	62.80	0.60	5.90	0.00	0.00	28.22	68.37
46	100.06	7.60	23.40	61.80	0.60	5.90	0.20	0.50	28.37	66.14
47	100.12	7.50	23.60	61.80	0.60	5.90	0.00	0.70	28.69	66.00
48	99.37	7.60	23.50	61.90	0.50	5.90	0.00	0.00	29.14	67.92
49	100.45	7.60	23.60	61.90	0.60	5.80	0.30	0.80	27.71	65.70
50	99.94	7.70	23.40	62.40	0.60	5.90	0.00	0.00	28.71	67.81
51	99.53	7.60	23.40	61.40	0.60	5.70	0.00	0.80	27.67	66.76
52	96.00									
53	100.46	7.60	23.60	62.20	0.60	5.90	0.00	0.50	28.59	66.64
54	99.77	7.70	23.30	62.00	0.50	5.80	0.00	0.50	28.16	67.64
55	99.08	7.60	23.20	61.50	0.60	5.60	0.00	0.60	27.46	67.44
56	99.81	7.30	23.50	62.30	0.60	5.70	0.00	0.50	28.65	66.40
57	100.27	7.80	23.60	62.50	0.60	5.70	0.00	0.00	27.77	68.76
58	101.10	7.60	23.90	62.80	0.60	5.90	0.00	0.40	28.66	66.81
59	99.59	7.50	23.20	61.50	0.60	5.60	0.20	0.90	27.28	66.11
60	99.85	7.70	23.30	61.80	0.60	5.80	0.00	0.60	27.92	67.08
61	99.73	7.90	23.20	61.60	0.60	5.70	0.00	0.80	26.96	67.61
62	99.48	7.70	23.60	62.10	0.50	5.70	0.00	0.00	28.18	68.88
63	99.69	7.50	23.50	61.70	0.50	5.80	0.00	0.50	28.66	67.06
64	91.79	4.40	24.10	54.80	0.70	6.40	1.00	0.50	39.39	49.01
65	99.63	7.20	24.10	60.90	0.40	6.40	0.00	0.60	31.64	64.40
66	98.58	6.80	24.80	59.10	0.30	7.30	0.30	0.00	36.14	60.93
67	98.28									
68	100.22	6.90	24.90	60.10	0.30	7.70	0.30	0.00	37.06	60.09
69	99.12	5.80	26.50	56.20	0.20	9.40	0.20	0.70	45.48	50.78
FIVE										
2	97.00									
3	93.00									
4	99.07	7.50	24.10	60.60	0.40	6.50	0.00	0.00	31.63	66.05
5	98.00									
6	97.00									
7	98.00									
8	99.60	7.60	24.10	60.80	0.40	6.40	0.00	0.40	30.70	65.98
9	98.52	7.40	23.80	60.40	0.40	6.60	0.00	0.00	32.25	65.43
10	98.84	7.50	24.00	60.50	0.50	6.50	0.00	0.00	31.45	65.67
11	99.02	7.10	24.20	59.60	0.40	6.50	0.20	0.80	31.84	62.94
12	99.33	7.20	24.50	59.80	0.50	6.80	0.00	0.60	32.77	62.79
13	98.00									
14	98.00									
15	98.00									
16	98.75	7.30	23.80	60.00	0.50	6.50	0.00	0.70	31.42	63.87
17	98.00									
18	98.00									
19	98.00									
20	98.78	7.10	23.90	60.00	0.50	6.50	0.00	0.80	31.90	63.05
21	98.00									
22	99.06	7.30	24.40	60.10	0.50	6.60	0.20	0.00	32.10	64.25
23	96.00									
24	98.00									
25	98.00									
26	99.45	7.00	24.30	60.20	0.50	6.90	0.00	0.50	33.77	61.99
27	99.88	7.30	24.40	61.10	0.60	6.40	0.00	0.00	31.49	65.00
28	100.48	7.30	24.60	61.50	0.50	6.60	0.00	0.00	32.34	64.74
29	99.01	7.30	24.00	60.60	0.50	6.50	0.00	0.00	32.01	65.06
30	99.59	7.50	24.10	60.30	0.50	6.50	0.00	0.60	30.96	64.65
31	99.39	7.40	24.00	60.40	0.60	6.50	0.00	0.40	31.22	64.31
32	97.00									
33	99.32	7.10	24.30	60.80	0.50	6.50	0.00	0.00	32.59	64.42

34	98.78	7.20	23.90	60.40	0.50	6.60	0.20	0.00	32.38	63.93
35	99.69	7.50	24.10	60.70	0.40	6.50	0.00	0.50	31.22	65.19
36	100.80	7.30	24.70	61.80	0.40	6.60	0.00	0.00	32.53	65.12
37	99.25	7.20	24.10	60.50	0.40	6.50	0.00	0.60	31.97	64.09
38	99.51	7.40	24.00	60.60	0.50	6.60	0.00	0.50	31.64	64.20
39	71.00									
40	99.61	7.40	24.10	60.60	0.50	6.30	0.00	0.70	30.49	64.80
41	99.30	7.60	23.90	61.10	0.50	6.20	0.00	0.00	30.17	66.93
42	99.00	7.30	23.70	60.50	0.40	6.30	0.00	0.70	30.93	64.87
43	100.40	7.50	24.10	61.20	0.50	6.40	0.00	0.70	30.55	64.79
44	98.86	7.30	23.80	61.00	0.40	6.40	0.00	0.00	31.86	65.77
45	99.26	7.20	23.90	60.60	0.40	6.50	0.20	0.40	31.90	63.94
46	92.00									
47	98.00									
48	99.69	7.10	21.70	64.20	3.70	3.10	0.00	0.00	15.23	63.12
49	97.00									
50	97.00									
51	96.00									
52	99.14	7.00	24.70	59.90	0.40	7.00	0.20	0.00	34.48	62.40
53	98.63	7.20	24.40	59.40	0.30	6.90	0.00	0.50	33.57	63.38
54	98.69	7.20	24.30	60.40	0.20	6.60	0.00	0.00	33.22	65.58
55	99.47	7.40	24.40	61.00	0.30	6.40	0.00	0.00	31.76	66.46
56	98.69	7.60	23.60	60.10	0.30	6.10	0.00	1.00	29.40	66.28
57	98.00									
58	78.00									
59	75.00									
60	77.00									
61	61.00									
62	77.00									
63	66.00									
64	83.00									
EIGHT	98.63	9.70	20.60	66.00	0.23	2.10	0.00	0.00	10.54	88.09
2	98.95	7.90	23.30	61.40	0.20	5.50	0.00	0.50	27.09	70.41
3	99.14	8.00	23.10	61.90	0.30	5.40	0.00	0.50	26.34	70.60
4	98.00									
5	99.32	7.90	23.30	61.40	0.30	5.60	0.20	0.50	27.08	69.13
6	99.43	7.80	23.70	60.70	0.30	6.10	0.20	0.70	28.90	66.87
7	99.21	7.80	23.90	61.30	0.30	6.00	0.00	0.00	29.31	68.95
8	100.37	7.60	24.30	61.50	0.30	6.30	0.00	0.40	30.54	66.68
9	97.00									
10	98.77	6.90	24.80	58.80	0.30	7.30	0.00	0.70	35.57	60.84
11	99.30	6.70	25.40	58.80	0.20	7.80	0.00	0.40	38.27	59.49
12	99.32	6.30	26.10	57.70	0.20	8.70	0.30	0.00	42.29	55.42
13	98.79	6.20	26.30	56.80	0.20	9.30	0.00	0.00	44.80	54.05
14	98.87	6.10	26.30	56.60	0.20	9.10	0.00	0.60	43.96	53.32
15	28.00									
16	26.00									
17	56.00									
18	46.00									
19	76.00									
20	76.00									
21	108.00									
22	102.00									
23	100.20	7.40	24.80	60.00	0.30	7.10	0.00	0.60	33.53	63.25
24										
25	99.89	7.50	24.20	61.20	0.20	6.30	0.00	0.40	30.99	66.77
26	99.71	8.00	23.30	61.30	0.30	5.60	0.00	1.20	26.56	68.66
27	98.93	7.70	23.40	61.80	0.40	5.70	0.00	0.00	28.34	69.29
28	100.21	7.80	23.80	61.50	0.30	5.90	0.00	0.80	28.36	67.84
29	99.82	7.50	23.90	61.10	0.30	6.20	0.30	0.70	29.89	65.43
30	99.50	7.30	24.20	60.20	0.30	6.50	0.00	1.00	31.54	64.10
31	98.73	7.40	24.00	60.60	0.30	6.50	0.00	0.00	32.10	66.13
32	98.80	7.30	23.80	60.50	0.40	6.30	0.40	0.00	31.04	65.08
33	99.18	7.50	23.70	60.90	0.40	6.00	0.20	0.50	29.30	66.29

34	98.66	7.60	23.50	60.30	0.40	6.00	0.00	0.90	28.96	66.39
35	99.50	7.30	24.00	61.50	0.40	6.30	0.00	0.00	31.52	66.10
36	98.51	7.40	23.70	60.20	0.40	6.20	0.00	0.50	30.48	65.84
37	98.72	7.40	23.90	60.60	0.40	6.30	0.00	0.00	31.24	66.40
38	99.02	7.00	24.00	60.30	0.40	6.60	0.30	0.50	32.60	62.56
39	100.31	7.20	24.80	61.30	0.30	6.70	0.00	0.00	33.36	64.87
40	99.66	7.00	24.80	60.70	0.20	6.90	0.00	0.00	34.84	63.96
41	93.00									
42	82.00									
43	99.61	6.90	25.20	59.50	0.30	7.40	0.30	0.00	36.14	60.98
44	1.00									
45	55.00									
46	101.28	5.90	25.20	62.50	0.40	6.40	0.90	0.00	35.06	58.49
47	100.21	7.10	24.70	60.50	0.20	7.40	0.40	0.00	35.58	61.77
48	90.00									
49	99.90	6.90	25.20	59.50	0.30	7.70	0.30	0.00	37.06	60.09
50	100.10	7.00	25.40	59.20	0.30	7.50	0.00	0.70	35.88	60.60
51	100.80	7.00	25.40	59.50	0.30	7.80	0.00	0.80	36.69	59.59
52	98.00									
53	98.83	7.40	23.90	59.80	0.40	6.60	0.25	0.50	31.53	63.97
54	99.92	7.50	24.20	60.90	0.40	6.70	0.20	0.00	32.05	64.92
55	98.77	7.40	23.80	60.30	0.40	6.60	0.20	0.00	32.00	64.93
56	99.07	7.20	24.30	60.40	0.30	6.70	0.20	0.00	33.10	64.37
57	98.00									
58	96.00									
59	84.00									
60	98.64	6.50	24.50	59.80	0.40	6.70	0.20	0.60	34.50	60.57
61	96.00									
62	99.13	6.60	24.70	59.00	0.30	7.50	0.20	0.70	36.88	58.73
63	93.00									
64	84.00									
65	98.00									
66	99.93	6.70	25.20	59.30	0.40	7.70	0.00	0.60	37.33	58.78
67	100.32	6.70	25.50	59.60	0.30	7.60	0.00	0.60	37.24	59.41
68	99.93	6.50	25.50	59.00	0.30	8.20	0.00	0.60	39.72	56.98
69	99.90	6.90	25.30	59.40	0.30	8.00	0.00	0.00	38.38	59.91
70	99.14	6.80	24.90	59.00	0.30	7.60	0.00	0.60	36.92	59.77
71	99.44	7.10	24.60	59.70	0.30	7.10	0.20	0.50	34.25	61.97
72	98.50	7.40	24.20	59.70	0.30	6.90	0.00	0.00	33.42	64.85
73	99.62	7.40	24.30	60.20	0.40	6.50	0.00	0.80	31.25	64.38
74	99.17	7.40	23.60	60.40	0.40	6.30	0.30	0.80	30.24	64.27
75	99.31	7.60	23.60	61.10	0.40	6.10	0.00	0.60	29.53	66.59
76	98.00									
77	99.37	7.70	23.50	61.20	0.40	5.80	0.20	0.50	28.10	67.52
78	99.51	7.50	24.00	60.30	0.40	6.20	0.00	1.00	29.82	65.28
79	99.50	7.50	23.70	60.40	0.50	6.40	0.50	0.50	30.15	63.93
80	98.00									
81	90.00									
82	15.00									
83	61.00									
84	92.00									
85	106.00									
86	104.00									
87	98.00									
88	97.00									
89	99.94	7.10	24.70	60.20	0.20	7.00	0.00	0.70	34.20	62.78
90	98.89	7.00	24.60	59.50	0.20	7.10	0.00	0.50	35.02	62.47
91	27.00									
92	91.00									
93	94.00									
94	100.74	7.60	24.70	61.90	0.50	6.00	0.00	0.00	29.49	67.59
95	98.81	7.60	24.70	61.90	0.50	6.00	0.00	0.00	29.49	67.59
96	99.20	6.40	25.50	58.50	0.30	7.80	0.30	0.50	38.53	57.21
97	99.38	6.60	25.30	58.80	0.30	7.90	0.00	0.50	38.59	58.34

98	100.45	6.50	25.60	59.30	0.30	7.90	0.30	0.60	38.39	57.16
99	99.33	6.20	25.40	58.80	0.30	8.10	0.00	0.60	40.50	56.09
100	99.62	6.60	25.20	58.50	0.40	8.00	0.20	0.70	38.18	57.00
101	72.00									
102	33.00									
103	84.00									
104	95.72									
105	83.00									
106	92.00									
107	92.00									
108	99.47	7.70	23.70	61.80	0.30	5.90	0.00	0.00	29.22	69.01
109	99.69	7.20	24.60	60.20	0.30	6.70	0.00	0.70	32.74	63.67
110	99.70	7.30	24.50	60.30	0.30	6.70	0.00	0.60	32.54	64.15
111	99.13	6.90	25.00	59.30	0.20	7.70	0.00	0.00	37.70	61.13
112	98.97	6.70	24.80	59.20	0.30	7.40	0.00	0.60	36.62	60.00
113	99.27	6.90	25.10	58.60	0.30	7.80	0.00	0.60	37.20	59.55
114	99.04	6.90	24.90	58.90	0.30	7.60	0.00	0.50	36.69	60.28
115	99.65	6.90	24.70	59.70	0.30	7.30	0.00	0.70	35.57	60.84
116	98.63	6.90	24.40	59.00	0.40	7.10	0.00	0.90	34.55	60.76
117	98.87	7.00	24.30	59.50	0.40	6.80	0.30	0.50	33.25	61.95
118	98.97	7.50	24.30	59.40	0.40	6.70	0.00	0.70	31.71	64.24
119	100.30	7.30	24.60	60.60	0.40	6.80	0.20	0.40	32.60	63.33
120	99.72	7.40	24.20	61.00	0.40	6.50	0.30	0.00	31.55	65.00
121	100.10	7.00	24.70	60.00	0.30	7.10	0.20	0.70	34.37	61.31
122	97.00									
123	99.44	7.40	24.20	60.60	0.30	6.30	0.00	0.60	30.92	65.73
124	98.94	7.60	24.00	60.00	0.30	6.40	0.00	0.70	30.64	65.84
125	98.00									
126	99.31	7.60	23.80	61.40	0.40	5.90	0.20	0.00	29.08	67.80
127	98.00									
128	98.55	7.60	23.40	61.10	0.30	5.90	0.20	0.00	29.26	68.20
129	99.40	7.70	23.70	61.30	0.30	5.90	0.00	0.60	28.76	67.92
130	99.65	7.80	23.70	61.10	0.30	6.00	0.00	0.80	28.70	67.52
131	99.33	7.70	23.40	61.10	0.30	6.00	0.30	0.40	28.93	67.18
132	98.92	7.60	23.90	59.90	0.30	6.50	0.00	0.60	31.05	65.69
133	96.00									
134	99.05	7.10	24.50	58.90	0.20	7.30	0.00	1.00	34.88	61.39
135	99.63	6.90	25.10	58.90	0.20	7.40	0.20	0.80	35.73	60.28
136	83.00									
137	97.00									
138	98.00									
139										
140	99.39	7.80	23.50	61.60	0.40	5.50	0.00	0.60	26.94	69.14
141	97.00									
142	99.14	6.90	25.00	58.90	0.30	7.60	0.00	0.60	36.59	60.12
143	98.54	6.90	24.90	58.50	0.20	7.50	0.00	0.50	36.59	60.92
144	99.15	7.40	24.10	59.70	0.30	6.70	0.20	0.70	31.93	63.82
NINE										
2	82.00									
3	77.00									
4	90.00									
5	98.00									
6	98.76	6.30	25.60	57.50	0.20	8.30	0.30	0.60	40.49	55.62
7	81.00									
8	80.00									
9	98.50	6.10	25.70	57.30	0.30	8.60		0.70	42.21	54.18
10	99.11	6.10	25.60	57.70	0.30	8.50	0.30	0.60	41.56	53.97
11	84.00									
12	99.51	6.70	25.00	59.50	0.30	7.70	0.30		37.72	59.39
13	96.00									
14	99.21	6.90	24.70	59.30	0.40	7.30		0.60	35.46	60.65
15	98.73	7.10	24.10	59.70	0.50	6.90		0.50	33.47	62.33
16	97.00									
17	99.92	7.20	24.20	60.40	0.40	6.80	0.20	0.70	32.63	62.52

18	97.00									
19	98.95	7.50	23.50	60.60	0.50	6.20		0.70	29.88	65.42
20	99.18	7.20	24.10	60.70	0.50	6.40	0.30		31.59	64.31
21	98.94	7.10	23.90	60.80	0.50	6.60			32.93	64.10
22	99.53	7.40	23.80	60.90	0.50	6.30		0.60	30.57	64.97
23	98.00									
24	98.00									
25	99.40	7.30	24.10	60.50	0.50	6.30	0.30	0.50	30.57	64.10
26	98.35	7.10	23.60	59.90	0.50	6.40	0.30	0.40	31.54	63.31
27	98.74	6.90	24.30	59.60	0.40	7.20		0.40	35.33	61.27
28	98.54	7.20	24.30	59.10	0.40	7.00		0.70	33.52	62.39
29	92.00									
30	98.00									
31	98.00									
32	98.00									
33	98.00									
34	98.00									
35	98.53	7.20	24.30	59.70	0.40	6.80			33.49	64.17
36	98.99	7.30	23.90	60.30	0.40	6.40		0.60	31.36	64.72
37	98.51	7.10	24.00	59.40	0.40	6.80		0.60	33.25	62.83
38	99.60	7.00	24.60	59.40	0.40	7.10		1.00	34.16	60.95
39	99.91	6.90	24.80	59.80	0.40	7.20	0.20	0.60	34.88	60.49
40	98.69	7.10	24.50	59.80	0.50	6.80			33.59	63.47
41	99.27	6.90	24.60	59.70	0.40	7.10		0.70	34.73	61.08
42	98.59	6.70	24.30	59.60	0.40	7.00		0.50	35.23	61.01
43	99.20	6.90	24.40	59.50	0.40	7.20		0.90	34.87	60.47
44	98.59	7.00	24.10	59.20	0.40	6.70	0.20	0.90	32.70	61.83
45	98.96	7.20	24.10	59.40	0.50	6.90		0.90	32.84	62.01
46	94.00									
47	98.58	7.10	23.90	59.80	0.30	6.80		0.60	33.45	63.20
48	99.17	7.20	24.30	59.60	0.50	7.00	0.30	0.50	33.13	61.66
49	98.00									
50	98.59	7.20	24.10	59.90	0.30	6.50		0.60	32.16	64.47
51	99.18	7.50	23.70	60.50	0.30	6.10		1.10	29.58	65.81
52	99.76	7.90	23.50	61.50	0.30	5.70		0.80	27.42	68.78
53	99.03	7.80	22.90	61.20	0.50	5.70	0.20	0.80	27.14	67.22
54	99.37	7.80	23.40	61.80	0.40	5.50		0.40	27.08	69.51
55	99.23	7.80	23.10	61.90	0.50	5.30	0.20	0.40	26.00	69.25
56	99.21	7.70	23.40	61.80	0.40	5.50		0.50	27.25	69.05
57	99.10	7.90	22.90	61.40	0.50	5.40	0.30	0.70	25.83	68.39
58	99.28	7.90	23.30	61.30	0.60	5.40		0.80	25.91	68.59
59	99.42	8.10	23.00	62.10	0.40	5.10	0.20	0.50	24.68	70.95
60	99.53	7.90	23.10	62.30	0.50	5.20		0.50	25.54	70.21
61	98.86	7.80	22.80	62.20	0.50	5.20	0.40		25.71	69.80
62	98.70	8.00	22.80	61.30	0.50	5.10		1.00	24.62	69.89
63	99.12	8.30	22.50	62.40	0.50	5.00	0.30		23.98	72.04
64	98.00									
65	99.59	8.10	22.70	62.70	0.50	4.80	0.20	0.60	23.38	71.38
66	99.00									
67	98.00									
68	99.02	8.00	23.40	60.60	0.50	5.80	0.20	0.40	27.30	68.14
69	98.88	7.80	23.40	60.60	0.30	5.60		1.10	27.10	68.30
70	99.01	7.90	23.60	60.50	0.40	5.80	0.30	0.60	27.45	67.65
71	98.00									
72	99.04	7.60	23.90	60.30	0.30	6.40		0.50	30.80	66.18
73	99.91	7.20	24.60	61.10	0.30	6.50	0.20		32.43	65.01
74	97.00									
75	99.34	7.40	23.90	61.80	0.30	5.70	0.30		28.96	68.04
76	98.00									
77	98.00									

THIRTI	83.00									
2	81.00									
3	100.25	6.50	25.90	58.90	0.20	7.90	0.00	0.80	38.85	57.85
4	99.74	7.50	24.70	59.50	0.20	6.60	0.00	1.20	31.34	64.45
5	98.98	8.50	22.60	63.10	0.23	4.60	0.00	0.00	22.71	75.94
6	100.84	9.20	22.30	64.90	0.23	3.70	0.00	0.40	17.76	79.89
7	83.00									
8	76.00									
9	93.00									
10	98.00									
11	99.30	9.60	20.90	65.20	0.21	2.70	0.00	0.70	13.04	83.92
12	98.63	7.80	23.50	61.40	0.30	5.60	0.00	0.00	27.90	70.32
13	100.20	8.10	23.80	62.70	0.30	5.20	0.00	0.00	25.72	72.51
14	99.75	7.30	24.40	61.20	0.30	6.50	0.00	0.00	32.39	65.83
15	98.00									
16	98.92	6.60	24.70	59.80	0.30	7.20	0.30	0.00	36.48	60.52
17	78.00									
18	79.00									
19	83.00									
20	82.00									
21	74.00									
22	80.00									
23	99.88	6.20	26.00	58.20	0.20	8.50	0.00	0.80	41.69	55.02
24	98.58	6.20	25.70	57.50	0.20	8.20	0.00	0.70	40.93	56.00
25	98.84	6.40	25.60	57.60	0.30	8.30	0.20	0.50	40.16	56.04
26	99.34	6.50	25.80	58.30	0.20	8.50	0.00	0.00	41.46	57.38
27	93.00									
28	91.00									
29	93.00									
30	81.00									
31	83.00									
32	89.00									
33	100.12	6.50	26.20	58.80	0.20	8.40	0.00	0.00	41.18	57.66
34	99.93	6.20	26.10	58.40	0.20	8.40	0.00	0.60	41.62	55.59
35	98.00									
36	99.08	6.40	25.50	57.80	0.20	8.40	0.00	0.70	40.78	56.23
37	99.32	6.50	26.00	57.90	0.30	8.40	0.30	0.00	40.47	56.68
38	100.31	6.60	25.80	58.30	0.20	8.50	0.20	0.60	40.17	56.44
39	99.95	6.60	25.70	59.60	0.20	7.90	0.00	0.00	39.34	59.47
40	99.35	6.50	25.70	58.00	0.00	8.50	0.00	0.70	41.18	56.99
41	98.00									
42	100.18	6.60	25.90	58.20	0.20	8.40	0.30	0.60	39.73	56.50
43	99.43	6.30	26.10	58.40	0.20	8.40	0.00	0.00	41.92	56.89
44	99.31	6.40	25.60	58.10	0.40	8.10	0.00	0.80	39.34	56.25
45	98.57	6.60	25.30	58.30	0.30	8.00	0.00	0.00	39.41	58.83
46	98.00									
47	99.00									
48	83.00									
49	99.68	7.20	24.30	60.60	0.30	6.40	0.00	0.90	31.57	64.27
50	92.00									
51	89.00									
52	99.56	7.60	24.10	60.80	0.30	6.30	0.00	0.50	30.46	66.50
53	100.03	7.80	24.10	61.00	0.30	6.40	0.00	0.50	30.27	66.76
54	99.07	7.60	24.00	61.00	0.30	6.30	0.00	0.00	30.87	67.38
55	99.31	8.80	22.20	63.30	0.30	4.20	0.00	0.60	20.19	76.54
56	99.23	7.80	23.50	61.20	0.40	5.90	0.00	0.50	28.42	67.99
57	98.92	7.90	23.30	61.50	0.30	5.50	0.00	0.40	27.00	70.18
58	97.00									
59	99.06	8.40	23.00	62.20	0.30	5.20	0.00	0.00	25.05	73.23
60	99.31	8.40	22.90	62.70	0.40	5.00	0.00	0.00	24.18	73.52
61	99.20	7.60	24.00	61.30	0.25	5.90	0.20	0.00	29.34	68.40

Hydrogen and oxygen isotopes for biotite within the feldspar porphyry and for andesite dykes and their selvedges.

Sample Nun	Line Numbe	Yield (µmol	□DV-SMOW (‰)	Run	d18O
296	10624	1.9	-70.5	1894	7.6
177	10625	1.9	-65	1849	7
211	10628	2.4	-76.3	1855	5.2
212	10629	2.1	-69.9	1854	5.9
239	10630	1.9	-77.4	1850	5.9
273	10633	Bottle broke	n.a.	1853	5.5
306	10634	1.7	-79	1901	6.6
292	10635	1.4	-72.8	1900	11.9
259	10638	1.7	-79.8	1851	5.8
267	10637	Small - not ı	-54.8	1852	6.1

Hydrogen standards

Sample Nun	Line Numbe	Yield (µmol	□DV-SMOW (‰)
DTW - Std	10626	Sample size	-51.7
DTW - Std	10627	Sample size	-51.4
DTW - Std	10631	Sample size	-50.5
DTW - Std	10632	Sample size	n.a.
DTW - Std	10636	Sample size	-52.7
		SUMMARY	Mean = -51.6 ± 0.8‰
			(Should be -51.9‰)

Oxygen standards

	11.294
	10.101
	10.511
	10.667
	10.694
	10.202
	10.749
	10.186
	10.807
	10
	10.166
Mean	10.49
St. Dev	0.39
± %	3.8
Should be	10.3

Data for EPMA transects across veins.

	92 SiO2	Na2O	MgO	Al2O3	K2O	CaO	TiO2	Total
#1	99.323	0.001	0	0.076	0.011	0.008	0.015	99.434
#2	99.466	0	0	0.026	0.002	0.006	0.008	99.508
#3	99.241	0	0	0.025	0.002	0.007	0.005	99.28
#4	99.905	0.004	0.005	0.04	0.008	0.004	0.007	99.974
#5	99.496	0.003	0	0.015	0.006	0.001	0.015	99.536
#6	99.796	0	0	0.013	0.006	0	0	99.815
#7	98.234	0.001	0.008	0.017	0.005	0.007	0.003	98.275
#8	99.785	0.001	0.002	0.032	0.008	0	0.007	99.835
#9	98.97	0.001	0	0.03	0.005	0.003	0.013	99.022
#10	100.112	0.003	0	0.03	0.004	0	0.012	100.16
#11	100.033	0	0	0.049	0.01	0.008	0.02	100.121
#12	99.162	0.003	0.003	0.017	0.004	0.007	0	99.196
#13	100.219	0	0	0.013	0	0.006	0	100.238
#14	100.044	0.001	0	0.036	0.006	0.004	0.012	100.103
#15	99.246	0.003	0.007	0.157	0.07	0.008	0	99.49
#16	99.652	0.001	0.002	0.032	0.007	0.013	0.007	99.714
#17	13.734	0.012	0	0.032	0.019	0.315	0.003	14.117
#18	98.465	0.003	0.002	0.034	0.006	0.014	0.002	98.526
#19	99.479	0.031	0	0.038	0.024	0.015	0.002	99.588
#20	99.999	0.004	0	0.025	0.002	0.006	0.01	100.047
#21	98.784	0.003	0.002	0.123	0.024	0.013	0.013	98.962
#22	99.573	0	0	0.026	0.001	0.014	0.008	99.623
#23	100.365	0	0	0.03	0.005	0.006	0.017	100.422
#24	99.766	0	0	0.019	0.002	0.006	0.015	99.808
#25	100.172	0	0	0.015	0.002	0	0.007	100.197
#26	100.138	0.003	0	0.019	0	0	0.012	100.17
#27	49.58	0.05	0.022	0.34	0.111	0.133	0.03	50.265
#28	100.277	0	0.002	0.021	0.005	0.001	0.012	100.317
#29	100.014	0	0.002	0.015	0.002	0.006	0.017	100.056
#30	100.196	0.001	0.002	0.019	0.008	0.004	0.01	100.24
#31	100.232	0.003	0	0.049	0	0.01	0.01	100.304
#32	100.114	0	0	0.015	0.006	0.001	0.005	100.142
#33	99.973	0.008	0	0.009	0.005	0.004	0.002	100.002
#34	99.967	0	0	0.032	0.001	0.006	0.007	100.013
#35	100.097	0	0	0.015	0	0.004	0.007	100.123
#36	100.191	0	0.003	0.019	0.001	0.013	0.008	100.235
#37	96.903	0.007	0	0.019	0	0.003	0.008	96.94
#38	99.539	0	0	0.03	0.014	0	0.007	99.59
#39	100.457	0	0.002	0.011	0.002	0	0.002	100.474
#40	99.126	0	0.01	0.006	0.004	0.011	0.007	99.163
#41	0.12	0.008	0	0.015	0.004	0	0	0.147
#42	98.23	0	0	0.013	0.008	0.011	0.008	98.271
#43	100.35	0.001	0	0.013	0.006	0.001	0.008	100.379
#44	99.203	0.013	0.005	0.019	0.004	0.007	0.003	99.255
#45	100.035	0.011	0	0.013	0.005	0	0	100.064
#46	99.468	0	0	0.025	0.002	0	0.017	99.512
#47	100.14	0	0	0.004	0	0	0.002	100.145
#48	100.273	0	0.005	0.026	0.006	0.007	0.015	100.332
#49	99.216	0	0.002	0.021	0.005	0.003	0	99.246
#50	106.115	0.007	0.003	0.053	0.006	0.006	0.002	106.191
#51	98.687	0.023	0.002	0.019	0.01	0.011	0.003	98.755
#52	99.905	0	0.002	0.032	0.008	0.008	0.017	99.972
#53	100.08	0.007	0	0.026	0.005	0.001	0.008	100.127
#54	99.678	0	0	0.028	0	0.006	0.005	99.717
#55	98.974	0.003	0	0.032	0.012	0.014	0.012	99.047
#56	100.127	0	0	0.036	0.006	0.006	0.012	100.186
#57	99.83	0.003	0.012	0.54	0.12	0	0.005	100.51

#58		100.191	0.001	0.005	0.019	0.002	0.001	0.007	100.227
#59		100.313	0.003	0.002	0.034	0	0.008	0	100.359
#60		22.709	0.013	0.005	0.125	0.024	0.311	0.003	23.19
#61		100.024	0	0	0.025	0.002	0.004	0.008	100.064
#62		92.317	0.07	0.012	0.219	0.039	0.092	0.018	92.766
#63		100.313	0	0.002	0.036	0	0.008	0.003	100.362
#64		100.014	0.003	0	0.026	0.002	0.008	0.017	100.07
#65		100.067	0	0	0.009	0.005	0.006	0.003	100.091
#66		100.296	0	0	0.004	0.005	0.001	0.007	100.312
#67		100.3	0	0	0.04	0.001	0.007	0.007	100.356
#68		99.892	0	0	0.064	0.006	0.01	0.003	99.975
#69		100.322	0.003	0	0.04	0.002	0.001	0	100.368
#70		100.3	0.004	0.005	0.136	0.011	0.004	0.012	100.472
#71		99.652	0.004	0.002	0.015	0.001	0.008	0	99.683
#72		98.978	0.007	0	0.11	0.006	0.022	0	99.123
#73		100.228	0	0.002	0.017	0.006	0.01	0	100.262
#74		100.243	0	0.002	0.015	0.001	0.01	0	100.27
#75		99.881	0.008	0	0.028	0.004	0.004	0.002	99.927
#76		99.43	0.011	0.003	0.051	0.016	0.011	0	99.522
#77		100.024	0	0.002	0.015	0.001	0.003	0.01	100.055
#78		99.954	0	0	0.025	0.006	0.003	0	99.986
#79		100.296	0	0	0.021	0.004	0.006	0.003	100.329
#80		97.943	0	0.003	0.021	0.005	0.007	0.013	97.992
#81		100.219	0	0.003	0.019	0	0.01	0.005	100.256
#82		99.962	0.003	0	0.026	0.007	0.006	0.002	100.006
#83		100.309	0.003	0.002	0.053	0	0.018	0.008	100.393
#84		99.714	0	0.003	0.023	0	0.001	0.003	99.745
#85		100.215	0	0	0.013	0	0.007	0	100.235
#86		95.754	0.022	0.008	0.132	0.022	0.027	0.002	95.967
#87		99.95	0.001	0	0.025	0.001	0.003	0.005	99.984
#88		1.343	0	0.027	0.072	0.014	1.251	0	2.707
#89		100.243	0	0	0.006	0.007	0.001	0	100.258
#90		100.412	0	0	0.015	0.005	0.008	0.002	100.441
#91		98.298	0	0.003	0.094	0.007	0.003	0.007	98.412
#92		100.078	0	0	0.013	0.004	0.001	0	100.095
#93		100.072	0	0.002	0.017	0.001	0	0.005	100.097
#94		99.881	0.001	0.002	0.008	0	0.011	0.002	99.905
#95		100.467	0.001	0.003	0.015	0.01	0.001	0.002	100.501
#96		100.029	0.003	0	0.013	0.001	0.006	0.005	100.057
#97		100.044	0.005	0	0.011	0.002	0.003	0.003	100.069
#98		100.029	0.005	0.003	0.013	0.001	0	0	100.052
#99		100.384	0.005	0.005	0.036	0.01	0.004	0.008	100.452
#100		99.749	0	0	0.013	0	0.006	0	99.768
	122								
#51		100.256	0.003	0	0.017	0.002	0.006	0.012	100.32
#52		69.411	1.41	0.003	18.061	13.937	0.018	0	102.909
#53		100.589	0.008	0	0.019	0	0.01	0.018	100.677
#54		100.429	0.004	0	0.013	0	0.008	0.007	100.48
#55		101.287	0	0.007	0.04	0	0.004	0.007	101.371
#56		99.609	0	0.002	0.017	0	0.007	0.012	99.646
#57		100.345	0	0	0.017	0.001	0.01	0.008	100.442
#58		97.631	0.024	0.023	0.242	0.025	0.076	0.02	98.104
#59		100.448	0	0.002	0.043	0.004	0	0.008	100.522
#60		75.369	0.205	0.174	1.963	0.188	0.653	0.105	79.328
#61		100.153	0	0.003	0.013	0.001	0.001	0.003	100.186
#62		100.264	0	0.003	0.081	0.013	0.004	0.005	100.379
#63		104.615	0.013	0.01	0.102	0.011	0.025	0.012	104.818
#64		104.429	0.047	0.022	0.155	0.013	0.048	0.005	104.76
#65		99.573	0	0	0.015	0.004	0.006	0.007	99.637
#66		100.324	0	0.003	0.023	0.002	0.003	0.012	100.379
#67		100.733	0.003	0.003	0.03	0.001	0.004	0.003	100.78
#68		100.638	0	0	0.026	0.004	0.008	0.007	100.697
#69		100.446	0.003	0	0.021	0	0	0.012	100.489
#70		100.698	0	0	0.015	0.002	0.003	0.005	100.763

#71	100.482	0.004	0	0.028	0	0.004	0.012	100.568
#72	97.147	0.007	0.008	0.11	0.025	0.074	0.02	97.46
#73	100.35	0	0	0.015	0.006	0.004	0.013	100.395
#74	100.737	0.003	0	0.026	0.002	0.011	0.01	100.8
#75	100.889	0	0	0.017	0.008	0.003	0.01	100.932
#76	100.504	0.004	0	0.057	0.001	0.01	0.018	100.615
#77	100.502	0	0	0.026	0.002	0.007	0.01	100.547
#78	100.84	0	0.005	0.028	0.004	0.004	0.023	100.943
#79	100.63	0	0	0.021	0.002	0.001	0.002	100.678
#80	100.728	0.004	0	0.026	0	0.003	0.017	100.79
#81	100.384	0	0	0.025	0.001	0	0.013	100.441
#82	100.549	0.003	0	0.059	0.013	0.003	0.033	100.68
#83	100.037	0	0	0.03	0.006	0.01	0.018	100.13
#84	100.628	0	0	0.017	0	0.003	0.018	100.676
#85	100.557	0.008	0	0.025	0	0.007	0.018	100.625
#86	100.256	0	0	0.023	0.002	0.007	0.025	100.338
#87	100.29	0	0.002	0.026	0	0.015	0.022	100.36
#88	100.615	0	0.003	0.038	0.006	0.021	0.017	100.75
#89	100.273	0.004	0	0.015	0.005	0	0.012	100.32
#90	100.825	0	0	0.034	0.023	0.017	0.023	100.933
#91	100.27	0	0	0.045	0.018	0	0.02	100.364
#92	100.707	0	0	0.013	0	0	0.01	100.747
#93	100.728	0.003	0.003	0.036	0.008	0.008	0.015	100.829
#94	100.634	0	0	0.017	0.001	0.001	0.01	100.7
#95	100.707	0	0.003	0.004	0.004	0.01	0.007	100.747
#96	100.315	0	0	0.028	0.001	0.014	0.027	100.398
#97	100.523	0	0.002	0.077	0.007	0.013	0.028	100.669
#98	100.647	0.003	0	0.023	0.005	0.004	0.028	100.716
#99	100.715	0	0	0.023	0	0	0.02	100.828
#100	65.036	0.944	0	19.484	15.929	0	0.007	101.475

151	SiO2	Na2O	MgO	Al2O3	K2O	CaO	TiO2	Total
#1	100.251	0	0.002	0.013	0.005	0.011	0.003	100.307
#2	98.298	0.018	0.007	0.537	0.661	0.014	0.005	99.653
#3	99.569	0.001	0.002	0.008	0	0.014	0.007	99.62
#4	98.848	0.009	0.007	0.017	0.007	0.003	0.002	98.898
#5	97.87	0.027	0.007	0.015	0.004	0.01	0.007	97.976
#6	100.551	0	0	0.008	0.002	0	0.012	100.578
#7	100.285	0.032	0	0.013	0.018	0.013	0.018	100.466
#8	85.334	0	0.007	0.064	0.01	0.011	0.015	85.52
#9	99.177	0	0.008	0.021	0.001	0.001	0.017	99.448
#10	98.172	0.003	0.002	0.123	0.008	0.01	0	98.359
#11	100.38	0.005	0	0.008	0.004	0.015	0	100.424
#12	100.42	0	0.005	0.011	0.007	0.008	0.012	100.484
#13	100.294	0	0.005	0.023	0	0.003	0.003	100.356
#14	99.637	0	0	0.008	0.008	0.013	0.003	99.67
#15	99.12	0	0	0.013	0.002	0	0.013	99.172
#16	100.339	0.001	0.003	0.03	0.007	0	0.01	100.429
#17	100.164	0	0.003	0.015	0.005	0.004	0.005	100.212
#18	99.87	0	0.005	0.017	0.002	0.001	0.015	99.922
#19	100.258	0	0	0.008	0.002	0.006	0.003	100.341
#20	99.532	0	0	0.008	0.005	0.006	0.008	99.571
#21	100.521	0	0	0.015	0.002	0.001	0.01	100.583
#22	100.442	0	0.002	0.013	0.005	0.003	0.01	100.505
#23	100.437	0	0.002	0.004	0.001	0.01	0.01	100.472
#24	99.903	0.005	0.007	0.015	0.002	0.006	0.002	99.965
#25	99.954	0	0	0.009	0	0.001	0.002	100.006
#26	101.171	0	0.01	0.019	0.001	0.017	0.01	101.234
#27	100.784	0	0.007	0.008	0	0.004	0.012	100.845
#28	100.553	0	0.002	0.013	0.002	0.013	0.007	100.594
#29	101.312	0	0	0.013	0.002	0.008	0.008	101.371
#30	100.35	0	0	0.019	0.001	0	0.01	100.408
#31	100.596	0	0.002	0.023	0.001	0.01	0.008	100.643
#32	100.94	0	0	0.038	0.006	0.01	0.002	101.034
#33	100.677	0	0.002	0.021	0.006	0.011	0.01	100.766

#34	100.812	0	0.007	0.023	0	0.003	0	100.864
#35	100.17	0	0.003	0.011	0	0.017	0.02	100.221
#36	100.594	0	0.003	0.229	0.046	0.006	0.008	100.907
#37	100.705	0	0.002	0.021	0.002	0.001	0.01	100.763
#38	100.895	0.004	0.005	0.017	0.001	0.006	0	100.971
#39	100.476	0	0	0.008	0.005	0.004	0.003	100.557
#40	100.705	0	0	0.023	0.004	0.018	0.012	100.781
#41	99.738	0	0	0.04	0.005	0.01	0.012	99.816
#42	100.891	0	0	0.036	0	0.001	0.01	100.958
#43	100.844	0.005	0.002	0.03	0.007	0.01	0.012	100.97
#44	100.81	0	0.002	0.013	0.001	0.014	0	100.869
#45	100.549	0	0.003	0.013	0	0.001	0.008	100.581
#46	100.48	0.02	0.015	0.043	0.013	0.003	0.008	100.608
#47	101.051	0	0	0.009	0.007	0.006	0.008	101.083
#48	100.35	0	0	0.008	0.002	0.013	0.005	100.394
#49	100.514	0	0.007	0.009	0.007	0.003	0.002	100.576
#50	101.128	0	0	0.009	0.008	0.013	0.008	101.186

Detection limits (% Element)

	Si	Na	Mg	Al	K	Ca	Ti
#1	12.09	0.785	1.57	3.175	1.045	1.28	2.645
#2	13.49	0.775	1.61	3.255	1.07	1.28	2.705
#3	12.11	0.795	1.645	3.16	1.05	1.23	2.625
#4	13.81	0.835	1.675	3.175	1.055	1.28	2.605
#5	12.27	0.825	1.65	3.185	1.015	1.285	2.725
#6	13.73	0.785	1.64	3.14	1.025	1.255	2.675
#7	13.41	0.815	1.69	3.265	1.02	1.255	2.77
#8	12.63	0.785	1.6	3.1	1.03	1.155	2.605
#9	12.23	0.765	1.62	3.16	1.035	1.2	2.65
#10	12.85	0.795	1.61	3.14	1.04	1.26	2.705
#11	13.37	0.795	1.5	3.21	0.97	1.235	2.575
#12	13.17	0.82	1.62	3.165	1.045	1.245	2.535
#13	13.65	0.84	1.695	3.145	1.085	1.16	2.8
#14	13.43	0.815	1.545	3.105	1.08	1.19	2.69
#15	12.91	0.81	1.585	3.25	1.065	1.215	2.745
std	0.6142591	0.0221897	0.0532447	0.05062	0.0289581	0.0429285	0.0742454
3*std	1.8427774	0.066569	0.1597342	0.1518599	0.0868743	0.1287855	0.2227362
std.% of el	46.74	11.28	60.32	52.92	32.86	38.61	59.95
c/s/na on stc	1176.583	76.111	1022.705	1266.236	373.686	402.758	1027.123
c/s/na/100%	2517.2935	674.74291	1695.4658	2392.7362	1137.2063	1043.1443	1713.2994
Det. limit (3	0.073	0.010	0.009	0.006	0.008	0.012	0.013

Sample 155.0 (Type 1)

Correction of values: Correction Factor = 8.593*10e-7te2+0.9924t-0.22

Corrected values

Inclusion	Te°C	Tm(h)°C	Tm(i)°C	Tm(d2)°C	Th°C	Homog	Fill	Salinity
2A1	-20.6	X	-0.3	X	306.3	L	70.0	0.5
2.0	-21.1	X	-2.2	X	375.6	L	50.0	3.6
3.0	-26.5	X	X	X	383.1	L	55.0	X
4.0	-26.0	X	-2.9	X	X	L	50.0	4.7
5.0	-30.5	X	-3.2	X	380.1	L	55.0	5.2
6.0	-28.2	X	-2.8	X	380.1	L	50.0	4.5
7.0	-41.9	X	-33.0	X	306.3	L	90.0	X
8.0	X	X	-3.2	X	379.1	L	60.0	5.2
9.0	-33.5	-20.1	-3.2	X	380.1	L	60.0	5.2
10.0	-27.0	X	-2.9	X	379.1	L	60.0	4.7
11.0	-37.4	-23.6	-12.5	X	377.1	L	80.0	16.5
12.0	X	X	-1.9	X	X	L	90.0	3.1
13.0	X	X	X	X	375.1	L	60.0	X
14.0	X	X	X	X	375.1	L	60.0	X
2B1	-52.3	X	-28.7	243.4	359.2	L	80.0	33.1
2.0	-54.3	X	-25.5	218.5	376.1	L	85.0	31.8
3.0	-51.3	X	-26.9	245.4	363.2	L	85.0	33.2
4.0	-49.3	X	X	245.4	370.1	L	85.0	33.2
5.0	-54.8	X	-26.2	245.4	386.1	L	90.0	33.2
6.0	-48.3	X	-27.6	245.4	256.4	L	70.0	33.2
7.0	-47.8	X	-28.0	245.4	367.1	L	85.0	33.2
8.0	-52.3	X	-28.6	245.4	368.1	L	85.0	33.2
9.0	-50.8	X	-28.5	245.4	366.1	L	85.0	33.2
10.0	-50.3	X	-28.4	245.4	364.1	L	85.0	33.2
11.0	-49.3	X	-27.3	245.4	349.2	L	85.0	33.2
12.0	-26.5	X	-2.4	X	374.1	L	45.0	3.9
13.0	-27.5	X	-2.3	X	376.1	L	55.0	3.8
14.0	-28.5	X	-6.3	X	312.0	L	50.0	9.6
2C1	-26.5	X	-0.7	X	373.1	L	50.0	1.2
2.0	X	X	-1.8	X	374.1	L	52.5	3.0
3.0	-50.3	X	X	X	237.5	L	90.0	X
4.0	-50.3	X	X	X	210.1	L	90.0	X
5.0	-48.3	X	-25.5	X	X	L	90.0	X
6.0	X	-23.9	-7.7	X	273.3	L	90.0	11.3
7.0	-31.0	-22.7	-9.8	X	394.1	L	50.0	13.8
8.0	-43.4	X	-24.3	X	288.3	L	92.5	X
9.0	-41.4	X	-22.5	X	358.2	L	85.0	X
10.0	-33.5	-24.4	-11.0	X	413.1	L	70.0	15.0
11.0	X	X	X	375.1	229.5	L	90.0	43.0
12.0	X	X	X	388.1	219.5	L	90.0	44.3
13.0	X	X	X	X	255.4	L	90.0	X
14.0	-33.5	-24.7	-17.8	X	375.1	L	70.0	20.8
15.0	-54.3	X	X	378.1	240.4	L	82.5	43.3
16.0	-55.3	X	X	X	303.3	L	85.0	X
17.0	-35.4	-23.0	-4.7	X	388.1	L	55.0	7.4
18.0	-28.5	-23.0	-12.9	X	354.2	L	55.0	16.8
19.0	-27.5	X	-5.2	X	309.2	L	60.0	8.1
20.0	-27.5	X	-1.7	X	375.1	L	50.0	2.8
21.0	-25.5	X	-0.8	X	375.1	L	50.0	1.3
22.0	-26.5	-20.5	-4.7	X	383.1	L	50.0	7.4
23.0	-20.6	X	-0.8	X	374.1	L	55.0	1.3
24.0	-40.4	-24.6	-15.7	X	285.3	L	90.0	19.2
25.0	X	X	-0.5	X	381.1	L	50.0	0.9
26.0	-38.4	-24.3	-1.2	X	X	L	90.0	2.0
27.0	-31.5	X	-0.8	X	374.1	L	50.0	1.3
28.0	-25.5	X	-0.9	X	373.1	L	50.0	1.5
29.0	X	X	-1.0	X	373.1	L	55.0	1.7
30.0	-25.5	-23.3	-11.1	X	386.1	L	50.0	15.1
1B 2	X	X	-1.4		376.6	L	80.0	2.3
3.0	-27.4	X	-0.8		372.7	L	60.0	1.3
4.0	-28.6	X	-3.4		370.6	L	60.0	5.5
5.0	-25.9	X	-3.1		366.5	L	70.0	5.0
6.0	-28.3	X	-1.2		X		85.0	2.0
7.0	-26.4	X	-1.2		372.5	L	75.0	2.0

8.0	-25.4	X	-1.4		231.6 L	85.0	2.3
C 2	-25.4	X	-19.3		376.0 L	82.5	21.9
3.0	-31.5	-21.9	-10.9		296.2 L	70.0	14.8
4.0	-36.5	X	-0.8	450.0	421.2 L	80.0	1.3
D 2	-27.9	X	-0.4		388.5 C	50.0	0.7
4.0	X	X	-0.2		380.5 C	70.0	0.3
5.0	X	X	-0.2		383.5 C	70.0	0.3
6.0	-30.0	X	-0.6		384.0 L	70.0	1.0
7.0	-24.9	X	-0.1		382.2 C	70.0	0.2
8.0	-30.5	X	-1.0		X	80.0	1.7
9.0	-25.4	X	-0.1		379.3 C	70.0	0.2
10.0	-25.9	X	-0.1		381.0 C	70.0	0.2
11.0	-33.5	X	-20.3		373.9 L	85.0	22.6
13.0	X	X	X		381.4 C	90.0	26.2
14.0	-33.5	X	-0.6		386.9 L	70.0	1.0
17.0	-26.9	X	-13.8		397.0 L	X	17.6
18.0	-35.0	X	X		376.5 L	X	0.0
75.0							

Sample 156.0 (Type 1)
Correction of values: Correction Factor = -2.819*10e-6te2+0.9992t-0.53

Inclusion	Corrected values Te°C	Tm(h)°C	Tm(i)°C	Tm(d2)°C	Th°C	Homog		Fill	Salinity
BA1	X	-22.8	-9.8	X	344.8	L		60.0	13.8
2.0	X	X	-2.5	X	344.8	L		65.0	4.1
3.0	X	X	-19.5	X	337.9	L		50.0	22.0
4.0	X	X	-2.5	X	345.7	L		60.0	4.1
5.0	X	X	-2.1	X	342.8	L		65.0	3.5
6.0	X	X	-2.0	X	345.7	L		70.0	3.3
7.0	-48.1	X	-23.1	X	351.6	L		80.0	X
8.0	X	X	X	X	351.6	L		55.0	X
9.0	-40.5	X	-23.3	X	352.6	L		70.0	X
10.0	X	X	-2.4	X	357.5	L		55.0	4.0
11.0	X	X	-2.0	X	359.4	L		50.0	3.3
12.0	X	X	-2.2	X	359.4	L		50.0	3.6
13.0	X	X	-1.9	X	365.3	L		60.0	3.2
14.0	X	X	-2.3	X	365.3	L		55.0	3.8
15.0	X	X	-2.5	X	365.3	L		50.0	4.1
BB1	X	X	-3.2	X	337.9	L		80.0	5.2
2.0	X	X	-23.0	278.0	274.1	L		90.0	35.2
3.0	X	X	X	237.7	272.1	L		90.0	32.8
4.0	X	X	-3.4	X	340.8	L		70.0	5.5
5.0	X	X	-3.2	X	337.9	L		60.0	5.2
6.0	X	X	X	X	343.8	L		60.0	X
7.0	X	X	X	X	289.8	L		85.0	X
8.0	X	X	X	X	282.0	L		90.0	X
9.0	X	X	X	242.6	285.9	L		80.0	33.0
10.0	X	X	-3.5	X	346.7	L		60.0	5.7
11.0	X	X	-3.1	X	351.6	L		50.0	5.1
12.0	-48.0	X	X	X	314.4	L		75.0	X
13.0	X	X	X	X	309.5	L		80.0	X
14.0	-45.6	X	-29.5	X	338.9	L		80.0	X
15.0	-45.6	X	X	217.9	317.3	L		80.0	31.7
16.0	-45.6	X	X	217.9	345.7	L		70.0	31.7
17.0	X	X	-1.3	X	X		0.0	65.0	2.2
18.0	-44.5	X	X	X	335.0	L		70.0	X
19.0	-44.5	X	X	208.1	326.1	L		80.0	31.3
A1	X	X	-1.8	X	338.9	L		60.0	3.0
2.0	X	X	-2.2	X	340.8	L		55.0	3.6
3.0	X	X	-1.8	X	335.9	L		50.0	3.0
4.0	X	X	-2.0	X	340.8	L		55.0	3.3
5.0	X	X	-1.8	X	340.8	L		65.0	3.0
6.0	X	X	-1.8	X	341.8	L		60.0	3.0
7.0	X	X	-2.1	X	340.8	L		60.0	3.5
8.0	X	X	-2.4	X	341.8	L		60.0	4.0
9.0	X	X	-2.0	X	339.9	L		55.0	3.3
11.0	X	X	-6.9	X	345.7	L		50.0	10.4
12.0	-35.5	-25.5	-23.7	X	356.5	L		75.0	X
13.0	X	X	X	232.7	257.4	L		80.0	32.5
14.0	X	X	X	264.2	264.2	L		80.0	34.3
15.0	X	X	-2.2	X	341.8	L		55.0	3.6
16.0	X	X	-3.4	X	342.8	L		50.0	5.5
17.0	X	X	X	262.3	282.0	L		80.0	34.2
18.0	X	X	X	257.4	273.6	L		80.0	33.9
19.0	X	X	X	208.1	242.6	L		95.0	31.3
20.0	X	X	X	198.2	286.9	L		80.0	30.8

Sample 308.0

Correction of values: Correction Factor = -2.819*10e-6te2+0.9992t-0.53

Inclusion	Corrected values Te°C	Tm(h)°C	Tm(i)°C	Tm(d2)°C	Th°C	Homog	Fill	Salinity

BRITISH LIBRARY

IMAGING SERVICES NORTH

Boston Spa, Wetherby
West Yorkshire, LS23 7BQ
www.bl.uk

PAGE MISSING IN ORIGINAL

Sample 93.0 (Type 2)

Correction of values: Correction Factor = -2.819*10e-6te2+0.9992t-0.53

Corrected values

Inclusion	Te°C	Tm(h)°C	Tm(i)°C	Tm(d2)°C	Th°C	Homog	Fill	Salinity
1.0	-28.5	X	-3.4	X		414.2 V	50.0	5.5
2.0	-28.0	X	-3.9	X		314.4 V	50.0	6.3
3.0	-28.5	X	-3.1	X		316.3 V	50.0	5.1
4.0	-27.5	X	-6.7	X		404.4 V	52.5	10.1
5.0	-28.0	X	-7.5	X		404.4 V	52.5	11.1
6.0	X	X	-4.6	X		428.8 V	50.0	7.3
7.0	-29.5	X	-4.5	X		425.9 C	52.5	7.1
8.0	-30.5	X	-4.1	X		409.3 V	50.0	6.6
9.0	-29.0	X	X	X		453.1 C	52.5	X
10.0	-34.5	-23.7	-12.8	X	X		70.0	16.7
11.0	-21.0	X	-1.7	X		394.6 V	50.0	2.8
12.0	-29.5	X	-3.8	X		394.6 V	57.5	6.1
13.0	-28.5	X	-3.4	X		394.6 V	50.0	5.5
14.0	-29.5	X	-7.5	X		340.8 V	50.0	11.1
15.0	-28.5	-21.0	-5.2	X		404.4 V	50.0	8.1
16.0	-24.5	X	-5.2	X		399.5 V	50.0	8.1
17.0	-24.5	X	-3.5	X		414.2 V	50.0	5.7
18.0	X	X	-3.5	X		389.8 V	50.0	5.7
19.0	X	X	-3.5	X		399.5 V	50.0	5.7
20.0	X	X	-3.5	X		404.4 V	50.0	5.7
21.0	-20.5	X	-1.9	X		399.5 V	50.0	3.2
22.0	-20.5	X	-2.0	X		409.3 V	50.0	3.3
23.0	-27.5	X	-6.5	X		413.2 V	50.0	9.9
24.0	-20.5	X	-2.1	X		419.0 V	50.0	3.5
25.0	-24.5	X	-3.5	X		419.0 V	50.0	5.7
26.0	-24.5	X	-8.2	X		394.6 V	50.0	12.0
27.0	-24.5	X	-3.5	X		419.0 V	60.0	5.7
28.0	-23.5	X	-6.1	X		409.3 V	50.0	9.4
29.0	X	X	-1.8	X		409.3 V	50.0	3.0
30.0	X	X	-3.3	X		404.4 V	50.0	5.4
31.0	X	X	-1.8	X		402.5 V	50.0	3.0
32.0	-28.5	X	-2.2	X		399.5 V	50.0	3.6
33.0	-28.5	X	-3.7	X		428.8 V	50.0	6.0
34.0	X	X	-1.6	X		482.3 V	50.0	2.7
35.0	-51.6	X	-24.2	X	X		80.0	X
36.0	X	X	X	X		365.3 L	80.0	X
37.0	X	X	X	X		350.6 L	82.5	X
38.0	X	X	X	X	X		90.0	X
39.0	X	X	X	X		350.6 L	85.0	X
40.0	X	X	X	350.6		350.6 L	90.0	40.7
41.0	X	X	X	360.4		321.2 L	90.0	41.6
42.0	-58.1	X	-43.3	X		380.0 L	95.0	X
43.0	X	X	X	433.7		331.0 L	90.0	49.1
44.0	X	X	X	350.6		350.6 V	80.0	40.7
45.0	X	X	X	321.2		340.8 L	85.0	38.3
46.0	X	X	X	X		340.8 L	92.5	X
47.0	-43.5	X	-30.5	394.6		350.6 L	85.0	44.9
48.0	-23.5	X	-7.8	X		477.5 L	55.0	11.5
49.0	X	X	X	X		305.5 L	80.0	X
50.0	-56.6	X	-37.5	X		350.6 L	85.0	X
51.0	X	X	X	X		370.2 L	90.0	X
52.0	X	X	X	X		350.6 L	87.5	X
53.0	-55.6	X	-37.5	X		380.0 L	80.0	X

Sample 123.0 (Type 2)

Correction of values: Correction Factor = -2.819*10e-6te2+0.9992t-0.53

Inclusion	Corrected values Te°C	Tm(h)°C	Tm(i)°C	Tm(d2)°C	Th°C	Homog	Fill	Salinity
1.0	-27.5	X	-2.5	X		355.5 L	60.0	4.1
2.0	X	X	X	X		375.1 L	40.0	X
3.0	-30.5	X	-2.4	X		367.3 L	65.0	4.0
4.0	X	X	-2.4	X		350.6 L	60.0	4.0
5.0	X	X	-2.6	X		364.3 L	80.0	4.3
6.0	X	X	X	267.2		286.9 L	85.0	34.5
7.0	X	X	-2.9	X		363.4 L	55.0	4.7
8.0	X	X	-3.0	X		358.5 L	75.0	4.9
9.0	X	X	-2.9	X		359.4 L	70.0	4.7
10.0	X	X	-3.0	X		359.4 L	70.0	4.9
11.0	X	X	-2.4	X		363.4 L	50.0	4.0
13.0	X	X	-0.9	X		361.4 L	50.0	1.5
14.0	X	X	-4.4	X		358.5 L	65.0	7.0
15.0	X	X	-0.9	X		362.4 L	50.0	1.5
16.0	X	X	-1.1	X		362.4 L	50.0	1.9
17.0	-43.0	X	X	X		226.8 L	90.0	X
18.0	-43.0	X	-27.5	267.2		296.7 L	90.0	34.5
19.0	X	X	X	X		241.6 L	90.0	X
20.0	X	X	X	X		241.6 L	90.0	X
21.0	X	X	-0.8	X		365.3 L	50.0	1.4
22.0	X	X	-0.9	X		365.3 L	50.0	1.5
23.0	X	X	-2.8	X		352.6 L	55.0	4.6
24.0	X	X	-3.3	X		343.8 L	70.0	5.4
25.0	X	X	-1.4	X		351.6 L	65.0	2.4
26.0	X	X	-4.4	X		272.1 L	70.0	7.0
27.0	X	X	-2.9	X		314.4 L	75.0	4.7
28.0	-53.1	X	X	X	X	L	85.0	X
29.0	X	X	-5.9	X		352.6 L	65.0	9.1
30.0	X	X	X	X		302.6 L	75.0	X
31.0	X	X	-1.3	X		333.0 L	60.0	2.2
32.0	-44.5	X	-23.6	X		279.0 L	50.0	X
33.0	X	X	-4.4	X		347.7 L	85.0	7.0
34.0	-45.6	X	-25.0	277.0		311.4 L	85.0	35.1
35.0	X	X	-1.7	X		357.5 L	55.0	2.8
36.0	X	X	X	X		257.4 L	80.0	X
37.0	X	X	-3.0	X		363.4 L	85.0	4.9
38.0	X	X	-4.2	X		352.6 L	50.0	6.7
39.0	X	X	-1.4	X		331.0 L	60.0	2.4
40.0	X	X	-2.5	X		342.8 L	70.0	4.1
41.0	X	X	-2.5	X		313.4 L	85.0	4.1
42.0	X	X	-2.2	X		335.9 L	65.0	3.6
43.0	X	X	-2.4	X		355.5 L	50.0	4.0
44.0	X	X	-23.8	237.7		356.5 L	85.0	32.8
45.0	-48.6	X	-27.8	237.7		302.6 L	80.0	32.8
46.0	X	X	-2.5	X		341.8 L	60.0	4.1
47.0	X	X	X	227.8		308.5 L	80.0	32.2
48.0	-49.1	X	-29.4	227.8		301.1 L	75.0	32.2

Sample 247.0 (Type 2)
Correction of values: Correction Factor = -2.819*10e-6te2+0.9992t-0.53
Corrected values

Inclusion	Te°C	Tm(h)°C	Tm(i)°C	Tm(d2)°C	Th°C Homog	Fill	Salinity
1.0	-31.0	-23.5	-6.1	X	358.5 L	70.0	9.4
2.0	-31.0		-3.8	X	381.0 L	60.0	6.1
3.0	-31.0	-20.7	X	X	431.7 V	50.0	X
4.0	X	X	-2.5	X	380.0 L	50.0	4.1
5.0	X	X	-0.8	X	346.7 L	60.0	1.4
6.0	-34.0	X	-7.5	X	341.8 L	70.0	11.1
7.0	-50.6	X	-33.5	326.1	252.4 L	90.0	38.7
8.0	-50.6	X	X	296.7	252.4 L	90.0	36.4
9.0	-46.6	X	-32.5	316.3	275.1 L	90.0	37.9
10.0	X	X	X	326.1	235.7 L	85.0	38.7
11.0	X	X	X	296.7	209.0 L	90.0	36.4
12.0	-28.5	-23.3	-11.8	X	X L	80.0	15.8
13.0	-30.0	-23.4	-9.5	X	363.4 L	60.0	13.4
14.0	-30.5	-23.6	-9.0	X	321.2 V	60.0	12.9
15.0	X	X	X	X	360.4 L	50.0	X
16.0	X	X	-2.3	X	356.5 L	50.0	3.8
17.0	X	X	X	286.9	282.9 L	90.0	35.8
18.0	X	X	X	X	X	75.0	X
19.0	X	X	X	327.1	276.1 L	90.0	38.8
20.0	X	X	X	296.7	262.3 L	85.0	36.4
21.0	X	X	X	270.2	262.3 L	90.0	34.7
22.0	-34.5	X	X	321.2	252.4 L	90.0	38.3
23.0	X	X	-1.3	X	336.9 L	50.0	2.2
24.0	X	X	-43.5	X	345.7 L	60.0	X
25.0	X	X	-3.5	330.1	259.3 L	90.0	5.7
26.0	X	X	-1.8	X	362.4 L	60.0	3.0
27.0	X	X	-2.1	X	352.6 L	55.0	3.5
28.0	X	X	-2.1	X	371.2 L	50.0	3.5
29.0	X	X	-2.8	X	372.2 L	50.0	4.6
30.0	X	X	X	335.9	227.8 L	90.0	39.5
31.0	X	X	X	282.0	218.9 L	90.0	35.4
32.0	X	X	-31.5	331.0	179.4 L	95.0	39.1
C1	X	X	-2.1	X	311.4 L	80.0	3.5
2.0	X	X	-1.2	X	381.0 L	50.0	2.0
3.0	X	X	-1.3	X	379.0 L	50.0	2.2
4.0	X	X	-1.2	X	381.0 L	50.0	2.0
5.0	X	X	-5.4	X	392.7 L	50.0	8.4
6.0	X	X	X	277.0	217.9 L	90.0	35.1
7.0	X	X	X	X	378.0 L	50.0	X
8.0	X	X	X	X	378.0 L	50.0	X
9.0	X	X	-1.1	X	381.9 L	50.0	1.9
10.0	X	X	-1.3	X	384.9 L	50.0	2.2
11.0	X	X	-1.8	X	373.1 L	50.0	3.0
12.0	X	X	-9.7	X	352.6 L	80.0	13.7
13.0	X	X	-4.1	X	392.7 L	50.0	6.6
14.0	X	X	-2.2	X	381.9 L	50.0	3.6
15.0	X	X	-1.1	X	384.9 L	50.0	1.9
16.0	-29.5	X	-1.5	X	372.2 L	50.0	2.5
17.0	-46.1	X	-25.3	277.0	277.0 L	90.0	35.1
18.0	X	X	X	X	360.4 L	60.0	X
19.0	X	X	-3.0	X	359.4 L	50.0	4.9
20.0	X	X	X	277.0	245.5 L	85.0	35.1
21.0	X	X	-2.0	X	384.9 V	50.0	3.3
22.0	-50.6	X	X	X	257.4 L	85.0	X
23.0	X	X	X	X	270.2 L	90.0	X
24.0	X	X	X	227.8	281.0 L	80.0	32.2
25.0	X	X	-3.6	X	403.4 L	50.0	5.8
26.0	X	X	-3.4	X	404.4 L	50.0	5.5
27.0	X	X	-2.4	X	404.4 L	50.0	4.0
28.0	X	X	-2.8	X	400.5 L	50.0	4.6
29.0	-30.5	X	-3.6	X	396.6 L	55.0	5.8
30.0	X	X	-33.5	326.1	291.8 L	90.0	38.7

Sample 289.0 (Type 2)

Correction of values: Correction Factor = -2.819*10e-6te2+0.9992t-0.53

Corrected values

Inclusion	Te°C	Tm(h)°C	Tm(i)°C	Tm(d2)°C	Th°C Homog	Fill	Salinity
A1	X	X	-23.7	X	X	60.0	X
2.0	X	X	X	X	375.1 V	40.0	X
3.0	X	X	-10.7	X	375.1 V	50.0	14.7
4.0	X	X	-23.7	X	X	55.0	X
5.0	X	X	-3.5	X	375.1 V	50.0	5.7
6.0	X	X	-4.3	X	375.1 V	40.0	6.9
7.0	X	X	-8.9	X	X	55.0	12.8
8.0	X	X	X	203.1	291.8 L	80.0	31.0
9.0	X	X	X	282.0	253.4 L	90.0	35.4
10.0	X	X	-24.2	X	X	60.0	X
11.0	X	X	X	X	X	50.0	X
12.0	X	X	-24.7	X	416.1 L	70.0	X
13.0	X	X	-6.8	X	375.1 V	55.0	10.3
14.0	X	X	-20.8	X	438.5 L	70.0	22.9
15.0	X	X	-26.6	247.5	315.3 L	80.0	33.3
16.0	X	X	X	X	392.7 L	80.0	X
17.0	X	X	-4.5	X	380.0 V	50.0	7.1
18.0	X	X	-33.5	X	384.9 V	40.0	X
19.0	X	X	-4.7	X	X	60.0	7.4
21.0	X	X	X	272.1	340.8 L	80.0	34.8
BA1	X	X	-26.3	X	388.8 L	80.0	X
2.0	X	X	X	X	355.5 L	75.0	X
4.0	X	X	-36.1	X	287.9 L	80.0	X
5.0	X	X	X	X	311.4 L	70.0	X
6.0	X	X	-22.5	268.2	414.2 L	80.0	34.5
BB1	X	X	X	X	414.2 L	60.0	X
2.0	X	X	-10.2	X	462.9 L	50.0	14.2
3.0	X	X	-10.5	X	462.9 L	50.0	14.5
4.0	X	X	-6.3	X	409.3 L	50.0	9.6
5.0	X	X	-27.3	X	437.6 L	80.0	X
6.0	X	X	X	X	367.3 L	80.0	X
BC1	X	X	-33.0	282.9	316.3 L	80.0	35.5
2.0	X	X	X	263.3	343.8 L	90.0	34.2
4.0	X	X	X	X	330.1 L	85.0	X
5.0	X	X	X	X	257.4 L	85.0	X
6.0	X	X	X	X	279.0 L	90.0	X
7.0	X	X	X	X	299.6 L	80.0	X
8.0	X	X	X	193.2	284.9 L	90.0	30.6
9.0	X	X	X	193.2	284.9 L	90.0	30.6
11.0	X	X	X	-6.9	394.6 V	50.0	26.2
12.0	X	X	X	-2.5	394.6 V	50.0	26.2

Sample 84.0 (Type 3)
Correction of values: Correction Factor = 8.593*10e-7te2+0.9924t-0.22

Inclusion	Corrected values Te°C	Tm(h)°C	Tm(i)°C	Tm(d2)°C	Th°C	Homog	Fill	Salinity
15.0	-27.0	X	-0.8		382.1	V	50.0	1.3
16.0	X	X	-1.0		385.1	V	50.0	1.7
17.0	X	-24.0	-5.7		438.1	C	50.0	8.8
18.0	X	X	-3.2		409.1	V	50.0	5.2
19.0	-33.0	-24.2	-3.2		430.1	V	50.0	5.2
20.0	-32.0	X	-6.8		485.1	V	50.0	10.2
27.0	-41.9	X	-25.9	153.8	412.1	L	80.0	29.1
28.0	X	X	X	298.3	273.3	H	90.0	36.6
29.0	-53.8	X	-32.0	303.3	303.3	L	90.0	36.9
30.0	-36.9	-23.0	-18.8				80.0	21.5
31.0	-28.0	X	-5.8				60.0	8.9
32.0	-54.8	X	-32.0		330.2	L	90.0	
33.0	X	X	X	303.3	288.3	L	85.0	36.9
34.0	-27.0	X	-4.1		496.1	V	50.0	6.5
35.0	X	X	X	303.3	283.3	L	90.0	36.9
36.0	-33.0	-22.9	-15.3		468.1	L	60.0	18.9
37.0	X	X	-3.3		466.1	V	50.0	5.3
A1	X	X	-51.0	314.2	314.2	L	90.0	37.7
2.0	X	X	-50.5	303.3	316.2	L	90.0	36.9
3.0	X	X	-1.2		390.1	V	50.0	2.0
4.0	-19.6	X	-2.0		394.1	V	50.0	3.3
5.0	X	-23.8	-17.7				75.0	20.7
6.0	X	X	-1.8		406.1	V	50.0	3.0
7.0	-28.3	X	-2.6		406.1	V	50.0	4.2
8.0	X	X	-1.9		406.1	V	50.0	3.1
9.0	X	X	-30.5	253.4	303.3	L	90.0	33.6
10.0	-53.8	X	-30.5	263.4	315.2	L	90.0	34.2
11.0	X	X	X	313.2	273.3	H	90.0	37.7
12.0	X	X	X	313.2	298.3	H	90.0	37.7
13.0	X	X	X	313.2	273.3	H	80.0	37.7
14.0	X	X	X	313.2	273.3	H	90.0	37.7
21.0	-35.9	-23.3	-18.0		328.2	L	90.0	20.9
22.0	-34.9	X	-5.1		334.2	C	55.0	7.9
23.0	-33.0	X	-4.1		437.1	C	50.0	6.5
24.0	-34.9	X	-4.3		433.1	V	50.0	6.8
25.0	X	X	X		406.1	C	50.0	26.2
26.0	-54.8	X	-37.2	313.2	272.3	H	80.0	37.7
B1	X	X	-1.3		388.1	V	50.0	2.2
2.0	-54.8	X	-31.9	158.8	314.2	L	80.0	29.2
3.0	-37.9	X	-20.7		436.1	L	70.0	22.8
4.0	-29.0	X	-10.1		481.1	C	60.0	14.1
5.0	-35.9	X	-19.3		405.1	L	50.0	21.9
6.0	-34.9	-22.8	-10.4		488.1	C	80.0	14.4
7.0	X	X	X	233.5	296.3	L	80.0	32.5
8.0	-29.0	X	-1.4		405.1	V	50.0	2.3
9.0	X	X	X	296.3	299.3	L	90.0	36.4
10.0	-29.0	X	-7.4		473.1	V	50.0	10.9
11.0	-20.1	X	-2.0		408.1	V	50.0	3.3
12.0	-28.0	X	-5.0		473.1	V	50.0	7.8
13.0	X	X	-1.0		396.1	V	50.0	1.7
14.0	X	X	X		286.3	L	90.0	
15.0	-21.1	X	-1.6		415.1	V	50.0	2.6
16.0	X	X	X		286.3	L	85.0	
17.0	-36.9	-23.6	-7.8		458.1	V	50.0	11.4
18.0	-54.8	X	-30.9	158.8	331.2	L	75.0	29.2
19.0	-53.8	X	-31.9	158.8	331.2	L	80.0	29.2
20.0	X	X	X	178.7	318.2	L	85.0	30.0
21.0	-32.5	-23.6	-10.7		488.1	D	55.0	14.7
22.0	-32.5	X	-23.6		426.1	L	85.0	
23.0	X	X	-1.0		404.1	V	50.0	1.7

Sample 285.0 (Type 3)

Correction of values: Correction Factor = -2.819*10e-6te2+0.9992t-0.53

Inclusion	Corrected values Te°C	Tm(h)°C	Tm(i)°C	Tm(d2)°C	Th°C	Homog	Fill	Salinity
A1	X	X	-3.8	X	434.6	V	50.0	6.1
2.0	X	X	-2.4	X	405.4	V	50.0	4.0
3.0	X	X	X	X	411.2	V	50.0	
4.0	X	X	-4.8	X	409.3	V	50.0	7.6
5.0	X	X	X	X	409.3	V	50.0	
6.0	X	X	X	X	409.3	V	50.0	
7.0	X	X	-10.8	X	453.1	V	55.0	14.8
8.0	X	X	X	X	406.4	L	50.0	
9.0	X	X	X	X	394.6	V	60.0	
10.0	X	X	-3.0	X	409.3	V	55.0	4.9
11.0	X	X	-3.0	X	409.3	V	50.0	4.9
12.0	X	X	-3.3	X	404.4	V	50.0	5.4
13.0	X	X	-7.0	X	448.3	V	50.0	10.5
14.0	X	X	-1.7	X	335.9	V	45.0	2.8
16.0	X	X	X	X	218.9	L	80.0	
B1	X	X	-1.3	X	345.7	V	45.0	2.2
2.0	X	X	-1.3	X	384.9	V	50.0	2.2
4.0	X	X	-2.4	X	380.0	V	50.0	4.0
5.0	X	X	-10.7	X	X	V	60.0	14.7
6.0	X	X	-2.6	X	398.5	V	50.0	4.3
7.0	X	X	-2.6	X	384.9	V	45.0	4.3
8.0	X	X	-4.5	X	395.6	V	50.0	7.1
9.0	X	X	-4.5	X	400.5	V	50.0	7.1

Sample 273.0 (Type 3)

Correction of values: Correction Factor = 8.593*10e-7te2+0.9924t-0.22

Corrected values

Inclusion	Te°C	Tm(h)°C	Tm(i)°C	Tm(d2)°C	Th°C	Homog	Fill	Salinity
A14	-19.1	X	-0.7	X	X		50.0	1.2
15.0	-34.0	-23.6	-18.5	X	390.1	L	80.0	21.3
16.0	-43.9	X	-18.7	X	423.1	L	50.0	21.4
17.0	-30.5	X	-1.8	X	366.1	L	50.0	3.0
19.0	-54.3	X	-27.0	X	352.2	L	90.0	
20.0	-29.3	-20.1	-3.8	X	398.1	L	60.0	6.1
21.0	-33.0	-22.7	-4.0	X	394.1	L	70.0	6.4
22.0	-39.9	-23.0	-15.9	X	373.1	L	90.0	19.4
23.0	-19.8	X	-1.7	X	383.1	L	50.0	2.8
24.0	-30.0	X	-1.7	X	383.1	L	80.0	2.8
25.0	-26.0	X	-3.0	X	388.1	L	50.0	4.9
26.0	-21.6	X	-2.8	X	383.1	L	60.0	4.5
27.0	X	X	-1.2	X	376.1	L	50.0	2.0
47.0	X	X	-0.3	X	382.1	L	60.0	0.5
48.0	-20.1	X	-2.2	X	374.1	L	60.0	3.6
49.0	-54.8	X	-30.0	X	358.2	L	80.0	
50.0	-52.8	X	-29.7	X	366.1	L	90.0	
51.0	-46.8	X	-30.3	X	353.2	L	95.0	
52.0	X	X	-0.2	X	377.1	L	50.0	0.4
53.0	-48.3	X	-24.6	X	366.1	L	80.0	
B7	-19.6	X	-0.8	X	378.6	L	60.0	1.3
8.0	-54.8	X	-37.0	238.5	X	L	95.0	32.8
9.0	-35.4	-24.9	-20.8	X	345.2	L	80.0	22.9
10.0	-32.0	-23.9	-6.0	X	373.1	L	80.0	9.2
11.0	-18.1	X	-0.6	X	378.6	L	60.0	1.0
12.0	X	X	-1.5	X	402.1	L	50.0	2.5
13.0	-45.9	X	X	X	344.2	L	90.0	
14.0	X	X	-1.7	X	372.1	L	50.0	2.8
15.0	X	X	X	X	288.3	L	90.0	
16.0	-54.8	X	-30.9	X	342.2	L	80.0	
17.0	X	X	X	X	334.2	L	80.0	
18.0	-34.9	-23.0	-20.5	X	418.1	L	80.0	22.7
19.0	-53.8	X	-30.4	X	X	L	90.0	
20.0	-53.8	X	-30.0	X	356.2	L	90.0	
21.0	-53.8	X	-29.2	X	338.2	L	90.0	
22.0	-20.6	X	-4.0	X	395.6	L	60.0	6.4
23.0	-54.8	X	-28.2	X	344.2	L	80.0	
24.0	X	X	X	X	308.2	L	90.0	
25.0	X	X	X	X	330.2	L	90.0	
26.0	-54.8	X	-37.4	X	334.2	L	90.0	
27.0	-44.4	X	-30.0	X	352.2	L	90.0	
28.0	-53.8	X	-27.3	X	337.2	L	90.0	
29.0	-53.8	X	-28.6	X	271.3	L	90.0	
30.0	X	X	X	X	271.3	L	95.0	
31.0	-55.1	X	-30.1	178.7	X	L	80.0	30.0
32.0	-43.9	X	-26.5	X	X	L	90.0	
33.0	-43.9	-24.9	-23.8	X	383.1	L	80.0	
A1	X	-23.8	-13.2	X	363.2	L	65.0	17.1
2.0	-34.4	-23.2	-15.9	X	382.1	L	60.0	19.4
3.0	-26.5	X	-2.8	X	383.1	V	40.0	4.5
4.0	X	X	X	X	378.1	L	50.0	
5.0	X	-24.3	-15.6	X	380.1	L	70.0	19.1
6.0	X	-23.1	-16.2	X	383.1	L	80.0	19.6
7.0	-32.0	-24.9	-15.6	X	378.1	L	70.0	19.1
8.0	-43.9	-23.8	-13.7	X	381.1	L	70.0	17.5
9.0	X	-23.2	-11.7	X	263.4	L	95.0	15.7
10.0	-41.9	-29.2	-10.6	X	279.3	L	95.0	14.6
11.0	-27.0	-24.1	-15.9	X	382.1	L	90.0	19.4
12.0	-27.0	-23.8	-16.2	X	382.1	L	75.0	19.6
13.0	X	X	-1.9	X	388.1	V	40.0	3.1

Sample 122.0 (Type 4)
Correction of values: Correction Factor = 8.593*10e-7te2+0.9924t-0.22

Inclusion	Corrected values Te°C	Tm(h)°C	Tm(i)°C	Tm(d2)°C	Th°C	Homog	Fill	Salinity
4.0	-52.3	X	X	X	298.3	L	95.0	X
5.0	X	X	X	X	298.3	L	90.0	X
8.0	X	X	-7.9	X	408.1	L	70.0	11.5
10.0	-34.9	-23.6	-14.4	X	363.2	L	85.0	18.1
12.0	X	X	X	X	350.2	L	75.0	X
13.0	-36.9	-23.9	X	X	399.1	L	80.0	X
14.0	X	-23.4	-7.0	X	401.1	L	75.0	10.4
15.0	-20.6	X	-4.3	X	X	L	60.0	6.8
17.0	-26.5	X	-6.3	X	370.1	L	60.0	9.6
18.0	-34.1	X	-0.3	X	366.1	L	60.0	0.5
20.0	-52.3	X	-39.8	X	298.3	L	90.0	X
21.0	-20.1	X	-3.5	X	328.2	V	60.0	5.6
22.0	-55.0	X	-39.9	X	298.3	L	95.0	X
23.0	-20.6	X	-2.5	X	364.1	L	55.0	4.1
24.0	-21.1	X	-2.3	X	362.2	L	60.0	3.8
25.0	-43.9	X	X	X	338.2	L	90.0	X
26.0	-40.9	-23.5	-14.1	X	324.2	L	90.0	17.9
27.0	-41.9	X	-24.0	X	363.2	L	90.0	X
28.0	-26.5	X	X	X	351.2	L	90.0	X
29.0	-20.6	X	-3.9	X	358.2	L	70.0	6.2
30.0	-27.5	X	-6.9	X	373.1	L	65.0	10.3
31.0	-38.9	X	-24.2	X	325.2	L	90.0	X
32.0	-26.5	X	X	X	361.2	L	90.0	X
33.0	-20.6	X	-3.1	X	X	L	85.0	5.0
34.0	-26.0	X	-7.2	X	324.2	L	85.0	10.7
35.0	-50.8	X	-20.7	X	443.1	L	75.0	22.8
36.0	-45.9	X	-26.0	X	X	L	70.0	X
37.0	X	X	-34.4	X	318.2	L	90.0	X
39.0	-26.5	X	-10.8	X	X	L	50.0	14.8
40.0	-55.8	X	-28.9	X	303.3	L	90.0	X
41.0	-35.9	X	-6.9	X	390.1	L	70.0	10.3
42.0	X	X	-4.8	X	369.1	L		7.5
43.0	-46.8	X	-25.4	X	333.2	L		X
44.0	-45.9	X	-26.9	X	341.2	L		X
45.0	-20.1	X	-6.4	X	403.1	L		9.7
46.0	-34.9	X	-2.0	X	333.2	L		3.3
47.0	-39.9	X	-19.0	X	345.2	L		21.7
48.0	-39.9	X	-23.6	X	X	L		X
49.0	-55.8	X	-31.8	X	310.2	L		X
50.0	-20.6	X	-7.9	X	393.1	L		11.5
A 1	-66.7	X	-29.7	X	X	L	95.0	X
2.0	-51.8	X	-23.4	X	228.5	L	95.0	X
3.0	-29.5	X	X	X	X	L	70.0	X
4.0	-31.0	X	X	X	339.2	L	70.0	X
5.0	X	X	X	X	332.2	L	45.0	X
6.0	-41.9	X	-5.9	X	358.2	L	80.0	9.0
7.0	-58.2	X	-23.9	X	327.7	L	80.0	X
8.0	-48.2	X	-23.4	X	326.2	L	75.0	X
9.0	-29.0	-10.2	-23.0	X	322.2	L	80.0	X
10.0	-30.0	-10.3	-23.5	X	329.2	L	82.5	X
11.0	-41.9	-2.9	-23.5	X	281.3	L	92.5	X
12.0	-27.0	X	-7.6	X	345.7	L	82.5	11.2
13.0	-64.7	X	-32.7	X	282.3	L	92.5	X
15.0	-57.3	X	-30.9	X	298.3	L	87.5	X
16.0	-34.0	-22.5	-3.5	X	339.7	L	75.0	5.6
17.0	-34.8	-16.2	-3.4	X	343.2	L	70.0	5.5
18.0	-27.0	X	-4.4	X	339.7	L	77.5	6.9
19.0	-33.0	X	-4.3	X	336.7	L	70.0	6.8
20.0	-23.0	X	-3.6	X	334.2	L	77.5	5.8
21.0	-30.0	X	-4.5	X	335.7	L	70.0	7.1
22.0	-30.0	X	-3.6	X	338.7	L	75.0	5.8
B 1	-78.6	X	-50.4	406.1	258.4	L	95.0	46.1
2.0	-72.6	X	-42.4	406.1	282.3	L	90.0	46.1
3.0	-76.6	X	-22.0	X	334.2	L	82.5	X

4.0	-29.0	X	-10.9	X	372.1 L	70.0	14.9
5.0	-72.6	X	X	297.3	296.8 L	95.0	36.5
6.0	-74.6	X	-50.8	296.3	283.3 L	92.5	36.4
7.0	-31.0	X	-8.2	X	358.3 L	80.0	11.9
8.0	X	X	-9.4	X	343.7 L	75.0	13.4
9.0	-74.6	X	-49.8	297.3	295.3 L	90.0	36.5
10.0	-72.6	X	-49.5	368.1	271.8 L	95.0	42.3
11.0	-30.0	X	-8.2	X	374.6 L	80.0	11.9
C 1	-54.8	X	X	X	X L	95.0	X
2.0	X	X	-11.3	X	356.2 L	80.0	15.3
3.0	X	X	-2.8	X	333.2 L	80.0	4.5
4.0	X	X	-3.1	X	336.2 L	77.5	5.0
5.0	-26.0	-14.1	-6.7	X	324.2 L	85.0	10.1
6.0	-26.0	X	-2.6	X	345.2 L	75.0	4.2
7.0	-29.0	X	-12.9	X	338.7 L	77.5	16.8
8.0	-29.5	-12.9	-2.6	X	329.2 L	70.0	4.2
9.0	-34.9	X	-19.9	X	349.2 L	87.5	22.3
10.0	-30.2	X	-4.1	X	343.2 L	80.0	6.5
11.0	X	X	-4.4	X	358.2 L	80.0	6.9
12.0	-24.0	X	-1.5	X	333.4 L	60.0	2.5

Sample 151.0 (Type 4)

Correction of values: Correction Factor = 8.593*10e-7te2+0.9924t-0.22

Inclusion	Corrected values Te°C	Tm(h)°C	Tm(i)°C	Tm(d2)°C	Th°C	Homog		Fill	Salinity
1.0	-19.6	X	-1.2	X	366.1	L		50.0	2.0
2.0	X	X		X	376.1	L		80.0	X
3.0	X	X		413.1	268.4	L		92.5	46.9
4.0	X	-22.0	-5.6	X	359.7	L		60.0	8.6
5.0	X	X	-4.8	X	355.2	L		65.0	7.5
6.0	-19.1	X	-2.9	X	345.7	L		60.0	4.7
7.0	X	X	-3.0	X	368.1	L		55.0	4.9
8.0	X	X	-5.8	X	355.2	L		80.0	8.9
9.0	X	X		X	348.2	L		80.0	X
10.0	X	X		X	351.2	L		55.0	X
11.0	X	X	-4.1	X	349.2	L		75.0	6.5
12.0	-20.6	X	-4.8	X	350.2	L		65.0	7.5
13.0	X	X	-2.2	X	359.2	L		60.0	3.6
14.0	-27.5	X	-2.8	X	360.2	L		50.0	4.5
15.0	X	X		X	361.2	L		80.0	X
16.0	-20.1	X	-2.5	X	358.2	L		60.0	4.1
17.0	-19.6	X	-2.6	X	361.2	L		55.0	4.2
18.0	-54.8	X	-42.9	303.3	303.3	L		80.0	36.9
19.0	X	-23.4	-10.1	X	398.1	L		55.0	14.1
20.0	X	X		328.2	237.5	L		90.0	38.8
21.0	-27.0	X	-5.3	X	376.1	L		55.0	8.2
1.0	-44.9	X	-25.8	X	365.1	L		85.0	X
2.0	-45.2	X	-23.8	310.2	381.1	L		80.0	37.4
3.0	-38.9	X	-25.7	X	X		0.0	75.0	X
4.0	-40.9	X	-25.4	X	364.1	L		85.0	X
5.0	-49.8	X		X	335.2	L		85.0	X
6.0	-26.5	X	-5.9	X	478.1	V		50.0	9.0
7.0	X	X		X	315.2	L		90.0	X
8.0	X	X		X	298.3	L		85.0	X
9.0	X	X		X	358.2	L		80.0	X
10.0	-27.0	X	-6.0	X	478.1	V		45.0	9.2
11.0	-38.9	-26.0	-24.1	X	X	V		50.0	X
12.0	-39.9	-24.5	-16.2	423.1	408.1	L		75.0	19.6
13.0	-19.1	X	-4.0	X	403.1	V		50.0	6.4
14.0	-25.0	X		X	470.1	V		50.0	X
15.0	X	X		X	273.3	L		95.0	X
16.0	X	X	-6.2	X	478.1	V		50.0	9.4
17.0	-29.0	X	-8.2	X	398.1	L		60.0	11.9
18.0	X	X	-3.5	X	382.1	L		50.0	5.6
19.0	-29.0	X	-8.3	X	325.2	L		80.0	12.0
20.0	X	X		X	278.3	L		90.0	X
21.0	X	X	-3.6	X	448.1	V		50.0	5.8
1.0	X	X		293.3	334.2	L		90.0	36.2
2.0	-52.8	X	-27.0	X	385.1	L		75.0	X
3.0	X	X		X	258.4	L		90.0	X
4.0	-41.9	X	-19.2	X	478.1	V		50.0	21.8
5.0	-26.1	X	-7.0	X	478.1	V		45.0	10.4
6.0	X	X		X	321.2	L		85.0	X
7.0	X	X		283.3	413.1	L		85.0	35.5
8.0	-46.8	X	-25.0	293.3	382.1	L		80.0	36.2
9.0	-27.5	X	-11.1	X	413.1	V		45.0	15.1
10.0	X	X		313.2	332.2	L		85.0	37.7
11.0	X	X		X	343.2	L		85.0	X
12.0	X	X		324.2	313.2	L		80.0	38.5
13.0	X	X		388.1	363.2	L		85.0	44.3
14.0	X	X		341.2	313.2	L		85.0	39.9
A 1	-30.5	X	-7.1	X	416.1	L		55.0	10.6
2.0	-29.1	X	-7.1	X	435.1	L		60.0	10.6
3.0	-73.6	-11.2	-7.1	X	X	L		40.0	10.6
4.0	-25.4	X	-2.2	X	X	L		45.0	3.6
5.0	-43.0	X	-5.3	X	363.2	L		70.0	8.2
B1	-68.6	X	-24.5	X	361.2	L		70.0	X
2.0	X	X	-24.3	X	354.2	L		80.0	X
4.0	-43.5	X	-4.7	X	443.1	V		45.0	7.4
5.0	-29.3	X	-6.2	X	433.1	V		45.0	9.4
6.0	-67.6	X	-38.6	X	303.3	L		90.0	X
7.0	-29.5	X	-6.4	X	440.1	V		50.0	9.7

8.0	-31.5	X	-6.0	X	440.1 V	45.0	9.2
9.0	-31.5	-8.9	-6.4	X	X L	75.0	9.7
C 1	-31.4	-11.0	-4.7	X	513.1 C	50.0	7.4
2.0	X	X	-6.0	X	X V	45.0	9.2
3.0	X	X		X	336.2 L	87.5	X
4.0	-65.6	X	-34.4	X	349.2 L	82.5	X
5.0	-27.1	X	-8.2	X	508.1 L -D	55.0	12.0
6.0	-27.8	X	-7.4	X	X L	85.0	11.0
7.0	-40.5	-24.4	-17.6	X	392.1 L	82.5	20.7
8.0	-38.5	-20.7	-17.3	X	404.1 L	80.0	20.4
9.0	-41.8	X	-14.7	X	491.1 L	87.5	18.4
10.0	X	X		X	352.2 L	90.0	X
11.0	-50.9	X		X	423.1 V	50.0	X
D 1	X	X		X	X L	45.0	X
2.0	X	X		X	418.1 V	45.0	X
4.0	X	X		X	411.1 L	85.0	X
5.0	X	X		X	326.2 L	82.5	X
6.0	X	X		X	X V	50.0	X
7.0	X	X		X	495.1 L	65.0	X
8.0	X	X		X	X V	45.0	X
9.0	X	X		X	395.1 L	75.0	X
10.0	X	X		X	363.2 L	87.5	X
11.0	-50.9	X		X	319.1 L	90.0	X
12.0	-53.6	X	-28.4	X	346.2 L	90.0	X
14.0	-53.6	X	-23.6	X	346.2 L	90.0	X

Sample 82.0 (Type 4)

Correction of values: Correction Factor = -2.819*10e-6te2+0.9992t-0.53

Corrected values

Inclusion	Te°C	Tm(h)°C	Tm(i)°C	Tm(d2)°C	Th°C	Homog		Fill	Salinity
1.0	-45.8	X	-25.1	X	317.3			65.0	X
2.0	X	X	X	284.9	320.3	L		80.0	35.6
3.0	X	X	X	320.3	318.3	L		80.0	38.2
4.0	X	X	X	318.3	380.0	L		80.0	38.1
5.0	X	X	-4.3	X	380.0	V		45.0	6.9
6.0	X	X	X	X	380.0	V		40.0	X
7.0	X	X	-24.7	X	404.4	V		45.0	X
8.0	X	X	-4.3	X	404.4	V		45.0	6.9
9.0	X	X	-1.6	X	425.9	V		45.0	2.7
10.0	X	X	-24.7	X	425.9	V		70.0	X
11.0	X	X	-24.5	316.3	296.7	H		70.0	37.9
12.0	X	X	X	X	388.8	L		85.0	X
13.0	-43.5	X	-23.5	X	388.8	L		70.0	X
14.0	X	X	-2.9	X	399.5	V		45.0	4.7
15.0	X	X	-5.8	X	456.1	C		45.0	9.0
16.0	X	-23.6	X	X	429.8	L		60.0	X
17.0	-44.5	-24.3	X	X	X		0.0	90.0	X
18.0	X	X	X	X	347.7	L		90.0	X
19.0	X	X	X	X	484.3	V		50.0	X
20.0	X	X	-5.0	X	464.8	V		50.0	7.9
21.0	X	X	X	X	376.1	L		50.0	X
22.0	X	X	-3.3	X	395.6	V		50.0	5.4
23.0	X	X	-24.5	X	X		0.0	80.0	X
24.0	X	X	-2.0	X	384.9	V		45.0	3.3
25.0	X	X	-17.0	X	384.9	V		45.0	20.2
26.0	X	X	-17.0	X	409.3	L		70.0	20.2
27.0	X	X	-24.5	X	X		0.0	70.0	X
28.0	X	X	-22.1	X	X		0.0	70.0	X
29.0	X	X	-3.0	X	X		0.0	70.0	4.9
30.0	X	X	-25.9	X	362.4	L		70.0	X
31.0	X	X	-2.0	X	389.8	V		55.0	3.3

Sample 153.0

Correction of values: Correction Factor = 1.169 x 10e-5te2 + 1.0042t - 0.33

Corrected values

Inclusion	Te°C	Tm(h)°C	Tm(i)°C	Tm(d1)°C	Th°C	Homog	Fill	Salinity
ChipC A1	-24.6	X	-0.5		332.6	L	50.0	0.8
2.0	-22.4	X	X		312.2	L	55.0	

Sample 92.0 (Type 5a)
Correction of values: Correction Factor = 8.593*10e-7te2+0.9924t-0.22
Corrected values

Inclusion	Te°C	Tm(h)°C	Tm(i)°C	Tm(d2)°C	Th°C Homog	Fill	Salinity
1.1	-64.7	X	-52.3	323.2	323.2 L	90.0	38.4
1.2	-28.5	-21.1	-1.0		395.1 V	45.0	1.7
1.3	-28.4	X	X		399.1 V	50.0	26.2
1.4	-52.3	-33.5	-25.5		337.2 L	80.0	26.2
1.5	-21.1	X	-2.2		408.1 V	50.0	3.6
1.7	-29.0	X	-1.1		408.1 V	45.0	1.8
1.8	-44.4	X	-24.2			90.0	26.2
1.9	-45.4	-39.4	X	352.2	360.2 L	90.0	40.9
1.1	-28.5	X	-0.8	X	399.1 V	40.0	1.3
1.1	-28.4	-23.4	-8.2	X	X	55.0	11.9
1.1	-54.8	X	-41.9	X	X	92.5	X
2.1	-27.5	-23.4	-10.9	X	X		14.9
2.2	-62.2	X	-34.4	X	333.2 L		X
2.3	-30.3	X	X	X	304.3 V		X
2.4	-30.0	-23.7	-11.4	X	X		15.4
2.6	-28.5	-24.2	X	X	X		X
2.8	-34.4	-25.0	X	X	396.1 L		X
3.1	-28.0	-24.0	X	X	403.1 V	50.0	X
3.2	X	X	-2.0	X	382.1 V	45.0	3.3
3.3	X	X	-2.7	X	378.1 V	50.0	4.4
3.4	-27.5	X	X	X	389.1 V	40.0	X
3.5	-31.5	X	-9.1	X	X	50.0	12.9
3.6	-34.4	-24.0	-14.0	X	515.1 L	70.0	17.8
3.7	-43.4	-29.0	-24.3	X	423.1 L	70.0	X
3.8	-44.9	-29.0	-29.0	X	368.1 L	92.5	X
3.1	-34.9	X	-2.2	X	398.1 V	45.0	3.6
4.1	-38.9	-24.5	-13.0	X	X	60.0	16.9
4.2	-42.4	X	X	X	313.2 L	92.5	X
4.3	-42.4	X	-27.8	X	351.2 L	95.0	X
4.4	-33.5	X	-19.8	X	456.1 L	80.0	22.2
4.5	-30.5	X	-0.7	X	399.1 V	50.0	1.2
4.6	-30.5	-23.1	-5.4	X	448.1 V	50.0	8.4
4.7	-46.3	X	-23.9	X	X	60.0	X
4.9	-22.5	X	-1.8	X	398.1 V	60.0	3.0
4.1	-26.5	-23.6	-5.6	X	448.1 C	60.0	8.6
4.1	-28.0	-22.6	-5.3	X	448.1 V	50.0	8.2
4.1	-30.5	X	-2.9	X	X	45.0	4.7
4.1	-27.5	-23.6	-8.2	X	X	60.0	11.9
Zone 1 1	X	X	X	248.4	301.2 L	80.0	33.4
3.0	-55.6	X	-1.8	248.4	324.9 L	80.0	2.9
4.0	-58.6	X	-28.1	X	X L	92.5	X
5.0	-27.2	X	-2.8	X	405.1 V	20.0	4.6
6.0	-56.6	X	-38.5	X	X L	95.0	X
7.0	-26.9	X	-2.5	X	405.1 V	45.0	4.0
8.0	-27.5	X	X	X	405.1 V	40.0	X
9.0	-48.5	X	-24.8	X	X L	70.0	X
10.0	-46.8	X	-39.2	X	317.2 L	85.0	X
11.0	-28.1	X	-6.2	X	405.1 V	35.0	9.4
12.0	-22.3	X	-0.9	X	405.1 V	40.0	1.5
13.0	-29.3	X	-3.0	X	405.1 V	55.0	4.8
14.0	-21.4	X	-2.7	X	405.1 V	40.0	4.4
15.0	-27.7	X	-6.5	X	405.1 V	50.0	9.8
16.0	-25.1	X	-6.0	X	405.1 V	50.0	9.2
17.0	-55.6	X	-27.7	248.4	322.9 L	90.0	33.4
Zone 2 1	-61.6	X	-37.4	X	351.0 L	90.0	X
2.0	-26.4	X	-2.3	X	396.6 V C	60.0	3.8

3.0	-37.5	X	-8.8	X	439.1 V	70.0	12.7
4.0	-26.9	X	-2.1	X	376.1 C	60.0	3.4
5.0	-41.5	X	-24.2	X	431.1 L	80.0	X
6.0	-42.7	X	-24.4	X	453.4 L	90.0	X
7.0	-43.5	X	-24.4	X	422.6 L	80.0	X
8.0	-41.0	X	X	X	358.7 L	85.0	X
9.0	-58.1	X	-36.5	X	X L	95.0	X
10.0	-44.5	X	-28.2	X	353.5 L	85.0	X
11.0	-58.1	X	-31.5	X	354.8 L	90.0	X
12.0	-48.5	X	-25.8	X	388.1 L	77.5	X
13.0	-28.8	X	-2.1	X	388.1 V	50.0	3.4
14.0	-62.6	X	-43.2	438.1	329.6 L	90.0	49.7
15.0	-26.4	X	-1.2	X	382.6 C	55.0	2.0
16.0	-26.9	X	-1.2	X	385.5 C	55.0	2.0
Zone 3 1	-68.6	X	-40.0	240.9	349.7 L	90.0	32.9
2.0	-67.6	X	-40.5	X	343.8 L	90.0	X
3.0	-66.6	X	-39.5	X	343.9 L	90.0	X
4.0	-70.6	X	-38.2	238.7	364.6 L	80.0	32.8
5.0	-70.6	X	-40.5	X	336.5 L	87.5	X
6.0	-27.9	X	-1.1	X	X L	40.0	1.8
7.0	-32.0	X	-0.3	X	X L	40.0	0.4
Chip B 1	-45.5	X	-24.3	X	376.3 L	80.0	X
2.0	-46.0	X	-24.4	X	377.4 L	85.0	X
3.0	-22.4	X	-0.9	X	390.5 C	50.0	1.5
4.0	-28.0	X	-1.2	X	385.1 C	50.0	2.0
5.0	-28.6	X	-3.2	X	396.1 L	65.0	5.2
6.0	-20.7	X	-1.2	X	391.6 L	50.0	2.0
7.0	-26.6	X	-3.2	X	399.7 L	55.0	5.2
8.0	X	X	-2.8	X	398.7 L	55.0	4.6
9.0	-28.9	X	-4.7	X	401.8 L	60.0	7.4
10.0	-24.2	-10.9	-5.7	X	401.6 L	50.0	8.7
11.0	-26.4	X	-5.3	X	405.0 L	50.0	8.2
12.0	-27.1	-9.3	-5.2	X	405.0 L	50.0	8.0
13.0	-34.5	X	-12.9	316.0	315.0 L	80.0	16.8
16.0	-29.3	X	X	X	399.7 L	55.0	X
17.0	-30.1	X	-4.6	X	408.3 L	60.0	7.3
18.0	-29.8	X	-0.7	X	374.5 L	50.0	1.2
19.0	X	X	X	X	375.9 L	45.0	X
20.0	-34.5	-21.2	-6.5	X	415.8 L	60.0	9.8
21.0	-54.6	X	X	X	376.4 L	75.0	X
22.0	-34.5	-22.9	-17.6	X	412.9 L	55.0	20.7
23.0	-31.1	X	-8.3	X	424.6 L	55.0	12.1
24.0	-51.5	X	X	274.2	326.6 L	85.0	34.9
25.0	-30.5	X	-4.9	X	413.9 L	60.0	7.7
26.0	-52.6	X	-27.7	X	327.2 L	85.0	X
27.0	-28.4	X	-3.2	X	399.6 L	65.0	5.2
28.0	-54.1	-22.1	-12.9	X	413.9 L	55.0	16.8
29.0	X	X	X	X	320.0 L	75.0	X
30.0	X	X	X	X	326.2 L	75.0	X

Sample 24.0 (Type 5a)
Correction of values: Correction Factor = -2.819*10e-6te2+0.9992t-0.53
Corrected values

Inclusion	Te°C	Tm(h)°C	Tm(i)°C	Tm(d2)°C	Th°C	Homog	Fill	Salinity
A1	-49.6	X	-40.5	280.0	230.8	L	90.0	35.3
2.0	-48.1	X	X	222.9	228.8	L	85.0	32.0
3.0	-48.1	X	X	252.4	233.7	L	90.0	33.6
4.0	-48.1	X	X	275.1	223.8	L	80.0	35.0
5.0	X	X	X		214.0	L	80.0	26.2
6.0	-48.1	X	X	252.4	233.7	L	85.0	33.6
7.0	X	X	X				80.0	
8.0	-49.6	X	-33.9	232.7	255.4	L	70.0	32.5
9.0	X	X	X	252.4	238.6	L	80.0	33.6
10.0	X	X	X				40.0	
11.0	X	X	X	227.8	267.2	L	80.0	32.2
12.0	X	X	X				40.0	
13.0	X	X	X	257.4	239.6	L	90.0	33.9
14.0	X	X	X		199.2	L	90.0	26.2
15.0	X	X	X	247.5	188.3	L	80.0	33.3
16.0	X	X	X	247.5	258.3	L	80.0	33.3
17.0	X	X	X	247.5	229.8	L	80.0	33.3
18.0	X	X	X				50.0	
B1	X	X	-2.0	X	399.5	V	45.0	3.3
2.0	X	X	-16.0	X	X		80.0	19.5
3.0	X	X	X	X	399.5	V	45.0	
4.0	-49.6	X	-36.5	X	230.8	L	90.0	
5.0	X	X	X	X	399.5	V	45.0	
6.0	X	X	X	X	399.5	V	45.0	
7.0	X	X	X	X	399.5	V	45.0	
8.0	X	X	X	X	399.5	V	45.0	
9.0	X	X	X	X	399.5	V	45.0	
10.0	-49.6	X	-36.5	X	236.7	L	85.0	
C1	X	X	-1.9	X	398.5	V	50.0	3.2
2.0	X	X	-2.0	X	388.8	V	50.0	3.3
3.0	X	X	X	X	390.7	V	50.0	
4.0	-48.1	X	X	X	233.7	L	90.0	
5.0	-48.1	X	X	X	237.7	V	90.0	
6.0	X	X	-2.4	X	388.8	V	50.0	4.0
7.0	X	X	X	X	X			
8.0	X	X	X	X	393.7	V	50.0	
9.0	-27.5	X	-5.5	X	421.0	C	60.0	8.6

Sample 61.0 (Type 5a)

Correction of values: Correction Factor = -2.819*10e-6te2+0.9992t-0.53

Corrected values

Inclusion	Te°C	Tm(h)°C	Tm(i)°C	Tm(d2)°C	Th°C	Homog	Fill	Salinity
A1	X	X	-4.3	X	414.2	V	55.0	6.9
2.0	X	X	-1.9	X	380.0	V	50.0	3.2
3.0	X	X	-1.8	X	394.6	V	50.0	3.0
4.0	X	X	-1.7	X	380.0	V	50.0	2.8
5.0	X	X	-2.3	X	380.0	V	50.0	3.8
6.0	X	X	-2.3	X	380.0	V	50.0	3.8
7.0	X	X	-3.8	X	380.0	V	50.0	6.1
8.0	X	X	-29.5	X	X		55.0	
9.0	X	X	-2.0	X	X		55.0	3.3
10.0	X	X	X	198.2	347.7	L	80.0	30.8
11.0	X	X	X	X	409.3	V	50.0	X

12.0	X	X	X	321.2	290.8 L	80.0	38.3
13.0	X	X	X	321.2	293.7 L	90.0	38.3
14.0	X	X	X	X	409.3 V	60.0	X
15.0	X	X	X	X	380.0 L	80.0	X
16.0	X	X	-1.9	X	409.3 V	50.0	3.2
17.0	X	X	-1.3	X	380.0 C	50.0	2.2
18.0	X	X	-0.8	X	381.9 V	50.0	1.4
19.0	X	X	-3.5	X	406.4 V	55.0	5.7
20.0	X	X	-2.3	X	407.3 C	55.0	3.8
21.0	X	X	X	X	390.2 L	65.0	
22.0	X	X	-0.6	X	380.0 C	50.0	1.0
23.0	X	X	X	X	349.7 L	70.0	
24.0	X	X	X	X	X	70.0	
25.0	X	X	X	X	366.3 L	80.0	
26.0	X	X	X	X	404.4 L	80.0	
27.0	X	X	X	X	399.5 L	80.0	
b1	X	X	-8.7	X	X	60.0	12.6
2.0	X	X	-5.1	X	X	50.0	8.0
3.0	X	X	-7.7	X	422.0 L	60.0	11.4
4.0	X	X	-8.7	X	419.0 L	50.0	12.6
5.0	X	X	-0.7	X	380.0 V	50.0	1.2
6.0	X	X	-4.7	X	420.0 V	50.0	7.4
7.0	X	X	-8.5	X	433.7 V	50.0	12.3
8.0	X	X	-2.9	X	412.2 V	45.0	4.7
9.0	X	X	-2.8	X	408.3 V	55.0	4.6
10.0	X	X	-1.3	X	375.1 V	50.0	2.2
11.0	X	X	X	167.5	360.4 L	80.0	
12.0	X	X	X	223.8	360.4 L	80.0	
13.0	X	X	-5.1	X	420.0 C	55.0	8.0
14.0	X	X	X	174.5	356.5 L	90.0	

Sample 61.0 (cont'd)

Correction of values: Correction Factor = 1.169 x 10e-5te2 + 1.0042t - 0.33

	Corrected values						
Inclusion	Te°C	Tm(h)°C	Tm(i)°C	Tm(d1)°C	Th°C Homog	Fill	Salinity
A 1	-27.4	X	-3.4		V	55.0	5.5
2.0	-28.2	X	-3.8		422.0 L	52.5	6.0
3.0	-28.4	X	-18.4		422.0 L	67.5	21.2
5.0	-48.0	X	X			85.0	
6.0	-57.6	X	-18.9	200.0	318.0 L	80.0	21.6
7.0	-60.6	-26.1	-3.4		352.7 L	85.0	5.5
8.0	-63.6	X	-47.5	280.0	318.7 L	82.5	35.3
B 1	-29.1	X	-4.9		441.0 V	60.0	7.7
2.0	-28.3	X	-4.6		438.0 V	45.0	7.3
8.0	-28.9	X	-5.9		400.0 V	55.0	9.0
9.0	-23.4	X	-5.6		400.0 V	65.0	8.6
10.0	X	X	-1.8		400.0 V	55.0	2.9
Z2 1	-41.5	X	-11.3			55.0	15.2
2.0	-42.0	X	-24.6		383.0 L	72.5	
3.0	X	X	-9.4			55.0	13.3
4.0	-26.4	X	-23.7		V	55.0	
5.0	-60.6	X	X	242.0	376.0 L	85.0	33.0
Z4 1	X	X	-15.0			50.0	18.6
2.0	-30.5	X	-24.4		433.0 L	67.5	
3.0	X	X	X		329.0 L	90.0	
Z7 1	X	X	X		375.0 V	55.0	
4.0	28.3	X	X		399.0 L	60.0	
5.0	-28.8	X	-9.9		V	65.0	13.9
6.0	-29.1	X	X		L	45.0	
7.0	-29.5	X	-2.8		V	65.0	4.6
Z8 1	-55.1	X	-3.2		451.0 CV	75.0	5.2
2.0	-55.1	X	23.5			75.0	
3.0	-42.1	X	-15.8		473.0 CV	50.0	19.3
4.0	-29.4	X	-5.3		L	50.0	8.2
5.0	-41.8	X	-26.4		L	60.0	
6.0	-42.5	X	-19.2			75.0	21.8

Sample 100.0 (Type 5b)
Correction of values: Correction Factor = 8.593*10e-7te2+0.9924t-0.22

	Corrected values							
Inclusion	Te°C	Tm(h)°C	Tm(i)°C	Tm(d2)°C	Th°C	Homog	Fill	Salinity
A1	-27.5	X	-2.5	X	396.1	C	50.0	4.1
2.0	X	X	-2.7	X	397.1	C	50.0	4.4
3.0	-26.5	X	-2.9	X	399.1	C	60.0	4.7
4.0	X	X	-2.6	X	396.1	C	50.0	4.2
5.0	-27.0	X	-2.6	X	401.1	C	50.0	4.2
6.0	X	X	-2.9	X	403.1	C	50.0	4.7
7.0	X	X	-2.8	X	403.1	C	55.0	4.5
9.0	X	X	-3.2	X	403.1	C	50.0	5.2
10.0	X	X	-2.8	X	392.1	L	55.0	4.5
11.0	X	X	-2.8	X	395.1	C	50.0	4.5
13.0	X	X	-2.6	X	395.6	L	50.0	4.2
C1	X	X	X	383.1	347.2	H	90.0	43.8
2.0	X	X	X	308.2	325.2	L	90.0	37.3
3.0	-54.8	X	X	263.4	345.2	L	90.0	34.2
4.0	X	X	X	323.2	323.2	L	90.0	38.4
5.0	-53.8	X	X	321.2	372.1	L	85.0	38.3
6.0	-52.8	X	X	223.5	346.2	L	85.0	32.0
7.0	X	X	-0.9	X	388.1	V	50.0	1.5
8.0	-52.8	X	X	X	342.2	L	80.0	X
9.0	X	X	X	X	303.3	L	90.0	X
10.0	X	X	X	363.2	340.2	H	80.0	41.9
11.0	X	X	X	X	408.1	V	50.0	X
13.0	-46.8	X	-23.0	X	403.1	L	80.0	X
14.0	X	X	X	263.4	303.3	L	80.0	34.2
15.0	X	X	X	263.4	336.2	L	90.0	34.2
16.0	X	X	-1.8	X	407.1	V	50.0	3.0
17.0	X	X	-25.6	218.5	349.2	L	90.0	31.8
18.0	X	X	-2.6	X	408.1	V	50.0	4.2
19.0	X	X	X	243.4	373.1	L	80.0	33.1
20.0	X	X	-20.7	X	X	0.0	60.0	22.8
21.0	-54.3	X	-25.7	X	356.2	L	80.0	X
22.0	X	X	X	X	X	0.0	80.0	X
23.0	X	X	X	333.2	291.3	H	90.0	39.2
24.0	X	X	X	X	295.3	L	85.0	X
25.0	X	X	X	X	413.1	L	55.0	X
1 1	X	X	X	X	433.1	V	35.0	X
3.0	-35.5	X	-12.9	X	X	0.0	50.0	16.8
5.0	X	X	X	X	421.1	L	55.0	X
8.0	X	X	X	X	363.2	V	35.0	X
9.0	-27.6	X	-1.3	X	406.6	C	55.0	2.2
10.0	X	X	X	X	363.2	V	35.0	X
14.0	-29.4	X	-1.2	X	X	0.0	45.0	2.0
15.0	-69.6	X	-1.0	X	360.2	L	85.0	1.7
16.0	-47.0	X	-28.4	X	X	0.0	80.0	X
17.0	-28.4	X	X	X	398.1	C	50.0	X
18.0	-21.9	X	-1.8	X	393.2	C	45.0	2.9
19.0	X	X	-1.6	X	394.6	C	35.0	2.6
20.0	-28.4	X	-3.4	X	X	0.0	50.0	5.5
2 1	X	X	-37.5	X	324.7	L	80.0	X
2.0	-60.6	X	-35.5	X	312.7	L	82.5	X
3.0	X	X	X	X	323.2	L	87.5	X
4.0	-48.5	X	-33.2	X	X	0.0	80.0	X
5.0	X	X	-1.8	X	X	0.0	45.0	2.9
6.0	-37.5	X	-1.0	X	X	0.0	45.0	1.7
8.0	-40.5	X	X	X	X	0.0	55.0	X
9.0	-42.5	X	-24.3	X	X	0.0	80.0	X
11.0	-28.8	X	-0.8	X	X	0.0	40.0	1.3
12.0	-47.5	X	-29.4	X	X	0.0	80.0	X
13.0	-31.4	X	-8.4	X	X	0.0	60.0	12.2
14.0	X	X	-13.6	X	X	0.0	80.0	17.4
15.0	-45.5	X	X	X	X	0.0	90.0	X
16.0	-44.3	X	X	X	326.7	L	X	X
17.0	-43.2	X	-30.7	X	X	0.0	80.0	X
3.2	X	X	X	X	326.1	L	80.0	X

3.0	-48.0	X	X	X	339.7 L		90.0	X
4.0	-31.5	X	-7.3	X	X	0.0	55.0	10.9
5.0	-45.5	X	-27.4	X	X	0.0	70.0	X
6.0	-52.5	X	-35.5	X	X	0.0	75.0	X
7.0	-58.1	X	-29.4	X	326.7 L		90.0	X
8.0	-58.1	X	-29.4	X	339.2 L		90.0	X
10.0	-28.3	X	-1.2	X	X	0.0	60.0	2.0
11.0	X	X	-29.8	X	X	0.0	90.0	X
12.0	-28.9	X	X	X	X	0.0	65.0	X

Sample 91.0 (Type 5b)

Correction of values: Correction Factor = -2.819*10e-6te2+0.9992t-0.53

Corrected values

Inclusion	Te°C	Tm(h)°C	Tm(i)°C	Tm(d2)°C	Th°C Homog	Fill	Salinity
A1	X	X	-2.1	X	381.9 C	50.0	3.5
2.0	X	X	-3.3	X	394.6 L	55.0	5.4
3.0	X	X	-2.5	X	382.9 C	50.0	4.1
4.0	X	X	-1.3	X	381.9 L	55.0	2.2
5.0	X	X	-1.3	X	373.1 L	50.0	2.2
6.0	X	X	-2.3	X	381.0 L	50.0	3.8
7.0	X	X	-1.7	X	374.1 C	50.0	2.8
8.0	X	X	-2.8	X	382.9 C	55.0	4.6
9.0	X	X	-2.3	X	403.4 C	50.0	3.8
10.0	X	X	-2.2	X	381.0 L	50.0	3.6
11.0	X	X	-1.4	X	381.4 L	50.0	2.4
12.0	X	X	-1.9	X	379.0 L	50.0	3.2
15.0	X	X	-1.3	X	380.0 L	50.0	2.2
16.0	X	X	-1.6	X	384.9 L	55.0	2.7
17.0	X	X	-1.7	X	380.0 L	55.0	2.8
18.0	X	X	-1.0	X	381.0 L	50.0	1.7
19.0	X	X	-10.6	X	402.5 L	70.0	14.6
20.0	X	X	-8.5	X	389.8 L	70.0	12.3
21.0	X	X	-6.7	X	391.7 L	60.0	10.1
22.0	X	X	-6.7	X	389.8 L	70.0	10.1
23.0	X	X	-5.3	X	402.5 L	55.0	8.3
24.0	X	X	-6.4	X	381.4 L	70.0	9.8
B1	X	X	-4.6	X	399.5 C	60.0	7.3
2.0	X	X	-4.4	X	397.6 C	60.0	7.0
3.0	X	X	-4.7	X	404.4 L	50.0	7.4
4.0	X	X	-4.5	X	400.5 V	50.0	7.1
5.0	X	X	-5.1	X	393.7 L	50.0	8.0
6.0	X	X	X	X	368.2 C	50.0	#VALUE!
7.0	X	X	X	X	368.2 C	50.0	#VALUE!
8.0	X	X	-5.9	X	404.4 L	55.0	9.1
9.0	X	X	X	X	397.6 L	60.0	#VALUE!
10.0	X	X	-3.8	X	396.6 L	50.0	6.1
11.0	X	X	X	X	399.5 V	50.0	#VALUE!
12.0	X	X	-2.6	X	393.7 L	55.0	4.3
13.0	X	X	-2.3	X	375.1 V	50.0	3.8
14.0	X	X	-3.8	X	400.5 L	60.0	6.1
15.0	X	X	-3.7	X	401.5 L	50.0	6.0
16.0	X	X	-2.4	X	374.1 C	50.0	4.0
17.0	X	X	X	X	401.5 L	50.0	#VALUE!
18.0	X	X	-2.4	X	393.7 L	50.0	4.0
19.0	X	X	-2.3	X	385.8 V	50.0	3.8
20.0	X	X	-2.5	X	398.5 C	50.0	4.1
21.0	-45.6	X	X	X	386.8 L	95.0	X
22.0	X	X	X	282.0	292.8 L	95.0	35.4
23.0	X	X	-34.5	305.5	321.2 L	90.0	37.1

Sample 97.0 (Type 6)
Correction of values: Correction Factor = -2.819*10e-6te2+0.9992t-0.53
Corrected values

Inclusion	Te°C	Tm(h)°C	Tm(i)°C	Tm(d2)°C	Th°C	Homog	Fill	Salinity
B1	X	X	-2.5	X		360.4 L	50.0	4.1
2.0	X	X	-2.4	X		356.5 L	50.0	4.0
3.0	X	X	-2.5	X		363.4 L	60.0	4.1
4.0	X	X	-2.6	X		360.4 L	50.0	4.3
5.0	X	X	X	X		360.4 L	70.0	#VALUE!
6.0	X	X	-2.4	X		357.5 L	50.0	4.0
7.0	X	X	-2.7	X		340.8 L	65.0	4.4
8.0	X	X	-2.4	X		347.7 L	60.0	4.0
9.0	X	X	-2.2	X		365.3 L	50.0	3.6
10.0	X	X	-2.2	X		345.7 L	60.0	3.6
11.0	X	X	-2.7	X		355.5 L	50.0	4.4
12.0	X	X	-2.5	X		363.4 L	55.0	4.1
13.0	X	X	-2.2	X		351.6 L	50.0	3.6
14.0	X	X	X	X		347.7 L	50.0	#VALUE!
A1	X	X	-2.4	X		327.1 L	55.0	4.0
2.0	X	X	-2.1	X		329.1 L	65.0	3.5
3.0	X	X	-2.1	X		353.6 L	60.0	3.5
4.0	X	X	-2.4	X		352.6 L	65.0	4.0
5.0	X	X	-2.1	X		352.6 L	70.0	3.5
6.0	X	X	-2.5	X		353.1 L	60.0	4.1
7.0	X	X	-2.2	X		328.6 L	70.0	3.6
8.0	X	X	-2.1	X		346.7 L	60.0	3.5
9.0	X	X	-2.1	X		331.0 L	80.0	3.5
10.0	X	X	-2.1	X		360.4 L	50.0	3.5
11.0	X	X	-1.9	X		357.5 L	55.0	3.2
12.0	X	X	-2.0	X		327.1 L	65.0	3.3
13.0	X	X	-2.1	X		345.2 L	60.0	3.5
14.0	X	X	-2.2	X		323.2 L	60.0	3.6
15.0	X	X	-1.8	X		346.7 L	50.0	3.0
16.0	X	X	-1.8	X		349.7 L	60.0	3.0
17.0	X	X	-1.8	X		345.7 L	60.0	3.0
18.0	X	X	-1.8	X		358.5 L	50.0	3.0
19.0	X	X	-2.4	X		362.4 L	50.0	4.0
20.0	X	X	-1.9	X		356.5 L	50.0	3.2
21.0	X	X	-2.1	X		343.8 L	50.0	3.5
22.0	X	X	-1.9	X		331.0 L	65.0	3.2
23.0	X	X	-2.1	X		359.4 L	50.0	3.5
24.0	X	X	-2.2	X		355.5 L	50.0	3.6
25.0	X	X	X	X		360.4 L	50.0	#VALUE!
26.0	X	X	-1.8	X		347.7 L	50.0	3.0
27.0	X	X	-1.8	X		358.0 L	50.0	3.0
28.0	X	X	-1.8	X		353.6 L	55.0	3.0
29.0	X	X	-1.8	X		356.5 L	50.0	3.0
30.0	X	X	-1.9	X		357.0 L	60.0	3.2
31.0	X	X	-1.9	X		356.5 L	50.0	3.2
32.0	X	X	X	X		366.8 L	60.0	#VALUE!
33.0	X	X	-1.9	X		353.6 L	50.0	3.2
34.0	X	X	-1.9	X		348.7 L	50.0	3.2
35.0	X	X	-2.0	X		343.8 L	65.0	3.3
36.0	X	X	-1.8	X		355.5 L	55.0	3.0
37.0	X	X	-1.8	X		345.7 L	60.0	3.0
38.0	X	X	X	X		365.3 L	50.0	#VALUE!
39.0	X	X	-1.9	X		348.7 L	50.0	3.2
40.0	X	X	X	X		351.6 L	60.0	#VALUE!
41.0	X	X	-1.8	X		313.4 L	55.0	3.0
42.0	X	X	-1.7	X		341.8 L	60.0	2.8
43.0	X	X	-1.8	X		348.7 L	55.0	3.0
44.0	X	X	-1.8	X		346.7 L	60.0	3.0

Sample 74.0 (Type 6)
Correction of values: Correction Factor = -2.819*10e-6te2+0.9992t-0.53

Inclusion	Corrected values Te°C	Tm(h)°C	Tm(i)°C	Tm(d2)°C	Th°C	Homog	Fill	Salinity
1.0	-45.6	X	-27.3	X		334.5 L	65.0	#VALUE!
2.0	X	X	-2.2	X		373.1 L	60.0	3.6
3.0	X	X	-2.2	X		372.2 L	55.0	3.6
4.0	X	X	-2.3	X		374.1 L	50.0	3.8
5.0	-44.5	X	-26.7	X		374.1 L	50.0	#VALUE!
6.0	X	-25.5	-12.5	X		376.6 L	60.0	16.5
7.0	-38.5	X	-6.7	X		385.8 L	55.0	10.1
8.0	X	X	-10.3	X		379.5 L	50.0	14.3
9.0	X	X	-6.7	X		382.7 L	65.0	10.1
10.0	X	X	-2.7	X		380.0 L	50.0	4.4
11.0	X	X	-5.7	X		386.8 L	50.0	8.8
12.0	X	X	-2.6	X		379.0 L	50.0	4.3
13.0	X	X	-2.2	X		370.2 L	60.0	3.6
14.0	X	X	-2.2	X		371.2 L	55.0	3.6
15.0	X	X	X	X		371.2 L	50.0	#VALUE!
16.0	X	X	-1.9	X		366.3 L	50.0	3.2
17.0	-40.5	X	-11.8	X		375.1 L	65.0	15.8
18.0	X	X	-2.9	X		373.1 L	60.0	4.7
19.0	X	X	-2.9	X		376.1 L	55.0	4.7
20.0	X	X	-2.7	X		372.2 L	55.0	4.4
21.0	X	X	-2.1	X		374.1 L	50.0	3.5
22.0	X	X	-1.6	X		369.2 L	60.0	2.7
23.0	X	X	-2.0	X		370.2 L	50.0	3.3
24.0	X	X	-1.6	X		370.2 L	50.0	2.7
25.0	X	X	-2.0	X		371.2 L	55.0	3.3
26.0	X	X	-8.9	X		377.1 L	65.0	12.8
27.0	X	X	-8.8	X		375.1 L	65.0	12.7
28.0	X	X	-8.8	X		377.1 L	70.0	12.7
29.0	X	X	-8.7	X		374.1 L	70.0	12.6
30.0	X	X	-8.7	X		376.1 L	65.0	12.6
31.0	X	X	-2.2	X		372.2 L	65.0	3.6
32.0	X	X	-2.1	X		373.1 L	55.0	3.5
33.0	X	X	-2.0	X		377.1 L	50.0	3.3
34.0	X	X	-2.5	X		376.1 L	65.0	4.1
35.0	X	X	X	X		360.4 L	60.0	#VALUE!
36.0	X	X	-8.7	X		375.1 L	60.0	12.6
37.0	X	X	-8.6	X	X	L	50.0	12.4
38.0	X	X	-8.5	X	X	L	65.0	12.3
39.0	X	X	-8.8	X		376.1 L	50.0	12.7
40.0	X	X	-8.7	X		384.9 L	55.0	12.6
41.0	X	X	X	X		382.9 L	65.0	#VALUE!
42.0	X	X	-2.3	X	X	L	50.0	3.8

Sample 103.0 (Type 6)

Correction of values: Correction Factor = -2.819*10e-6te2+0.9992t-0.53

Corrected values

Inclusion	Te°C	Tm(h)°C	Tm(i)°C	Tm(d2)°C	Th°C	Homog		Fill	Salinity
1.0	X	X	-3.8	X		390.2	0.0	60.0	6.1
2.0	X	X	-2.7	X		390.2 L		60.0	4.4
3.0	X	X	-2.4	X		390.7 L		50.0	4.0
4.0	X	X	-2.8	X		389.3 L		55.0	4.6
5.0	X	X	-2.3	X		388.3 L		60.0	3.8
6.0	X	X	-2.5	X		388.8 L		50.0	4.1
7.0	X	X	-2.5	X		389.3 L		60.0	4.1
8.0	X	X	-2.9	X		389.3 L		50.0	4.7
9.0	X	X	-2.9	X		388.3 L		50.0	4.7
10.0	X	X	-2.7	X		388.3 L		55.0	4.4
11.0	X	X	-3.5	X		389.8 L		55.0	5.7
12.0	X	X	-2.4	X		388.8 L		50.0	4.0
13.0	X	X	-2.4	X		386.8 L		55.0	4.0
14.0	X	X	-2.6	X		385.8 L		55.0	4.3
15.0	X	X	-2.4	X	X		0.0	50.0	4.0
16.0	X	X	-2.7	X		393.7 C		50.0	4.4
17.0	X	X	-2.3	X		389.8 L		50.0	3.8
18.0	X	X	-2.4	X		390.2 L		55.0	4.0
19.0	X	X	-2.5	X		389.8 L		60.0	4.1
20.0	X	X	-2.6	X		396.1 C		50.0	4.3
21.0	X	X	-2.7	X		391.7 L		55.0	4.4
22.0	X	X	-2.6	X		399.5 V		50.0	4.3
23.0	X	X	X	X		392.7 C		60.0	#VALUE!
24.0	X	X	-2.4	X		392.7 C		55.0	4.0
25.0	X	X	-2.5	X		396.6 C		50.0	4.1
26.0	X	X	-2.5	X		387.8 L		50.0	4.1
27.0	X	X	-2.5	X		388.8 L		55.0	4.1
28.0	X	X	-2.6	X		388.8 L		55.0	4.3
29.0	X	X	-2.5	X		388.8 L		50.0	4.1
30.0	X	X	-2.7	X		394.6 C		60.0	4.4
31.0	X	X	-2.8	X		391.7 L		60.0	4.6
32.0	X	X	-2.5	X		391.7 L		55.0	4.1
33.0	X	X	-2.7	X		387.8 L		50.0	4.4
34.0	X	X	-2.7	X		392.2 C		50.0	4.4
35.0	X	X	-2.5	X		389.8 C		55.0	4.1
36.0	X	X	-2.5	X		389.8 L		50.0	4.1
37.0	X	X	-2.5	X		390.7 L		50.0	4.1
38.0	X	X	-2.4	X		387.8 L		55.0	4.0
39.0	X	X	-2.5	X		388.8 L		55.0	4.1
40.0	X	X	-2.5	X		388.8 L		50.0	4.1

Oxygen isotope results

Type	Sample number	Lab number	Phase analysed	Delta 1	Delta 2	d18O SMOW	Calculated d18O (Min	Max	Temp (C) Min	Max
1	155A	2545	Quartz	-5.16	-22.55	9.3				
	156A	2554	Quartz	-5.22	-22.13	9.7				
2	93A		Quartz			8.9	-2.1	1.5	375	600
	93B	1862	Magnetite	-5.39	-27.35	2.2	4.1	7.6	375	600
	Repeat	2576		-5.58	-29.07	2.6	3.7	7.3	375	600
	123A		Quartz			8.7	1.7	5.3	375	600
	123B	1863	Magnetite	-5.63	-23.57	8.4	3.0	6.6	375	600
	Repeat	2577		-5.58	-28.77	6.4	5.7	9.2	375	600
	Repeat	2585		-5.36	-24.17	7.6	2.7	6.2	375	600
	247A	2546	Quartz	-5.11	-21.60	10.3	-1.8	1.8	375	600
	247B	1861	Magnetite	-5.38	-24.58	7.3	-1.2	2.4	375	600
	Repeat	2578		-5.58	-28.77	2.9	5.0	8.6	375	600
	Repeat	2586		-5.47	-28.21	3.5	5.1	8.6	375	600
	289A	2547	Quartz	-5.12	-22.22	9.7	3.6	7.2	375	600
	Repeat	1838		-5.24	-22.28	9.7	4.3	7.9	375	600
	289B	1902	Magnetite	-4.97	-23.74	8.3	4.7	8.2	375	600
	Repeat	2579		-5.41	-22.91	8.9	5.1	8.7	375	600
3	43	2564	Quartz	-5.17	-21.81	10.1	4.6	6.0	345	399
	84	2584	Quartz	-5.31	-22.21	9.7	4.2	5.6	345	399
	285	2565	Quartz	-5.27	-21.89	10.0	4.6	6.3	345	419
4	41	2574	Quartz	-5.26	-21.76	10.1	5.4	6.3	372	411
	82	2575	Quartz	-5.29	-21.95	9.9	5.2	6.1	372	411
	122	2542	Quartz	-5.13	-22.12	9.8	2.2	4.4	281	349
	130	2555	Quartz	-5.18	-21.99	9.9	5.2	6.1	372	411
	151A	2543	Quartz	-5.17	-21.56	10.3	4.5	7.2	331	446
	151B	2544	Quartz	-5.14	-21.75	10.1	4.3	7.0	331	446
5	61	2573	Quartz	-5.25	-20.69	11.2	6.0	7.1	353	398
	24A	2556	Quartz	-5.21	-20.42	11.5	6.3	7.4	353	398
	24B	2557	Quartz	-5.21	-21.49	10.4	5.2	6.3	353	398
	29A	2566	Quartz	-5.18	-21.51	10.4	5.2	6.3	353	398
	29B	2567	Quartz	-5.11	-21.33	10.6	5.4	6.5	353	398
	92A	1826	Quartz	-5.21	-21.56	10.4	5.2	6.3	353	398
	92B	1827	Quartz	-5.47	-22.88	10.1	4.9	6.0	353	398
	91A	2568	Quartz	-5.20	-21.11	10.8	5.6	6.7	353	398
	91B	2569	Quartz	-5.12	-18.38	13.6	2.0	9.4	200	395
	Repeat	2587		-5.03	-14.41	17.7	6.1	13.5	200	395
	100A	1828	Quartz	-5.22	-22.21	9.8	4.6	5.7	353	398
	100B	1829	Quartz	-5.14	-19.64	13.4	1.8	9.2	200	395
	Repeat	1846		-5.09	-14.51	17.8	6.2	13.7	200	400
	Repeat	1905		-4.81	-17.83	14.3	2.7	10.1	200	395
	Repeat	2588		-5.00	-14.89	17.2	5.6	13.1	200	395
6	74	2558	Quartz	-5.10	-19.88	12.1		7.4		373
	Repeat	2583		-5.18	-20.51	11.4		6.7		373
	97	2559	Quartz	-5.16	-20.51	11.1		5.8		350
	103	2560	Quartz	-5.13	-20.51	11.4		7.1		390

A=Marginal
B=Core

Sulphur isotope geochemistry

Sample type	Sample number	Lab number	Phase analysed	d66SO2	2sigma	d34S CDT
Type 1 veins	155	SA5444	C'pyrite	-7.485	0.019	-0.05
	84	SA5611	Pyrite	-7.159	0.01	0.08
Type 2 veins	93	LS2939	C'pyrite	*		-2.93
	repeat	LS2940	C'pyrite	*		-2.21
	123	LS2937	Pyrite	*		3.00
Type 5 veins	24	SA5607	MoS2	-6.484	0.025	0.84
	repeat	SA5453	MoS2	-6.826	0.017	0.30
	29	SA5604	MoS2	-6.506	0.012	0.81
	91	SA5610	MoS2	-6.943	0.036	0.32
		SA5445	Pyrite	-6.673	0.013	0.47
	92	SA5609	MoS2	-6.613	0.023	0.69
	repeat	SA5448	MoS2	-5.958	0.017	1.30
	100	SA5601	MoS2	-6.521	0.024	0.80
		SA5439	Pyrite	-6.492	0.022	0.68
	repeat	SA5612	Pyrite	-6.646	0.016	0.66
Type 6 veins	38	SA5621	Pyrite	-6.134	0.017	1.23
	48	SA5451	Pyrite	-6.634	0.016	0.52
	50	SA5623	Pyrite	-6.545	0.023	0.77
	62	SA5616	Pyrite	-6.723	0.027	0.57
	68	SA5615	Pyrite	-6.846	0.03	0.43
	74	SA5608	Pyrite	-6.712	0.013	0.58
	97	SA5438	Pyrite	-6.755	0.015	0.38
	98	SA5622	Pyrite	-6.248	0.023	1.10
	103	SA5441	Pyrite	-6.225	0.017	0.99
	141	SA5442	Pyrite	-6.216	0.013	1.00

Calculation of water solubility in the suspension layer.

1. Calculate in K_w^{ma} for pressure (P) and temperature (K)

$$\ln K_w^{ma} = 5.00 + (\ln P)(4.481\times10^{-8}T^2 - 1.51\times10^{-4}T - 1.137) + (\ln P)^2(1.831\times10^{-8}T^2 - 4.882\times10^{-5}T + 4.656\times10^{-2}) + 7.80\times10^{-3}(\ln P)^3 - 5.012\times10^{-4}(\ln P)^4 + T(4.754\times10^{-3} - 1.621\times10^{-6}T)$$

2. Calculate $\ln K_w^{rockmelt} = \ln K_w^{ma} + 0.47 \times (1-(X_{ab} + X_{or} + X_{an})$

Where X_i are eight-oxygen normative components in the melt composition in question

3. Determine $X_w m$ (mol. fraction of water)

$$X_w^m = 0.5 + \frac{\ln (a_w / 0.25 \times \ln K_w^{rockmelt})}{(6.52-2667)/T}$$

where a_w = activity of water

Sample	FP Melt								
Oxide	Weight %	Adjusted to 100%	Molecular weight	Molecular x 1000	Ab NaAlSi3O8	Or KAlSi3O8	An CaAl2Si2O8	Qtz Si4O8	Sum of moles
SiO2	67.49	77.42	60	1290.4	123.8	168.4	0.0	249.5	
Al2O3	12.85	14.74	102	144.5	41.3	56.1	0.0		
Na2O	2.23	2.56	62	41.3	41.3				
K2O	4.6	5.28	94	56.1		56.1			
CaO	0	0.00	56	0.0			0.0		
	87.17	100			41.3	56.1	0.0	249.5	346.9
			Mole fractions		0.118	0.161	0.000	0.716	1.0
			Formula weights		262	278	278	240	Fw8
					31.00	44.76	0.00	171.76	**248**

Calculated K factor ($0.47 \times (1-(X_{ab} + X_{or} + X_{an})) = 0.338715$

Calculation of melt composition in the suspension layer at Quebrada Blanca

1. Fresh average composition of feldspar porphyry
2. Total composition of the phenocryst assemblage; 40% Plagioclase, 5% Quartz, 2% Magnetite
3. Composition minus the composition of the phenocryst assemblage; 40% Plagioclase, 5% Quartz, 2% Magnetite
4. Recalculated to 100% (H_2O determined)

	1	Plag	Qtz	Magnetite	2	3	4
SiO2	66.39	24.744	5		29.744	36.65	67.49
Al2O3	16.67	9.6933			9.6933	6.98	12.85
FeO	3.69			1.4	1.4	2.29	4.22
MgO	1.30					1.30	2.39
CaO	2.34	2.4949			2.4949	0.00	0.00
NaO	4.28	3.0675			3.0675	1.21	2.23
K2O	2.50					2.50	4.60
P2O5	0.19					0.19	0.35
TiO2	0.44					0.44	0.81
MnO	0.03					0.03	0.06
H2O-						5.00	5.00
Total						51.59	100.00
Ba	686	10			10	676	1126
Sr	489	160			160	329	549
Cr	88					88	147
Cu	610					610	1017
Ni	25					25	42
Zn	148					148	247
Zr	122					122	203
Mo	36					36	60

Calculation of melt composition in the porphyry at Yerington

1. Fresh average composition of feldspar porphyry
2. Composition minus the composition of the phenocryst assemblage; 40% Plagioclase, 5% Quartz, 2% Magnetite
3. Recalculated to 100% (H_2O determined)

1	Oligoclase	Microcline	Quartz	2	3
68.1	11.716	10.151	10.9	35.333	64.87
15.6	4.131	3.02		8.449	15.51
2.42				2.42	4.44
0.98				0.98	1.80
2.84	0.5958			2.2442	4.12
4.32	1.808	0.411		2.101	3.86
3.35		2.018		1.332	2.45
0.14				0.14	0.26
0.37				0.37	0.68
0				0	0.00
1.1				1.1	2.02
99.22				54.4692	100

Percentage of phenocrysts

	Phenocryst	Rock
oligoclase	36.5	18.25
microcline	31.2	15.6
quartz	21.8	10.9
Hornblende	3.2	1.6
biotite	5	2.5

Feldspar compositions

Oligo	Si	64.1	11.71582
	Al	22.6	4.130696
	Ca	3.26	0.595844
	Na	9.89	1.807636
		99.85	18.25
Microcline		64.2	10.15123
		19.1	3.020069
		2.6	0.411109
		12.76	2.017596
		98.66	15.6

SAMPLES TAKEN

Hole Number 71 Grid Coordinates Total Length

Sample Number	Depth	Subject
1	57.85	8mm qtz /cpy (ox) vein in ig breccia
2	90.57	?
3	100.10	qtz vein with weak mineralisation in feldspar porphyry
4	106.00	2cm qtz /cc vein qtz selvage? in feldspar porphyry
5	116.05	5mm cc / py vein with st qtz selvage
6	127.40	1cm qtz / mo (cpy) vein in qtz monzonite (sericite)
7	131.70	qtz / py veins possibly some mo
8	145.70	thick qtz vein with diss cc cut by py / cc vein cut by qtz veinlet
9	164.00	py / cc veins with qtz-ser selvages in igneous breccia
10	214.65	development of qtz obliterating cpy/py/bn veinlet
11	224.70	1cm qtz vein with diss sulphides in qtz monzonite
12	235.70	1cm qtz / py vein with feldspar halo
13	240.40	two phase 3cm qtz cpy / bn or mo vein
14	314.60	angular qtz clasts with mo veinlets in igneous breccia

Hole Number 102A Grid Coordinates Total Length

Sample Number	Depth	Subject
15	539.60	?
16	518.40	1cm bi(chlor)/cpy / mo / qtz no selvage cuts qtz vein with k-spar selvage
17	515.40	2cm qtz ((mo/cpy)) vein with k-spar selvage
18	470.80	feld / qtz / cpy / bio vug fills in locally brecciated zone
19	439.20	2.5cm qtz / cpy / py vein
20	387.50	1cm qtz (((cpy))) vein with wk k-spar selvage
21	384.95	6mm qtz (cpy / mo) veins no haloes
22	371.90	2.5cm qtz (cpy) vein with qtz-ser-chlor selvage cuts mo veinlet
23	356.50	1cm py (qtz) vein with wk k-spar selvage
24	344.60	two phase 1cm qtz mo / cpy vein with k-spar selvage in feld / bio rock
25	293.00	multiphase qtz / feld / biotite vein with bands of biotite. in bio rock
26	263.50	4mm qtz vein with st k-spar selvage

Hole Number 109 Grid Coordinates Total Length

Sample Number	Depth	Subject
27	96.25	?
28	122.70	veinlet with st qtz selvage fringed by thin bio or to / qtz selvage
29	193.50	5mm qtz /mo / py vein no selvage st ser silicic rock
30	194.60	possible a type veins
31	204.15	3cm qtz / mo / cv vein some chrysocolla no selvage
32	235.35	4cm qtz / mo /cpy vein
33	236.00	2mm cpy (py) vein with qtz selvage in st ser qtz monzonite
34	239.60	stockwork of cpy and mag/bio veinlets with st sericite haloes

Hole Number 60 Grid Coordinates Total Length

Sample Number	Depth	Subject
35	48.70	?
36	138.60	3mm cpy / bn / qtz vein wk ser in ser qtz monzonite
37	144.50	tourmaline crystals
38	170.70	3cm py (cv) / qtz vein v strong qtz- ser halo
39	173.30	8mm qtz (cpy (cc)) vein wk sericite
40	174.00	1.5cm qtz vein with k-spar core in st silicic rock

Hole Number 62 Grid Coordinates Total Length

Sample Number	Depth	Subject
41	66.60	8mm qtz vein or unmineralised qtz veins
42	69.45	8mm qtz (cpy(cv)) vein with st ser selvage in qtz monzonite (ser)
43	84.05	2cm thick qtz vein with central cv w ser granodiorite w ser w bio
44	97.75	2.5cm qtz / cpy veins with biotite / qtz selvages

Hole Number 74 Grid Coordinates Total Length

Sample	Depth	Subject
45	264.95	1.5cm qtz vein with core of cpy/py with st qtz halo cuts qtz/py vein and qtz veinlet in silicic qtz monzonite
46	263.20	?
47	250.45	2cm band of py in ser matrix cuts through qtz ((cpy)) band in qtz monzonite
48	226.10	1.5cm qtz vein with core of py st qtz? silicic qtz monzonite
49	215.75	to breccia contact
50	207.40	5mm py vein cuts 5mm qtz (py) vein no selvages bio qtz monzonite
51	178.50	py / to / alunite vein with ser selvage cut by qtz / alunite vein no selvage in m ser qtz monzonite
52	158.80	qtz /py(cv) veinlet from to breccia al selvage
53	111.80	6mm qtz / py vein in to breccia also infilling vugs
54	67.20	1cm qtz / py (ox) vein in clast within breccia
55	18.55	to / alunite veins

Hole Number 155 Grid Coordinates Total Length

Sample Number	Depth	Subject
56	132.90	1.5cm qtz (mo/cpy) vein in mg granodiorite
57	135.25	8mm qtz / py(cv) vein ser halo fringed with bio
58	155.60	py(cv) qtz vein with ser or kaolinite st qtz - ser halo
59	175.60	6mm qtz / py (cv) vein with qtz selvage in fresh granodiorite
60	190.50	8-10cm thick qtz (((qtz / cpy))) vein in bio granodiorite
61	209.20	2cm qtz vein with cpy core st qtz - ser selvage in granodiorite
62	247.90	7mm py (qtz) vein with qtz o bio o k-spar selvage in bio andesite
63	259.30	1.4cm qtz ((mo/py)) vein wk ser halo in granodiorite
64	270.35	3mm qtz (py) vein st qtz-ser-bio halo cut by 5mm qtz / cpy vein similar halo but weaker
65	283.35	6-7mm qtz vein with large agglom of hem / mag st qtz ser halo in m bio w ser granodiorite

Hole Number 133 Grid Coordinates Total Length

Sample Number	Depth	Subject
66	121.00	possible a type veins in st ser qtz monzonite
67	129.50	1.2cm qtz / py vein (cv) no selvage in st ser rock
68	143.45	1.4cm py (qtz) vein st qtz-ser selvage in m bio granodiorite
69	152.65	7mm qtz (py(cv)) vein wk ser in bio granodiorite (wk ser)
70	165.60	?
71	189.60	two phase? 8mm qtz vein outer qtz inner qtz / py qtz selvage in grano
72	200.80	?
74	206.30	1cm qtz / mo ((py)) vein wk sericite selvage in st ser rock
75	206.55	?
76	212.90	?
77	265.60	?
78	272.30	1.2cm qtz (py) vein st qtz - ser halo possibly after k-spar in bio grano

Hole Number 100 Grid Coordinates Total Length

Sample Number	Depth	Subject
79	133.30	6mm qtz (py(cv)) vein k-spar (ser)
80	136.00	contact between qtz porphyry and qtz monzonite
81	143.30	5mm qtz (py) vein wk k-spar selvage barrier to bio and ser
82	143.50	6mm qtz / py vein with qtz - ser halo is cut by 3mm qtz vein in m ser diorite
83	148.40	1.5cm qtz ((py)) vein and k-spar selvage in m ser granodiorite
84	151.70	5mm qtz (cpy/py) vein lacking a halo cuts 8mm qtz (((py))) vein in m sericite biotite granodiorite
85	156.50	5mm qtz (py) vein with qtz selvage is cut by 4mm qtz mo/py vein without a selvage m ser granodiorite

Hole Number 32

Sample Number	Depth	Subject
86	57.70	5mm qtz vein no halo in sericite leached qtz porphyry
87	100.70	?
88	105.80	hem ((alunite)) vein with qtz selvage in hem / silicic material
89	172.80	?
90	192.00	4mm qtz (py(cv)) vein cutting breccia
91	197.05	1.5cm qtz / py(cv) in fg breccia silicic
92	209.00	?
93	282.50	5mm cpy/py(cv) vein with k-spar (ser) halo. in to rich rock

Hole Number 6

Sample Number	Depth	Subject
94	74.75	6mm py / qtz vein in qtz diorite (ser)
95	84.90	composite qtz / py vein with biotite selvage and later zeo/alun/clays
96	110.15	1cm qtz / py vein lacking selvage
97	122.75	5mm qtz / py ((mo)) vein with k-spar selvage (ser)
98	139.10	3cm py / qtz vug fills with unusual bn type tarnishes
99	170.40	4mm qtz / py / hem vein with k-spar or qtz-ser selvage

Hole Number 53

Sample Number	Depth	Subject
100	290.70	2cm qtz vein with py core and mo borders no selvage in m to rock
101	287.50	1cm qtz vein no halo in to / ser rock
102	284.30	6mm qtz ((cpy/mo)) vein with wk qtz - ser halo in to / ser rock
103	263.70	1cm qtz/py/hem vein no selvage m sericite silicic rock
104	212.70	8mm qtz (cpy(cv)) vein no selvage silicic rock
105	179.15	py (cv) vein with qtz selvages in ser / kaolinised rock
106	125.75	1cm qtz vein with qtz halo in igneous breccia ser / bleached

Hole Number 134 Grid Coordinates Total Length

Sample Number	Depth	Subject
107	41.60	1.3cm qtz vein ((cpy(ox))) no halo in st ser leached rock
108	44.40	strange flow texture in igneous breccia
109	104.00	2-15mm qtz vein (((cv))) no selvage st ser feld-rich qtz monzonite
110	155.70	1cm qtz / mo / py vein with ser core in m ser st silicic rock
111	173.55	6-7mm qtz ((py)) vein lacking selvage in bio ser rock
112	174.80	5mm qtz / py(cv) vein with k-spar (ser) selvage m ser st silicic
113	195.70	1.3cm py ((qtz)) vein k-spar prior to st silicic of rock
114	229.75	7mm qtz ((py)) vein wk qtz halo in m ser f (bi) porphyry
115	255.70	1.5cm qtz / py(cv) vein lacking obvious halo in m bio silicic rock
116	263.45	bio / py vug fillings in igneous breccia
117	269.95	1.5-2cm qtz ((py)) vein no halo st bio ser rock

Hole Number 14

Sample Number	Depth	Subject
118	20.80	?
119	36.72	1cm qtz vein with trace cpy no halo in st biotite st sericite rock
120	51.90	8mm qtz / py /feld vein with strong qtz selvage m sericite f-porphyry
121	81.75	6mm qtz / feld? (cpy) no halo m sericite f-porphyry
122	80.95	4mm-1cm qtz (cpy (cv)) vein no halo in biotitised rock
123	95.65	1.8cm qtz (py(mo)) vein lacking halo cut by breccia matrix granodiorite

Hole Number 88 Grid Coordinates Total Length

Sample Number	Depth	Subject
124	24.75	1.5-2cm qtz vein with no halo is cut by feld rich intrusion st ser qtz monzonite
125	37.90	1.5-2cm qtz vein ((cv)) wk qtz halo in fresh granodiorite
126	39.30	4-8mm granular qtz veins no haloes ser granodiorite
127	59.85	7mm qtz / mo (py) vein without a halo cuts 5mm qtz vein with wk k-spar (ser)
128	74.40	1cm qtz (mo?/py) vein without a selvage is cut by igneous
129	83.50	1.5cm qtz ((py)) vein without a selvage in st bio / m ser granodiorite
130	112.00	3mm py ((qtz)) vein st qtz selvage in m ser ig breccia matrix

Hole Number 69 Grid Coordinates Total Length

Sample Number	Depth	Subject
131	48.85	1.5cm qtz / feld (cv/mo) vein with wk qtz halo in m bio /ser diorite
132	49.50	1cm qtz vein with mo at edges and cpy in core no halo st ser diorite
133	67.20	3mm (py/cpy)? bi / qtz st k-spar selvage in wk ser / bio diorite
134	94.40	5mm-1cm cpy / mo /qtz vein with qtz o k-spar m ser / bio diorite
135	97.40	3mm qtz / py vein with strong bio halo in bio granodiorite

Hole Number 51

Sample Number	Depth	Subject
136	0.80	8cm qtz vein (ox) no halo in sericite leached qtz monzonite
138	108.40	8mm qtz / py (cv) vein with qtz halo in w sericite diorite
139	128.30	5mm qtz / py vein with weak k-spar cuts 6mm qtz ((mo/py)) vein with wk k-spar. in diorite (ser / bio)
140	133.55	8mm py vein with fresh py and chrysocolla silicic qtz monzonite
141	141.20	4mm py / qtz vein with st qtz halo in m sericite / biotite diorite
142	161.35	1.5cm py/qtz vein no halo st silicic rock
143	170.45	1cm qtz ((mo/py)) vein with qtz selvage. in st ser diorite
144	180.25	strange chalcedonic breccia matrix
145	195.20	5mm qtz (py(cv)) vein no halo st silicic rock
146	228.10	3cm qtz (mo/py) vein with no halo

Hole Number 111A Grid Coordinates Total Length

Sample Number	Depth	Subject
147	185.45	1.6cm qtz (py) vein with ser/qtz/bio halo truncated by igneous breccia
148	188.20	5cm qtz (((py))) vein no halo in ser / bio porphyry
149	213.00	possible a type veins milky qtz ((py)) in silicic bio chlor qtz M
150	284.80	ig breccia with vugs infilled by cpy bi(chlor) and 5mm qtz vein ser halo
151	289.70	2cm qtz ((mo/py)) vein fractured by igneous breccia
152	304.05	large clast of vein qtz in igneous breccia
153	335.40	1cm qtz vein no selvage in m silicic qtz monzonite
154	443.60	5mm qtz (mo) vein with wk k-spar selvage in bio qtz monzonite
155	516.80	5mm qtz / feld / py vein no selvage bio diorite / qtz monzonite
156	563.50	3.5-4cm qtz vein no selvage w ser qtz monzonite

DDH	Sample Number	From Desde	To Hasta	Nature of sample
14	309	79.90	80.00	Feldspar Porphyry
14	201	107.17	107.25	Mafic dyke
23	294	69.70	69.75	MoS2 vein
23	295	159.25	159.37	Feldspar Porphyry
29	323	174.26	174.30	Mafic dyke
29	324	179.36	179.41	Mafic dyke
29	325	194.95	195.00	A-type vein
32	243	104.00	104.08	Tourmaline Breccia
32	244	115.92	116.00	Tourmaline Breccia
32	245	271.95	271.55	Granodiorite
51	213	136.25	136.40	Fresh mafic dyke
51	214	231.15	231.35	Fresh mafic dyke
53	215	239.10	239.20	Qtz-Magnetite-Cpy vein
53	216	270.80	271.00	Granodiorite
53	217	277.50	277.58	Qtz-Biotite-Cpy vein
60	203	46.10	46.20	Tourmaline Breccia
60	204	110.95	111.05	Tourmaline Breccia
60	205	144.90	145.00	Tourmaline Breccia
60	206	154.15	154.24	Tourmaline Breccia
60	207	176.87	176.95	Tourmaline Breccia
60	208	174.80	174.90	Tourmaline Breccia
60	209	180.45	180.51	Tourmaline Breccia
62	210	85.50	85.62	Brecciated Granodiorite
62	211	95.00	95.13	A-type vein
62	212	96.30	96.45	Feldspar Porphyry
65	275	92.30	92.36	Tourmaline Breccia
65	276	93.40	93.47	Tourmaline Breccia
65	277	140.85	140.90	Granodiorite
65	278	164.60	164.70	Granodiorite
65	279	168.34	168.40	Magnetite in igneous breccia
65	280	173.51	173.63	Mafic dyke
65	281	181.55	181.60	Tourmaline Breccia
65	282	184.85	184.90	Tourmaline Breccia
65	283	193.78	193.88	Granodiorite
65	284	201.05	201.13	Magnetite-rich breccia
67	268	169.10	169.22	Granodiorite
67	269	174.04	174.14	MoS2 vein

DDH	Sample Number	From Desde	To Hasta	Nature of sample
69	202	75.15	75.25	Granodiorite, altered
70	265	119.25	119.34	Granodiorite
70	266	138.35	138.43	A-type vein
70	267	167.20	167.35	Feldspar Porphyry
71	310	93.25	93.35	Feldspar Porphyry
71	232	150.12	150.22	Vuggy Breccia
71	233	239.00	239.15	Granodiorite
71	234	228.95	229.00	Mafic dyke
71	235	229.25	229.35	Mafic dyke
71	236	338.65	338.79	Granodiorite
73	297	185.20	185.31	Feldspar Porphyry
74	218	166.90	167.00	Tourmaline Breccia
74	219	260.12	260.20	Qtz-Cpy vein with Biotitic halo
74	220	260.85	261.05	Granodiorite
89	292	88.15	88.30	Mafic dyke
89	293	89.50	89.60	Mafic dyke / clasts
97	296	89.55	89.67	Feldspar Porphyry
102A	237	292.30	292.45	Granodiorite
102A	307	306.85	306.90	Mafic dyke
102A	238	348.50	348.62	Granodiorite
102A	239	424.00	424.10	Feldspar porphyry
102A	240	449.50	449.60	Qtz-rich Cpy vein
102A	306	526.20	526.25	Mafic dyke
102A	241	528.16	528.29	Mafic-Granodiorite contact
102A	242	544.10	544.20	Probable A-type vein
105	287	101.40	101.49	Granodiorite with Biotite and K-s
105	288	127.70	127.75	A-type vein
105	289	132.60	132.65	A-type vein
105	290	135.30	135.41	Granodiorite
105	291	137.75	137.80	A-type vein
109	246	237.75	237.85	Vein with Chlorite
109	247	241.64	241.70	Vein with chlorite
109	248	249.40	249.52	Granodiorite

DDH	Sample Number	From Desde	To Hasta	Nature of sample
111A	221	211.50	211.60	Vuggy Breccia
111A	222	241.65	241.80	Vuggy Breccia
111A	223	275.65	275.75	Igneous Breccia
111A	224	307.54	307.62	Igneous Breccia
111A	225	382.15	382.25	Igneous Breccia
111A	226	509.33	509.39	A-type vein
111A	227	511.70	511.78	A-type vein
111A	308	513.65	513.70	Mafic dyke
111A	228	525.00	525.12	Feldspar Porphyry - Granodiorite
111A	298	538.70	538.80	Mafic dyke
111A	229	546.80	546.90	A-type vein
111A	230	548.45	548.53	Qtz-Biotite-Chlorite vein
111A	231	556.65	556.85	Granodiorite
131	270	105.07	105.17	Breccia with molybdenite
131	271	119.81	119.90	Breccia with molybdenite
131	272	182.50	182.60	Feldspar Porphyry
131	273	176.00	176.10	Feldspar Porphyry
131	274	123.45	123.51	Feldspar Porphyry
133	255	172.70	246.00	Mafic dyke
133	257	179.50	179.65	Feldspar porphyry
133	258	182.35	182.50	Granodiorite
134	259	186.02	186.17	Feldspar Porphyry
134	260	231.00	231.12	Feldspar Porphyry
134	261	277.25	277.38	Feldspar Porphyry
134	262	255.50	255.60	Granodiorite
134	263	259.50	259.57	Igneous Breccia
134	264	276.80	276.92	Granodiorite

DDH	Sample Number	From Desde	To Hasta	Nature of sample
152	299	242.12	242.27	Granodiorite
152	300	246.40	246.52	Granodiorite
152	311	275.60	275.66	Granodiorite
152	312	276.08	276.14	Granodiorite
152	313	277.83	277.87	Granodiorite
152	314	278.60	278.55	Granodiorite
152	315	278.93	278.97	Granodiorite
152	301	279.65	279.75	Mafic dyke
152	302	282.25	282.83	Mafic dyke
152	316	288.69	288.79	Granodiorite
152	317	290.25	290.30	Granodiorite
152	318	291.50	291.55	Granodiorite
152	319	292.20	292.25	Granodiorite
152	320	292.60	292.66	Granodiorite
152	321	293.85	293.90	Granodiorite
152	303	337.65	337.78	Granodiorite
152	304	357.20	357.32	Mafic dyke
152	305	405.10	405.25	Granodiorite
155	249	140.85	140.90	Granodiorite
155	326	198.80	198.85	Granodiorite
155	327	200.85	200.90	Granodiorite
155	328	202.60	202.65	Granodiorite
155	329	203.10	203.15	Granodiorite
155	330	204.60	204.65	Granodiorite
155	250	205.10	205.20	Granodiorite
155	331	205.65	205.70	Granodiorite
155	332	207.90	207.95	Granodiorite
155	333	209.65	209.70	Granodiorite
155	334	210.40	210.45	Granodiorite
155	252	210.50	210.60	Possible A-type veins in mafic ma
155	335	210.75	210.80	Mafic dykes
155	251	212.12	212.18	Mafic dyke
155	253	218.70	218.85	Granodiorite
155	254	245.50	245.57	A-type vein
155	256	245.88	172.80	Mafic dyke
157	285	24.60	24.63	A-type vein in feldspar porphyry
157	286	65.30	65.39	Granodiorite

DIAMOND DRILL HOLE LOCATIONS AND DETAILS

Hole #	**Date in notes**	Northings	**Eastings**	Total Depth	**Collar Elevation**	
6	**18/9/95**	7,678,274	**519,065**	192.27	**4103.20**	
14	**20/9/95**	7,677,887	**519,100**	149.00	**4152.15**	
32	**17/9/95**	7,677,910	**521,047**	292.05	**4402.30**	
51	**22/9/95**	7,678,094	**520,573**	238.30	**4332.05**	
53	**18/9/95**	7,678,035	**520,915**	297.73	**4372.08**	
60	**12/9/95**	7,677,896	**520,606**	181.48	**4352.25**	
62	**12/9/95**	7,678,299	**520,502**	110.08	**4292.47**	
69	**21/9/95**	7,678,295	**520,906**	105.20	**4263.32**	
71	**9/9/95**	7,678,096	**520,100**	338.79	**4280.45**	
74	**14/9/95**	7,677,899	**520,502**	267.00	**4338.47**	
88	**21/9/95**	7,677,915	**519,399**	131.07	**4206.79**	
100	**16/9/95**	7,678,299	**519,602**	178.85	**4276.17**	
102A	**10/9/95**	7,678,201	**519,999**	554.75	**4290.88**	
109	**11/9/95**	7,678,100	**519,201**	273.35	**4252.52**	
111A	**23/9/95**	7,678,100	**519,501**	716.60	**4238.92**	
133	**15/9/95**	7,678,297	**520,095**	288.20	**4292.24-I**	
134	**19/9/95**	7,678,117	**519,693**	303.60	**4272.63**	
155	**15/9/95**	7,677,901	**520,100**	296.20	**4299.26**	